ORGANIC AMMONIUM SALTS OF GROUP VI OXOMETALATES AND THIOMETALATES: SYNTHESIS, SPECTROSCOPIC, THERMAL, X-RAY STRUCTURE AND REACTIVITY STUDIES

A Thesis Submitted

In partial Fulfillment of the Requirements

For the Degree of

DOCTOR OF PHILOSOPHY

By

SUNDER NARAYAN DHURI

547

DHU/ Org

T- 338

To the

**DEPARTMENT OF CHEMISTRY
GOA UNIVERSITY
TALEIGAO PLATEAU
GOA 403 206 INDIA**

NOVEMBER 2005

J. k. Lahiri; 18.8.2006
(G.K. LAHIRI)

Dedicated to Devi Mahalaxmi, Brahmani and

To My Late Grand Father

The inspiration and the strength behind this work

STATEMENT

I hereby declare that the matter embodied in this thesis entitled, "Organic Ammonium Salts of Group VI Oxometalates and Thiometalates: Synthesis, Spectroscopic, Thermal, X-ray Structure and Reactivity Studies" is the result of investigations carried out by me in the Department of Chemistry, Goa University, Goa, India, under the supervision of Dr. B. R. Srinivasan.

In keeping with the general practice of reporting scientific observations, due acknowledgement has been made wherever the work described is based on the findings of other investigators.
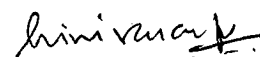
Sunder N. Dhuri

Goa University

November 2005

I

CERTIFICATE

This is to certify that the work entitled, ''Organic Ammonium Salts of Group VI Oxometalates and Thiometalates: Synthesis, Spectroscopic, Thermal, X-ray Structure and Reactivity Studies'' presented in this thesis has been carried out by Mr. Sunder N. Dhuri under my supervision and the same has not been submitted elsewhere for the award of a degree.

(Dr. B.R. Srinivasan)
Guiding Teacher
Department of Chemistry
Goa University

Goa University

November 2005

CERTIFICATE

Certified that the work entitled, "Organic Ammonium Salts of Group VI Oxometalates and Thiometalates: Synthesis, Spectroscopic, Thermal, X-ray Structure and Reactivity Studies" presented in this thesis has been carried out by Mr. Sunder N. Dhuri under the supervision of Dr. B. R. Srinivasan, Department of Chemistry, Goa University and the same has not been submitted elsewhere for the award of a degree. Mr. Dhuri has satisfactorily completed all the course requirements for the Ph.D. degree program. The courses include: i) General Spectroscopy ii) Coordination Chemistry iii) General Seminar.

Head,
Department of Chemistry
Goa University
Head,
Department f Chemi t y
GOA UNIVERSITY.

Goa University

November 2005

Acknowledgement

TABLE OF CONTENTS

LIST OF ABBREVIATIONS

Å	Angstrom unit, 10^{-10} m
AR	Analytical reagent
cm^{-1}	Unit of wave number
nm	Nanometer
ε	Molar absorptivity
υ	Frequency
en	Ethylenediamine
1,3-pn	1,3-propanediamine
1,4-bn	1,4-butanediamine
dien	Diethylenetriamine
dipn	Dipropylenetriamine
pip	Piperazine
1,4-dmp	1,4-dimethylpiperazine
tmen	N,N,N',N'-tetramethylethylenediamine
tren	Tris(2-ethylamine)amine
trans-1,2-cn	(±) Trans-1,2-cyclohexanediamine
(2-pip-1-EtNH$_2$)	2-piperazin-1-ethylamine
mipa	Monoisopropylamine
N,N'-dm-1,3-pn	N,N'-dimethyl-1,3-propanediamine
N-Me-en	N-methylethylenediamine
dbtmen	N,N'-dibenzyl-N,N,N',N'-tetramethyethylenediammonium
DMF	N,N-dimethyl formamide
DMSO	Dimethyl sulphoxide
DEPT	Distortionless enhancement by polarization transfer
TG	Thermogravimetry
DSC	Differential scanning calorimetry
DTA	Differential thermal analysis
EDX	Energy dispersive X-ray analysis
ESEM	Environmental semi electron microscopy
ESR	Electron spin resonance
NMR	Nuclear magnetic resonance
S.D.	Standard deviation
e.s.d.	Estimated standard deviation

SYNOPSIS

The thesis entitled, *"Organic Ammonium Salts of Group VI Oxometalates and Thiometalates: Synthesis, Spectroscopic, Thermal, X-ray Structure and Reactivity Studies"* consists of five chapters as depicted in **Scheme I**. The first chapter reviews the work carried out by various researchers in this field and highlights of the known work are presented. The second chapter deals with scope of the present investigation. The details of experimental work, which include synthesis and reactivity studies, are discussed in the Chapter 3. The characterisation of synthesised complexes by various analytical techniques is described in the fourth chapter. The final chapter summarizes the present work and the thesis ends with some recommendations for future work.
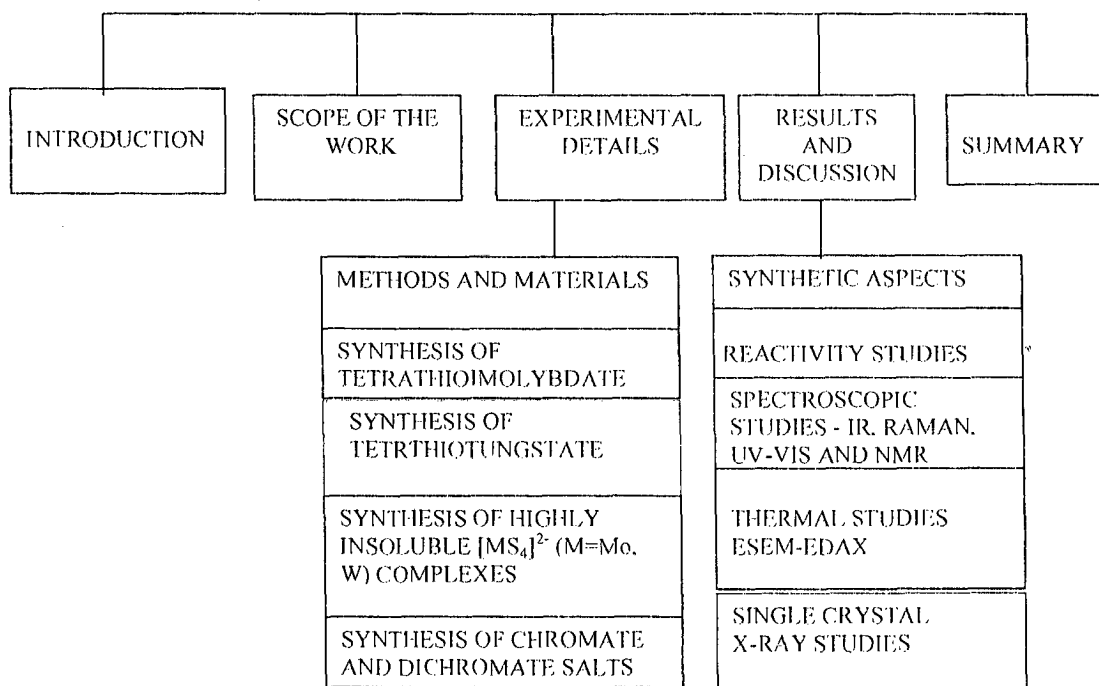
Scheme I

The first chapter reviews the known chemistry of M-X complexes (M= Mo, W and Cr, X= S, O). The elements of group VI (Mo and W) are essential trace elements for many organisms, including human beings and animals. Molybdenum is required for almost all molybdenum enzymes containing sulfur atoms [1]. Many sulfur-bridged compounds of tungsten, a congener of molybdenum, are also known. Molybdenum is also present as the Fe/Mo cofactor of nitrogenase [2] and oxidoreductase enzymes [3]. The sulfur complexes of group VI metals Mo [4] and W [5] are a unique class of

compounds encompassing an unusually wide range of metal-sulfur stoichiometry, metal oxidation states, coordination geometries and different bonding modes of sulfido ligands. The structural diversity exhibited by Mo/W-S complexes can be evidenced from the structural characterisation of a variety of Mo/W-S complexes and this is an important reason for the continuing research in this rapidly growing field. The Mo-S complexes $[MoS(S_4)_2]^{2-}$, $[Mo_2(S)_2(\mu-S)_2(S_2)_2]^{2-}$, $Mo_2(S)_2(\mu-S)_2(S_4)(S_2)]^{2-}$, $[Mo_2(S)_2(\mu-S)_2(S_4)_2]^{2-}$, $[SMo(MoS_4)_2]^{2-}$ etc. which can be prepared from $[MoS_4]^{2-}$ by reacting with the appropriate reagents, serve as a few examples, to illustrate the structural diversity encountered in Mo-S chemistry [6-10]. It is well documented that the $[MoS_4]^{2-}$ ion can behave like a bidentate ligand to form sulphur bridged multi-metal complexes [11,12]. Like $[MoS_4]^{2-}$, $[WS_4]^{2-}$ has been used as a reagent for the synthesis of several structurally diverse W-S complexes such as $[W_2(S_2)_2(\mu-S)_2(S_4)_2]^{2-}$ [9], $[W_2(S)_2(\mu-S)(\eta^2-S_2)_4]^{2-}$ [13], $[W_2(S)_2-(SH)(\mu-\eta^3-S_2)(\eta^2-S_2)_3]^-$ [14], $[W(WS_4)_2]^{2-}$ [15], $[SW(WS_4)_2]^{2-}$, $[W_3S_{10}]^{2-}$ [16], $[(W_2S_4)(WS_4)_2]^{2-}$ [17]. Although the ammonium salts of tetrathiometalates of the group VI metals $(NH_4)_2[MS_4]$ (M = Mo, W) were first investigated by Berzelius [18,19] in the beginning of the nineteenth century, much of its chemistry has been developed only in the last three decades primarily by Müller and coworkers [11].

In recent years, the chemistry of soluble metal sulfide complexes is emerging as a frontier area of research in view of the relevance of metal sulfide compounds in hydrosulfurisation (HDS), hydrodeoxygenation (HDO), hydrodenitrogenation (HDN) and hydrometallation (HDM), and application in energy, environmental, and material science [20]. The use of organic ammonium tetrathiomolybdates and tetrathiotungstates as precursor materials for the preparation of highly dispersed MoS_2 and WS_2 catalysts respectively is showing much promise in the field of hydrodesulfurisation (HDS) catalysis [21]. It has also been reported that the chemical properties of $[MoS_4]^{2-}$ can be substantially changed by surrounding it with organic ammonium cations for example cetyltriethylammonium [22]. The synthesis and HDS activity of Ni-Mo-S [23] and Co-Mo-S catalyst [24] both derived from thiomolybdates have been reported recently.

The use of thiomolybdate as a versatile reagent for the preparation of a variety of compounds and also its relevance in bioinorganic chemistry and medicine has been

reviewed [25]. In recent years the use of tetrathiomolybdate for the treatment of metastatic cancer has added an entire new dimension to its chemistry [26,27]. Recently the reactivity characteristics of $[MoS_4]^{2-}$ towards trialkyl phosphine like PMe_3 (Me is methyl) have been reported emphasizing the role of proton sources for S transfer [28]. A possible reason for the differing reactivity of $(NH_4)_2[MoS_4]$ and $(Et_4N)_2[MoS_4]$ has been attributed to short H-bonding contacts between the cation and anion in $(NH_4)_2[MoS_4]$ [28], a structural feature which is absent in $(Et_4N)_2[MoS_4]$ [29]. The use of Mo-S complexes like $(NH_4)_2[Mo_2S_{12}]$ [30], $(C_5H_{12}N)_2[MoS_4]$ [31], $[(PhCH_2)N(C_2H_5)_3]_2[MoS_4]$ [32,33], $(NH_4)_2[MoS_4]$ [34,35] as sulfur transfer reagents in organic syntheses, for the preparation of organo-sulfur compounds has added an extra dimension to the known Mo-S compounds. It has recently been shown by Bensch and coworkers that phase pure sulfido complexes of Mo and W like $[Ni(en)_3][MoS_4]$ (en is ethylenediamine) [36], $[Ni(en)_3][WS_4]$ [37], $[Co_2(tren)_3][MoS_4]_2$ [38], $[Ni(tren)_2][WS_4]$ (tren is tris(2-aminoethylamine)) [39] and $[Mn(dien)_2][MoS_4]$ (dien is diethylenetriamine) [40] can be prepared under mild solvothermal conditions. In this context, the study of the reactivity characteristics of $[MS_4]^{2-}$ complexes with different organic bases like en and other related amines can be useful to understand the influence of the chemical and geometrical properties of the solvent on the product formation.

The second chapter outlines the scope of the present work. A primary aim of the present investigation is to develop simple synthetic strategies for the convenient synthesis of newer organic ammonium tetrathiomolybdates and tetrathiotungstates using readily available starting materials. It may be noted that several reported extended network systems derived from $[MoS_4]^{2-}$ and $[WS_4]^{2-}$ have been assembled under solvothermal conditions. It is of interest to develop synthetic methods for the construction of M-S complexes under ambient conditions. In this context two different synthetic methods along with the previously used simple cation exchange method, are used for the syntheses of a variety organic ammonium tetrathiometalates. The use of organic amines with differing H-bonding donors and steric factors can lead to the formation of structurally different extended network compounds. Hence various organic amines with different steric factors and different number of potential H-bonding donors have been chosen in this work. The different organic amines used in this work are depicted in **Scheme II**.

The third chapter describes the full details of the experimental aspects of the present work, which includes the synthesis of organic ammonium tetrathiometalates, oxochromates as well as their reactivity studies. The reaction sequences employed for the synthesis are summarized in **Scheme III. Scheme IV** summarizes the reactivity studies of the synthesized complexes. As a part of reactivity study of tetrathimolybdates and tetrathiotungstates, a convenient method has been developed for the quantitative estimation of $[MS_4]^{2-}$ core. Here aqueous or organic solution of $[MS_4]^{2-}$ complexes was reacted with $[Ni(en)_3]^{2+}$ solution which results in formation of highly insoluble $[Ni(en)_3][MS_4]$ (M= Mo,W). This method has been used to correctly formulate the earlier reported ammonium tetracosathioheptamolybdate as ammonium tetrathiomolybdate [41].

The synthetic aspects and physicochemical as well the structural investigations of newly synthesized complexes are described in fourth chapter. The complexes synthesized in the present work have been studied by a variety of methods (**Scheme V**) and the details of these investigations are elaborated in this chapter. The formation of the organic ammonium tetrathiometalates has been achieved by using different synthetic routes as shown in **Scheme III**. The syntheses of ammonium salts of $[MS_4]^{2-}$ (M = Mo ,W) are known from the days of Berzelius. This method (reaction 1) involves passing a rapid stream of H_2S gas into an aqueous ammoniacal solution of heptamolybdate (in case of Mo) or tungstic acid (in case of W) which results in the formation of well known $(NH_4)_2[MoS_4]$ or $(NH_4)_2[WS_4]$ complexes. This method has been slightly modified in the present work (method A) (reaction 2) and an organic amine has been used instead of ammonia.

$$[Mo_7O_{24}]^{6-} \text{ or } [MO_4]^{2-} + H_2O + NH_3 \xrightarrow{H_2S} (NH_4)_2[MS_4] \qquad \dots 1$$

$$[Mo_7O_{24}]^{6-} \text{ or } [MO_4]^{2-} + \text{organic amine} \xrightarrow{H_2S} \text{organicammonium}[MS_4] \qquad \dots 2$$

$NH_2-CH_2-CH_2-NH_2$

en

$NH_2-CH_2-CH_2-CH_2-NH_2$

1,3-pn

$CH_3-CH(NH_2)-CH_2-NH_2$

1,2-pn

$(CH_3)_2N-(CH_2)_2-N(CH_3)_2$

tmen

$NH_2-(CH_2)_2-NH-(CH_2)_2-NH_2$

Dien

$NH_2-(CH_2)_4-NH_2$

1,4-bn

$N(CH_2-CH_2-NH_2)_3$

tren

$NH_2-(CH_2)_3-NH-(CH_2)_3-NH_2$

dipn

$NH_2-(CH_2)_6-NH_2$

1,6-hn

$NH_2-CH_2-CH_2-NH-CH_3$

N-Meen

$CH_3-NH_2-(CH_2)_3-NH-CH_3$

N-N'-dm-1,3-pn

$NH_2-(CH_2)_2-C(CH_3)_2-NH_2$

2-2-dm-1,3-pn

$NH_2-(CH_2)_2-NH-(CH_2)_2-NH-(CH_2)_2-NH_2$

trien

$CH_3-CH(NH_2)-CH_3$

iso-prNH$_2$

$[Ph-CH_2-N(CH_3)_2-(CH_2)_2-(CH_3)_2N-CH_2-Ph]Br_2.2H_2O$

dbtBr$_2$·2H$_2$O

pip

1, 4-dmpip

dabco

trans(±)1,2-diaminocyclohexane
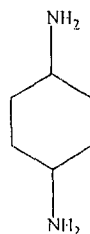
trans 1,4-diaminocyclohexane

NH_2-NH_2

hydrazine

Scheme II

X

H$_2$[MO$_4$]   H$_2$[MO$_4$]

Berzelius Method | Method A

(NH$_4$)$_2$[MS$_4$] — Method B →   Organic ammonium[MS$_4$]
                                         (M = Mo, W)

                                                 | Method C

Method A = Modified Berzelius Method   R$_4$NX
Method B = Base promoted Cation Exchange
Method C = Simple cation exchange

Scheme III

MS$_3$ [R$_4$N]$_2$[MS$_4$]
                                    [Ph$_4$P]$_2$[MS$_4$]

H$^+$ [R$_4$N]$^+$ 2[Ph$_4$P]$^+$

[Zn(en)$_3$]$^{2+}$ [Cu(en)$_2$]$^{2+}$

[Zn(en)$_3$][MS$_4$] ←   (NH$_4$)$_2$[MS$_4$]   → [Cu(en)$_2$][MS$_4$]
                          (M = Mo or W)

                                        Organic amine

[Ni(en)$_3$]$^{2+}$ [Cu(NH$_3$)$_4$]$^{2+}$

[Ni(en)$_3$][MS$_4$]   [Cu(NH$_3$)$_4$][MS$_4$]   Organic ammonium [MS$_4$]

Sheme IV

XI

X-RAY ANALYSIS

IR

ESEM EDAX

RAMAN

$[MX_4]^{2-}$ (M= Mo, W, Cr) (X=S, O)

TG-DTA

UV-VIS

CHEMICAL ANALYSIS

NMR

Scheme V

The organic ammonium tetrathiometalate complexes can also be prepared by base promoted cation exchange method (method B) where in a weak base like NH_3 of $(NH_4)_2[MS_4]$ is replaced by stronger base organic amine. The base promoted cation exchange method can be shown as follows (reaction 3).

$(NH_4)_2[MS_4]$ + organic amine $\longrightarrow$ organicammonium$[MS_4]$ + $2\,NH_3$ …3

The base promoted cation exchange method has been shown to be a convenient as well as general method for the high yield synthesis of organic ammonium tetrathiometalates. $(trenH_2)[MS_4] \cdot H_2O$ (M= Mo, W) (tren is tris(2-aminoethyl)amine) complexes are the first examples of structurally characterized hydrated organic diammonium tetrathiometalates obtained by this method.

Two highly insoluble organic ammonium tetrathiometallate complexes namely (dbt)[MoS$_4$] and (dbt)[WS$_4$] have been synthesized by simple cation exchange method (method C) where in aqueous ammoniacal solution of (NH$_4$)$_2$[MS$_4$] was reacted with aqueous solution dbtB$_2$.2H$_2$O (dbt is N,N'-dibenzyl-N,N,N'N'-tetramethylethylene-diammonium) as shown in below equation 4.

$$(NH_4)_2[MS_4] \ + \ (dbt)Br_2 \cdot 2H_2O \ \longrightarrow \ (dbt)[MS_4] + 2\ NH_4Br + 2\ H_2O \quad \ldots \ 4$$
$$(M = Mo, W)$$
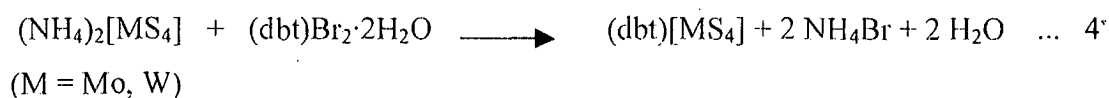
The chemistry of thiometalates has been extended to the corresponding oxochromates and this work has resulted in the isolation of two organicdiammonium oxochromate salts namely ethylenediammonium chromate (enH$_2$)[CrO$_4$] and ethylenediammonium-dichromate (enH$_2$)[Cr$_2$O$_7$] (equation 5 and 6).

$$(NH_4)_2[CrO_4] \ + \ (enH_2)Cl_2 \ \longrightarrow \ (enH_2)[CrO_4] + 2\ NH_4Cl \qquad \ldots \ 5$$

$$(NH_4)_2[Cr_2O_7] \ + \ (enH_2)Cl_2 \ \longrightarrow \ (enH_2)[Cr_2O_7] + 2\ NH_4Cl \qquad \ldots \ 6$$

A combination of UV-Vis, IR, Raman and NMR spectroscopic techniques has been used for the characterisation of new complexes investigated in this work. The UV-Visible spectra of tetrathimolybdate and tetrathiotungstate complexes exhibit characteristic bands due to charge transfer transitions of tetrahedral [MoS$_4$]$^{2-}$ and [WS$_4$]$^{2-}$ moieties respectively. IR and Raman spectra of almost all new complexes synthesised in this work show splitting of M-S vibration. The maximum splitting of Mo-S and W-S bands are observed in the IR spectra of (pipH$_2$)[MoS$_4$] and (pipH$_2$)[WS$_4$] complexes respectively which can be attributed to differing degree of distortion of the [MS$_4$] tetrahedron. The splitting of M-S bands in these complexes is further revealed from the crystal structure determination as evidenced by short and long M-S bond lengths.

The newer organic ammonium tetrathiometalates prepared in this work has also been studied by thermoanalytical techniques. The final residue obtained after thermal decomposition of these complexes was characterized by elemental analysis, X-ray powder pattern and ESEM–EDAX studies. On heating at higher temperatures, organic

ammonium tetrathiometalates decompose to form carbon containing amorphous metal disulfides. Organic ammonium tetrathiotungtates are thermally more stable than the corresponding tetrathiomolybdates as evidenced from the thermal investigation of these complexes.

Several salts of organic ammonium tetrathiomolybdates, tetrathiotungstates and oxochromates have been structurally characterized. The salient structural features of a few structurally characterized tetrathiometalates are described below.

The crystal structures of organic ammonium tetrathiometalate consists of organic ammonium cations which are connected to tetrahedral $[MS_4]^{2-}$ dianions via weak H-bonding interactions (N-H....S). In ethylenediammonium tetrathiotungstate (enH$_2$)[WS$_4$] [42], the W-S bond distances vary from 2.1851(14) to 2.1943(13) Å with S-W-S angles ranging from 108.66(7) to 110.08(6)° indicating small distortion of $[WS_4]^{2-}$ anion (Fig 1). The (enH$_2$)[WS$_4$] is isostructural with the corresponding ethylenediammonium tetrathiomolybdate (enH$_2$)[MoS$_4$] [43]. In 1,3-propanediammonium tetrathiomolybdate (1,3-pnH$_2$)[MoS$_4$] [44], the S-Mo-S angles vary from 108.16(3) and 110.43(3)° with Mo-S bond lengths ranging from 2.1699(8) to 2.1882(7) Å with an average of 2.1815 Å (Fig 2). The N-H...S angles ranging from 128.74 to 162.97° indicate different degree of S...H bond strengths (Fig 3). The W analogue [45] of (1,3-pnH$_2$)[MoS$_4$] shows similar type of structural features (Fig. 4). The crystal structure of N,N,N',N'-tetramethylethylenediammonium tetrathiomolybdate (tmenH$_2$)[MoS$_4$] [44] (Fig. 5 and Fig. 6) and the corresponding W analogue (tmenH$_2$)[WS$_4$] [45] (Fig. 7) consist of (tmenH$_2$)$^{2+}$ dication and $[MS_4]^{2-}$ dianion linked to each other via weak H-bonding interactions (N-H...S) leading to a slight distortion of [MS$_4$] tetrahedron. The elongation of W-S lengths due to H-bonding interactions (N-H...S) has been also observed in crystal structure of 1,4-dimethylpiperazinium tetrathiotungstate (1,4-dmpH$_2$)[WS$_4$] (Fig. 8) [46]

Piperazinium tetrathiomolybdate (pipH$_2$)[MoS$_4$] [47] exhibits interesting structural features as S-Mo-S angles vary from 108.66(3) to 110.04(3)° and Mo-S bond distances ranges from 2.1683(8) to 2.2114(8) Å (Fig. 9). The difference between the longest and the shortest Mo-S bond distances of 0.0431 Å in (pipH$_2$)[MoS$_4$] is very large compared to those observed in known tetrathiomolybdates. The elongation of Mo-S bond distances in (pipH$_2$)[MoS$_4$] can be attributed to the observed short H-

bonding contacts (2.379-2.884 Å) between cation and anion, which result in an extended three-dimensional network as shown in (Fig. 9). Similar structural trends are observed in the corresponding W analogue (pipH₂)[WS₄] [48] (Fig. 10). The crystal structures of hydrated (trenH₂)[MoS₄] H₂O (tren is tris (2-aminoethyl)amine) [47] and (trenH₂)[WS₄] H₂O [48] show two types of H-bonding interactions as shown in (Fig. 11) and (Fig. 12). The two Cr complexes namely (enH₂)[CrO₄] and (enH₂)[Cr₂O₇] has been structurally characterized and shown to exhibit N-H...O interactions [49].

The final chapter summarizes the results of the present work. A few of the important results are as follows:

1. A simple base promoted cation exchange method has been developed for the convenient synthesis of crystalline organic ammonium tetrathiometalates and oxochromates.

2. $[MX_4]^{2-}$ (M= Mo, W, Cr; X= O, S) core is stable in alkaline medium.

3. Acidification of $[MS_4]^{2-}$ core results in the formation of highly insoluble amorphous MS_3 as the ultimate product.

4. The splitting of M-S bands in the IR region of tetrathiometalates has been attributed to different degree of tetrahedral MS_4 distortion.

5. The shift in N-H vibrations to lower frequency in the IR spectra of organic ammonium tetrathiometalates can be attributed to H-bonding interactions.

6. The two complexes viz (trenH₂)[MoS₄] H₂O and (trenH₂)[WS₄]·H₂O are the first examples of structurally reported hydrated organic ammonium tetrathiometalates

7. Both hydrated (trenH₂)[MS₄] H₂O (M=Mo, W) complexes undergo interesting reversible hydration.

8. Tetrathiotungstate complexes are thermally more stable than corresponding tetrathiomolybdates complexes.

9. Elemental analysis of thermolysis products shows considerable amount of carbon content.

10. X-ray powder pattern of thermal product indicates the formation of amorphous metal sulfides.

11. The structure of organic ammonium tetrathiometalates complexes consists of tetrahedral $[MS_4]^{2-}$ (M= Mo or W) dianions which are connected to organic ammonium cations via weak H-bond interactions (N-H---S). The structural

characterization of several $[MS_4]^{2-}$ complexes with different cations indicates the structural flexibility of the tetrahedral $[MS_4]^{2-}$ core.

12. The strength and number of H- bonds affect the M-S bond lengths in $[MS_4]^{2-}$ complexes while Cr-O bond lengths in oxochromates.

13. Piperazinium tetrathiomolybdate and tetrathiotungstate show maximum splitting of M-S band in IR and Raman spectra compared to other complexes indicating the maximum distortion of $[MS_4]$ tetrahedron.

14. The longest Mo-S bond length (2.2114 Å) is observed in $(pipH_2)[MoS_4]$ and longest W-S bond length (2.2147 Å) is observed in $(pipH_2)[WS_4]$ indicating maximum distortion of $[MS_4]$ tetrahedron.

15. $(dbtmen)[MS_4]$ (M=Mo,W) complexes are the first examples of highly insoluble organic ammonium $[MS_4]$ compounds.

16. A convenient method has been developed for the quantitative estimation of $[MS_4]^{2-}$ core in the tetrathiometalates by using $[Ni(en)_3]Cl_2.2H_2O$.

The thesis ends with some recommendations for future work.

Selected References

1. E. I. Stiefel, *Prog. Inorg. Chem.*, **22** (1977) 1.
2. B. Burgess, *Chem. Rev.*, **90** (1990) 1377.
3. E. I. Stiefel, D. Coucouvanis and N. E. Newton, Eds., *Molybdenum Enzymes, Cofactors, and Model Systems; ACS Symposium,* Series 535 (1993).
4. D. Coucouvanis, *Adv. Inorg. Chem.*, **45** (1998) 1.
5. T. Shibhahara, *Coord. Chem. Rev.*, **123** (1993) 73.
6. E. D. Simhon, N. C. Baenziger, M. Kanatzidis, D. Coucouvanis, *J. Am. Chem. Soc.*, **103** (1981) 1218.
7. W. H. Pan, M. A. Harmer, T. R. Halbert, E. I. Stiefel, *J. Am. Chem. Soc.*, **106** (1984) 459
8. M. Draganjac, E. Simhon, L. T. Chan, M. Kanatzidis, N.C. Baenziger, D. Coucouvanis, *Inorg. Chem.*, **21** (1982) 3321.
9. S. A. Cohen, E. I. Stiefel, *Inorg. Chem.* **24** (1985) 4657.
10. W. H. Pan, M. E. Leonowicz, E. I. Stiefel, *Inorg. Chem.*, **22** (1983) 672.
11. A. Müller, E. Diemann, R. Jostes, H. Bögge, *Angew. Chem.*, **93** (1981) 957; *Angew. Chem. Int. Ed. Engl.* **20** (1981) 934 and references therein.
12. B. R. Srinivasan, S. Sarkar, *Inorg. Chem.*, **29** (1990) 3898.
13. J. M. Manoli, C. Potvin, F. Sécheresse, *Inorg. Chem.*, **26** (1987) 340.
14. F. Sécheresse, J. M. Manoli, C. Potvin, *Inorg. Chem.*, **25** (1986) 3967.
15. S. Bhaduri, J. A. Ibers, *Inorg. Chem.*, **25** (1986) 3.
16. A. Müller, E. Diemann, U. Wienböker, H. Bögge, *Inorg. Chem.*, **28** (1989) 4046.
17. F. Sécheresse, J. Lefebvre, J. C. Daran, Y. Jeannin, *Inorg. Chem.*, **21** (1982) 1311.
18. J. J. Berzelius, *Poggendorffs Ann. Phys.Chem.*, **7** (1826) 262.
19. J. J. Berzelius, *Poggendorffs Ann. Phys. Lpz.*, **8** (1826) 277.
20. T. Rauchfuss, *Inorg. Chem.*, **43** (2004) 14 and references cited therein.
21. G. Alonso, G. Berhault, A. Aguilar, V. Collins, C. Ornelas, S. Fuentes, R. R. Chianelli, *J. Catal.*, **208** (2002) 359.
22. I. Bezverkhyy, P. Afanasiev, M. Lacroix, *Mater. Res. Bull.*, **37** (2002) 161.
23. F. Pedraza, S. Fuentes, *Catal. Lett.*, **65** (2000) 107.
24. H. Nava, C. Ornelas, A. Aguilar, G. Berhault, S. Fuentes, G. Alonso, *Catal. Lett.*, **86** (2003) 257.
25. S. H. Laurie, *Eur. J. Inorg. Chem.*, (2000) 2443.
26. G. J. Brewer, R. D. Dick, D. K. Grover, V. LeClaire, M. Tseng, M. Wicha, K. Pienta, B. D.Redman, T. Jahan, V. K. Sondak, M. Strawderman, G. Lecarpentier, S. D. Merajver, *Clinical Cancer Res.*, **6** (2000) 1.
27. G. N. George, I. J. Pickeing, H. H. Harris, J. Galler, D. Klein, J. Lichtmannegger, K. H. Summer, *J. Am. Chem. Soc.*, **125** (2003) 1704.
28. D. E. Schwarz, T. B. Rauchfuss, S. R. Wilson. *Inorg. Chem.*, **42** (2003) 2410.
29. M. G. Kanatzidis, D. Coucouvanis, *Acta Cryst.*, **C39** (1983) 835.
30. J. G. MacDonald, D. N. Harpp, *Tetrahedron Lett.*, **25** (1984) 703.
31. P. Dhar, S. Chandrasekaran, *J. Org. Chem.*, **54** (1989) 2998.
32. A. R. Ramesha, S. Chandrasekaran *Synth. Commun.*, **22** (1992) 3277.
33. S. Sinha, P. Illakumaran, S. Chandrasekaran, *Tetrahedron Lett.*, **65** (1999) 14769.
34. P. Illakumaran, K. R. Prabhu, S. Chandrasekaran, *Synth. Commun.*, **27** (1997) 4031.
35. N. Devan, D. Sureskumar, I. Beadham, K. R. Prabhu, S. Chandrasekaran, *Indian J. Chem.*, **41B** (2002) 2112.
36. J. Ellermeier, C. Näther, W. Bensch, *Acta Cryst.*, **C55** (1999) 501.

37. J. Ellermeier, *Ph.D. thesis, Christian-Albrecht Universität-Kiel*, (March 2002).
38. J. Ellermeier, W. Bensch, *Z. Naturforsch. Teil B.*, **56** (2001) 611.
39. J. Ellermeier, R. Stähler, W. Bensch, *Acta Cryst.*, **C58** (2002) m70.
40. J. Ellermeier, W. Bensch, *Monatsh. Chem.*, **133** (2002) 945.
41. B. R. Srinivasan, S. N. Dhuri and A. R. Naik, *Tetrahedron Lett.*, **45** (2004) 2247.
42. B. R. Srinivasan, S. N. Dhuri, C. Näther, W. Bensch, *Acta Cryst.*, **E58** (2002) m622.
43. B. R. Srinivasan, B. K. Vernekar, K. Nagarajan, *Indian J. Chem.*, **40A** (2001) 563
44. B. R. Srinivasan, S. N. Dhuri, C. Näther, W. Bensch, *Inorg. Chim. Acta.*, **358** (2005) 279.
45. B. R. Srinivasan, S. N. Dhuri, C. Näther, W. Bensch, *Acta Cryst.*, *C* **59** (2003) m124.
46. B. R. Srinivasan, S. N. Dhuri, C.Näther, W. Bensch, *Acta Cryst.*, *E* **59** (2003) m681.
47. B. R. Srinivasan, S. N. Dhuri, M. Poisot, C. Näther, W. Bensch, *Z. Naturforsch.*, **59b** (2004) 1083.
48. B. R. Srinivasan, S. N. Dhuri, M. Poisot, C. Näther, W. Bensch, *Z. Anorg. Allg. Chem* (in press).
49. B. R. Srinivasan, S. N. Dhuri, C. Näther, W. Bensch, *Indian J. Chem.*, **42A** (2003) 2735.
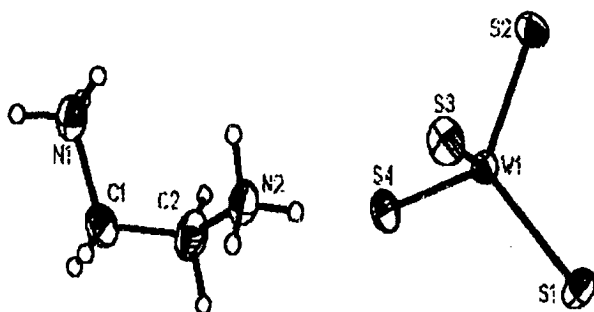
Fig. 1 Crystal structure of (enH₂)[WS₄] with labeling and displacement ellipsoids drawn at the 50% probability level.
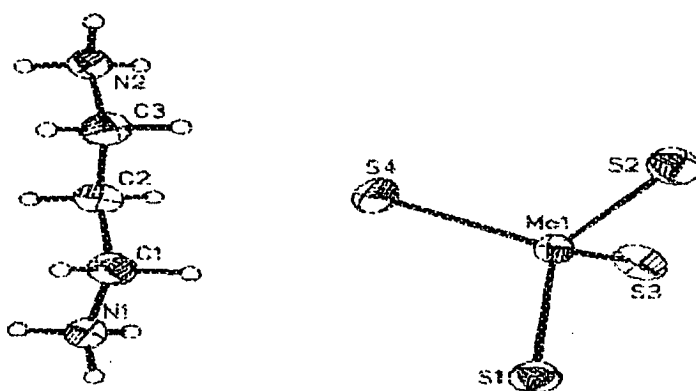
Fig 2. Crystal structure of (13-pnH₂)[MoS₄] with labeling and displacement ellipsoids drawn at the 50% probability level.
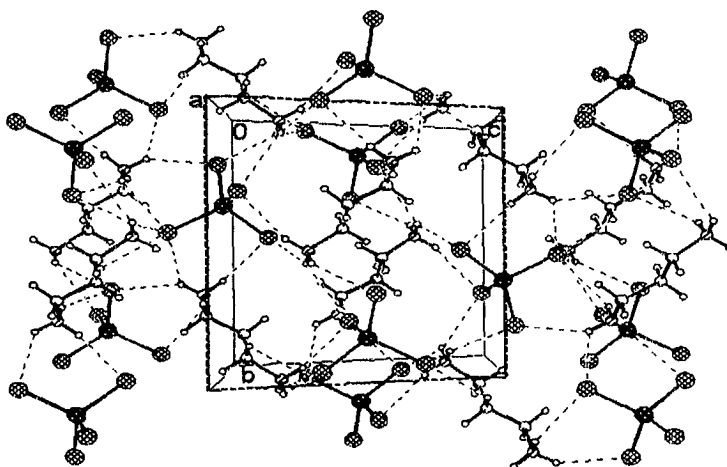
Fig 3. Crystal structure of (1,3-pnH₂)[MoS₄], with view along the a-axis (hydrogen bonding is shown as dashed lines).
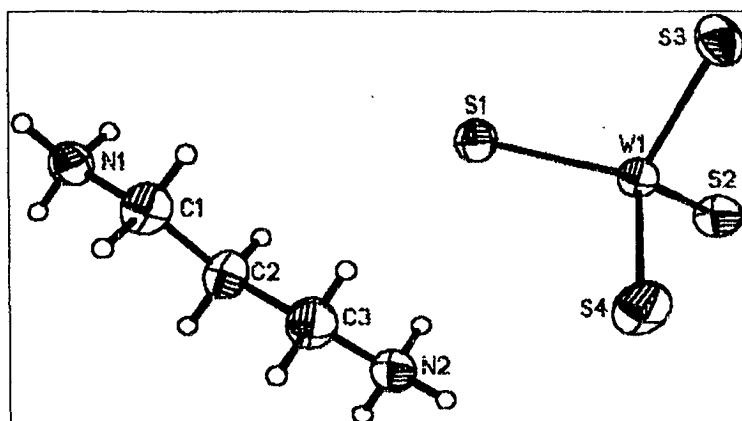
Fig 4. Crystal structure of the anion and cation in $(1,3\text{-pnH}_2)[WS_4]$ with labeling and displacement ellipsoids drawn at the 50% probability level.
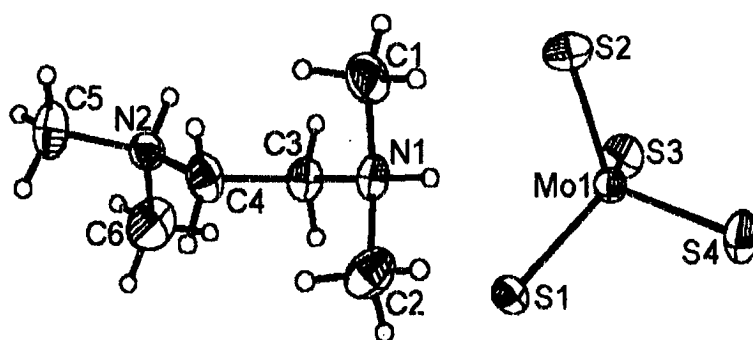
Fig 5. Crystal structure of the anion and cation in $(\text{tmenH}_2)[MoS_4]$, with labeling and displacement ellipsoids drawn at the 50% probability level.
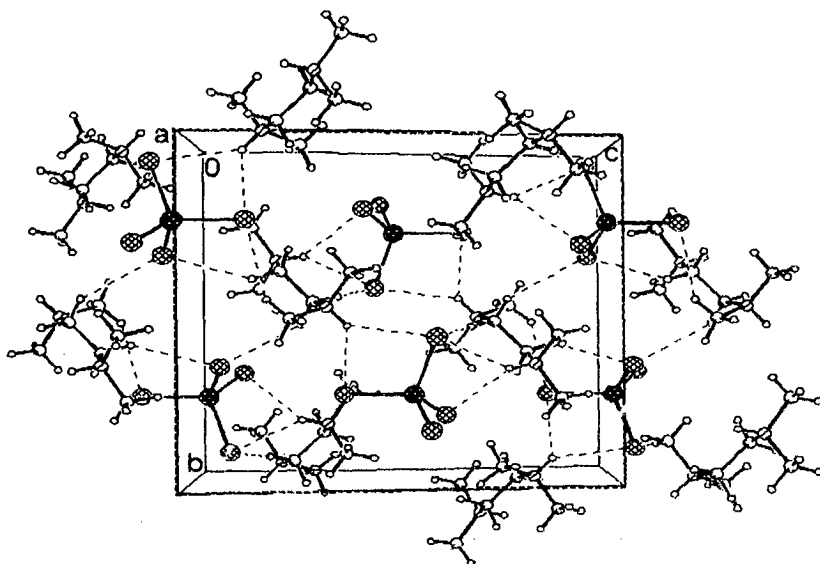
Fig 6 Crystal structure of the anion and cation in (tmenH₂)[MoS₄], with view along the a-axis (hydrogen bonding is shown as dashed lines).
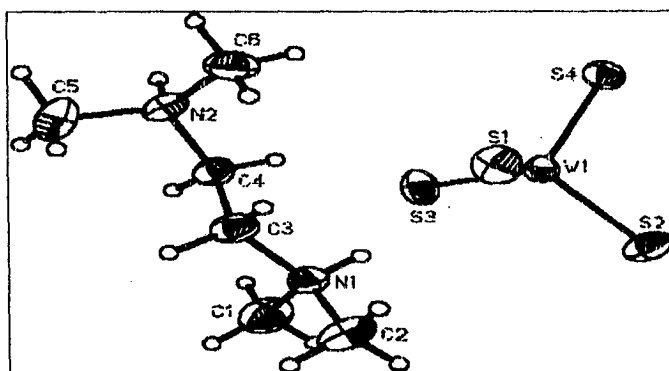
Fig. 7. Crystal structure of the anion and cation in (tmenH₂)[WS₄], with labeling and displacement ellipsoids drawn at the 50% probability level.
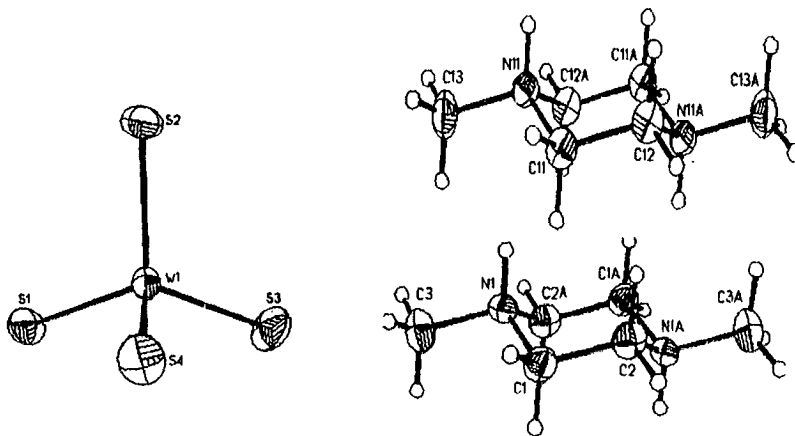
Fig. 8 Crystal structure of the anion and cation in (1,4-dmpH₂)[WS₄], with labeling and displacement ellipsoids drawn at the 50% probability level.
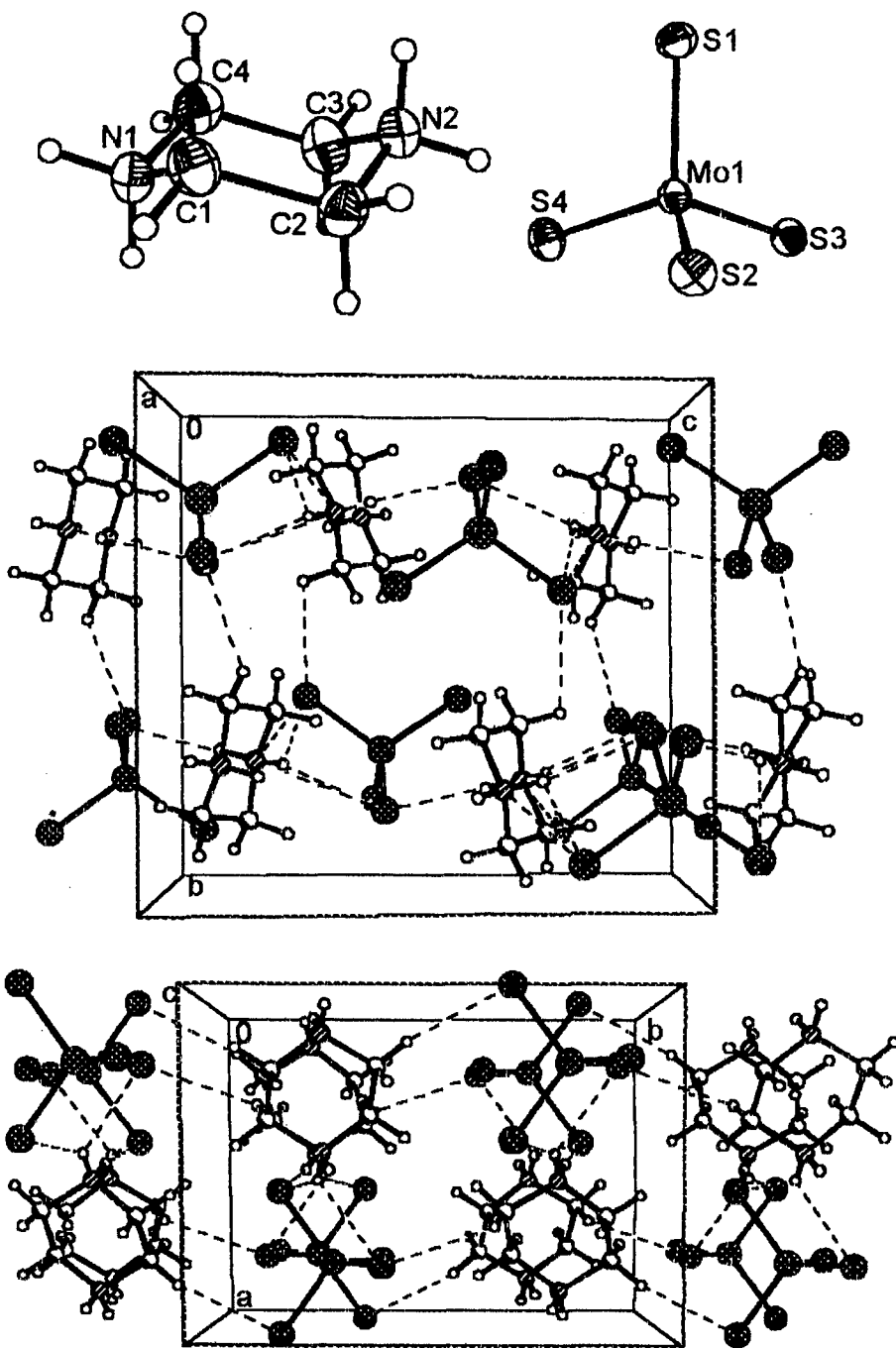
Fig. 9 Crystal structure of (pipH₂)[MoS₄] with labeling and displacement ellipsoids drawn at the 50% probability level (top), with view in the direction of the crystallographic a-axis (middle) and c-axis (bottom) (hydrogen bonding is shown as dashed lines).
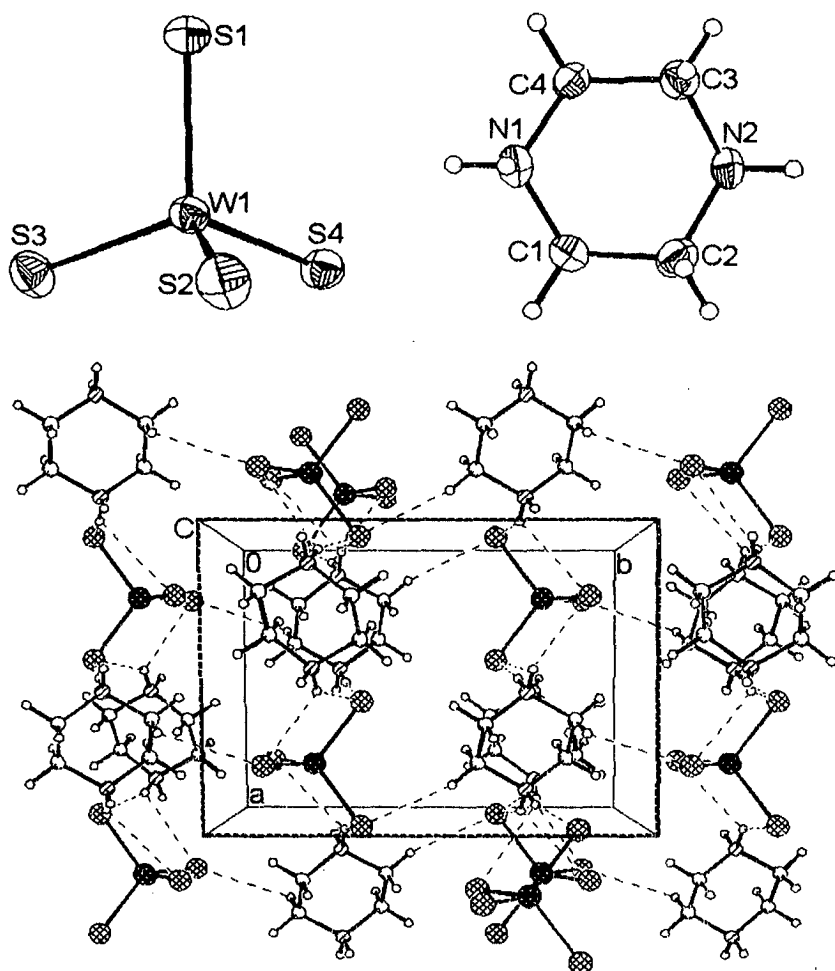
Fig. 10 Crystal structure of (pipH$_2$)[WS$_4$] with view of the [WS$_4$]$^{2-}$ anion (top: left) and the (pipH$_2$)$^{2+}$ cation (top: right) with labeling and displacement ellipsoids drawn at the 50% probability level and of the packing in the direction of the c-axis (bottom) (hydrogen bonding is shown as dashed lines).
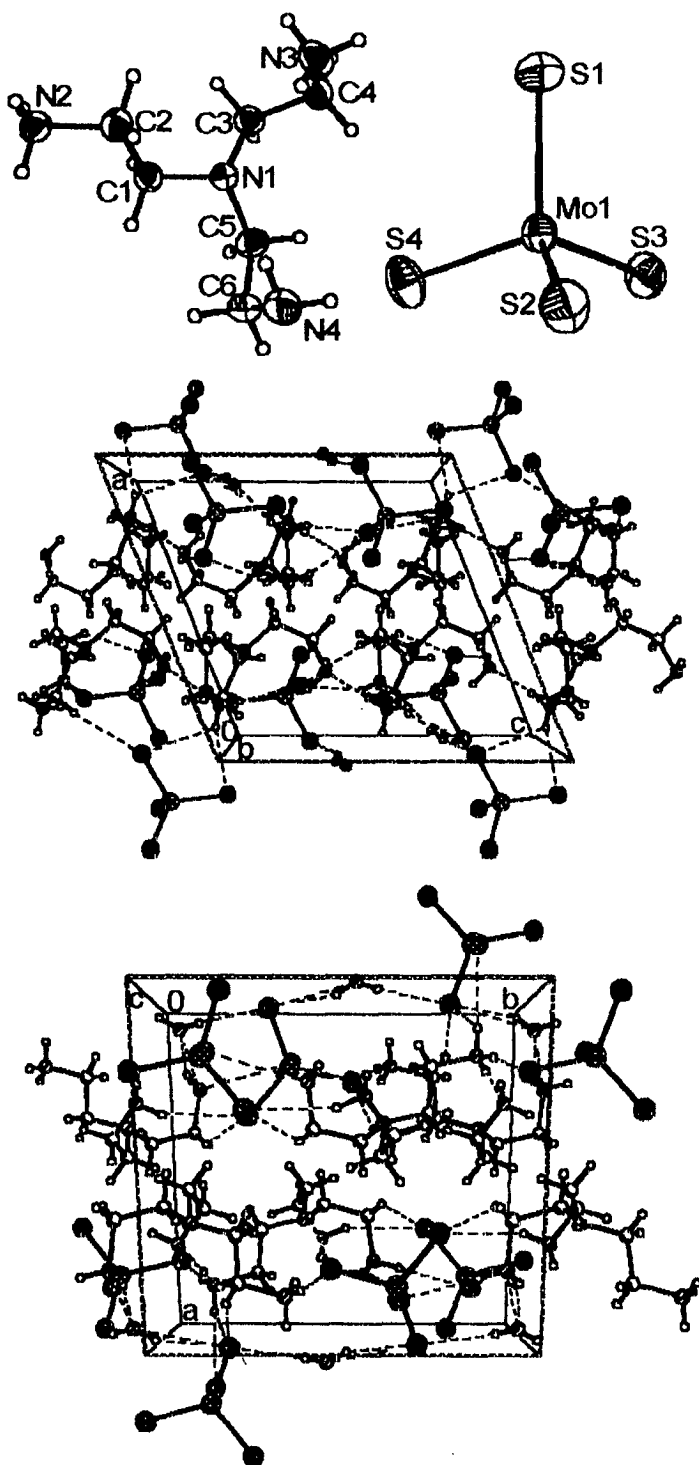
Fig. 11 Crystal structure of (trenH$_2$)[MoS$_4$]·H$_2$O with labeling and displacement ellipsoids drawn at the 50% probability level (top), with view in the direction of the crystallographic a-axis (middle) and c-axis (bottom) (hydrogen bonding is shown as dashed lines).
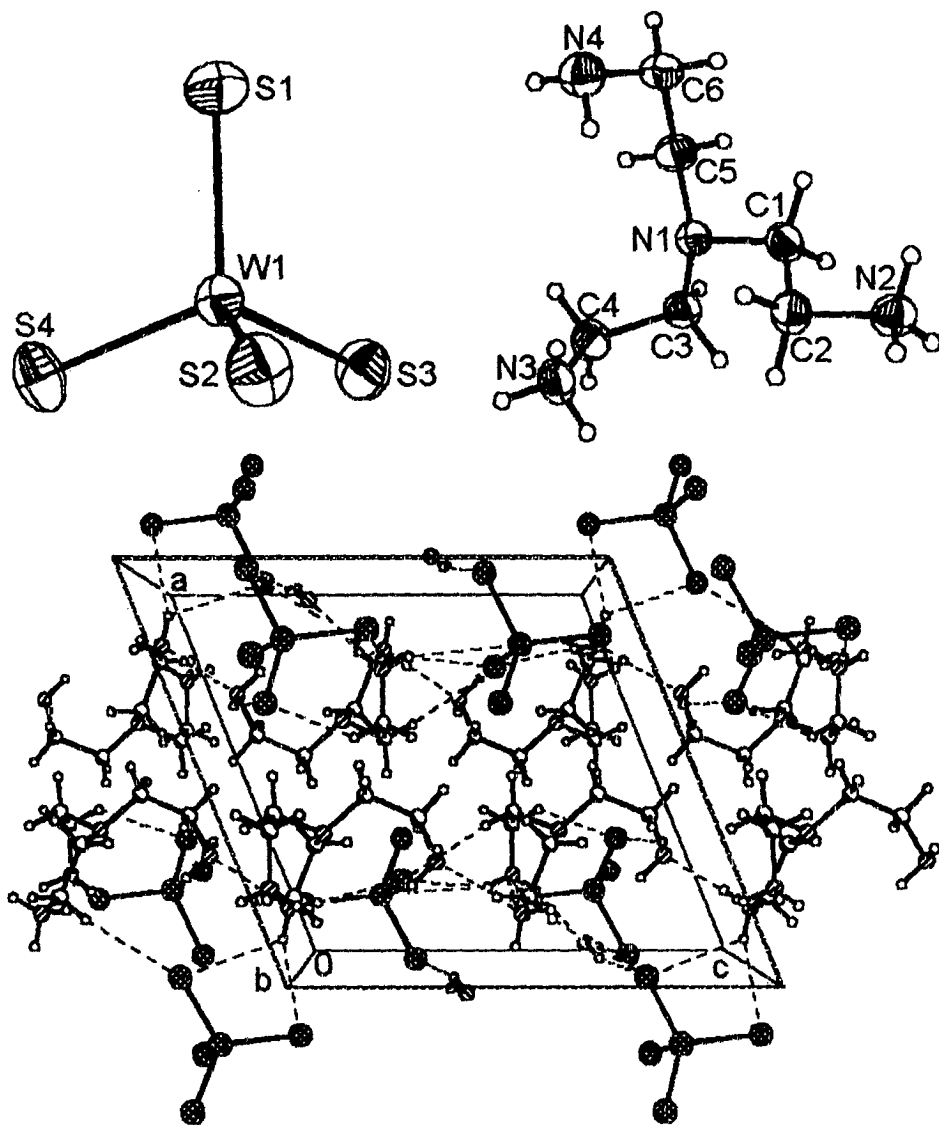
Fig 12. Crystal structure of (trenH$_2$)[WS$_4$]·H$_2$O with view of the [WS$_4$]$^{2-}$ anion (top: left) and the (trenH$_2$)$^{2+}$ cation (top: right) with labeling and displacement ellipsoids drawn at the 50% probability level and of the packing in the direction of the c-axis (bottom) (hydrogen bonding is shown as dashed lines).

CHAPTER 1

INTRODUCTION

The group VI elements especially molybdenum (Mo) and tungsten (W) are essential trace elements for many organisms, including human beings and animals. Both Mo and W exhibit several oxidation states in their compounds in addition to different stereochemistries. Sulfur-ligated molybdenum as well as and its congener tungsten centers are known to exist as active metal sites in variety of enzymes [1-3]. Molybdenum occurs in nature as molybdenite (MoS_2) or wulfenite ($PbMoO_4$). Molybdenum-sulfur compounds are very important in several enzymes, such as xanthine oxidase, sulfite oxidase, aldehyde oxidase, oxidoreductase enzymes etc. The tungstoenzymes have been classified into principal families AOR (aldehyde oxido-reductase) and F(M)DH (formate dehydrogenase, FDH and N-formylmethanofurano dehydrogenase, FMDH) [3]. Iron-molybdenum-sulfur cluster is present as the Fe/Mo cofactor of nitrogenase [4-6], which is responsible for the fixation of nitrogen. Mo occurs in more than thirty enzymes and may be replaced by W or V in some cases. The natural sources of tungsten include wulframite ($FeWO_4$), scheelite ($CaWO_4$) and stolzite ($PbWO_4$). W is the only element in the third transition metal series known to have biological functions and occurs in many enzymes [3]. The chemistry of Mo and W has been described as the most complex of the transition elements [7].

1.1 Focus on applications of group VI metal tri- and dichalcogenides

In recent years, transition metal sulfides are key to many topological challenges in inorganic chemistry, catalysis, energy, environment and materials [8]. The field of catalytically active transition metal sulfides has been reviewed [9-10]. The extensive research on sulfur rich metal complexes has proven to be fruitful with respect to novel structures, development of methods and chemical transformations, including catalytic processes. The role of metal sulfides in biological and industrial catalysis indicates that this area holds tremendous potential for continued theoretical and practical applications. The existence of many metal sulfides of group VI elements

1

has been reported in the literature. Of these only the disulfides [MS_2], trisulfides [MS_3], (M= Mo, W), sesquisulfide Mo_2S_3 and also Mo_2S_5 are well studied. These compounds have potential industrial applications and have been used in industrial settings as catalysts, photovoltaic materials [11], solid-state lubricants [12-13] and cathode materials for high energy density batteries [14] due to their interesting material properties. The solution chemistry of these sulfides is unknown owing to their high insolubility and mainly solid-state studies have been carried out [15]. The metal disulfides MS_2 (M = Mo, W) are particularly useful in the petroleum industry as hydrodesulphurization (HDS) catalysts [16-17] in order to prevent emissions of atmospheric pollutants since sulfur present in crude oil is directly responsible for the production of sulfur oxides by combustion of fuels. They are also central to hydrotreating catalysis, which includes removal of nitrogen (hydrodenitrogenation, HDN), oxygen (hydrodeoxygenation, HDO) and metals (hydrodemetalation, HDM), from petroleum products.

The amorphous trichalcogenides MX_3 (M = Mo, W; X = S, Se) have interesting electrochemical and physical properties. The structure of MX_3 type of sulfides have been established by EXAFS technique and shown to exhibit metal-metal bonds in these compounds [18]. The disulfide MS_2 exhibits two structures. Of these one consists of discrete bridged sulfido groups and the other is a layered structure. In the layered structure of MoS_2, each Mo ion is surrounded by six sulfur anions in a trigonal prismatic arrangement resulting in a sandwich-layered configuration. These layers are held together by weak van der Waals interactions. The anisotropic layered structure property of MoS_2 makes it useful as a host material for intercalated compounds giving rise to interesting conductive properties [16,19]. The active centers of MoS_2-based catalysts are located on the edges of the layers, where sulfur vacancies are formed. Therefore, catalytic activity of bulk or supported MoS_2 depends strongly on its dispersion. In this context a brief review of metal sulfides focusing on their synthesis is presented below.

1.2 Synthesis of molybdenum and tungsten sulfides

A variety of methods have been reported for the syntheses of metal di- or trichalcogenides. The dispersed MoS_2 has been obtained by thermal decomposition of $(NH_4)_2[MoS_4]$ [20]. Over the past few decades considerable efforts have been placed

on the synthesis of different kinds of nanotubes. A particularly significant breakthrough in WS_2 and MoS_2 nanotube synthesis was made by Tenne and co-workers [21, 22] through the gas-phase reaction between MoO_3 or WO_{3-x} and H_2S in a reducing atmosphere at elevated temperatures. Several other methods like metathesis reactions [23] or gas-phase decomposition of $Mo(CO)_6$ in the presence of H_2S [24] are also reported in the literature. The reductive sulfiding of the oxide is usually difficult and does not proceed in a reproducible manner [25]. MoS_2 has been also synthesized from the reactions of $(NH_4)_2[MoS_4]$ with hydroxylamine and hydrazine [26]. A soft aqueous reaction between $(NH_4)_2[MoS_4]$ and hydrazine to give dispersed MoS_2 with high surface area has been also documented [27]. Furthermore, it is reported that multiwall nanotubes of many of the layered metal dichalcogenides could be prepared by the thermal decomposition of the respective ammonium thiometalate precursor [28]. The WS_2 nanotubes have been synthesized on a relatively large scale by thermal decomposition of amorphous/nano $(NH_4)_2[WS_4]$ in a floating hydrogen and thiophene atmosphere at temperature of 360-450 °C [29]. In this report, the amorphous $(NH_4)_2[WS_4]$ precursor has been obtained by ball milling $(NH_4)_2[WS_4]$.

In recent years, the use of tetraalkylammonium tetrathiomolybdates as precursor material for the preparation of MoS_2 catalysts is showing much promise in the field of HDS catalysis [30,31]. The nature of the alkyl group in the precursors has been shown to affect the surface area, pore size distribution as well as HDS selectivity. The thermal decomposition of tetraalkylammonium thiometalates is an interesting alternative method of preparation of highly active MoS_2 and WS_2 catalysts with controlled stoichiometry [32,33]. The modification of the composition of ' precursor thio salts leads to a sharp increase of surface area with the bulkiness of cation, and appearance of sponge-like morphology [34]. The use of tetraalkylammonium thiometalates for the synthesis of carbon containing mesoporous MoS_2 and WS_2 catalysts with high surface area and catalytic activity [35] has added an extra dimension to the field of transition metal chalcogenides. The role of carbon in the formulation of such HDS catalysts is not completely understood, but it is possible that carbon, at least partly, is included in the arrangement of active sites. In a recent report it has been shown that molybdenum carbide has high activity in hydro processing reactions which is produced by carburizing of alumina supported ammonium molybdate in a CH_4/H_2 reactant stream. Mo_2C/Al_2O_3 showed three times

higher activity in HDS process than MoS_2/Al_2O_3 catalyst [36]. The precursor composition is an important factor for the synthesis of highly active MS_2 type of catalysts. The synthesis and HDS activity of heterometallic sulfides like Ni-Mo-S catalysts [37] and Co-Mo-S catalysts [38] both derived from thiomolybdates has been recently reported. In this context, the present work on the *synthesis, reactivity studies and structural aspects of group VI thiometalates* has been undertaken and results of the investigation are presented in this thesis. An overview of the existing literature on the synthesis and reactivity characteristics of tetrathiometalates is presented in the following section of this chapter.

1.3 Tetrathiomolybdates and tetrathiotungstates

In general the term thiometalate is used to refer to any of the sulfur complexes of the early transition elements. In the present work the term tetrathiometalates refers to the $[MS_4]^{2-}$ (M = Mo, W) anions where only two metals Mo, and W of group VI are considered. These tetrahedral anions exhibit interesting chemical properties and occupy a special position in coordination chemistry, as they are unique ligands, which are purely inorganic in nature, and give rise to sulfur bridged multimetallic compounds. The tetrathiometalates of the early transition elements are the simplest soluble metal sulfides and include $[ReS_4]^-$ [39], $[VS_4]^{3-}$ [40], $[MoS_4]^{2-}$ and $[WS_4]^{2-}$. The complexes of other metal such as $K_3[NbX_4]$ and $K_3[TaX_4]$ (X = S, Se) are reported in the literature [41]. The transition metal chalcogenides like $[CrS_4]^{2-}$, $[MnS_4]^-$ are not known. A simple explanation for their non-existence can be given based on the strong oxidizing properties of Cr(VI) and Mn(VII) in these compounds. However the chemistry of $[MoS_4]^{2-}$ and $[WS_4]^{2-}$ is by far the most highly developed area and extensively studied by several researchers. In the beginning of the 19th century, Berzelius investigated the synthesis of the ammonium tetrathiometalates by passing H_2S into an aqueous ammonical solutions of molybdate and tungstate [42,43]. Sixty years later Krüss [44] and Corleis [45] reported the synthesis of ammonium tetrathiomolybdate and ammonium tetrathiotungstate respectively. However, much of the work in this area has been carried out in the last three decades primarily by Müller and coworkers [46,47] since the reported synthesis of $[Ni(MS_4)_2]^{2-}$ (M = Mo, W) complexes [48].

1.4. Synthesis of tetrachalcogenometalates

The tetrathiomolybdates and tetrathiotungstates can be synthesized by a variety of methods, like passing H_2S into an aqueous ammonical solution of oxometalate, oxidative decarbonylation of $M(CO)_6$, or by the direct reaction of alkali metal sulfide Rb_2S_3 with Mo/W in the presence of S_8 etc. All the known methods of reported synthesis are summarized in Table 1.1. All these reactions can be classified and understood, depending upon the type of sulfiding agents such as H_2S, elemental S_8, polysulfides etc used. The details of these methods with an emphasis on their importance in the synthesis of tetrachalcogenometalates are described below.

Table 1.1 Synthesis of tetrathio/selenometalates

Metal source/amine/additional requirements	Chalcogen source	Tetrathio/selenometalate	Ref.
$[MO_4]^{2-}$ + NH_4OH	H_2S	$(NH_4)_2[MS_4]$	42-45 49,50
$(NH_4)VO_3$ + NH_4OH	H_2S	$(NH_4)_3[VS_4]$	51
Re_2O_7 + NH_4OH + $(n-Bu_4N)Cl$	H_2S	$(n-Bu_4N)[ReS_4]$	51
MoO_3 + NH_4OH	H_2Se	$(NH_4)_2[MoSe_4]$	52
$(NH_4)_6[Mo_7O_{24}]\cdot 4H_2O$	H_2Se	$(NH_4)_2[MoSe_4]$	53
WO_3 + NH_4OH	H_2Se	$(NH_4)_2[WSe_4]$	54
$Na_2MoO_4\cdot 2H_2O$+ Et_4NCl + Et_3N	$(dmos)_2Se$	$(Et_4N)_2[MoSe_4]$	55
$(NH_4)_2[WO_4]$ + NH_4OH	$(dmos)_2Se$	$(NH_4)_2[WSe_4]$	55
$W(t-Nbu_2)(t-NHBu_2)$	H_2Se	$(t-BuNH_3)_2[WSe_4]$	53
$M(CO)_6$ + Ph_4PBr	K_2Se_3	$(Ph_4P)_2[MSe_4]$	56-57
$M(CO)_6$ + Ph_4PBr	K_2S	$(Ph_4P)_2[MS_4]$	56
Re_2O_7 + Et_4NCl	$(NH_4)_2S_x$	$(EtN)[ReS_4]$	58
Et_4NCl + CH_3CN	$(NH_4)_2[MS_4]$	$(N_4Et)_2[MS_4]$	59
Et_4NOH + H_2O	$(NH_4)_2[MS_4]$	$(N_4Et)_2[MS_4]$	50
$NaOH$	$(NH_4)_2[MoS_4]$	$Na_2[MoS_4]\cdot 3\cdot 5H_2O$	60
MoO_3 + CH_3OH	K_2S	$K_2[MoS_4]$	61
$CsCl$	$(NH_4)_2[MoS_4]$	$Cs_2[MoS_4]$	62

Metal source/amine/additional requirements	Chalcogen source	Tetrathio/selenometalate	Ref.
$RbI + AgI + en + (NH_4)_2[MoS_4]$	S_8	$Rb_2[MoS_4]$	63
$Rb_2S_3 + W$	S_8	$Rb_2[WS_4]$	64
$V + CH_3OH$	Cs_2S_3	$Cs_2[VS_4]$	65
$VO_2 + Rb_2S_3 + CH_3OH$	Rb_2S_3	$Rb_3[VS_4]$	65
$NiBr_2 + (NH_4)_2[MoS_4] + en$	S_8	$[Ni(en)_3][MoS_4]$	66
$NiBr_2 + (NH_4)_2[WS_4] + en$ (180^0C)	$(NH_4)_2[WS_4]$	$[Ni(en)_3][WS_4]$	67
$NiCl_2·6H_2O + en$ $(130\,^{o}C)$	$(NH_4)_2[WS_4]$	$[Ni(en)_3][WS_4]$	67
$MnCl_2·4H_2O + en$	$(NH_4)_2[MoS_4]$	$[Mn(en)_3][MoS_4]$	67
$MnBr_2 + en$	$(NH_4)_2[MoS_4]$	$[Mn(en)_3][WS_4]$	67
$Co[MoO_4] + tren$	S_8	$[Co_2(tren)_3][MoS_4]_2$	68
$NiCl_2·6H_2O + Na_2[WO_4]·2H_2O + en$	S_8	$[Ni(tren)_2][WS_4]$	69
$Mn[MoO_4] + dien$	S_8	$[Mn(dien)_2][MoS_4]$	70
$Na_2[WO_4] + CTAB$	CH_3CSNH_2	$(CTA)_2[WS_4]$	71
$CTAB$	$(NH_4)_2[MS_4]$	$(CTA)_2[MS_4]$	72, 73
$[MO_4]^{2-} + organic\ amine$	H_2S	organic ammonium$[MS_4]$	74-79
$(Ph_4P)Cl$	$(NH_4)_2[MX_4]$	$(Ph_4P)_2[MX_4]$	80,53
$[(PhCH_2)N(C_2H_5)_3]Cl$	$(NH_4)_2[MoS_4]$	$[(PhCH_2)N(C_2H_5)_3]_2[MoS_4]$	81, 82
Organic amine	$(NH_4)_2[MS_4]$	organic ammonium$[MS_4]$	75, 79, 83-88
$(R_4N)Br + NaOH$	$(NH_4)_2[MS_4]$	$(R_4N)_2[MS_4]$	72,89-90

M = Mo, W; X = S, Se, Et = ethyl, Bu = butyl, R = methyl, ethyl, propyl, butyl, pentyl, hexyl, heptyl and octyl, Ph = phenyl, organic amines used; en = Ethylenediamine, dien = Diethylenetriamine, trien = Triethylenetetramine, tren = tris(2-aminoethyl)amine, 1,4-bn = 1,4-Butanediamine, 1,4-dmp = 1,4-Dimethylpiperazine, pip = Piperazine, 1,3-pn = 1,3-Propanediamine, tmen = N,N,N'N'-tetramethylethylenediamine, Et_2NH = Diethylamine, mipa = Monoisopropylamine, N-Me-en = N-methylethylenediamine, N,N'-dm-1,3-pn = N,N'-dm-1,3-propanediamine ; CTAB = Cetyltrimethylammonium bromide

The tetrachalcogenometalates can be prepared by passing H_2S gas into an ammonical solution of heptamolybdate $[Mo_7O_{24}]^{6-}$ or oxotungstates $[WO_4]^{2-}$ [42-43]. The method was first developed by Berzelius and later has been used by several researchers [44-45, 49-50]. The reaction of an aqueous tetraoxomolybdate $[MoO_4]^{2-}$ or tetraoxotungstate $[WO_4]^{2-}$ with H_2S gas occurs by the stepwise substitution of oxo-ligand by sulfido group forming trioxomonothio $[MoO_3S]^{2-}$, dioxodithio $[MoO_2S_2]^{2-}$, monooxotrithio $[MOS_3]^{2-}$ and the tetrathio $[MS_4]^{2-}$ species. The substitution mechanism of oxo ligands by sulfido ligands in $[MO_4]^{2-}$ is shown in Scheme I.

$$[MO_4]^{2-} \xrightarrow{H_2S} [MO_3S]^{2-} \xrightarrow{H_2S} [MO_2S_2]^{2-} \xrightarrow{H_2S} [MOS_3]^{2-} \xrightarrow{H_2S} [MS_4]^{2-}$$
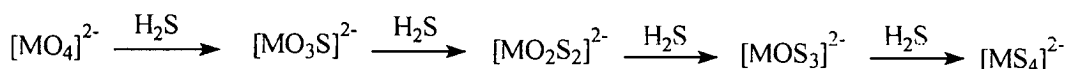
Scheme I

The reaction time with hydrogen sulfide gas, temperature and concentration of counter cations used in the reaction are all important factors to be considered for the preparation and isolation of various thiometalates. The rate of formation of thiometalates depends markedly on the nature of the central metal atom involved. The greater the electron density on oxygen atom, the higher is the rate of formation of thiometalate [91]. The stability of the thiomolybdates decreases with increasing oxygen content. The dioxodithioanion $[MO_2S_2]^{2-}$ and trithioanions $[MOS_3]^{2-}$ have been isolated in good yields by adding appropriate counter cationic species [50]. Recently Holm and coworkers [92], have reported the isolation of the tetrahedral monosulfido species $[MO_3S]^{2-}$ (see 1.1 and 1.2) previously obtained from the aqueous system $[MO_4]^{2-}$ / H_2S. In this report, $[MO_3S]^{2-}$ has been obtained in good yields, by the reaction of $[MO_4]^{2-}$ with $(Ph_3C)(PF_6)/(Et_4N)(SH)$ in acetonitrile. In the same report, the reaction of $(Et_4N)[MoO_3(OSiPh_3)]$ to yield $[MO_3S]^{2-}$ has been mentioned. These reactions serve as new methods for terminal oxo/sulfide conversion.

$$[MoO_3(OSiPh_3)]^- + HS^- \rightarrow [MoO_3S]^{2-} + Ph_3SiOH \qquad (1.1)$$

$$[MO_4]^{2-} + Ph_3C^+ + HS^- \rightarrow [MO_3S]^{2-} + Ph_3COH \qquad (1.2)$$
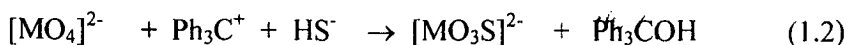
The electronic spectra of the $[MoO_4]^{2-}/H_2S$ reaction system as a function of time is well documented. When hydrogen sulfide gas is passed into an aqueous solution of oxometalate, a change in the electronic spectrum is observed. The characteristic bands of all the species with general formula $[MO_{4-n}S_n]^{2-}$ [n = 1-4] appear in succession. The synthesis of $[MoS_4]^{2-}$ is kinetically more facile since a very short duration (30 min. at 60 ^{0}C) is needed for the reaction. In contrast the preparation of tetrathiotungstate requires drastic reaction conditions, and requires about eight hours of H_2S passing at 60 ^{0}C [50]. In other words practically ammonium tetrathiomolybdate is easier to prepare and even longer reaction times do not have any effect on the product. $(NH_4)_3[VS_4]$ has been synthesized by passing H_2S gas at a moderate rate through an ice-cooled solution of NH_4VO_3 in NH_4OH for 8 h [51]. The use of hydrogen selenide instead of hydrogen sulfide leads to the formation of $[MSe_4]^{2-}$ (M = Mo, W) complexes. A sulfur analogous anion of Se namely $[MOSe_3]^{2-}$ is also reported in the literature [93].

The organic ammonium tetrathiomolybdates can be prepared by the exhaustive hydrogen sulfide treatment of an aqueous molybdic acid solution in the presence of a organic diamine (reaction 1.3). In this method the well-known classical reaction of H_2S with oxomolybdate is modified by using an organic diamine instead of ammonia to afford the corresponding organic ammonium salt. The usefulness of this method can be evidenced by the preparation of several organic ammonium tetrathiomolybdates like $(Et_2NH_2)_2[MoS_4]$ [74], $(enH_2)[MoS_4]$ [75], $(trienH_2)[MoS_4]$, [76] and $(dienH_2)[MoS_4]$ [78], $(piperidinium)_2[MS_4]$ (M = Mo ,W) [78], (1,3-pnH$_2$)[MoS$_4$] and $(tmenH_2)[MoS_4]$ [79].

$$[MO_4]^{2-} + \text{organic amine} \xrightarrow[60\,^0C]{H_2S} \text{organic diammonium}[MS_4] \qquad 1.3$$
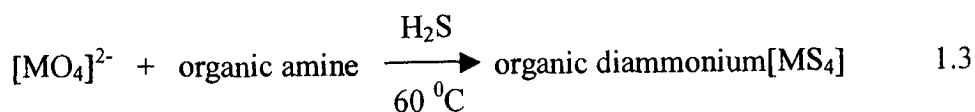
The cation exchange reactions are simple metathesis reactions that can be used for the preparation of organic ammonium as well as alkali metal thiometalates. In this reaction a simple exchange of the cations (ammonium with alkali metal or organic ammonium cation) between two reacting salts under aqueous conditions or some times non-aqueous media takes place. Holm *etal* have reported the synthesis of tetraethylammonium tetrathiometalate $(Et_4N)_2[MS_4]$ by the metathesis reaction between $(NH_4)_2[MS_4]$ and Et_4NCl in CH_3CN [59].

8

$$(NH_4)_2[MS_4] + (Et_4N)Cl \longrightarrow (Et_4N)_2[MS_4] + 2\,NH_4Cl \downarrow \qquad (1.4)$$

A similar reaction between an organic ammonium halide and tetrathiometalate in aqueous medium instead of acetonitrile can be used for the formation of water insoluble complexes such as benzyltriethylammonium tetrathiomolybdate [82-83], and cetyltrimethylammonium tetrathiometalate [73,74]. The tetraphenylphosponium and tetraphenylarsonium thiometalates [80] have been also synthesized under aqueous conditions. The organic tetraselenomolybdate like tetraphenylphosphonium tetraselenomolybdate $(Ph_4P)_2[MoSe_4]$ have been prepared by the reaction between $(Ph_4P)Cl$ and $(NH_4)_2[MoSe_4]$ in aqueous medium [53] (1.5).

$$2\,(Ph_4P)Cl + (NH_4)_2[MoX_4] \longrightarrow (Ph_4P)_2[MoX_4] \downarrow + 2\,NH_4Cl \qquad (1.5)$$
$$(X = S, Se)$$
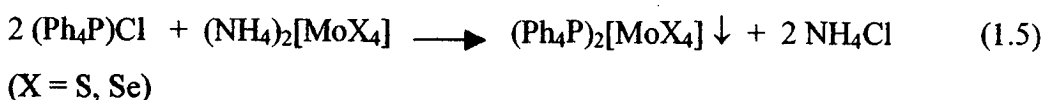
In recent years, solid-state reactions (green chemistry) are being developed for the synthesis of tetrathiometalates with a view to avoid the use of solvents. The reactive flux method which is an effective means of synthesizing metal chalcogenides, has been employed by Ibers and coworkers for the preparation of dirubidium tetrathiotungstate $Rb_2[WS_4]$ [64]. In this reaction solid Rb_2S_3, sulfur and metallic W were heated in a fused-silica tube under Ar atmosphere at high temperature. Such solid state routes are also known for the direct synthesis of $[MX_4]^{3-}$ (M = Nb, Ta; X = S, Se) complexes [41].

The use of solvo-or hydrothermal methods has resulted in the synthesis of a large number of compounds ranging from discrete molecular anions to three-dimensional frameworks. The new compounds obtained by this method exhibit fascinating structural features and interesting physical properties [94-96]. The sulfido complexes of Mo and W like $[Ni(en)_3][MS_4]$, $[Mn(en)_3][MS_4]$ [66,67], $[Co_2(tren)_3][MoS_4]_2$ [68], $[Ni(tren)_2][WS_4]$ [69], $[Mn(dien)_2][MoS_4]$ [70] etc. have been prepared under solvothermal conditions from a reaction mixture of oxometalate/thiometalate, elemental sulfur, amine and a bivalent metal salt under solvothermal conditions. In these compounds H-bonding interaction between the cationic metal amine complex and the thiometalate are observed which stabilize the overall structure. The fully inorganic dirubidium tetrathiomolybdate, $Rb_2[MoS_4]$ [63]

has been prepared in low yields by the reaction of $(NH_4)_2[MoS_4]$, AgI, RbI, elemental sulfur and en under solvothermal conditions.

McDonald *et al* have reported the synthesis of tetraalkylammonium tetrathiometalate $(Et_4N)_2[MS_4]$ by the reaction of an aqueous $(NH_4)_2[MS_4]$ with $(Et_4N)OH$ [50] (1.6). The use of alkali metal hydroxide such as NaOH (in place of $(Et_4N)OH$) with ammonium tetrathiomolybdate to give hydrated $Na_2[MoS_4]\cdot 3.5H_2O$ has been reported in the literature [60] (1.7). Several members of the tetraalkyl group like methyl, propyl, butyl, pentyl, hexyl, heptyl and octyl ammonium tetrathiometalates have been recently reported in the literature by Alonso *et al* [20, 72, 89-90] by slight modification of the procedure employed by McDonald. The synthesis involves the reaction of $(NH_4)_2[MS_4]$ with $(R_4N)X$ (R = alkyl; X = Cl, Br) in the presence of sodium hydroxide. The reaction of NaOH with $(R_4N)X$ generates the strong base $(R_4N)OH$ which then reacts with ammonium tetrathiometalates in aqueous medium as mentioned earlier.

$$2(Et_4N)OH + (NH_4)_2[MS_4] \xrightarrow{H_2O} (Et_4N)_2[MS_4] + 2NH_3 + 2H_2O \qquad (1.6)$$

$$(NH_4)_2[MS_4] + 2\,NaOH \xrightarrow{H_2O} Na_2[MoS_4]\cdot 3.5H_2O + NH_3 + 2H_2O \qquad (1.7)$$

$$(R_4N)X + NaOH \xrightarrow{H_2O} (R_4N)OH + NaCl \qquad (1.8)$$
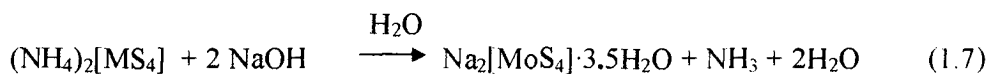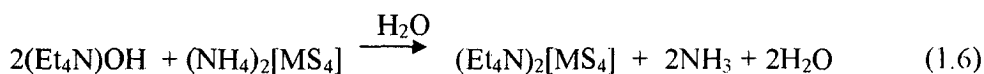
The tetrathiomolybdates and thiotungstates of several organic amines have been synthesized in good yields by the reaction between an aqueous solution of the ammonium salts of $[MoS_4]^{2-}$ or $[WS_4]^{2-}$ and organic amines. In this method the weaker base NH_3 of ammonium tetrathiomolybdate or tetrathiotungstate is replaced by the organic amines, which are stronger bases. This method can be described as a base promoted cation exchange reaction as shown below.

$$(NH_4)_2[MS_4] + \text{organic diamine} \xrightarrow{H_2O} \text{organic diammonium}[MS_4] \qquad (1.9)$$
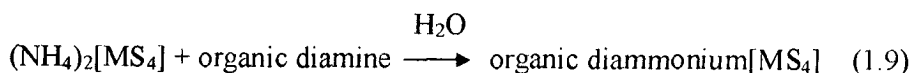
In the present work, the base promoted cation exchange method has been employed for the formation of several organic ammonium tetrathiometalates. The isolation of $(enH_2)[MS_4]$, $(1,3\text{-pnH}_2)[MS_4]$, $(tmenH_2)[MS_4]$, $(pipH_2)[MS_4]$,

(trenH$_2$)[MS$_4$]·H$_2$O, (1,4-dmpH$_2$)[WS$_4$], (1,4-bnH$_2$)[WS$_4$], (N-Me-enH$_2$)[MoS$_4$], (N,N'-dm-1,3-pnH$_2$)[MS$_4$] and (mipaH)$_2$[WS$_4$] accomplished by this reaction have been recently reported in the literature [75, 79, 83-88]. The formation of [MS$_4$]$^{2-}$ complexes under these conditions indicates the stability of the [MS$_4$]$^{2-}$ core in strongly alkaline medium. The formation of several organic ammonium tetrathiometalate by using different organic amines in this method indicates the generality of this reaction.

Kollis and coworkers have reported the synthesis of tetrathiometalates and tetraselenometalates of Mo and W by an oxidative decarbonylation method [56,57]. The high cost as well as toxicity of H$_2$Se has prompted the search of other Se reagents and therefore bis(dimethyloctylsilyl) selenide, (dmos)$_2$Se has been used as a source of Se instead of H$_2$Se for the isolation of tetraselenometalates. However under identical conditions, (dmos)$_2$Se reacts differently with vanadium and a dinuclear V-Se complex ion [V$_2$Se$_{13}$]$^{2-}$ [97] is formed. The tetraethylammonium salt of thioperrhenate [ReS$_4$]$^-$ has been obtained by reacting a methanolic polysufide solution, rather than H$_2$S, with the oxorhenate anion and tetraalkylammonium salt by warming at 45 ^{0}C for a short duration. The violet coloured tetrabutylammonium tetrathioperrhenate has been also isolated under identical reaction conditions.

1.5 Reactivity of tetrathiometalate complexes.

The soluble sulfides of the group VI metals Mo [98] and W [99] are unique as they exhibit unusually wide range of metal-sulfur stoichiometry, metal oxidation states, coordination geometries and different bonding modes of sulfido ligands. In thiometalates, sulfur can bind to a metal in the form of sulfido (S^{2-}), persulfido (S$_2^{2-}$) and tetrasulfido (S$_4^{2-}$) ligands. The structural diversity exhibited by Mo/W-S complexes is evidenced from the structural characterization of a variety of Mo/W-S complexes [100]. This is an important reason for the continuing research in this rapidly growing field. The tetrathiometalates are versatile reagents in inorganic synthesis and the reactivity of these compounds can be attributed to the transfer of electrons across M=S bond, in view of the presence of the metal in its highest oxidation state and the reducing nature of sulfide ligands. The reactions of tetrathiometalates are broadly classified into two categories:

i)   Those resulting in the formation of sulfur-rich polythiometalates and

ii)   Those resulting in the formation of heterometallic complexes.

1.5.1 Formation of sulfur rich polythiometalates

The tetrahedral $[MS_4]^{2-}$ (M = Mo, W) complexes are routinely used as starting materials for the preparation of a variety of structurally diverse di-, tri-, and tetranuclear polythiometalate complexes. The polythiometalates can be formed from the reaction of thiometalates with a variety of sulfur sources, which include a) polysufide b) elemental sulfur c) thiol and d) organic disulfide. The controlled acidification of thiometalates results in the formation of polythiometalates while the use of excess acid leads to the insoluble MS_3 as the final product. A variety of thiomolybdate complexes such as $[MoS(S_4)_2]^{2-}$, $[Mo_2(S)_2(\mu-S)_2(S_2)_2]^{2-}$, $[Mo_2(S)_2(\mu-S)_2(S_4)(S_2)]^{2-}$, $[Mo_2(S)_2(\mu-S)_2(S_4)_2]^{2-}$, $[SMo(MoS_4)_2]^{2-}$ have been synthesized from $[MoS_4]^{2-}$ and can serve as examples, to illustrate the structural diversity encountered in Mo-S chemistry [101-105]. A variety of structurally diverse dinuclear, trinuclear and tetranuclear thiotungstates like $[W_2(S_2)_2(\mu-S)_2(S_4)_2]^{2-}$ [104], $[W_2(S)_2(\mu-S)(\eta^2-S_2)_4]^{2-}$ [106], $[W_2(S)_2(SH)(\mu-\eta^3-S_2)(\eta^2-S_2)_3]^-$ [107], $[W(WS_4)_2]^{2-}$ [108], $[SW(WS_4)_2]^{2-}$, $[W_3S_{10}]^{2-}$ [109], $[(W_2S_4)(WS_4)_2]^{2-}$ [110] etc. with W in various oxidation states are reported in the literature and many of these have been obtained by the controlled acidification of $[WS_4]^{2-}$. All these polythiometalates can be used as good precursors for the synthesis of MS_2 (M = Mo, W) HDS catalysts. The reactions of thiometalate with polysulfides are summarized in Table 1.2.

Table 1.2 Reactions of chalcogenometalate with polysulfide

Metal source	Polysulfide	Final product	Ref.
$(NH_4)_2[MoS_4]$	$(NH_4)_2S_3$	$[MoS_9]^{2-}$	103
$(NH_4)_6[Mo_7O_{24}]$	$(NH_4)_2S_x$	$[Mo_3S_{13}]^{2-}$	111-113
$(NH_4)_6[Mo_7O_{24}]$	$(NH_4)_2S_x$	$[Mo_2S_{12}]^{2-}$	113-115
$(NH_4)_2[MoO_2S_2]$	$(NH_4)_2S_x$	$[Mo_2S_{12}]^{2-}$	113
$(NH_4)_6[Mo_7O_{24}]$	$(NH_4)_2S_x$ with NH_2OH	$[Mo_4(NO)_4S_{13}]^{4-}$	116
$(NH_4)_6[Mo_7O_{24}]$	$(NH_4)_2S_x$	$[Mo_2O_2S_8]^{2-}$	117-118
$[WO_4]^{2-} + SCN^- + H^+$	$(NH_4)_2S_x$	$[W_2O_2S_8]^{2-}$ $[W_2O_2S_{10}]^{2-}$	118-119
$(NH_4)_6[Mo_7O_{24}]$	$(NH_4)_2S_x$ + bpy	$[MoO(S_2)_2(bpy)]$	120
$[WO_4]^{2-} + NH_4(SCN)$ + HCl	$(NH_4)_2S_x$ + bpy	$[WO(S_2)_2(bpy)]$	120
$[VOCl_4]^{2-} + 1/8S_8$	Li_2S + bpy	$[VO(S_2)_2(bpy)]^-$	121
$MoO_3 + (Me_4N)Cl$	Na_2Se_2	$[Mo_3Se_{13}]^{2-}$	122
Re_2O_7	$(NH_4)_2S_3$	$[ReS_9]^-, [Re_2S_{16}]^{4-}$	58,123

The disulfide ligand, like its dioxygen analog, can exhibit terminal or bridged bonding with metals. A significant difference between the sulfur and oxygen ligand lies in the tendency to form polysulfide complexes containing S_x^{2-} units. The formation of polythiometalate depends on three factors namely, the amount of available sulfur, counter cations and the type of solvent employed. Thus the reaction of ammonium trisulfide $(NH_4)_2S_3$ with ammonium tetrathiomolybdate in the presence of tetraalkylammonium chloride leads to the formation of $(Et_4N)_2[Mo^{IV}S(S_4)_2]$. It is clear from this reaction that Mo(VI) gets reduced to Mo(IV) in the presence of polysufides. In addition, the presence of other reactants like NH_2OH or bipyridine can alter the course of the reaction giving unusual products. The addition of 2,2'-bipyridine (bpy) to a reaction mixture containing $[MoO_4]^{2-}$ or $(WO)^{3+}$ and $(S_x)^{2-}$ results in the formation of the discrete mononuclear bis(disulfido) complexes $[MO(S_2)_2(bpy)]$ [M = Mo, W] [120]. The reaction of oxomolybdates with aqueous ammonium polysulfide solution in the presence of hydroxylamine leads to the formation of several interesting polynuclear nitrosyl-molybdenum-sulfido clusters

[100,116,124-125]. [WS$_4$]$^{2-}$ complexes do not react with polysulfides in contrast to [MoS$_4$]$^{2-}$ complexes. The diselenides behave in a similar manner with Mo(VI) and W(VI) complexes. The Mo-Se complex ion [Mo$_3$Se$_{13}$]$^{2-}$ which is an analogue of [Mo$_3$S$_{13}$]$^{2-}$ is reported in the literature [123]. It is prepared by the reaction of sodium diselenide, molybdic acid and tetramethylammonium chloride under hydrothermal conditions. Polysufides are also known to reduce Re(VII) to Re(IV). The reaction of [ReO$_4$]$^{2-}$ with polysulfide gives rise to a variety of products like [ReS$_4$]$^-$, [ReS(S$_4$)$_2$]$^{2-}$, [ReO(S$_4$)$_2$]$^{2-}$, [Re$_2$S$_{16}$]$^{2-}$ etc. under different reaction conditions and counter cations used [58,123]. The reactions of thiometalates with elemental S to give polythiometalates are listed in Table 1.3.

Table 1.3 Reactions of chalcogenometalate with elemental chalcogen

Chalcogenometalate	Chalogen source	Final product	Ref.
(Et$_4$N)$_2$[MoS$_4$]	Sulfur or BzS$_3$Bz	(Et$_4$N)$_2$[MoS$_9$]	101
(Ph$_4$P)$_2$[MoS$_4$]	BzS$_3$Bz	(Ph$_4$P)$_2$[Mo$_2$S$_{10}$]	103
	Bz = benzyl		
(Et$_4$N)$_2$[MoOS$_3$]	S$_8$	(Et$_4$N)$_2$[MoOS$_8$]	103
(Et$_2$NH)$_2$[MoOS$_3$]	S$_8$	(Et$_2$NH)$_2$[MoOS$_8$]	126
(NH$_4$)$_2$[MoS$_4$]	S$_8$ at 95 ^{0}C	(NH$_4$)$_2$[Mo$_2$S$_{12}$]	104
(NH$_4$)$_2$[WS$_4$]	S$_8$ at 110 ^{0}C	(NH$_4$)$_2$[W$_2$S$_{12}$]	104
(Et$_4$N)$_2$[MoS$_4$]	S$_8$	[(S$_2$)OMoS$_2$Mo(O)(S$_3$O$_2$)]$^{2-}$	127
(Ph$_4$P)$_2$[MoSe$_4$]	Se$_8$	(Ph$_4$P)$_2$[MoSe$_9$]	55
(Ph$_4$As)$_2$[WSe$_4$]	Se$_8$	(Ph$_4$As)$_2$[WSe$_9$]	55

1.5.2. Induced electron transfer reactions

The tetrathiometalate anions with fully oxidized, d^0 metal centers and fully reduced sulfide ligands undergo internal induced electron transfer reaction. The reaction of (Et$_4$N)$_2$[MoS$_4$] with sulfur gives the well known complex [MoS$_9$]$^{2-}$ as shown below.

$$(Et_4N)_2[MS4] \quad 5/8\ S_8 \quad \dashrightarrow \quad (Et_4N)_2 \quad \text{[structure]} \quad (1.11)$$
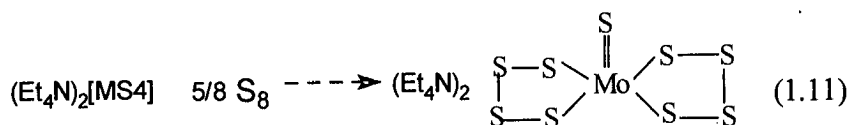
In this reaction, dibenzyl trisulfide (BzS$_3$Bz) can also be used as the source of sulfur. The oxidation of the coordinated (S)$^{2-}$ to (S$_4$)$^{2-}$ and the coupled reduction of Mo(VI) to Mo(IV) are brought about by elemental sulfur in an induced electron transfer pathway, wherein the electron transfer occurs from coordinated (S)$^{2-}$ to the Mo metal center. The attempts to exchange the (Et$_4$N)$^+$ with (Ph$_4$P)$^+$ in (Et$_4$N)$_2$[MoS(S$_4$)$_2$] has resulted in the formation of an altogether different compound (Ph$_4$P)$_2$[Mo$_2$S$_{10}$] [103]. A reaction of the oxotrithiomolybdate complex [MoOS$_3$]$^{2-}$ with sulfur gives [MoO(S$_4$)$_2$]$^{2-}$ complex which is also a hydrolysis product of [MoS(S$_4$)$_2$]$^{2-}$. The heating of ammonium tetrathiomolybdate, elemental sulfur, and tetraethylammonium bromide in DMF affords the dinuclear Mo(V) complex [Mo$_2$S$_{12}$]$^{2-}$ as shown below.

$$2 \ (NH_4)_2[MoS_4] + 5/8 \ S_8 \xrightarrow[2 \ (Et_4N)Br]{DMF, \ 95 \ ^\circ C, \ Ar} (Et_4N)_2[Mo_2S_{12}] + (NH_4)_2S + 2 \ NH_4Br \qquad (1.12)$$
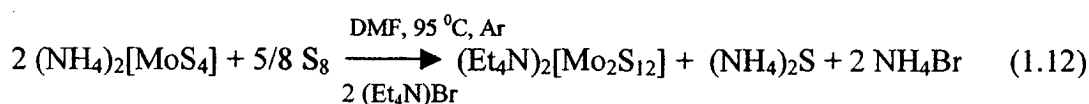
The reaction of ammonium tetrathiotungstate with elemental sulfur at elevated temperatures (110 $^\circ$C) in DMF leads to the formation of the dimeric W(V) complex as shown below.

$$2(NH_4)_2[WS_4] + 5/8 \ S_8 \xrightarrow[2(Et_4N)Br]{110 \ ^\circ C \ DMF} [W_2S_{12}]^{2-} + 2 \ NH_4Br + (NH_4)_2S \qquad (1.13)$$
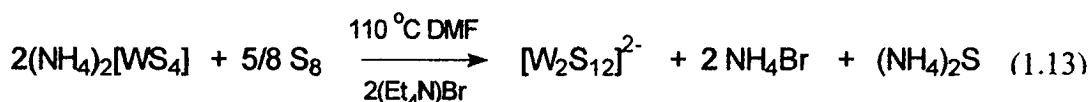
In this reaction, it is essential to note that failure in purging with Ar or N$_2$ results in significantly reduced yields of the dimer and reisolation of the starting material. This is not surprising because (NH$_4$)$_2$S, one of the products of the reaction, can combine with sulfur to form polysulfide which oxidizes the W(V) to W(VI). The above point gets credence from the fact that [WS$_4$]$^{2-}$ does not show any reactivity with polysulfide unlike [MoS$_4$]$^{2-}$. The reaction of ammonium tetrathiomolybdate with organic disulfides in DMF at 90 $^\circ$C results in the dimerisation of the tetrahedral [MoS$_4$]$^{2-}$ moiety with concomitant reduction of Mo(VI) to form [Mo$_2$S$_8$]$^{2-}$ as shown below.

$$2 \ [MoS_4]^{2-} + PhSSPh \ ----\!\!\rightarrow \qquad + \ 2 \ PhS^- \qquad (1.14)$$
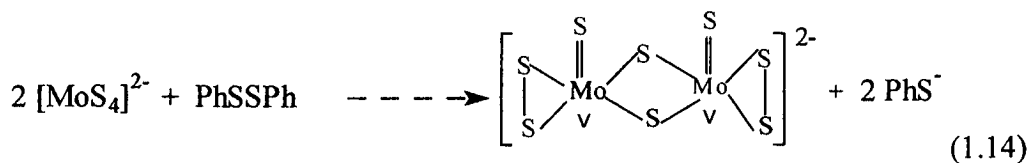
In the above transformation, the organic disulfide is reduced by two electrons while the metal center is reduced by one electron. The conversion of $[MoS_4]^{2-}$ to the dimeric $[Mo_2S_8]^{2-}$ complex can also be effected by the use of diphenyldiselenide at 90 ^{0}C or $[p\text{-}NO_2C_6H_4SSC_6H_4NO_2\text{-}p]$ at room temperature. The tungsten analogue $[W_2O_2(\mu\text{-}S)_2(S_2)_2]^{2-}$ has also been prepared by the oxidation of $(NH_4)_2[WOS_3]$ with elemental iodine [128]. The reaction of tetrathiometalates with tetramethylthiuram disulfides (TMDS) yields dithiocarbamate complexes. The reaction of $[MoS_4]^{2-}$ with TMDS forms an eight coordinate Mo(VI) complex while reaction of $[WS_4]^{2-}$ and $[MoO_2S_2]^{2-}$ with TMDS results in seven coordinate W(VI) and Mo(V) complexes respectively.

A comparison of the reactions of dithiobenzoate disulfide with $[ReS_4]^-$, $[MoS_4]^{2-}$, and $[WS_4]^{2-}$ has been reported. These reactivity studies showed that Re undergoes four-electron reduction, to form $[Re^{III}(S_2CC_6H_5)(S_3CC_6H_5)_2]$ (equation 1.16), Mo undergoes a two-electron reduction to form $[Mo^{IV}(S_2CC_6H_5)_4]$, and W undergoes no reduction at all, forming $[W^{VI}S(S_2)(S_2CC_6H_5)_2]$ by pure ligand redox reaction (Table 1.4).

$$(Et_4N)[Re^{VII}S_4] + 2[C_6H_5CS_2]_2 \longrightarrow [Re^{III}(S_2CC_6H_5)(S_3CC_6H_5)_2] + 2\,S^0 \quad (1.15)$$
$$+ (Et_4N)S_2CC_6H_5$$
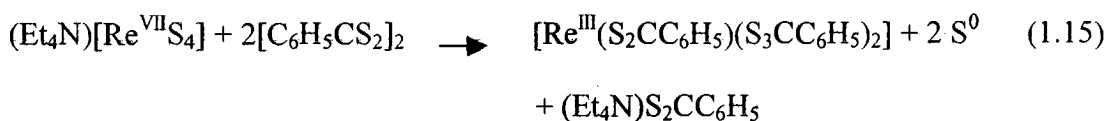
In the reaction of tetrathiometalate with tetraalkylthiuram disulfide, the same trend holds with rhenium undergoing a three-electron reduction to form $Re_2^{IV}(\mu\text{-}S)_2(S_2CNR_2)_4]$ [129b, 129c], molybdenum undergoing a one-electron reduction, to form $[Mo^VS_2((S_2CNR_2)_3]$ [129d] and tungsten undergoing no reduction, forming $[W^{VI}S(S_2)(S_2CNR_2)_2]$ [129d] (Table 1.4). The reaction of $(Et_4N)[Re^{VII}S_4]$ with dialkylxanthogen disulfide $[(ROCS_2)_2]$ results in the formation of $[Re_2^{IV}(\mu\text{-}S)_2(\mu\text{-}S_2)(S_2COR)_3]^-$ [129a].

$$2\,[Re^{VII}S_4]^- + 2\,[ROCS_2]_2 \longrightarrow Re^{IV}_2(\mu\text{-}S)_2(\mu\text{-}S_2)(S_2\text{-}COR)_3]^- + 4\,S + [ROCS_2]^- \quad (1.16)$$
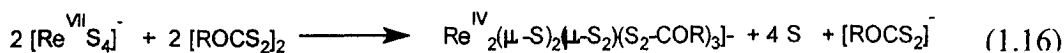
Table 1.4 Reactions between tetrathiometalates and disulfides

$[MS_4]^{n-}$	disulfide	Product	Ref.
$[Re^{VII}S_4]^-$	$(C_6H_5CS_2)_2$	$[Re^{III}(S_2CC_6H_5)(S_3CC_6H_5)_2]$	129a
$[Mo^{VI}S_4]^{2-}$	$(C_6H_5CS_2)_2$	$[Mo^{IV}(S_2CC_6H_5)_4]$	129a
$[W^{VI}S_4]^{2-}$	$(C_6H_5CS_2)_2$	$[W^{VI}S(S_2)(S_2CC_6H_5)_2]$	129a
$[Re^{VII}S_4]^-$	$(S_2CNR_2)_2$	$[Re_2^{IV}(\mu-S)_2(S_2CNR_2)_4]$	129b, 129c
$[Mo^{VI}S_4]^{2-}$	$(S_2CNR_2)_2$	$[Mo^V S_2((S_2CNR_2)_3]$	129d
$[W^{VI}S_4]^{2-}$	$(S_2CNR_2)_2$	$[W^{VI}S(S_2)(S_2CNR_2)_2]$	129d
$[Re^{VII}S_4]^-$	$(ROCS_2)$	$[Re^{IV}_2(\mu-S)_2(\mu-S_2)(S_2COR)_3]^-$	129a
$[W^{VI}S_4]^{2-}$	S_8	$[W^V_2S_2(\mu-S)_2(S_4)_2]^{2-}$	104
$[Mo^{VI}S_4]^{2-}$	S_8	$[Mo^{IV}_2S(S_4)_2]^{2-}$	103
$[Re^{VII}S_4]^-$	S_8	No reaction	129a

The ligand to metal charge transfer (LMCT) energy bands of tetrathiometalates present a possible parameter for correlating the extent of metal reduction in the above induced internal redox reactions. The position of the lowest energy LMCT band (LMCT1) reflects the energy it needs to move an electron from the sulfide to the metal center of tetrathiometalate anion. Looking at $LMCT_1$ band energies, one sees that $[W^{VI}S_4]^{2-}$ has the highest LMCT1 band at 25.5 x 10^3 cm^{-1}, followed by $[Mo^{VI}S_4]^{2-}$ with LMCT1 = 21.4 x 10^3 cm^{-1}, and $[Re^{VII}S_4]^-$ has the lowest LMCT$_1$ band at 19.8 x 10^3 cm^{-1}. As a result, it takes less energy to move an electron from S to Re than from S to W, and the reaction of the three tetrathiometalates with either dithiobenzoate disulfide or tetraalkylthiuram disulfide, leads to Re undergoing the largest reduction, followed by Mo and W, which is not at all reduced. In comparison, the LMCT1 of $[W^{VI}Se_4]^{2-}$, 21.6 x 103 cm^{-1}, is similar to that of $[Mo^{VI}S_4]^{2-}$ [47]. The reaction of $[W^{VI}Se_4]^{2-}$ with $(R_2NCS_2)_2$ is analogous to the

reaction of $[Mo^{VI}S_4]^{2-}$ with $(R_2NCS_2)_2$. Both follow an internal electron transfer pathway to produce $[W^VSe(R_2NCS_2)_3]$ and $[Mo^VS(R_2NCS_2)_3]$ respectively [130].

$$(W^{VI}Se_4)^{2-} + TMDS \ \text{---}\!\!\!\rightarrow\ [W^{VI}(Se_2)(R_2NCS_2)_3] \qquad 1.17$$
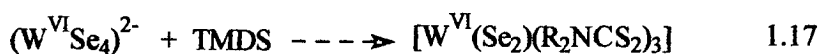
It is to be noted that the tetrathiometalate $[WS_4]^{2-}$ only reacts with S_8 upon heating to form $[W^V{}_2S_2(\mu\text{-}S)_2(S_4)_2]^{2-}$ and $[MoS_4]^{2-}$ reacts with S_8 at room temperature to produce $[Mo^{IV}S(S_4)_2]^{2-}$. However $[ReS_4]^-$ does not react at all with S_8 (Table 1.4). Though the reactions of $[WS_4]^{2-}$ and $[MoS_4]^{2-}$ with S seem to follow LMCT trends, the reaction of $[Re^{VII}S_4]^{2-}$ (with lowest LMCT1 energy band) with sulfur deviates from this pattern. In addition $[Mo^{VI}S_4]^{2-}$ reacts with diphenyl disulfide, $(C_6H_5S)_2$, to produce $[Mo_2S_8]^{2-}$ [129e] (equation 1.14) but $[Re^{VII}S_4]^-$ does not react.

The reaction of $[VS_4]^{2-}$ with TMDS results in the formation of the dinuclear $[V_2{}^{IV}(S_2)_2(R_2dtc)_4]$ [131], while use of dimethyldithiocarbamate $Me_2(dtc)$ and PhS^- instead of TMDS forms trinuclear $[V_3S_7(Me_2dtc)_3]^-$ complex. The reactivity characteristics of thiometalates with thiols have been reported in the literature. In DMF solvent ammonium tetrathiomolybdate reacts with thiophenol under Ar atmosphere at 90 ^{0}C to form the black trinuclear $[Mo_3S_9]^{2-}$ in good yields [105]. The W analogue of $[W_3S_9]^{2-}$ has also been obtained by a similar procedure at slightly higher temperatures.

1.5.2 Formation of heterometallic chalcogenides

Müller and coworkers have studied the ligational behaviour of the thiometalates and synthesized several heteronuclear complexes where the central metal ion can be either a transition metal or a non-transition metal and thiometalate can be any member of the series $(MS_{4-n}O_n)^{2-}$ [M = Mo, W; n = 0-2]. The tetrahedral $[MS_4]^{2-}$ (M = Mo, W) moiety has been used as a starting material for the synthesis of bis(thiometalato)metal complexes. The reaction of bivalent metal salts in the presence of bulky cation with thiometalates in aqueous medium results in the formation of bis(thiometalate) complexes like $[Ni(MS_4)_2]^{2-}$ [48], $[Co(WS_4)_2]^{2-}$ [132], $[Zn(WS_4)_2]^{2-}$ [133] etc. A general reaction for the formation of bis(thiometalato)metal complexes can be written as follows:

$$M'^{2+} + 2(XR_4)^+ + 2[MS_{4-n}O_n]^{2-} \dashrightarrow \left[\begin{array}{c} S \\ S \end{array} M \begin{array}{c} S \\ S \end{array} M' \begin{array}{c} S \\ S \end{array} M \begin{array}{c} S \\ S \end{array} \right]^{2-} \quad 1.18$$
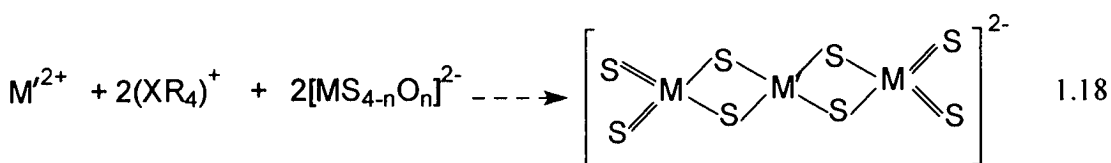
M'= Fe, Co, Ni, Pd, Pt, Zn, Cd, Hg,: M = Mo, W; X = As, P, R= Phenyl; n = 0, 1, 2

The tetrathiotungstate complex of tin namely $[Sn_2(WS_4)_4]^{4-}$ [134] has also been reported in the literature. In this complex, tetrathiotungstate behave like a tridentate ligand unlike bidentate in the above examples. It can also behave like a doubly bridging ligand as in $[Cl_2Fe(MoS_4)FeCl_2]^{2-}$ [126] and $[NH_4CuMoS_4]_n$ [135].

The aqueous reaction of ferrous salts with tetrathiometalate in the presence of tetraphenylphosphonium halide results in the formation of a polymeric species of approximate composition $(Ph_4P)_2[Fe(MS_4)_2]$ [136]. Besides bis(thiometalato)metal complexes, several other heterometallic sulfur complexes which include Ag-M-S [137], Mn/M/S [138], Ni/M/S [37], Cu/M/S [139], Pd/M/S [140] (M = Mo, W) have been reported in the literature. The Mn/M/S complexes $[(bpy)_2Mn(\mu-S)_2MS_2]$ where $[MS_4]^{2-}$ acts as bidentate ligand to Mn (II) have been synthesized from the reaction of aqueous alcoholic solution of $MnCl_2.H_2O$ and bpy with an aqueous solution of $(NH_4)_2[MS_4]$ (M = Mo,W] complex [138]. Recently heterometallic compound containing f-block element namely Ce has been reported [141]. In this report, the synthesis of a Ce-W-S complex $[Ce(dmf)_8]_2[WS_4]_3 \cdot H_2O$ (dmf = dimethylformamide) has been accomplished by the reaction of $(NH_4)_2[WS_4]$ and $CeCl_3.7H_2O$ in DMF. The structure of $[Ce(dmf)_8]_2[WS_4]_3.H_2O$ consists of $[WS_4]^{2-}$ tetrahedral anions and dmf coordinated Ce^{3+} cations with inclusion of water molecules. The synthesis of thioantimonates like $[Ni(dien)_2]_3[SbS_4]_2$, $[Co(tren)_2][Sb_2S_4]$, $[Ni(tren)_2][Sb_2S_4]$ [142] as well as the pure inorganic compound $Cs_3[TaS_4]$ has been also reported [143].

1.6 Biological relevance of thiometalates.

The synthesis and characterization of iron-thiometalate (Fe-M-S) (M =Mo, W) complexes as structural models for the Mo sites of nitrogenase has been the subject of research of many workers. The chemistry of Fe-M-S complexes derived from $[MS_4]^{2-}$ anions has been reviewed by Coucouvanis [144] and Averill [145]. A number of Fe-M-S complexes have been synthesized in recent years as possible models for Mo site of the nitrogenase enzyme. These models can be classified as i) cubane models and ii) linear models. A self-assembly of cubane clusters has been achieved by the reaction of ferric chloride with alkyl or aryl thiolates and tetrathiometalates in alcoholic solvents, which can be written as follows;

$$FeCl_3 \ + \ RS^- \ + \ [MS_4]^{2-} \ \longrightarrow \ \text{double cubane clusters} \qquad (1.19)$$

Linear [Fe-M-S] clusters with various stoichiometries of iron and M (M = Mo, W) have been synthesized and structurally characterized. The synthesis of different types of linear [Fe-M-S] clusters is presented in Scheme II. The novel hexanuclear cluster $[Fe_3(\mu_3-S)_2(WS_4)_3]^{4-}$, having a central $\{Fe_3(\mu_3-S)_2\}$ moiety, is formed from acetonitrile solutions of $[Fe(WS_4)]^{2-}$ in good yields [146]. Zumft and coworkers have reported the isolation of $[MS_4]^{2-}$ by mild hydrolysis of Mo-Fe protein from Clostridium Pasturanium [147].

Ammonium tetrathiomolybdate has been effectively used for the treatment of metastatic cancer [148-149]. Copper is an essential element serving as an important cofactor for more than thirty enzymes, many of which are of key importance, such as superoxide dismutase to combat radical formation, cytochrome c oxidase for cellular respiration, tyrosine oxidase in pigmentation, or lysyloxidase for connective tissue maturation [150]. However, a surplus of copper is toxic and leads to radical formation and oxidation of bio-molecules. Therefore, copper homeostasis is a key requisite for every organism. Thiomolybdates have been demonstrated to be able to remove Cu from the bodies of Cu-poisoned animals [151-153]. The tetrathiomolybdate $[MoS_4]^{2-}$, a good Cu chelator, has been used for the treatment of Wilson disease patients with neurological symptoms [154]. The uptake of tetrathiomolybdate by the liver and removal of copper in the liver of rats has been well documented [155-156].

Tetrathiomolybdate has been extensively used as a specific and selective chelator to remove copper accumulating in the form bound to metallothionein protein in the livers of patients suffering from Wilson disease without disruption of the metabolism of other essential metals such as Zn and Fe [157-158]. Cu–$[MoS_4]^{2-}$ heterometallic systems, in which Cu is flanked by N, S and O donor ligands, may be considered as models for protein–Cu–$[MoS_4]^{2-}$ systems because N, S and O are the potential donor sites in proteins [159]. In this context, the isolation of Cu/Mo/S cluster-containing protein from sulphate reducing bacteria *Desulfovibriogigas* (D. gigas) has been reported [160-162].
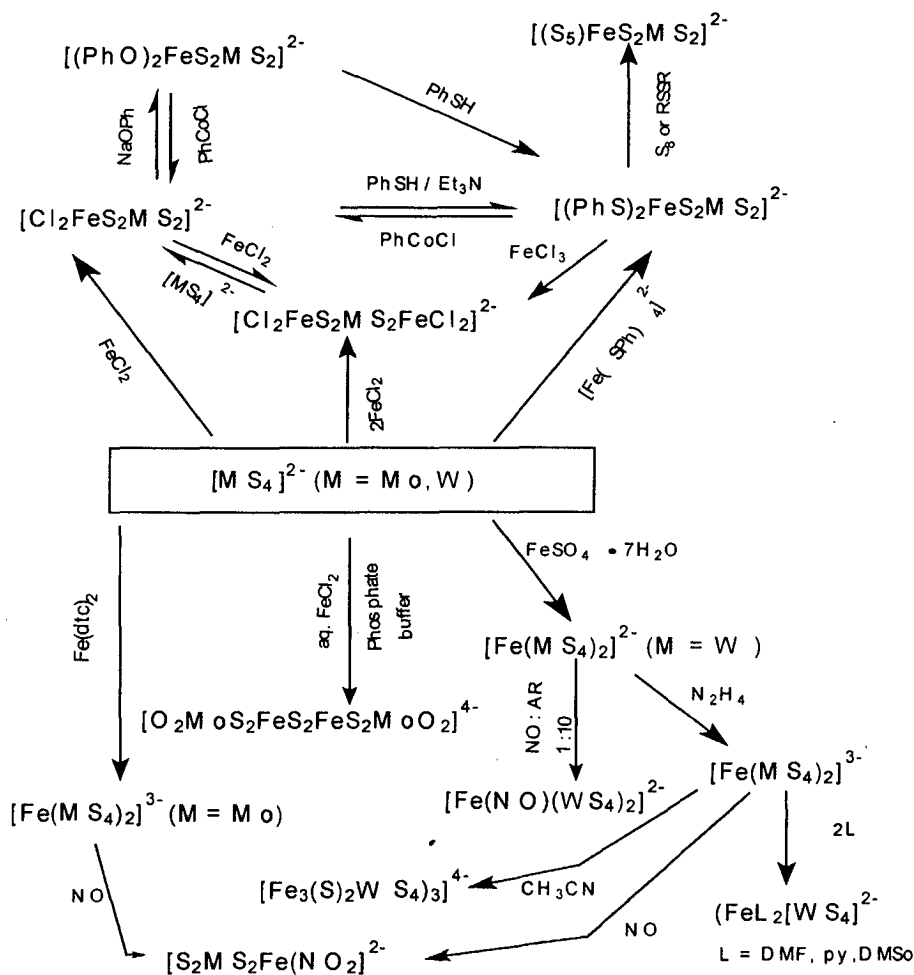
[MS₄]²⁻ THIOANIONS AS LIGANDS IN THE SYNTHESIS OF LINEAR Fe-M-S CLUSTERS

Scheme II

1.7 Thiometalates as sulfur transfer reagents in organic synthesis

The utility of thiometalates have gained importance in recent years in the field of organic synthesis as sulfur transfer reagents. Several Mo-S complexes like diammonium bis(μ-disulfido)tetrakis(disulfido)dimolybdate(V) $(NH_4)_2[Mo_2S_{12}]$, [163], piperidinium tetrathiomolybdate and tetrathiotungstate $(C_5H_{12}N)_2[MS_4]$ (M = Mo ,W) [79b], benzyltriethylammonium tetrathiomolybdate $[(PhCH_2N(C_2H_5)_3]_2$-$[MoS_4]$ [82-83], ammonium tetrathiomolybdate $(NH_4)_2[MoS_4]$ [164-165] have been used as sulfur transfer reagents in organic synthesis, for the preparation of organo-sulfur compounds. All the above-mentioned compounds have been shown to convert alkyl halides to alkyl disulfides. Chandrasekaran and coworkers have pioneered the use of benzyltriethylammonium tetrathiomolybdate in organic synthesis and have demonstrated this complex to be a versatile sulfur transfer reagent for the convenient synthesis of a variety of organic-sulfur compounds under mild reaction conditions [82-83, 166-169]. The alkylation reactions of $[WS_4]^{2-}$ with pyridine derivatives have been recently reported [170]. The utility of thiometalate in organic synthesis as sulfur transfer reagents is presented in Scheme III.
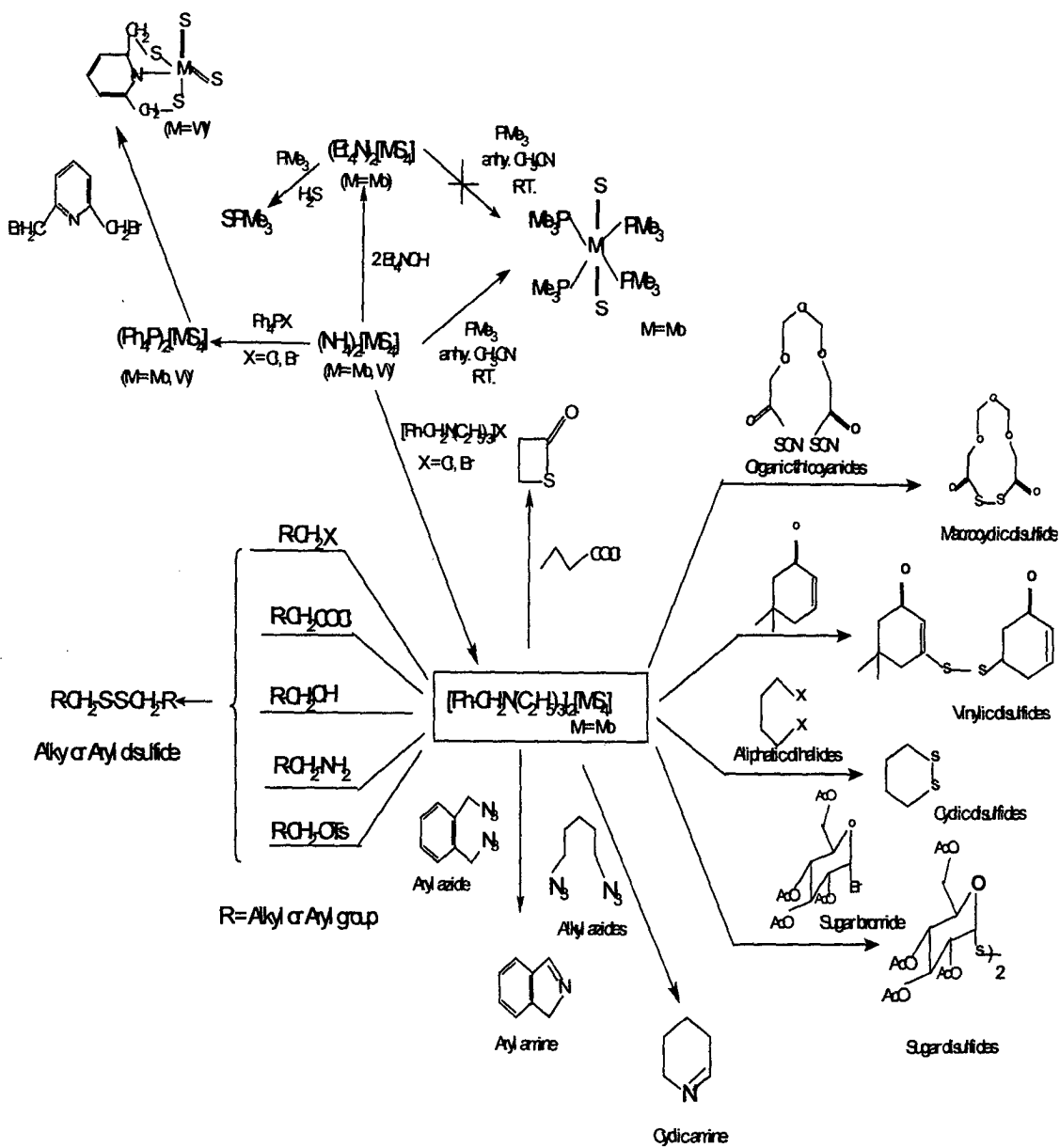
THE UTILITY OF [MS₄]²⁻ THIOANIONS IN ORGANIC SYNTHESIS AS SULFUR TRANSFER REAGENTS

Scheme III

1.8 Characterization of thiometalates

1.8.1 Spectroscopic Investigation

Several physical methods have been reported in the literature for the characterization of complexes containing tetrathiometalate moiety. The useful information on the structure, nature of the chemical bonding and stability of these compounds has been obtained.

i) UV-Visible spectroscopy

The simple tetrathiometalates have characteristic high intensity absorption bands in the UV-Visible region. The first indication of the type of bonding is given by metal-sulfur bond lengths which are significantly shorter than the sum of the ionic or covalent radii and thus suggest a bond order > 1 i.e. the involvement of pi-bonds [171-172]. The Mo-S bond length in $[MoS_4]^{2-}$ or $[MoOS_3]^{2-}$ lies between those for a double and single bonds. The proportion of pi-contribution in the respective metal-sulfur bonds of analogous species increases in the sequence V<Mo<W<Re. It is also appreciably higher compared to the thioanions of main group elements [173]. The electronic spectra of coordinated thiometalates are entirely different from that of the free thiometalates. Various physical measurements have demonstrated that in thiometalato complexes with central metal possessing open d-shells, there are strong metal-ligand interactions. The known complexes of the type $[M'(MS_{4-n}O_n)_2]^{2-}$ (M = Mo, W; M' = Fe, Co, Ni, Pd, Pt) show characteristic absorption bands whose positions are only roughly comparable to those in free thiometalates [47]

ii) Vibrational spectroscopy

The vibrational spectroscopy is a powerful tool for the inorganic chemist, which provides valuable structural information. The free tetrathiometalates have characteristic M=S stretching vibrations ($v_{(M-S)}$ 400-500 cm^{-1}) in their IR and Raman spectra. The vibrational spectroscopic analyses of many thiometalates have been done and the bands are assigned [174,175]. The IR spectra in the lower energy region (400-500 cm^{-1}) can be useful to distinguish, between free and coordinated thiometalates. The proof for the bidentate nature of the thiometalate ligands can be obtained from a simple vibrational analysis. The resonance Raman effect can be used as a sensitive probe for the detection of $[MS_4]^{2-}$ ligands and to make distinction between the

different modes of coordination (for example whether two S atom are bridging or all the four S atoms are bridging) of thiometalates. For the free tetrahedral $[MS_4]^{2-}$ anion, four characteristic vibrations $v_1(A_1)$, $v_2(E)$, $v_3(F_2)$ and $v_4(F)$ are expected. All four vibrations are Raman active while only v_3 and v_4 are IR active. Many tetrathiomolybdates exhibit a single strong band at around 475 cm^{-1} while tetrathiotungstates exhibit a strong signal around 455 cm^{-1} which can be assigned to the triply degenerate asymmetric stretching vibration (v_3) of the M=S bond [47,175].

1.8.2 Structural characterization

X-ray single crystal structures of $(NH_4)_2[MS_4]$ (M = Mo, W) have been reported several years ago and these compounds are shown to be isomorphous with β–K_2SO_4 [172]. The alkali metal tetrathiometalates $A_2[MS_4]$ (A = K, Cs, Rb; M = Mo, W) all of which crystallize in the orthorhombic space group *Pnma* are isostructural to $(NH_4)_2[MS_4]$ (M = Mo, W). The crystal structure of both $(NH_4)_2[MoS_4]$ [176] and $(NH_4)_2[WS_4]$ [177] have been recently reinvestigated considering the importance of H-bonding interactions in these compounds. The H...S contacts in the reinvestigated $[NH_4)_2[MoS_4]$, range from 2.55 to 3.02 Å. The Mo-S bonds are within 0.01 Å of those for $(Et_4N)_2[MoS_4]$ [178]. The Mo-S bond distance in $(NH_4)_2[MoS_4]$ [179] is 2.19 Å which is intermediate between that of a Mo-S single and M= S bond indicating the involvement of pi-bonding.

Several Mo/W-S complexes containing sulfide, disulfide, tetrasulfide bonded to Mo or W in different oxidation states have been structurally characterized, indicating the versatile ligational behaviour of the $(S)_x^{-2}$ (x = 1, 2, 3, 4 etc). The structures of the homometallic complexes $[M_3S_9]^{2-}$ (M = Mo, W) consists of two tetrahedral bidentate $[MoS_4]^{2-}$ units bound to a central square pyramidal $\{MS\}^{2+}$ [103]. Similarly the trimetallic complex $[W_3S_8]^{2-}$ consists of a central W^{2+} bound to $[WS_4]^{2-}$ units one on each side [106]. The central W atom has a square planar coordination of S atoms, while the terminal W atoms have a tetrahedral coordination. In general the M-S$_{term}$ bond lengths are shorter than the M-S$_{br}$ bonds (term is terminal, br is bridging). The Mo-S bond length in the polymeric complex $(NH_4)Cu[MoS_4]$ is 2.19 Å. The structure of this complex consists of a tetrahedral arrangement of S atoms around each Mo and Cu atoms with each tetrahedron sharing two corners with two of its neighbors [180].

The thiomolybdate can be visualized as doubly bridging ligand in this complex. In bis(tetrathiometalato) complexes of the type $[M'(MS_4)_2]^{2-}$, the arrangement of S atoms around the heterometal depends upon the nature of the central metal. When M' = Ni, Pd and Pt, the complexes are square planar whereas the complexes with M' = Co, Zn are tetrahedral. In all these complexes the M-S$_{term}$ bond lengths are shorter than that of the M-S$_{br}$ bond lengths. In the trinuclear complex $[(FeCl_2)_2(MoS_4)]^{2-}$, where the $[MoS_4]^{2-}$ bridges the two FeCl$_2$ units, all the S are bridging sulfurs and the Mo-S bond length is longer at 2.204 Å.

1.9 Oxochromates

Chromium (VI) based reagents are an important class of compounds, which are extensively used in organic syntheses to effect a variety of synthetic transformations [181,182]. The commonly used Cr(VI) reagents are chromium trioxide (CrO_3) in combination with a variety of organic compounds like acetic acid or acetic anhydride or pyridine etc. a mixture of sodium dichromate and concentrated sulphuric acid and pyridinium chlorochromate [183,184]. In the last two decades, chromium (VI) reagents in combination with amines have been widely used for the oxidation of alcohols to the corresponding carbonyl compounds [185]. It has been shown that the nature of the amine determines the oxidizing power of the chromate ion and this is inversely related to the donor strength of the associated amine ligand [185,186]. The two complexes (tmenH$_2$)[Cr$_2$O$_7$] [187] and (pipH$_2$)[CrO$_4$] [188], which contain tetramethylethylenediamine and the cyclic diamine piperazine in their diprotonated form, have been recently introduced as reagents in organic syntheses as mild oxidants.

The $[MO_4]^{n-}$ tetrahedron can be used as an acentric building block to create non-centrosymmetric materials. Based on this strategy, Poeppelmeier [189] and coworkers have reported the synthesis of novel dichromates having formula [M(py)$_4$]Cr$_2$O$_7$ (M=Cu, Zn or Cd). Of these, the Zn and Cu dichromates exhibit interesting structural features like neutral non-intersecting one-dimensional chains of M(py)$_4$Cr$_2$O$_7$ and nonlinear optical properties. Although a number of chromates and dichromates containing inorganic cations have been structurally characterized [191-197], relatively few structures of Cr(VI) compounds containing organic cations have

been determined [198-201]. An important aspect of the reported structures of the organic salts of Cr(VI) compounds is the identification of an extended H-bonding network in these systems. In view of the importance of chromates and dichromates in organic syntheses and also their emerging importance as useful materials, it is desirable to develop new synthetic methodologies for the preparation of such salts and also to determine the three dimensional structures. Hence, the study of Cr(VI) compounds has also been investigated in the present work.

CHAPTER 2

SCOPE OF THE PRESENT WORK

The chemistry of soluble metal sulfide complexes is currently a frontier area of research in view of the relevance of metal sulfide compounds in hydrodesulferization (HDS) catalysis, and the emerging importance of the layered metal disulfides in nanomaterials [8,202,203]. The soluble sulfides of the group VI metals W and Mo [98,99] are a unique class of compounds with a wide range of metal to sulfur stoichiometries, metal oxidation states, coordination geometries and bonding modes of the sulfido ligands. In recent years several extended network systems containing thiometalates have been assembled under solvothermal / hydrothermal conditions. In hydro or solvothermal method, a metal salt, S, an organic amine, an oxometalate / thiometalate are reacted at a high temperature and pressure in aqueous medium (hydrothermal) or in the presence of a structure-directing agent, which is usually an organic amine. These reactions lead to very unusual products, which exhibit novel as well as interesting structural features. Although these reactions are useful for the synthesis of newer oxo or thiometalate materials, one drawback of these reactions is the unpredictability of the final product. In addition, the special equipment needed like Teflon vessel, steel autoclave, controlled temperature oven etc. makes this method more expensive and also beyond the reach of many laboratories. In spite of this, the hydrothermal (or solvothermal) method is slowly emerging as an important synthetic route for the preparation of newer complexes, as phase pure products can be obtained in reasonably good yields. Several oxo as well as thiometalates have been prepared under solvothermal conditions in recent years. It is important to develop synthetic methods for the construction of M-S complexes under ambient conditions.

A primary aim of the present investigation is to develop simple synthetic strategies for the convenient synthesis of newer thiometalates using readily available starting materials. In this context, in our synthetic methodology, chemicals like molybdic acid, ammonia, organic amines, H_2S, water etc. have been used which are readily available. The H_2S use as the sulfiding agent was generated by the reaction of dilute HCl with ferrous sulfide sticks. Several tetrathiometalate $[MS_4]^{2-}$ complexes have been reported in the literature. Of them, many are known to be stabilized by the use of appropriate counter cations like alkali metal or tetraalkylammonium cations. The

structural characterization of a few alkali metal and tetraalkylammonium tetrathio-metalates has been well established.

The reactivity characteristics of $[MS_4]^{2-}$ can be altered by the choice of proper counter cations as explained below. The reactivity characteristics of $[MS_4]^{2-}$ with trimethylphoshine PMe_3 in the presence of simple cations like $(NH_4)^+$ and $(Et_4N)^+$ cations have been reported [176]. Here it has been shown that acetonitrile solutions of $(Et_4N)_2[MoS_4]$ and PMe_3 are stable, while acetonitrile solutions of $(NH_4)_2[MoS_4]$ and PMe_3 react to form the hexacoordinated Mo(IV) complex $[MoS_2(PMe_3)_4]$ indicating the role of proton sources for S transfer. A possible reason for this differing reactivity of $(NH_4)_2[MoS_4]$ and $(Et_4N)_2[MoS_4]$ can be attributed to the short H-bonding contacts between the cation and anion in $(NH_4)_2[MoS_4]$ [176], a structural feature which is absent in $(Et_4N)_2[MoS_4]$ [178]. However $(Et_4N)_2[MoS_4]$ catalyzes the reaction of PMe_3 and H_2S to give $SPMe_3$. In view of the nonreactivity of PMe_3 toward $(Et_4N)_2[MoS_4]$, it can be concluded that the S transfer is initiated by a proton source viz. H_2S with $[MoS_4]^{2-}$.

It has been reported that the chemical properties of $[MoS_4]^{2-}$ can be substantially changed by surrounding it with organic ammonium cations for example cetyltriethyl ammonium [73]. The use of such bulky cation can lead to the formation of highly dispersed MS_2 disulfides. The lamellar bis(cetyltrimethylammonium) tetrathiotungstate has recently been used as a precursor for the formation of bulk quantities of uniform WS_2 nanotubes [71]. In addition, tetrathiomolybdates like $[(PhCH_2)N(C_2H_5)_3]_2[MoS_4]$ [82-83, 166-169] has been extensively used as a sulfur transfer reagent for the synthesis of several organo-sulfur compounds under mild reaction conditions. The above discussions, clearly indicate the importance of organic ammonium thiometalates in material science and also the usefulness of the counter cations to alter the reactivity of $[MS_4]^{2-}$ complexes.

The reactivity of $[MS_4]^{2-}$ towards several organic substrates, such as dibenzyl trisulfide [101], diphenyl disulfide [102], 1,1-dithiolate disulfide, alkyl halides etc. has been investigated. However, the reactions of $MS_4]^{2-}$ with organic amines have not been studied in detail. These investigations are especially important in view of the accessibility of novel metal-sulfide complexes under mild solvothermal conditions using organic amines [129]. In our recent work [79,83-88], we have demonstrated the importance of hydrogen bonding interactions in the lengthening of M-S bond distances in $[MS_4]^{2-}$ by

surrounding it with a variety of organic amines in their protonated form. This clearly indicates that a rich chemistry of thiometalate can be developed by suitably changing the hydrogen bonding interactions between the cation and $[MoS_4]^{2-}$ dianion. These studies can then be useful to derive a structure-function correlation in terms of the M-S bond distances. Thus H-bonding interactions in thiometalates can be fine tuned by a proper choice of the amine, which differs in its bulkiness and also the number of potential H-bonding donors attached to nitrogen atoms. In this context the investigation entitled *"Organic Ammonium Salts of Group VI Oxometalates and Thiometalates: Synthesis, Spectroscopic, Thermal, X-ray Structure and Reactivity Studies"* has been undertaken and the results are discussed in a later chapter. In the present work, a variety of organic amines have been chosen for the reactions with ammonium tetrathiometalate to obtain new cationic tetrathiometalates. The amines used in this work include monoamines like isopropylamine, diamines such ethylenediamine, 1,3-propanediamine, 1,4-butanediamine, etc., triamines like diethylenetriamine, tetraamines like tris(2-aminoethyl)amine, cyclic diamines like piperazine etc. and shown in Scheme IV. The chemistry of tetrathiometalates has been extended for oxochromates.

$NH_2\text{-}CH_2\text{-}CH_2\text{-}NH_2$	$NH_2\text{-}CH_2\text{-}CH_2\text{-}NH\text{-}CH_3$	$(CH_3)_2N\text{-}(CH_2)_2\text{-}N(CH_3)_2$
(en)	(N-Me-en)	(tmen)
$NH_2\text{-}CH_2\text{-}CH_2\text{-}CH_2\text{-}NH_2$	$CH_3\text{-}NH_2\text{-}(CH_2)_3\text{-}NH\text{-}CH_3$	$NH_2\text{-}(CH_2)_4\text{-}NH_2$
(1,3-pn)	(N-N'-dm-1,3-pn)	(1,4-bn)
$[NH_2\text{-}(CH_2)_2]_2NH$	$[NH_2\text{-}(CH_2)_3]_2NH$	$N(CH_2\text{-}CH_2\text{-}NH_2)_3$
(dien)	(dipn)	(tren)

(pip)

(1, 4-dmp)

(dabco)

(trans-1,2-cn)

$CH_3\text{-}CH(NH_2)\text{-}CH_3$

(mipa)

(2-pip-1-EtNH$_2$)

$[Ph\text{-}CH_2\text{-}N(CH_3)_2\text{-}(CH_2)_2\text{-}(CH_3)_2N\text{-}CH_2\text{-}Ph]Br_2.2H_2O$

(dbtmen)Br$_2$·2H$_2$O)
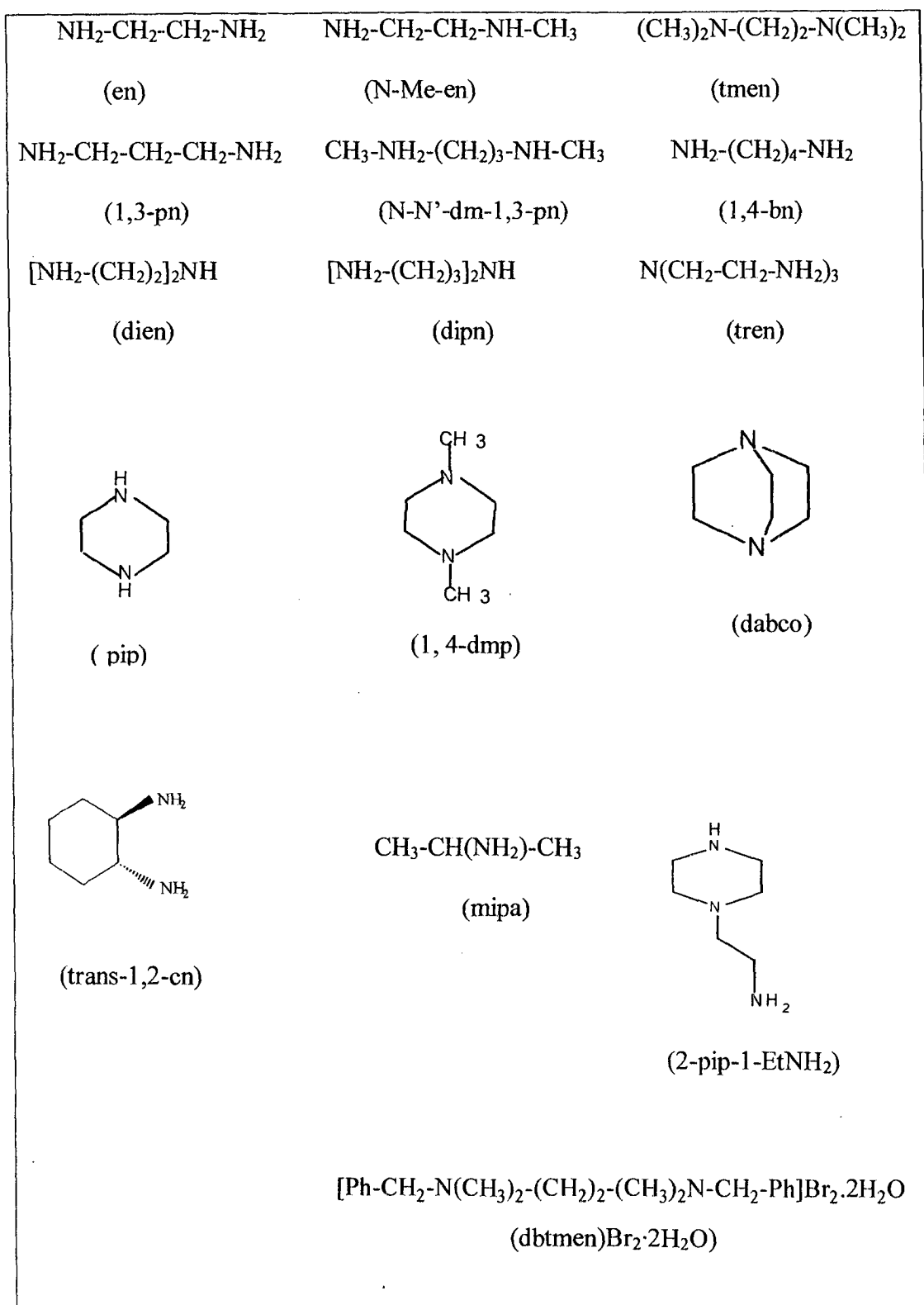
Scheme IV

CHAPTER 3
EXPERIMENTAL DETAILS

3.1 General considerations

Materials and methods

All the reactions were carried out using distilled water as a solvent, unless specified otherwise. All the amines, organic solvents, mineral acids and other chemicals were used in these investigations as obtained from commercial sources. The compounds $(NH_4)_2[MoS_4]$ [50], $(NH_4)_2[WS_4]$ [50], $[(PhCH_2)N(C_2H_5)_2][MoS_4]$ [81,82], $[Ni(en)_3]Cl_2.2H_2O$ [204] were prepared by literature methods. H_2S gas was generated by adding dilute hydrochloric acid into ferrous sulfide sticks (**CAUTION !** H_2S gas, organic amines and other chemicals such as benzyl bromide, mineral acids used in this work have been handled with the appropriate precautions). The pH of the solutions were determined using short-range pH paper as well as electronic pH meter (Model PHAN, Lab India). The mid IR spectra of the samples were recorded on a Shimadzu (model 8101A) (range 400 to 4000 cm^{-1}), IR Prestige-21 Fourier transform (SHIMADZU) (4000-250 cm^{-1}) infrared (IR) spectrometers at Department of Chemistry, Goa University and ATI Mattson Genesis (range 450-3000 cm^{-1}) (resolution 1 cm^{-1}) IR spectrometer at the Institut für Anorganische Chemie, Christian-Albrechts-Universität zu Kiel. The IR spectra of the compounds were recorded in a KBr matrix. The samples were ground with dry KBr into fine powders and pressed into transparent pellets (1 cm dia.). Far-IR spectra (range 80 to 500 cm^{-1}) were measured on a Bruker IFS 66 infrared spectrometer in pressed polyethylene discs. Raman spectra were measured in the region 100-3500 cm^{-1} on a Bruker FRA106 FT Raman spectrometer. ^1H and ^{13}C NMR spectra of the samples were recorded (in DMSO-d_6 or D_2O as solvent) on a Bruker 300 MHz instrument at the National Institute of Oceanography, Dona Paula, Goa and Bruker 400 MHz instrument at the Institut für Anorganische Chemie, Christian-Albrechts-Universität zu Kiel, Germany. In some cases ^{13}C DEPT have been recorded on a Bruker 400 MHz instrument in DMSO-d_6. UV-Visible (electronic) spectra of tetrathiometalates in dilute ammonia and chromates in water were recorded using matched quartz cuvettes on a Varian Cary 5 UV-VIS-NIR equipment and Shimadzu UV-1601

instrument. The C, H, N and S analyses were performed on a HEKA Tech Euro EA elemental analyzer. Thermal decomposition studies were performed in an electric furnace (Newtronic) fitted with a temperature controller in silica crucibles. TG-DTA measurements were performed simultaneously using the STA-409CD device (Netzsch). The thermal investigations were performed in Al_2O_3 crucibles using a heating rate of 4 ^{0}K/min and purged in a N_2 and Ar stream of 75 ml/min. DTA-TG-MS measurements were performed simultaneously using the STA-409CD device (Netzsch) with Skimmer coupling, which was equipped with quadrupole mass spectrometer QMA 400 (max. 512 amu) from Balzers. The MS measurements were performed in analogue and trend scan mode. The investigations were performed in Al_2O_3 crucibles under a dynamic helium atmosphere (flow rate 75 ml/min, purity 4.6) using a heating rate of 4 ^{0}C/min up to 500 ^{0}C. All measurements were corrected for buoyancy and current effects. The instrument was calibrated using standard reference materials. EDX analysis was performed with a Philips ESEM XL 30 scanning electron microscope equipped with an EDAX analyzer. X-ray powder patterns were recorded in transmission geometry using a STOE STADI P diffractometer (CuK_α = 1.54056 Å) at Institut für Anorganische Chemie, Christian-Albrechts-Universität zu Kiel, Germany and on X-ray diffractometer, system APD 2000, Ital Structures (Italy) at Department of Chemistry, Goa University.

3.2 Synthetic Procedures for Tetrathiometalates

3.2.1 Preparation of (NH$_4$)$_2$[MS$_4$] (M = Mo ,W) [50]

i. (NH$_4$)$_2$[MoS$_4$]

Ammonium heptamolybdate (3 g) was dissolved in water (5 ml) and ammonia (25 ml) mixture to obtain a clear solution (pH=12.1). Into this solution a rapid stream of H_2S gas was passed for ~30 min and the temperature was maintained at 60 ^{0}C. After 30-40 min, when deep red crystals were started appearing, the H_2S gas flow was stopped and the reaction mixture was left undisturbed to attain room temperature. The mixture was then cooled in a refrigerator for ~1 h and the crystals separated, were isolated by filtration, washed well with isopropyl alcohol (20 ml) and diethyl ether (20 ml). The compound was stored in a vacuum dessicator. Yield (4.1 g, ~92 % based on Mo). Anal. Found (calc.) for $N_2H_8MoS_4$: (NH$_4$) 13.85 (13.87), Mo 36.70 (36.85), S 49.11 (49.28), MoS$_4$ 85.85 (86.23).

The use of molybdic acid (MoO_3) or sodium molybdate instead of ammonium heptamolybdate under identical conditions also afforded good yield of ammonium tetrathiomolybdate.

ii. $(NH_4)_2[WS_4]$ [50]

Tungstic acid $H_2[WO_4]$ (10 g) was dissolved in water (20 ml) and ammonia (50 ml) mixture to obtain a white slurry (pH = 12.0). Into this solution a continuous and rapid stream of H_2S gas was passed for about 8 h and the temperature of reaction mixture was maintained at 60 °C. After every 1 h, about 5 ml of liquor ammonia was added. After 8 h, the mixture was filtered, and left undisturbed in a refrigerator to obtain yellow blocks of $(NH_4)_2[WS_4]$. The compound was isolated by filtration, washed well with isopropyl alcohol (30 ml) and diethyl ether (20 ml) and dried under vacuum. Yield (6 g). Anal. Found (calc.) for $N_2H_8WS_4$: WS_4 88.99 (89.65) %.

$$[MO_4]^{2-} + H_2O + NH_3 \xrightarrow[60°C]{H_2S} (NH_4)_2[MS_4] \qquad (3.1)$$
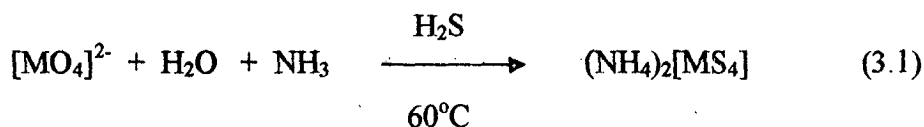
3.2.2 Preparation of $(enH_2)[MoS_4]$ 1 and $(enH_2)[WS_4]$ 2

Method I

MoO_3 (1.44 g, 10 mmol) was dissolved in aqueous ethylenediamine (en) (2 ml of en in 15 ml of H_2O) and stirred for 2 min to obtain a clear solution. Into this mixture a continuous and rapid stream of H_2S gas was passed for 30 min and the temperature of the reaction mixture was maintained at 60°C. After 30-40 min, deep red crystals started appearing in the solution. At this moment, H_2S gas stream was stopped and the reaction mixture left undisturbed to attain room temperature. Further mixture was cooled in a refrigerator for about 1 h to obtain red crystals of 1. The crystals were separated by filtration, washed with ice-cold water (20 ml) followed by isopropyl alcohol (20 ml) and diethyl ether (20 ml) and dried under vacuum. Yield was 2 g (70 % based on Mo). Anal. Found (calc.) for 1 ($C_2H_{10}N_2MoS_4$): C 8.42 (8.39), H 3.48 (3.53), N 9.81(9.78), S 46.16 (44.80), MoS_4 77.33 (78.31) %.

The use of ammonium heptamolybdate (2 g in 20 ml of water and 3 ml en) instead of MoO_3 in the above method afforded the formation of 1 (2.6 g, 80 % based

on Mo). The product obtained in this reaction had an identical IR spectrum and analyzed satisfactorily as the product from method I.
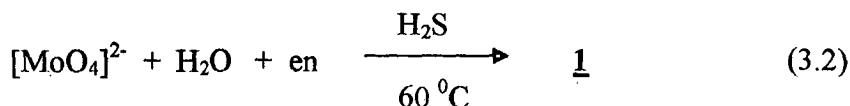
$$[MoO_4]^{2-} + H_2O + en \xrightarrow[60\,^\circ C]{H_2S} \underline{1} \qquad (3.2)$$

Method II

Freshly prepared $(NH_4)_2[MoS_4]$ (260 mg, 1 mmol) was dissolved in 15 ml of distilled water containing few drops of ammonia and then filtered. 1 ml of en was added in drops to the filtrate and left aside in a refrigerator for crystallization. After 1-2 days, red blocks of $\underline{1}$ slowly separated out from the solution. The deep red crystals were isolated by filtration, washed with ice-cold water (10 ml), isopropyl alcohol followed by diethyl ether (10 ml) and dried under vacuum. Yield was 200 mg (70 % based on Mo). The product obtained in this method had an identical IR spectrum and analyzed satisfactorily as the product from method I.

Compound $\underline{2}$ was prepared similarly. The use of $(NH_4)_2[WS_4]$ (348 mg, 1 mmol, in 6 ml water and 0.2 ml en) instead of $(NH_4)_2[MoS_4]$ in the above reaction resulted in the formation of complex $\underline{2}$ (230 mg, 60 % based on W). Anal. Found (calc.) for $\underline{2}$ $(C_2H_{10}N_2WS_4)$: C 6.46 (6.42), H 2.62 (2.70), N 7.38 (7.49), S 34.22 (34.27), % WS_4 82.28 (83.39 %). Both $\underline{1}$ and $\underline{2}$ are fairly stable in air, slightly soluble in water, freely soluble in ammonia, DMSO, DMF and insoluble in CH_3CN, CH_2Cl_2, toluene, alcohol etc.

$$(NH_4)_2[MS_4] + en \longrightarrow \underline{1}\,or\,\underline{2} + 2\,NH_3 \qquad (3.3)$$
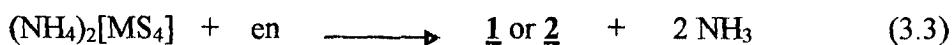
3.2.3 Preparation of (N-Me-enH₂)[MoS₄] $\underline{3}$ and (N-Me-enH₂)[WS₄] $\underline{4}$

Freshly prepared $(NH_4)_2[MoS_4]$ (260 mg, 1 mmol) was dissolved in 15 ml of distilled water and filtered. 0.3 ml of N-methylethylenediamine (N-Me-en) was added to the above solution and the resultant red coloured solution left aside for crystallization. The long red needles of $\underline{3}$ isolated after a day were washed with 5 ml of ice-cold water, isopropyl alcohol (10 ml) followed by diethyl ether (10 ml) and dried under vacuum. Yield was 240 mg (80 % based on Mo). Anal. Found (calc.) for $\underline{3}$ $(C_3H_{12}N_2MoS_4)$: C 9.34 (9.28), H 3.11 (3.12), N 6.88 (7.22), S 35.89 (33.04) %.

The reaction of $(NH_4)_2[WS_4]$ (350 mg, 1 mmol in 10 ml) instead of $(NH_4)_2[MoS_4]$ with 0.3 ml of N-Me-en resulted in the formation of yellow needles of **4** (300 mg, 77 % based on W). Anal. Found (calc.) for **4** $(C_3H_{12}N_2WS_4)$: C 12.09 (11.99), H 4.03 (4.03), N 8.98 (9.332), S 46.16 (42.70) %. The crystals of both **3** and **4** obtained by this method were suitable for X-ray studies, stable in air, slightly soluble in water and freely soluble in ammonia, DMSO, DMF and insoluble in CH_3CN, CH_2Cl_2, toluene, alcohol etc.

$$(NH_4)_2[MS_4] + \text{N-Me-en} \longrightarrow \underline{3} \text{ or } \underline{4} + 2\,NH_3 \qquad (3.3)$$

3.2.4 Preparation of $(tmenH_2)[MoS_4]$ **5** and $(tmenH_2)[WS_4]$ **6**

Method I

Complex **5** was prepared by passing H_2S gas into an aqueous MoO_3 solution (1 g, dissolved in 20 ml of water containing 2.5 ml of N,N,N',N'-tetramethylethylene-diamine, (tmen) for 30 min at 60°C. The mixture was left undisturbed and then cooled in a refrigerator for 1 h. The red needles of **5** were isolated by filtration and washed well with ice-cold water (20 ml), followed by isopropyl alcohol (20 ml) and diethyl ether (20 ml). Yield was 1.54 g (78 % based on Mo). Anal. Found (calc.) for **5** $(C_6H_{18}N_2MoS_4)$: C 21.06 (21.05), H 5.32 (5.31), N 7.99 (8.19), S 37.31 (37.41), MoS_4 65.07 (65.47) %.

$$[MoO_4]^{2-} + H_2O + \text{tmen} \xrightarrow{\text{H}_2\text{S}/60\,^{0}\text{C}} \underline{5} \qquad (3.4)$$
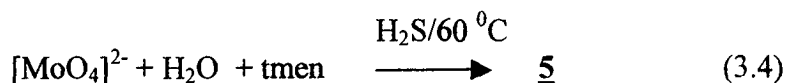
Method II

Freshly prepared $(NH_4)_2[MoS_4]$ (260 mg, 1 mmol) was dissolved in 10 ml of water containing few drops of ammonia and filtered. To the filtrate, tmen (0.5 ml) was added in drops at room temperature. A clear red colored solution was left aside in the refrigerator for crystallization. After 2 days, red blocks of **5** separated out from the solution. Yield was 257 mg (75 % based on Mo). The product obtained had an identical IR spectrum and analysed satisfactorily as the product in method I.

The use of $(NH_4)_2[WS_4]$ (348 mg, 1mmol dissolved in 10 ml of water and 0.4 ml of tmen) instead of $(NH_4)_2[MoS_4]$ in the above reaction afforded yellow blocks of compound **6** in good yields (254 mg, 60 % based on W). Anal. Found (calc.) for **6**

$(C_4H_{16}N_2WS_4)$: C 16.79 (16.74), H 4.15 (4.22), N 6.55 (6.51), S 30.89 (29.80), WS_4 72.59 (72.52) %. Both **5** and **6** are stable in air, slightly soluble in water, freely soluble in ammonia, DMSO, DMF and insoluble in CH_3CN, CH_2Cl_2, toluene, alcohol etc. The crystals obtained by this method were suitable for X-ray studies.

$$(NH_4)_2[MS_4] + tmen \longrightarrow \underline{5} \text{ or } \underline{6} + 2NH_3 \qquad (3.5)$$

3.2.5 Preparation of $(1,3\text{-pnH}_2)[MoS_4]$ $\underline{7}$ and $(1,3\text{-pnH}_2)[WS_4]$ $\underline{8}$

Method I

MoO_3 (1 g) was dissolved in water (20 ml) and 1,3-propanediamine, 1,3-pn (1 ml) mixture to obtain clear solution. A rapid stream of H_2S gas was bubbled through the solution for about 30 min and the temperature of the reaction mixture was maintained at 60 ^{0}C. After 30 min, when red needles of compound $\underline{7}$ started appearing in the solution, H_2S gas flow was stopped, the mixture was left undisturbed to attain room temperature and cooled in a refrigerator. The deep red crystals of $\underline{7}$ were isolated by filtration, washed with cold distilled water (20 ml), isopropyl alcohol (20 ml) followed by diethyl ether (20 ml) and dried under vacuum. Yield was 1.64 g (78 % based on Mo). Anal. Found (calc.) for $C_3H_{12}N_2MoS_4$: C 12.08 (12.00), H 4.09 (4.04), N 8.89 (9.34), S 42.62 (42.66), MoS_4 74.59 (74.64) %.

$$MoO_3 + H_2O + 1,3\text{-pn} \xrightarrow[60^{\circ}C]{H_2S} \underline{7} \qquad (3.6)$$
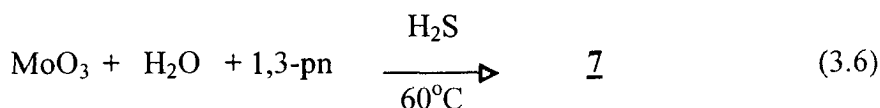
Method II

Freshly prepared ammonium tetrathiomolybdate $(NH_4)_2[MoS_4]$ (520 mg, 2 mmol) was dissolved in 15 ml of distilled water containing few drops of ammonia and then filtered. Into this red coloured solution, 1,3-pn (0.4 ml) was added in drops at room temperature and the mixture left undisturbed in a refrigerator for crystallization. After 2 days well-formed deep red blocks of $\underline{7}$ slowly separated from the solution. Yield was 550 mg (90 %). The product obtained in this method had an identical IR spectrum and analysed satisfactorily as the product from method I.

The use of $(NH_4)_2[WS_4]$ (348 mg, 1 mmol dissolved in 10 ml H_2O and 0.3 ml of 1,3-pn) instead of $(NH_4)_2[MoS_4]$ afforded orange-yellow blocks of $\underline{8}$ in good yields (254 mg, 60 % based on W). Anal. Found (calc.) for $\underline{8}$ $C_3H_{12}N_2WS_4$: C 9.29

(9.29), H 3.20 (3.12), N 7.16 (7.22), S 32.82 (33.04), WS$_4$ 79.83 (80.38) %. The red and yellow crystals of 7 and 8 respectively obtained by this method were suitable for X-ray studies. Both **7** and **8** are stable in air, slightly soluble in water, freely soluble in ammonia, DMSO, DMF and insoluble in CH$_3$CN, CH$_2$Cl$_2$, toluene, alcohol etc.

$$(NH_4)_2[MS_4] \quad + 1,3\text{-pn} \quad \longrightarrow \quad \underline{7} \text{ or } \underline{8} \quad + 2\,NH_3 \qquad (3.7)$$

3.2.6 Preparation of (N,N'-dm-1,3-pnH$_2$)[MoS$_4$] $\underline{9}$ and (N,N'-dm-1,3-pnH$_2$)[WS$_4$] $\underline{10}$

Freshly prepared (NH$_4$)$_2$[MoS$_4$] (260 mg, 1 mmol) was dissolved in 15 ml of distilled water and then filtered. To this clear solution, 0.3 ml of N,N'-dimethyl-1,3-propanediamine (N,N'-dm-1,3-pn) was added in drops at room temperature and left undisturbed for crystallization. After a day, well-formed red needles of $\underline{9}$ were obtained. The crystals were isolated by filtration, washed with ice-cold water (5 ml), isopropyl alcohol (10 ml) followed by diethyl ether (10 ml) and dried under vacuum. Yield (290 mg, 88 % based on Mo). Anal. Found (calc.) for C$_5$H$_{16}$N$_2$MoS$_4$: C 18.49 (18.28), H 4.91 (4.92), N 8.46 (8.53), S 39.19 (39.06) %.

Complex **10** was synthesized by using (NH$_4$)$_2$[WS$_4$] (175 mg, 0.5 mmol dissolved in 10 ml of water and 0.3 ml of N,N'-dm-1,3-pn instead of (NH$_4$)$_2$[MoS$_4$] in the above method in good yields (185 mg, 88 % based on W). Anal. Found (calc.) for **10** (C$_5$H$_{16}$N$_2$WS$_4$): C 14.53 (14.42), H 3.85 (3.88), N 6.33 (6.73), S 33.64 (30.96) %. Both **9** and **10** are stable in air, slightly soluble in water, freely soluble in ammonia, DMSO, DMF and insoluble in CH$_3$CN, CH$_2$Cl$_2$, toluene, alcohol etc. The crystals obtained by this method were suitable for single crystal structure determination.

$$(NH_4)_2[MS_4] \quad + N,N'\text{-dm-1,3-pn} \quad \longrightarrow \quad \underline{9} \text{ or } \underline{10} \quad + 2\,NH_3 \qquad (3.8)$$
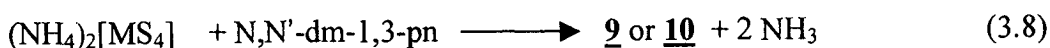
3.2.7 Preparation of (1,4-bnH$_2$)[MoS$_4$] $\underline{11}$ and (1,4-bnH$_2$)[WS$_4$] $\underline{12}$

Method I

MoO$_3$ (1 g) was dissolved in mixture of water (10 ml) and 1,4-butanediamine (14-bn) (2 ml) to obtain a clear solution. A continuous and rapid stream of H$_2$S gas was passed into this solution for 30 min and the temperature was maintained at 60°C.

After 30-40 min when red crystals started appearing in the solution, flow of H_2S gas stopped and the mixture was left undisturbed to attain room temperature. The deep red crystals of **11** were isolated after keeping the above mixture in refrigerator for about 1 h. The compound was filtered, washed with ice-cold water (5 ml), isopropyl alcohol (20 ml) followed by diethyl ether (20 ml) and dried under vacuum. Yield was 1.4 g (64 % based on Mo). Anal. Found (calc.) for **11** ($C_4H_{14}N_2MoS_4$): C 15.32 (15.28), H 4.55 (4.50), N 8.86 (8.91), S 41.63 (40.80), MoS_4 70.67 (71.31) %. The crystals obtained in this method were used of X-ray analysis.

$$MoO_3 + H_2O + 1,4\text{-bn} \xrightarrow[60\,^{0}C]{H_2S} \underline{\textbf{11}} \qquad (3.9)$$
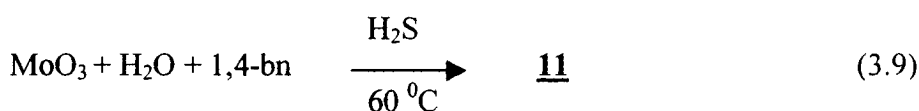
Method II

Freshly prepared $(NH_4)_2[MoS_4]$ (260 mg, 1 mmol) was dissolved in distilled water (15 ml) containing few drops of ammonia and then filtered. Into this red coloured solution, 1,4-bn (0.5 ml) was added in drops at room temperature. The reaction mixture was left undisturbed in a refrigerator. After 2 days, well-formed red blocks of **11** slowly separated out from the solution. The compound was filtered, washed with cold water (2 ml), isopropyl alcohol (10 ml) followed by diethyl ether (10 ml) and dried under vacuum. Yield was 200 mg (64 % based on Mo). The product had an identical IR spectrum and analyzed satisfactorily as the product in method I.

The use of $(NH_4)_2[WS_4]$ instead of $(NH_4)_2[MoS_4]$ in the above reaction resulted in the formation of compound **12** in good yields (300 mg, 74 % based on W). Anal. Found (calc.) for **12** ($C_4H_{14}N_2WS_4$): C 11.93 (11.94), H 3.51 (3.52), N 6.84 (6.69), S 33.91 (31.88), WS_4 76.59 (77.58) %. Both **11** and **12** fairly stable in air, slightly soluble in water, freely soluble in aqueous ammonia, DMSO, DMF and insoluble in CH_3CN, CH_2Cl_2, toluene, alcohol etc. The crystals obtained by this method were suitable for X-ray studies.

$$(NH_4)_2[MS_4] \quad + \quad 1,4\text{-bn} \longrightarrow \underline{\textbf{11}} \text{ or } \underline{\textbf{12}} + 2\,NH_3 \qquad (3.10)$$

3.2.8 Preparation of (dienH$_2$)[MoS$_4$] <u>13</u> and (dienH$_2$)[WS$_4$] <u>14</u>

Method I

MoO$_3$ (1.5 g) was dissolved in mixture of distilled water (20 ml) and diethylenetriamine (dien) (3 ml) to obtain a clear solution. Into this solution, a continuous and rapid stream of H$_2$S gas was passed for 30 min with temperature maintained at 60 ^{0}C. After 30-40 min, when deep red crystals of **13** were started appearing in the solution, the flow of H$_2$S gas was discontinued and mixture was left undisturbed to attain room temperature. The mixture was cooled in the refrigerator for about 1 h and the red needles of <u>13</u> were then isolated by filtration. The compound was washed with ice-cold water (10 ml), isopropyl alcohol (10 ml) followed by diethyl ether (10 ml) and dried under vacuum. Yield was 2.36 g (69 % based on Mo). Anal. Found (calc.) for <u>13</u> (C$_4$H$_{15}$N$_3$MoS$_4$): C 14.65 (14.58), H 4.56 (4.60), N 12.67 (12.76), S 38.87 (38.94), MoS$_4$ 67.76 (68.06) %.

$$MoO_3 + H_2O + dien \quad \xrightarrow[60\,^0C]{H_2S} \quad \underline{\textbf{13}} \qquad\qquad (3.11)$$
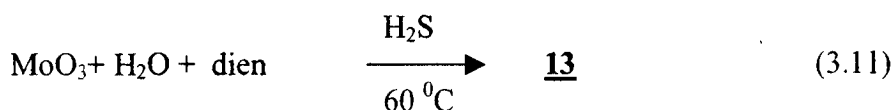
Method II

(NH$_4$)$_2$[MoS$_4$] (260 mg, 1 mmol) was dissolved in water (15 ml) containing few drops of ammonia, filtered and to the red coloured solution, dien (0.2 ml) was added in drops. The mixture was left undisturbed in the refrigerator and after 1-2 days, red needles of <u>13</u> were slowly started forming in the mixture. The crystals were isolated by filtration, washed with ice-cold water (10 ml), isopropyl alcohol (10 ml) followed by diethyl ether (10 ml) and dried under vacuum. Yield was 260 mg (79 % based on Mo). The product obtained had an identical IR spectrum and analyzed satisfactorily as the product in method I.

Compound <u>14</u> was prepared using similar synthetic protocol. Here instead of (NH$_4$)$_2$[MoS$_4$], (NH$_4$)$_2$[WS$_4$] (348 mg, 1 mmol in 10 ml of water) was treated with dien (0.3 ml). Yield was 240 mg (60 % based on W). Anal. Found (calc.) for <u>14</u> (C$_4$H$_{15}$N$_3$WS$_4$): C 11.63 (11.51), H 3.52 (3.60), N 9.94 (10.07), S 28.15 (30.74), WS$_4$ 74.0 (74.79) %. Both <u>13</u> and <u>14</u>, have good stability in air, are slightly soluble in water, freely soluble in ammonia, DMSO, DMF and insoluble in CH$_3$CN, CH$_2$Cl$_2$,

toluene, alcohol etc. The crystals obtained by this method were used for single crystal structure determination.

$$(NH_4)_2[MS_4] + dien \longrightarrow \underline{13} \text{ or } \underline{14} + 2 NH_3 \qquad (3.12)$$
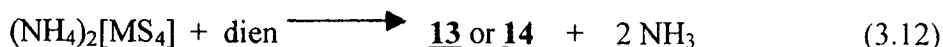
3.2.9 Preparation of (dipnH$_2$)[MoS$_4$] $\underline{15}$ and (dipnH$_2$)[WS$_4$] $\underline{16}$

An aqueous solution of freshly prepared $(NH_4)_2[MoS_4]$ (520 mg, 2 mmol in 50 ml of H_2O) was filtered and to the filtrate dipropylenetriamine, dipn (1 ml) was added in drops. The mixture was left undisturbed for crystallization and after a day, red plates of $\underline{15}$ started appearing in the solution. The crystals were isolated by filtration, washed with cold water (10 ml), followed by isopropyl alcohol (20 ml) and diethyl ether (20 ml) and dried under vacuum. Yield was 515 mg (72 % based on Mo). Anal. Found (calc.) for $\underline{15}$ ($C_6H_{19}N_3MoS_4$): C 20.15 (20.16), H 5.29 (5.37), N 11.57 (11.76), S 38.86 (35.88) %.

The reaction of an aqueous $(NH_4)_2[WS_4]$ (100 mg, in 5 ml water) instead of $(NH_4)_2[MoS_4]$ with dipn (0.3 ml) resulted in the formation of yellow plates of $\underline{16}$ in good yields (100 mg, 63 % based on W). Anal. Found (calc.) for $\underline{16}$ ($C_6H_{19}N_3WS_4$): C 16.36 (16.18), H 4.26 (4.30), N 9.933 (9.44), S 29.12 (28.80) %. Both, **15** and **16** are stable in air, slightly soluble in water but freely soluble in ammonia, DMSO, DMF and insoluble in CH_3CN, CH_2Cl_2, toluene, alcohol etc. The crystals obtained by this method were suitable for X-ray studies.

$$(NH_4)_2[MS_4] + dipn \longrightarrow \underline{15} \text{ or } \underline{16} + 2 NH_3 \qquad (3.13)$$

3.2.10 Preparation of (trenH$_2$)[MoS$_4$]·H$_2$O 17 and (trenH$_2$)[WS$_4$]·H$_2$O $\underline{18}$

Freshly prepared $(NH_4)_2[MoS_4]$ (520 mg, 2 mmol) was dissolved in 50 ml water and then filtered. To the filtrate, tris(2-aminoethyl)amine (tren) (0.5 ml) was added in drops and left undisturbed for crystallization. After a day, red blocks of 17 slowly separated from the solution and were isolated by filtration, washed with cold water (2 ml) followed by isopropyl alcohol (15 ml) and diethyl ether (20 ml) and the compound was dried under vacuum. Yield was 540 mg (70 % based on Mo). Anal.

Found. (calc.) for **17** ($C_6H_{22}N_4OMoS_4$): C 18.34 (18.45), H 5.71 (5.64), N 14.23 (14.35), S 32.63 (32.85), MoS_4 57.40 (57.42) %.

Compound **18** was obtained by adding tren (0.3 ml) to an aqueous solution of $(NH_4)_2[WS_4]$ (348 mg, 1 mmol in 10 ml water) and subsequent crystallization. Yield was 335 mg (70% based on W). Anal. Found (calc.) for **18** ($C_6H_{22}N_4OWS_4$): C 15.11 (15.06), H 4.72 (4.60), N 11.31 (11.63), S 26.23 (26.81) %. The crystals obtained by this method were suitable for X-ray studies.

$$(NH_4)_2[MS_4] + tren \longrightarrow \underline{\textbf{17}} \text{ or } \underline{\textbf{18}} + 2 NH_3 \qquad (3.14)$$
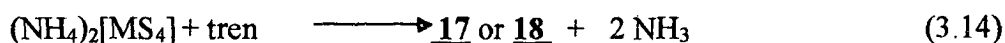
3.2.11 Preparation of anhydrous (trenH$_2$)[MoS$_4$] 19 and (trenH$_2$)[WS$_4$] 20

Powdered samples of **17** (400 mg) or $(trenH_2)[WS_4] \cdot H_2O$ **18** (300 mg) were heated separately in an electric furnace at 130°C and 140 °C respectively. This resulted in the formation of the anhydrous $(trenH_2)[MoS_4]$ **19** (381.5 mg) and $(trenH_2)[WS_4]$ **20** (288.8 mg). The complexes **19** and **20** were equilibrated over aqueous ammonia in a dessicator for ~2 h to obtain the original monohydrates 17 and **18** respectively as described in equation below. All the complexes **17-20** are stable in air, slightly soluble in water, freely soluble in ammonia, DMSO, DMF and insoluble in CH_3CN, CH_2Cl_2, toluene, alcohol etc.

$$(trenH_2)[MS_4] \cdot H_2O \underset{\Delta}{\overset{\Delta}{\rightleftharpoons}} \underline{\textbf{19}} \text{ or } \underline{\textbf{20}} + H_2O \qquad (3.15)$$

3.2.12 Preparation of (pipH$_2$)[MoS$_4$] 21 and (pipH$_2$)[WS$_4$] 22
Method I

MoO_3 (1 g) was dissolved in an aqueous solution of anhydrous piperazine, pip (1 g in 10 ml water) and stirred to obtain a clear solution. Into the solution, a continuous and rapid stream of H_2S gas was passed for 30 min, and the temperature was maintained at 60 °C. After about 30-40 min, when crystals started appearing in the solution, the flow of H_2S gas was stopped and the mixture was left undisturbed to attain room temperature. The mixture was then cooled in the refrigerator for 30-40 min and the crystalline blocks of **21** were isolated by filtration. The compound was washed with ice-cold water (20 ml), followed by isopropyl alcohol (10 ml) and ether

(10 ml) and dried under vacuum. Yield was 1.27 g (60 % based on Mo. Anal. Found (calc.) for **21** ($C_4H_{12}N_2MoS_4$): C 15.04 (15.38), H 3.83 (3.88), N 8.71 (8.97), S 40.95 (41.06), MoS_4 71.37 (71.77) %
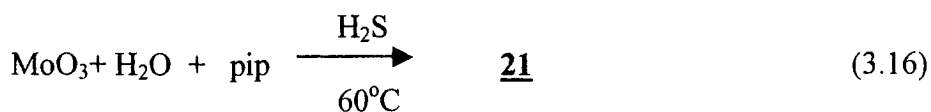
$$MoO_3 + H_2O + pip \xrightarrow[60^{\circ}C]{H_2S} \underline{\mathbf{21}} \qquad (3.16)$$

Method II

Freshly prepared $(NH_4)_2[MoS_4]$ (260 mg, 1 mmol) was dissolved in 15 ml of distilled water containing few drops of ammonia. The solution then was filtered, and to the filtrate, an aqueous solution pip (86 mg, 1 mmol in 5 ml water) was added in drops at room temperature. The reaction mixture was stirred and then filtered to obtain a clear solution. The solution was left undisturbed in the refrigerator. After 2 days, well-formed red blocks of **21** separated out from the solution. The crystals were isolated by filtration, washed well with cold water (2 ml), isopropyl alcohol (10 ml) and diethyl ether (10 ml). Yield was 200 mg (65 % based on Mo). The product obtained by this method had an identical IR spectrum and analysed satisfactorily as the product in method I.

The mixing of aqueous solutions of $(NH_4)_2[WS_4]$ (348 mg, 1 mmol, in 20 ml water) and anhydrous pip (86 mg, 1 mmol in 5 ml water) resulted in the formation of yellow blocks of **22** after 2 days in good yields (330 mg, 80 % based on W). Anal. Found (calc.) for **22** ($C_4H_{12}N_2WS_4$): C 12.18 (12.00), H 3.00 (3.03), N 7.03 (7.00), S 32.84 (32.04), WS_4 76.6 (78.0) %. Both **21** and **22** are stable in air, slightly soluble in water, freely soluble in ammonia, DMSO, DMF and insoluble in CH_3CN, CH_2Cl_2, toluene, alcohol etc.

$$(NH_4)_2[MS_4] + pip \longrightarrow \mathbf{21} \text{ or } \mathbf{22} + 2\,NH_3 \qquad (3.17)$$
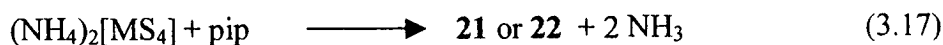
3.2.13 Preparation of (1,4-dmpH₂)[MoS₄] $\underline{\mathbf{23}}$ and (1,4-dmpH₂)[WS₄] $\underline{\mathbf{24}}$

Method I

MoO_3 (1 g) was dissolved in a mixture of water and 1,4-dimethylpiperazine, 1,4-dmp, (0.3 ml). Into this solution a continuous and rapid stream of H_2S gas was passed for about 30 min and the temperature of the reaction mixture was maintained at $60^{\circ}C$. After 30-40 min, red crystalline compound started appearing in the solution. The mixture was left undisturbed and then cooled in the refrigerator for about 1 h. The

red crystals of **23** were isolated by filtration, washed with cold water (15 ml), isopropyl alcohol (15 ml) and diethyl ether (15 ml) and dried under vacuum. Yield was 2.0 g (85 % based on Mo). Anal. Found (calc.) for **23** ($C_6H_{16}N_2MoS_4$): MoS_4 65.40 (65.86) %.

$$MoO_3 + H_2O + 1,4\text{-dmp} \xrightarrow[60\,^0C]{H_2S} \textbf{23} \tag{3.18}$$
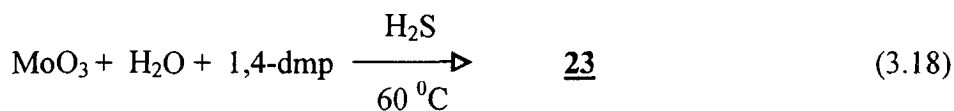
Method II

To an aqueous solution of $(NH_4)_2[MoS_4]$ (260 mg, 1 mmol in 15 ml of water), 1,4-dmp (0.5 ml) was added in drops and the mixture was left undisturbed in the refrigerator. After 2 days red crystals of **23** were isolated by filtration, washed with cold water (5 ml) followed by isopropyl alcohol (15 ml) and diethyl ether (15 ml) and dried under vacuum. Yield was 280 mg (80 % based on Mo). The product obtained had an identical infrared spectrum and analyzed satisfactorily as the product in method I.

The use of $(NH_4)_2[WS_4]$ (348 mg, 1mmol) instead of $(NH_4)_2[MoS_4]$ resulted in the formation of **24** in good yield (300 mg, 60 % based on W). Anal. Found (calc.) for **24** ($C_6H_{16}N_2WS_4$): C 16.87 (16.82), H 3.69 (3.77), N 6.92 (6.54), S 30.02 (29.95), WS_4 72.50 (72.86) %.

$$(NH_4)_2[MS_4] + 1,4\text{-dmp} \longrightarrow \textbf{23 or 24} + 2\,NH_3 \tag{3.19}$$
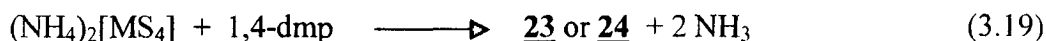
3.2.14 Preparation of (dabcoH)₂[MoS₄] 25 and (dabcoH)₂[WS₄] 26

MoO_3 (1g) was dissolved in a mixture of distilled water (10 ml) and aqueous triethylenediamine (dabco) (1 g in 10 ml) and into the clear solution, a continuous and rapid stream of H_2S gas was passed for 30 min. After 30-40 min, when crystalline material started appearing in the solution, the flow of H_2S gas was stopped and the mixture was left undisturbed. The deep red crystalline compound **25** was isolated after keeping the mixture in a refrigerator for about 1 h. The compound was washed with cold water (5 ml) followed by isopropyl alcohol (20 ml) and diethyl ether (20 ml) and dried under vacuum. Yield was 2.2 g (70 % based on Mo). Anal. Found (calc.) for **25**
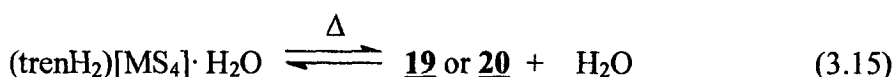
$(C_{12}H_{26}N_4MoS_4)$: C 30.77 (31.98), H 5.99 (5.83), N 12.06 (12.43), S 29.93 (28.47), MoS_4 49.75 (49.75).

$$MoO_3 + H_2O + dabco \xrightarrow[60^{\circ}C]{H_2S} \underline{\textbf{25}} \qquad (3.20)$$
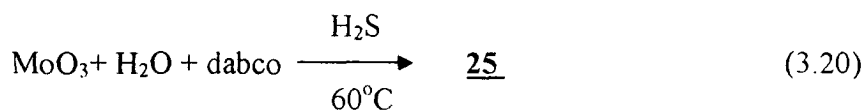
Compound **26** was prepared by mixing aqueous solutions of $(NH_4)_2[WS_4]$ (175 mg, 0.5 mmol in 10 ml water) and dabco (112.2 mg, 1 mmol in 10 ml H_2O). Yield (200 mg, 74 % based on W). Anal. Found (calc.) for **26** $(C_{12}H_{26}N_4WS_4)$: C 26.31 (26.76), H 4.86 (4.88), N 10.06 (10.40), S 23.23 (23.82), WS_4 57.92 (57.96) %.

3.2.15 Preparation of (2-pipH-1-EtNH₃)[MoS₄] · ½H₂O 27

Freshly prepared $(NH_4)_2[MoS_4]$ (260 mg, 1 mmol) was dissolved in 50 ml of distilled water containing few drops of NH_3. To the red coloured solution, 2-piperazine-1-ethylamine (2-pip-1-EtNH₂) (0.5 ml) was added and then the solution was filtered and left undisturbed for crystallization. After 2 days, the red needles of **27** were isolated, washed with ice-cold water (5 ml) followed by isopropyl alcohol (10 ml) and diethyl ether (10 ml). Yield (240 mg, 66.0% based on Mo). The crystals obtained by this method were suitable for X-ray studies. Anal. Found (calc.) for **27** $C_6H_{17}N_3MoS_4$ · ½ H_2O: C 19.62 (19.77), H 4.89 (4.98), N 11.39 (11.53), S 35.38 (35.19) %.

$$(NH_4)_2[MoS_4] + 2\text{-pip-1-EtNH}_2 \longrightarrow \underline{\textbf{27}} + 2NH_3 \qquad (3.21)$$
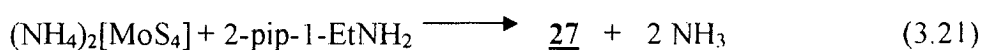
3.2.16 Preparation of (trans 1,2-cnH)₂[WS₄] 28

To an aqueous solution of $(NH_4)_2[WS_4]$ (348 mg, 1 mmol in 15 ml of water), (±) trans 1,2-diaminocyclohexane (trans-1,2-cn) (0.5 ml) was added and the mixture was left undisturbed for crystallization. After 2 days, yellow crystals of **28** were isolated by filtration, washed with cold water, followed by isopropyl alcohol (10 ml) and ether (10 ml). The compound was dried in air. Yield (400 mg, 73 % based on W). The crystals are stable in air, slightly soluble in water, freely soluble in ammonia, DMSO, DMF and insoluble in CH_3CN, CH_2Cl_2, toluene, alcohol etc. Anal. Found (calc.) for **28** $C_{12}H_{30}N_4WS_4$: C 26.38 (26.57), H 5.49 (5.58), N 10.08 (10.33), S 22.65 (23.64) %

$$(NH_4)_2[WS_4] + \text{trans-1,2-cn} \longrightarrow \underline{\textbf{28}} + 2NH_3 \qquad (3.22)$$

3.2.17 Preparation of (mipaH)₂[WS₄] $\underline{29}$

$(NH_4)_2[WS_4]$ (348mg, 1 mmol) was dissolved in 10 ml of distilled water and to this isopropyl amine, mipa (0.5 ml) was added in drops. The solution was left undisturbed for crystallization. After 1-2 days, yellow rectangular blocks of $\underline{29}$ were isolated by filtration, washed with ice cold water (5 ml) followed by isopropyl alcohol (10 ml) and diethyl ether (10 ml). The compound was dried in air. Yield (350 mg, 81 % based on W). Anal. Found (calc.) for $\underline{29}$ $C_6H_{20}N_2WS_4$: C 14.25 (16.66), H 4.24 (4.67), N 6.31 (6.48), S 33.07 (29.67) %.

$$(NH_4)_2[WS_4] + 2\,(mipa) \longrightarrow \underline{29} + 2\,NH_3 \qquad (3.23)$$

3.3 Synthesis of highly insoluble salts of tetrathiometalates

i. (dbtmen)Br₂·2H₂O $\underline{30}$

The reaction of tmen (1.3 ml in 10 ml CH_3CN) with benzyl bromide (2.3 ml) formed a crystalline powder of $\underline{30}$. (CAUTION! benzyl bromide is a strong eye irritant and has been handled with proper precaution). Yield = 4.0 g. The recrystallisation of $\underline{30}$ from water gave crystals of X-ray quality. The product analyzed satisfactorily as (dbtmen)Br₂·2H₂O. Anal. Found (calc.) for $\underline{30}$ $C_{20}H_{30}N_2Br_2$·2H₂O: C 48.63 (48.59), H 7.01 (6.95), N 5.68 (5.67) %.

ii. (dbtmen)[MoS₄] $\underline{31}$ and (dbtmen)[WS₄] $\underline{32}$

The addition of an aqueous solution of (dbtmen)Br₂·2H₂O (494 mg, 1 mmol in 20 ml H_2O) to an aqueous $(NH_4)_2[MoS_4]$ solution (260 mg, 1 mmol in 20 ml H_2O) resulted in the formation of polycrystalline orange-red (dbtmen)[MoS₄] $\underline{31}$ complex. The compound was washed well with distilled water (20 ml) and then air-dried. Yield (515 mg, 98 % based on Mo). Anal. Found (calc.) for $\underline{31}$ $(C_{20}H_{30}N_2MoS_4)$: C 45.09 (45.95), H 5.61 (5.80), N 5.30 (5.36), S 23.31 (24.54) %. The use of $(NH_4)_2[WS_4]$ (348 mg, 1 mmol in 20 ml H_2O) in the above reaction resulted in the formation of insoluble (dbtmen)[WS₄] $\underline{32}$. Anal. Found (calc.) for $C_{20}H_{30}N_2WS_4$: C 38.50 (39.33), H 4.81 (4.96), N 4.52 (4.59), S 19.49 (21.01) %.

$$(dbtmen)Br_2·2H_2O + (NH_4)_2[MS_4] \longrightarrow \underline{31}\ or\ \underline{32} + 2\,NH_4Br + 2H_2O \quad (3.24)$$
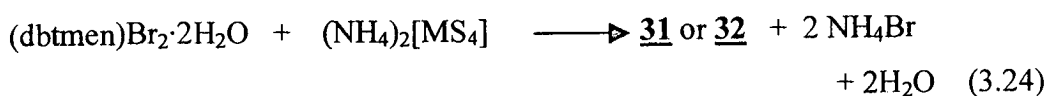
3.4 Reactivity Studies of tetrathiometalates

3.4.1 Reaction of $(NH_4)_2[MS_4]$ with $[(PhCH_2)N(C_2H_5)_3]Cl$

The reaction of an aqueous solution of $(NH_4)_2[MoS_4]$ (3.2 g in 30 ml water) with aqueous $[(PhCH_2)N(C_2H_5)_3]Cl$ (2.733 g dissolved in 20 ml of H_2O) solution under constant stirring for about 1 h resulted in the formation of $[(PhCH_2)N(C_2H_5)_3]_2[MoS_4]$. Yield (5.5 g, 73 % based on Mo). Anal. Found (calc.) for $C_{26}H_{44}N_2MoS_4$: C 51.08 (51.28), H 7.27 (7.30), N 4.58 (4.60), S 20.95 (21.06), Mo 15.67 (15.75), MoS_4 36.62 (36.82), MoO_3 22.23 (23.64) %, decomposition temp 130^0C, DSC onset temperature 130 ^0C. The use of $(NH_4)_2[WS_4]$ instead of $(NH_4)_2[MoS_4]$ results in the formation of $[(PhCH_2)N(C_2H_5)_3]_2[WS_4]$.

$$2\,[(PhCH_2)N(C_2H_5)_3]Cl + (NH_4)_2[MS_4] \longrightarrow [(PhCH_2)N(C_2H_5)_3]_2[MS_4] + 2\,NH_4Cl \qquad (3.25)$$
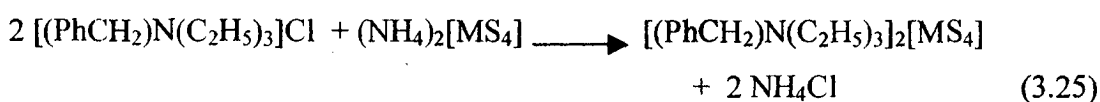
3.4.2 Reaction of $(NH_4)_2[MS_4]$ with (CTAB)

The mixing and stirring of aqueous solutions of $(NH_4)_2[MoS_4]$ (2 g, in 50 ml H_2O) and N-cetyl,N,N,N-trimethylammonium bromide (CTAB) (5.6 g in 20 ml H_2O) resulted in the formation of $(CTA)_2[MoS_4]$. Yield (5.9 g, 90 % based on Mo). Anal Found (calc) for $C_{38}H_{84}N_2MoS_4$: MoS_4 28.06 (28.26). The reaction of $(NH_4)_2[WS_4]$ with (CTAB) under identical conditions afforded $(CTA)_2[WS_4]$.

$$2\,(CTAB) + (NH_4)_2[MS_4] \longrightarrow (CTA)_2[MS_4] + 2\,NH_4Br \qquad (3.26)$$
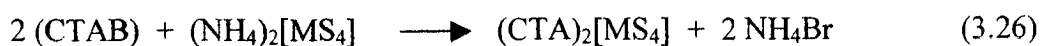
3.4.3 Reaction of $(NH_4)_2[MoS_4]$ with $[Ni(en)_3]Cl_2·2H_2O$

To an aqueous ammonical solution of $(NH_4)_2[MoS_4]$ (260 mg in 15 ml H_2O containing few drops of NH_3), $[Ni(en)_3]Cl_2·2H_2O$ (370 mg in 20 ml in H_2O) was added which resulted in the formation of the previously reported $[Ni(en)_3][MoS_4]$. The reaction mixture was kept aside for 1 h and filtered. The orange red polycrystalline compound was washed well with cold water till the washings were colorless and dried in vacuum and weighed to get 460 mg of of product. The use of ammonium terathiotunsgtate instead of tetrathiomolybdate, resulted in the formation of insoluble $[Ni(en)_3][WS_4]$. Anal. Found (calc.) for $[Ni(en)_3][MoS_4]$: C 18.68 (15.55), H 5.20 (5.23), N 16.93 (18.14), S 26.55 (27.79) %; $[Ni(en)_3][WS_4]$: C 12.90 (13.07), H 4.35 (4.40), N 14.97 (15.25), S 22.53 (23.27) %.

3.4.4 Reaction of [(PhCH$_2$N(C$_2$H$_5$)$_3$]$_2$[MoS$_4$] with [Ni(en)$_3$]Cl$_2$·2H$_2$O

[(PhCH$_2$N(C$_2$H$_5$)$_3$]$_2$[MoS$_4$] (609 mg) was dissolved in 20 ml of CH$_3$CN and slowly added in drops to an aqueous solution of [Ni(en)$_3$]Cl$_2$·2H$_2$O (370 mg in 20 ml) under stirring. The reaction mixture was kept aside for 1 h and filtered. The orange red polycrystalline [Ni(en)$_3$][MoS$_4$] was washed with cold water till the washings were colorless and dried in vacuum and weighed to get 460 mg of compound. (CTA)$_2$[MS$_4$] in CH$_3$CN reacts with aqueous solution of [Ni(en)$_3$]Cl$_2$·2H$_2$O to form [Ni(en)$_3$][MS$_4$] complexes in good yields in a similar way.

3.4. 5 Reaction of Cu(II) with (NH$_4$)$_2$[MS$_4$] in presence of ethylenediamine

CuSO$_4$.5H$_2$O (500 mg, 1 mmol) was dissolved in 10 ml H$_2$O and reacted with slight excess of en (10 ml) to obtain a dark blue coloured solution (pH =12). To this mixture, an aqueous (NH$_4$)$_2$[MoS$_4$] solution (520 mg in 30 ml water) was added in drops which resulted in the formation of red polycrystalline [Cu(en)$_2$][MoS$_4$] complex. The compound was washed with 20 ml of cold water and dried under vacuum. Yield = 684 mg. The reaction of (NH$_4$)$_2$[WS$_4$] (350 mg in 20 ml water) with Cu(II)-en mixture gave the insoluble yellow [Cu(en)$_2$][WS$_4$] complex.

$$Cu(II) + en + (NH_4)_2[MS_4] \rightarrow [Cu(en)_2][MS_4] \downarrow \qquad (3.27)$$
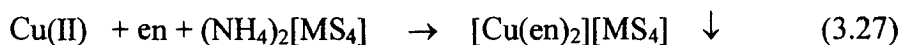
Use of ammonia instead of ethylenediamine in the above experiment gave nearly quantitative yield of red [Cu(NH$_3$)$_4$][MoS$_4$] and orange yellow [Cu(NH$_3$)$_4$][WS$_4$] complexes.

3.4.6 Reaction of (NH$_4$)$_2$[MS$_4$] with Zn^{2+} in the presence of ethylenediamine

ZnSO$_4$.7H$_2$O (287 mg, 1 mmol) was dissolved in 10 ml distilled water and to this solution 10 ml of en was added in drops. The solution was filtered and to the filtrate, (NH$_4$)$_2$[MoS$_4$] (260 mg in 20 ml water) was added which resulted in the formation of orange red [Zn(en)$_3$][MoS$_4$] complex. Yield = 415 mg. The reaction of (NH$_4$)$_2$[WS$_4$] instead of (NH$_4$)$_2$[MoS$_4$] afforded polycrystalline yellow [Zn(en)$_3$][WS$_4$] complex.

$$Zn^{2+} + en + (NH_4)_2[MS_4] \rightarrow [Zn(en)_3][MS_4] \downarrow \qquad (3.28)$$
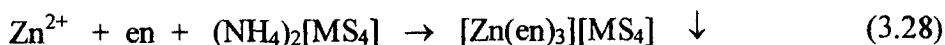
3.4.7 Reaction of (NH$_4$)$_2$[MS$_4$] with (Ph$_4$P)Br

A reaction of aqueous (NH$_4$)$_2$[MoS$_4$] (260 mg, 1mmol in 20 ml H$_2$O) and aqueous tetraphenylphosphonium bromide, (Ph$_4$P)Br (839 mg in 20 ml water) gave red polycrystalline (Ph$_4$P)$_2$[MoS$_4$] complex. Yield of the product was 820 mg. Anal. Found (calc.) for C$_{48}$H$_{40}$P$_2$MoS$_4$: C 63.24 (63.84), H 4.32 (4.47), S 14.29 (14.20). IR

data: 3046, 1581, 1480, 1435, 1313, 1189, 1107, 995, 723, 689, 527, 467 cm^{-1}. The use of $(NH_4)_2[WS_4]$ (350 mg, 1mmol) instead of ammonium tetrathiomolybdate in the above method, resulted in the formation polycrystalline yellow $(Ph_4P)_2[WS_4]$ complex. Anal. Found (calc.) for $C_{48}H_{40}P_2WS_4$: C 58.33 (58.17), H 3.98 (4.07), S 14.24 (12.94). IR data: 3075, 1574, 1486, 1435, 1313, 1190, 1107, 996, 758, 723, 690, 527, 451 cm^{-1}.

$$2\,(Ph_4P)Br \;+\; (NH_4)_2[MS_4] \;\rightarrow\; (Ph_4P)_2[MS_4] \;\downarrow\; +\; 2\,NH_4Br \qquad (3.29)$$
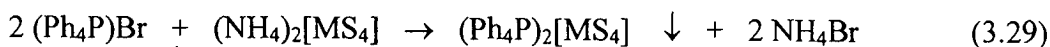
3.5 Syntheses of organic ammonium salts of oxometalates

3.5.1. Preparation of (enH₂)[CrO₄] $\underline{33}$

$K_2[CrO_4]$ (1.94 g, 0.01 mol) was dissolved in water (20 ml) and added to an aqueous solution of $(enH_2)Cl_2$ (1.33 g, 0.01 mol in 5 ml of water) was slowly added at room temperature. The yellow coloured solution thus obtained was filtered and kept in the refrigerator for crystallization. After 2 days, yellow block-like crystals were obtained. The crystalline product was filtered and washed with ice-cold water (~5 ml) and air-dried. Yield of the product obtained was 54 %. The crystals were suitable for X-ray studies. The reaction of $(enH_2)Cl_2$ with ammonium chromate instead of $K_2(CrO_4)$ also gave $(enH_2)[CrO_4]$ in good yields. The compound is stable in air, soluble in water, ammonia, DMSO, DMF etc. Anal. Found (calc.): Cr 29.1 (29.2 %).

$$A_2(CrO_4)\;(A = K\;or\;NH_4) + (enH_2)Cl_2 \longrightarrow \underline{33} \;+\; 2\,ACl \qquad (3.30)$$
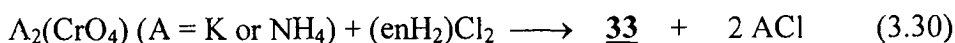
3.5.2. Preparation of (enH₂)[Cr₂O₇] $\underline{34}$

$K_2[Cr_2O_7]$ (2.94 g, 0.01 mol) was dissolved in water (25 ml) and $(enH_2)Cl_2$ (1.33 g, 0.01 mol) in water (10 ml) was slowly added at room temperature. The orange coloured solution thus obtained was filtered and kept aside for crystallization. After 2-3 day, orange crystalline blocks were obtained. The crystalline product was filtered and washed with ice-cold water (~10 ml) and air-dried. The yield of the product was 65 % based on Cr. The crystals obtained by this method were used for single crystal structure determination. The use of $(NH_4)_2(Cr_2O_7)$ instead of $K_2(Cr_2O_7)$ in the above reaction also gave crystals of $\underline{34}$ in good yield. Anal. Found (calc.): Cr 37.3 (37.4%). The compound is stable in air, soluble in water, ammonia, DMSO, DMF etc.

$$K_2(Cr_2O_7) + (enH_2)Cl_2 \longrightarrow (enH_2)[Cr_2O_7] \;+\; 2\,KCl \qquad (3.31)$$
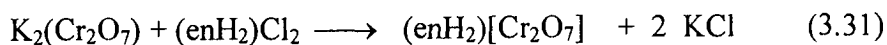
CHAPTER 4

RESULTS AND DISCUSSION

The characterizations of the new organic ammonium tetrathiometalates and tetraoxometalates synthesized in the present investigation have been achieved by using a combination of various analytical as well chemical techniques. The details of each method which include the newly developed gravimetric analysis of $[MS_4]^{2-}$ content (M = Mo or W), elemental analysis (C, H, N, S), IR, Raman, ^{1}H, ^{13}C and DEPT NMR, UV-Vis spectroscopic techniques, thermogravimetric methods like TG-DTA-DSC, electron microscopic techniques namely EDAX-ESEM, X-ray powder and single crystal X-ray diffractometry are described in this chapter. Scheme V summarizes the various techniques used for the characterization of the new complexes synthesized in the present work. In addition to the characterization part, this chapter also covers the synthetic aspects and reactivity characteristics of the tetrathiometalates and tetraoxochromates.
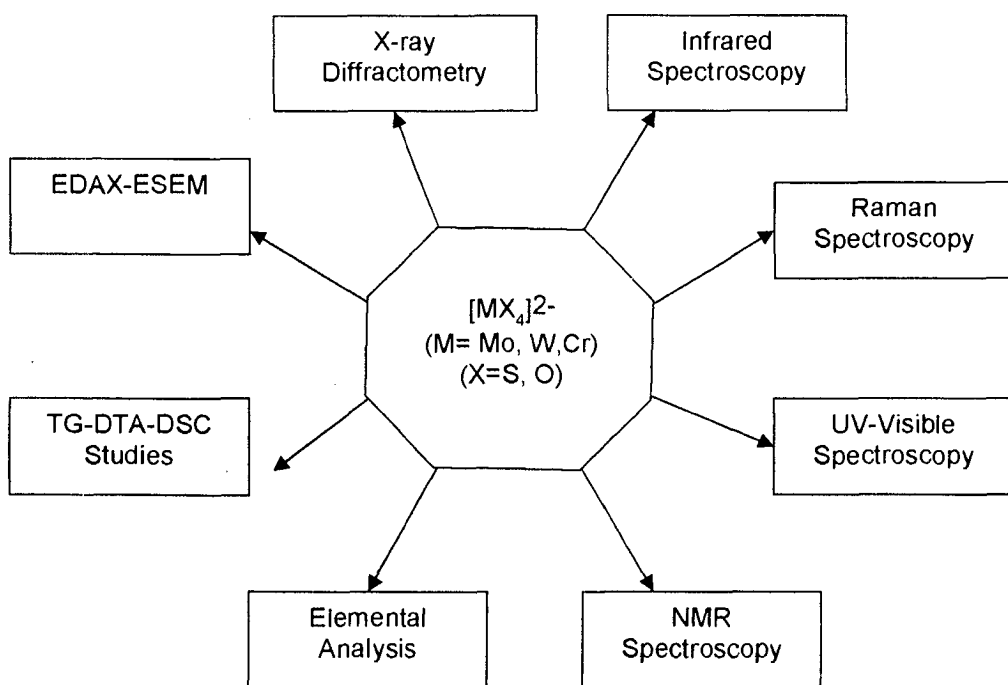
Scheme V

4.1. Synthetic aspects

The experimental details which include the synthetic and reactivity procedures for different organic ammonium tetrathiomolybdates, tetrathiotungstates oxochromates are described in Chapter 3. The new organic ammonium tetrathiometalates have been synthesized by a slight modification of the classical synthesis of tetrathiomolybdate first investigated by J.J. Berzelius in 1826 [42] as depicted in Scheme VI.

$$[MO_4]^{2-} \qquad\qquad\qquad\qquad [MO_4]^{2-}$$

Method A $\qquad\qquad\qquad\qquad\qquad\qquad$ Method A

$$(NH_4)_2[MS_4] \xrightarrow{\text{Method B}} \boxed{\begin{array}{c}\text{Organic ammonium } [MS_4] \\ (M = Mo, W)\end{array}}$$

Method C

$$[R_4N]X$$

Method A = passing of H_2S

Method B = base promoted Cation Exchange

Method C = simple cation exchange
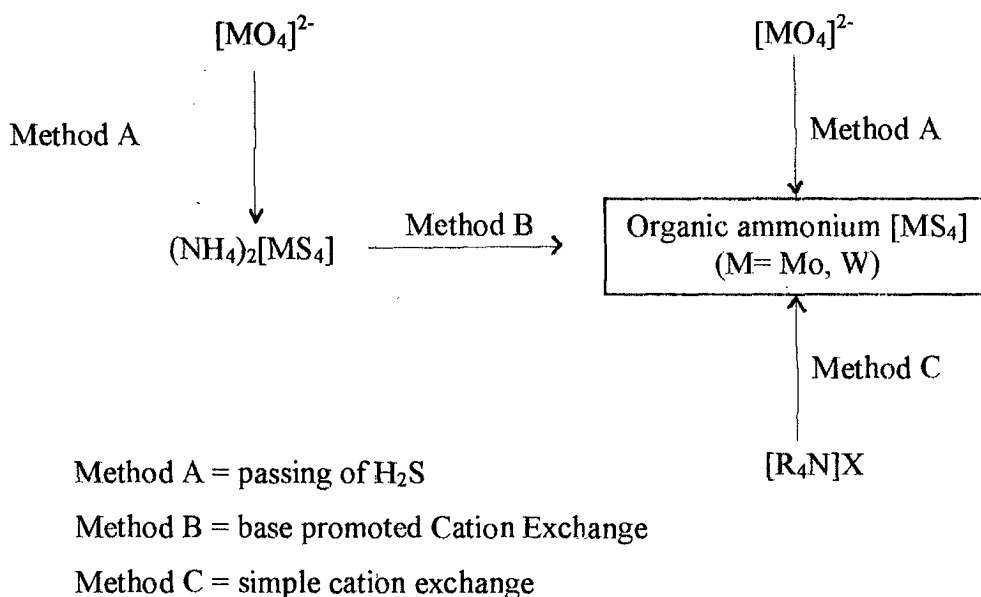
Scheme VI

The synthesis of the ammonium salts of $[MS_4]^{2-}$ (M = Mo, W) $(NH_4)_2[MoS_4]$ [42] and $(NH_4)_2[WS_4]$ [43] is known from the days of Berzelius who first investigated these reactions by passing H_2S gas into an ammoniacal molybdate or tungstate solution (4.1).

$$[MO_4]^{2-} + NH_3 \xrightarrow[60\,^0C]{H_2S} (NH_4)_2[MS_4] \qquad\qquad (4.1)$$
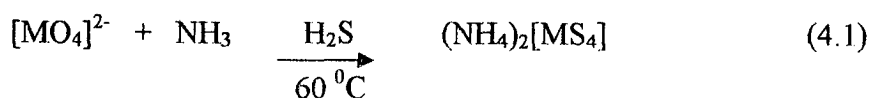
The preparation of these two salts by this method differs in terms of the duration of H_2S passing. $(NH_4)_2[MoS_4]$ can be synthesized by passing H_2S into an ammoniacal

solution for about 30 min at 60 ^{0}C while the synthesis of the corresponding W analogue requires H_2S passing for about six hours at same temperature. The passing of H_2S gas for even longer time under such alkaline conditions does not form any product other than $(NH_4)_2[MoS_4]$. In our recent report, we have shown that passing of H_2S gas into an ammoni cal solution of heptamolybdate for a longer period results only in the formation of ammonium tetrathiomolybdate [205] and not ammonium tetracosathioheptamolybdate $(NH_4)_6[Mo_7S_{24}]$ as has been reported by Kaushik et al [206]. Based on analytical data as well as the known stability of tetrahedral $[MoS_4]^{2-}$ in alkaline media, the heptanuclear complex $(NH_4)_6[Mo_7S_{24}]$ has been correctly formulated as $(NH_4)_2[MoS_4]$.

In the present work, the classical Berzelius synthetic protocol has been modified and an organic amine is used instead of ammonia and molybdic acid is used instead of heptamolybdate or sodium molybdate. The use of molybdic acid precludes the interference of NH_4^+ or Na^+ ions in the final product. Thus addition of organic amine into an aqueous slurry of molybdic acid followed by reaction with H_2S gas at 60 ^{0}C results in the formation of the corresponding organic ammonium tetrathiomolybdate as shown in Scheme VI. In the present work, a variety of organic amines, which have different steric bulk and different number of potential H-bonding donors (Scheme IV) have been used and a general reaction can be written as shown below.

$$[MO_4]^{2-} + \text{organic amine} \xrightarrow[60\,^\circ C]{H_2S} \text{organic ammonium } [MS_4] \quad (4.2)$$
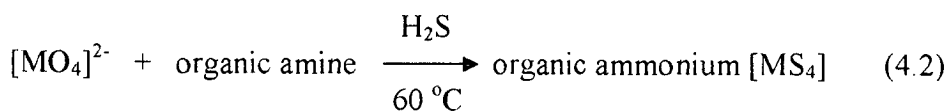
The same method can also be used for synthesis of the corresponding $[WS_4]^{2-}$ complexes indicating the generality of this method. The attempted synthesis of ammonium salts of $[CrS_4]^{2-}$ by passing H_2S gas into an ammonical solution of chromium trioxide was unsuccessful which can be explained based on the strong oxidizing properties of Cr(VI).

The organic ammonium tetrathiometalate complexes derived from the polyamines such as dien, trien etc can be obtained by this method in good yields. For example $(dienH_2)[MoS_4]$ which contains diprotonated dien has been synthesized as shown below.

$$[MoO_4]^{2-} + \text{dien} \xrightarrow[60\,°C]{H_2S} (\text{dienH}_2)[MoS_4] \qquad (4.3)$$
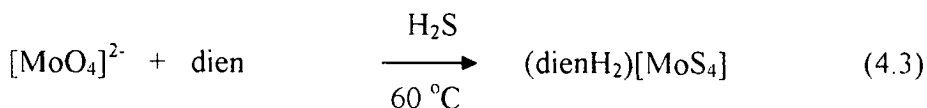
When H_2S gas was passed into an aqueous mixture of bicyclic amine like dabco and molybdic acid (1:1 or 2:1), only the monoprotonated product (dabcoH)$_2$[MoS$_4$] **25** is obtained.

$$[MoO_4]^{2-} + \text{dabco} \xrightarrow[60\,°C]{H_2S} (\text{dabcoH})_2[MoS_4] \qquad (4.4)$$
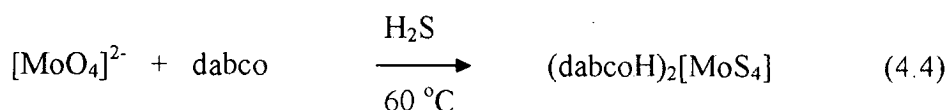
It is interesting to note that the use of other cyclic amines like piperazine or 1,4-dimethylpiperazine, in the above reaction results in the formation of the diprotonated products unlike in dabco.

$$[MoO_4]^{2-} + \text{pip} \xrightarrow[60\,°C]{H_2S} (\text{pipH}_2)[MoS_4] \qquad (4.5)$$
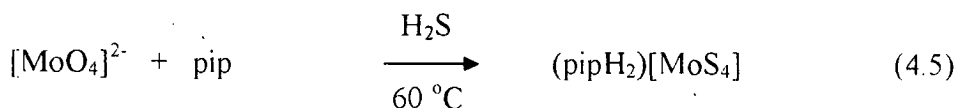
This method has been earlier reported for isolation of (Et$_2$NH$_2$)$_2$[MoS$_4$] (Et$_2$NH is diethyl amine) [74], (enH$_2$)[MoS$_4$] [75], (trienH$_2$)[MoS$_4$] [76] and (dienH$_2$)[MoS$_4$] [77] and piperidinium tetrathiomolybdate [78].

McDonald *et al* have reported synthesis of the (Et$_4$N)$_2$[MS$_4$][50] by adding a strong base such as (Et$_4$N)OH into an aqueous solution of ammonium tetrathiometalate. The facile substitution of ammonium cation by an organic tertaalkylammonium leads to the formation of (Et$_4$N)$_2$[MS$_4$] complexes as shown below.

$$(NH_4)_2[MS_4] + (Et_4N)OH \longrightarrow (EtN)_2[MS_4] + 2\,NH_3 + 2\,H_2O \quad (4.6)$$
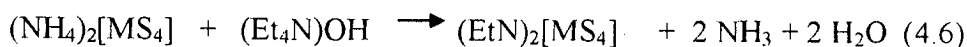
Alonso *et al* have reported the synthesis of several tetraalkylammonium tetrathiometalates [72,89-90] using a slight modification of the above method. The organic base i.e. tetraalkylammonium hydroxide has been generated *in situ* reaction of tetraalkylammonium chloride or bromide with NaOH further reacts with (NH$_4$)$_2$[MS$_4$] as mentioned earlier in 4.6.

$$(R_4N)X + NaOH \quad \rightarrow \quad (R_4N)OH + NaX \qquad (4.7)$$

In these reactions the alkyl group R can be methyl, ethyl, propyl, butyl, pentyl, hexyl, heptyl, octyl with X as either Cl⁻ or Br⁻. In the present investigation, the reaction of $(NH_4)_2[MS_4]$ has been investigated with a variety of organic amines instead of tetraethlyammonium hydroxide. The reaction is a base promoted cation exchange reaction and can be represented as shown below.

$$(NH_4)_2[MS_4] \quad + \quad \text{organic amine} \quad \rightarrow \quad \text{organic ammonium } [MS_4] + 2\ NH_3 \quad (4.8)$$
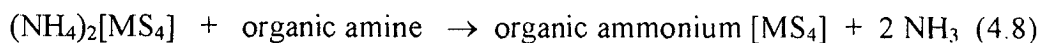
Thus several organic diammonium tetrathiometalates have been prepared in good yields by the reaction of an aqueous solution of ammonium salt of $[MoS_4]^{2-}$ or $[WS_4]^{2-}$ with the corresponding organic diamines in the present work. In this method, stronger base replaces the weaker base ammonia. The variety of organic diammonium tetrathiometalates synthesized by base promoted cation exchange method are listed in Table 4.1.1 The usefulness of this method lies in the high yield synthesis of tetrathiometalate under normal laboratory conditions. The method does not involve any sophisticated apparatus. The formation of a variety of organic ammonium tetrathiometalate complexes under ambient reaction conditions indicates the generality of this reaction.

It is interesting to note that although organic amine replaces ammonia in the above reaction, this method never gave quantitative yield of the organic ammonium tetrathiometalate. The observed yield can be attributed to the solubility of tetrathiometalate in aqueous ammonia which is formed during the course of the reaction. The base promoted cation exchange method has been used for the isolation of hydrated $(trenH_2)[MS_4] \cdot H_2O$ (M= Mo **17**, W **18**) complexes in good yields. These complexes are the first examples of structurally characterized hydrated organic diammonium tetrathiometalates. The use of a cyclic diamine, pip in above reaction results in the formation of $(pipH)_2[MS_4]$ (M = Mo **21**, W **22**). However it is worth to note that the reaction of **21** with different ratios of pip can give two products. When complex **21** is reacted with pip in 1:1 (MoS_4 : pip) molar ratio, only **21** is obtained.

Table 4.1.1 Organic ammonium tetrathiometalates

Tetrathiometalate source	Organic amine	Organic ammonium tetrathiometalate		Yield (%)
$(NH_4)_2[MoS_4]$	en	$(enH_2)[MoS_4]$	**1**	70
$(NH_4)_2[WS_4]$	en	$(enH_2)[WS_4]$	**2**	60
$(NH_4)_2[MoS_4]$	N-Me-en	$(N\text{-}Me\text{-}enH_2)[MoS_4]$	**3**	80
$(NH_4)_2[WS_4]$	N-Me-en	$(N\text{-}Me\text{-}enH_2)[WS_4]$	**4**	77
$(NH_4)_2[MoS_4]$	tmen	$(tmenH_2)[MoS_4]$	**5**	75
$(NH_4)_2[WS_4]$	tmen	$(tmenH_2)[WS_4]$	**6**	60
$(NH_4)_2[MoS_4]$	1,3-pn	$(1,3\text{-}pnH_2)[MoS_4]$	**7**	90
$(NH_4)_2[WS_4]$	1,3-pn	$(1,3\text{-}pnH_2)[WS_4]$	**8**	60
$(NH_4)_2[MoS_4]$	N,N'-dm-1,3-pn	$(N,N'\text{-}dm\text{-}1,3\text{-}pnH_2)[MoS_4]$	**9**	88
$(NH_4)_2[WS_4]$	N,N'-dm-1,3-pn	$(N,N'\text{-}dm\text{-}1,3\text{-}pnH_2)[WS_4]$	**10**	88
$(NH_4)_2[MoS_4]$	1,4-bn	$(1,4\text{-}bnH_2)[MoS_4]$	**11**	64
$(NH_4)_2[WS_4]$	1,4-bn	$(1,4\text{-}bnH_2)[WS_4]$	**12**	74
$(NH_4)_2[MoS_4]$	dien	$(dienH_2)[MoS_4]$	**13**	79
$(NH_4)_2[WS_4]$	dien	$(dienH_2)[WS_4]$	**14**	60
$(NH_4)_2[MoS_4]$	dipn	$(dipnH_2)[MoS_4]$	**15**	72
$(NH_4)_2[MoS_4]$	dipn	$(dipnH_2)[WS_4]$	**16**	63
$(NH_4)_2[MoS_4]$	tren	$(trenH_2)[MoS_4] \cdot H_2O$	**17**	70
$(NH_4)_2[WS_4]$	tren	$(trenH_2)[WS_4] \cdot H_2O$	**18**	70
$(NH_4)_2[MoS_4]$	pip	$(pipH_2)[MoS_4]$	**21**	65
$(NH_4)_2[WS_4]$	pip	$(pipH_2)[WS_4]$	**22**	80
$(NH_4)_2[MoS_4]$	1,4-dmp	$(1,4\text{-}dmpH_2)[MoS_4]$	**23**	80
$(NH_4)_2[WS_4]$	1,4-dmp	$(1,4\text{-}dmpH_2)[WS_4]$	**24**	60
$(NH_4)_2[WS_4]$	dabco	$(dabcoH)_2[WS_4]$	**26**	74
$(NH_4)_2[MoS_4]$	2-pip-1-EtNH₂	$(2\text{-}pipH\text{-}1\text{-}EtNH_3)[MoS_4] \cdot \frac{1}{2} H_2O$ **27**		66
$(NH_4)_2[WS_4]$	trans-1,2-cn	$(trans\text{-}1,2\text{-}cnH)_2[WS_4]$	**28**	73
$(NH_4)_2[WS_4]$	mipa	$(mipaH)_2[WS_4]$	**29**	81

On changing the ratio of MoS_4 : pip to 1:2, altogether new product $(pipH)_2[MoS_4]\cdot x$ pip can be obtained. The use of excess of pip in this reaction results in formation of the same product. The distinct comparison between the two complexes has been achieved by use IR and UV-Vis spectroscopy. The IR spectra of two complexes are quite different. The IR spectrum of **21** shows a broad signal at around 3000 cm^{-1} which can be attributed to the N-H region of $(pipH_2)^{2+}$ cations while the IR spectrum of second product is totally different which exhibit extra sharp signals in the N-H region at around 3300 cm^{-1} indicating the presence of free unprotonated pip. In addition to these signals, a broad signal at around 3000 cm^{-1} for N-H region is also observed which can originate from the singly protonated $(pipH)^+$ cation. The two reactions used for the isolation of **21** and $(pipH)_2[MoS_4] \cdot x$ pip are shown below.

$$(pipH_2)[MoS_4] \ + pip \ \longrightarrow \ (pipH_2)[MoS_4] \qquad\qquad (4.9)$$

$$(pipH_2)[MoS_4] \ + 2\ pip \ \longrightarrow \ (pipH)_2[MoS_4].x\ pip \qquad (4.10)$$
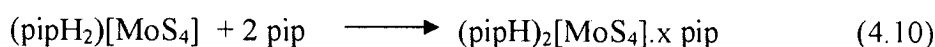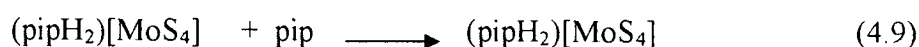
A simple cation exchange methodology (method C in Scheme VI) has been used in the present work for isolation of few organic ammonium tetrathiometalates. The two highly insoluble complexes of $[MS_4]^{2-}$ namely $(dbtmen)[MoS_4]$ and $(dbtmen)[WS_4]$ have been isolated in nearly quantitative yields by reacting $(dbtmen)Br_2\cdot2H_2O$ with the corresponding diammonium salts in aqueous media in 1:1 molar stoichiometry. The reaction between $(dbtmen)Br_2\cdot2H_2O$ and the corresponding ammonium salts of $[MoS_4]^{2-}$ and $[WS_4]^{2-}$ is shown below.

$$(dbtmen)Br_2\cdot2H_2O + (NH_4)_2[MS_4] \rightarrow \ \underline{\mathbf{31}}\ or\ \underline{\mathbf{32}} \ \ + 2\ NH_4Br \qquad (4.11)$$
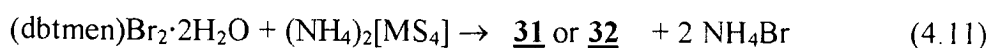
The previously reported complexes like $(CTA)_2[MoS_4]$ and $[(PhCH_2)N(C_2H_5)_3]_2[MoS_4]$ [72-73,81-82] have been synthesized using identical reaction protocol.

The chemistry of Mo/W-S has been extended to the corresponding oxochromates considering their structural similarities with thiometalates and extensive applications in material science and organic synthesis. A convenient

extensive applications in material science and organic synthesis. A convenient synthetic route for preparation of the two organic diammonium oxochromates is described in the present work. The reaction of an aqueous $(enH_2)Cl_2$ solution with $K_2[CrO_4]$ or $K_2[Cr_2O_7]$ in a 1:1 mole ratio readily affords the complexes $(enH_2)[CrO_4]$ **33** and $(enH_2)[Cr_2O_7]$ **34** in good yields and the product formation can be represented as shown below.

$$K_2[CrO_4] \ + \ (enH_2)Cl_2 \ \longrightarrow \ (enH_2)[CrO_4] + 2\,KCl \qquad (4.12)$$

$$K_2[Cr_2O_7] \ + \ (enH_2)Cl_2 \ \longrightarrow \ (enH_2)[Cr_2O_7] + 2\,KCl \qquad (4.13)$$

The more soluble KCl remains in solution and the organic diammonium chromates crystallize out from the reaction mixture. The reaction of $(NH_4)_2[CrO_4]$ or $(NH_4)_2[Cr_2O_7]$ with $(enH_2)Cl_2$ also affords the isolation of two chromates in good yields. Like in tetrathiometalates, the base promoted cation exchange method can also be used for oxochromates. The reaction of ammonium chromate with en leads to the formation of $(enH_2)[CrO_4]$. In this reaction the weaker base ammonia is replaced by the stronger base en resulting in product formation.

4.2 Reactivity studies

The reactivity characteristics of tetrathiometalates complexes have been investigated in this work. The reactions of $[MS_4]^{2-}$ (M= Mo, W) with different reagents are summarized in Scheme VII.

MS₃ $[R_4N]_2[MS_4]$ $[Ph_4P]_2[MS_4]$

H^+ $[R_4N]^+$ $2\ [Ph_4P]$

$[Zn(en)_3]^{2+}$ $(NH_4)_2[MS_4]$ $[Cu(en)_2]^{2+}$

$[Zn(en)_3][MS_4]$ (M = Mo or W) $[Cu(en)_2][MS_4]$

$[Ni(en)_3]^{2+}$ $[Cu(NH_3)_4]^{2+}$ Organic amine

$[Ni(en)_3][MS_4]$ $[Cu(NH_3)_4][MS_4]$ Organic ammonium$[MoS_4]$
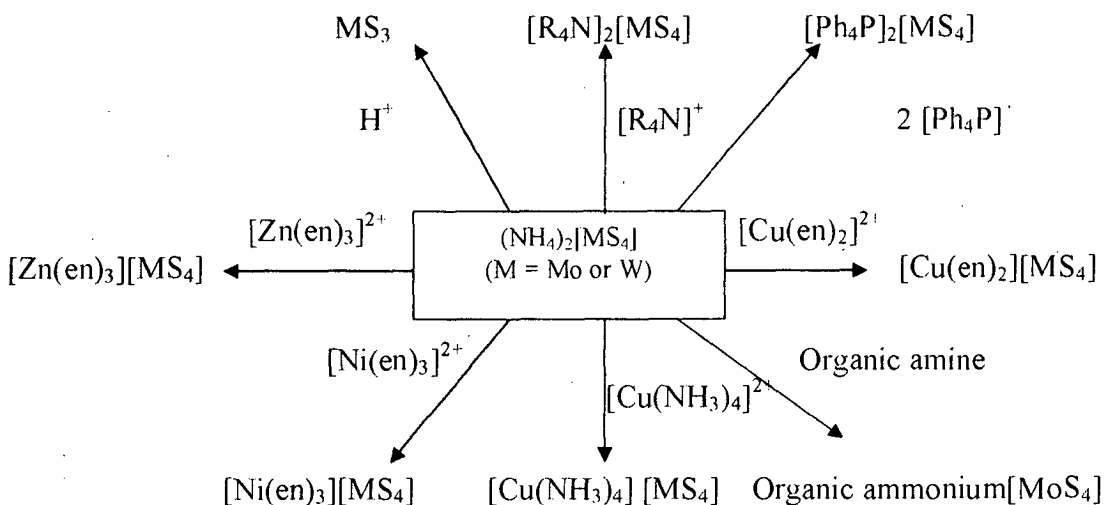
Scheme VII

The formulae for the complexes synthesized in this work have been proposed based on the analytical data (*vide supra*). All the complexes were analyzed satisfactorily. The tetrathiomolybdates synthesized in this work are quite stable in air but undergo surfacial morphological changes over a period of time unlike ammonium tetrathiomolybdate which slowly becomes black on exposure to air. This ageing process has been studied by IR spectral method and the surface change has been attributed to the slow decomposition of ammonium tetrathiomolybdate in air, via an induced electron transfer reaction, resulting in the formation of the dinuclear $[Mo_2O_2S_6]^{2-}$ complex. Most of the complexes are less soluble in water and insoluble in organic solvents like acetonitrile, dichloromethane etc but freely dissolve in aqueous ammoni- cal medium forming coloured solution. It is interesting to note that, among all the new organic ammonium tetrathiometalate complexes synthesized, the two complexes viz (dbtmen)[MoS₄] **31** and (dbtmen)[WS₄] **32** are highly insoluble in most common solvents like water, ammonia, NaOH, CH₃CN, CH₂Cl₂, etc. It can be

noted that the two reported complexes viz. $[(PhCH_2)N(C_2H_5)_3]_2[MoS_4]$ [72-73,81-82] and $(CTA)_2MoS_4]$ [72-73] which contain twenty-six and thirty-eight carbons each are soluble in organic solvents. The solubility of benzyltriethylammonium tetrathiomolybdate makes it useful as a sulfur-transfer reagent in organic synthesis for the formation of novel organo-sulfur compounds under mild reaction conditions. It appears that, the use of bulkier cations is essentially to enhance the solubility in organic solvents. This suggests that the solubility of organic ammonium salts in organic solvents can be improved by increasing the bulkiness of the cation in other words by increasing the number of carbon atoms. Interestingly this does not happen with the two complexes viz **31** and **32** which contain the bulkier dication $(dbtmen)^{2+}$ with twenty carbons each. Both **31** and **32** are highly insoluble in aqueous and non-aqueous solvents. The three bulkier cations $[(PhCH_2)N(C_2H_5)_3]^+$, $[CTA]^+$ and $(dbtmen)^{2+}$ contains fully alkylated organic cations and differ prepared in this work.

The existence of thiometalates as tetrahedral dianionic $[MX_4]^{2-}$ (M = Mo, W; X = O, S) compounds in the alkaline media is well documented [47,207]. In the present work, several new complexes have been isolated in alkaline media. The facile formation of $[MX_4]^{2-}$ complexes in alkaline media not only indicates the stability of the $[MX_4]^{2-}$ core in basic solution. Acidification of $[MoS_4]^{2-}$ results in formation of the insoluble MoS_3 as the ultimate product [15] [Scheme VII]. The condensation of $[MoS_4]^{2-}$ under controlled acidification to form polynuclear complexes like $[Mo_2OS_7]^{2-}$, $[Mo_2O_2S_9]^{2-}$, $[Mo_2S_{11}]^{2-}$ etc is well known [208,209]. The reactivity of $[MoS_4]^{2-}$ complexes with acids like hydrochloric have been studied in the present work. It is observed that the acidification of all the new complexes containing $[MoS_4]^{2-}$ core results in formation of the black insoluble MoS_3 as the ultimate product which exhibit featureless IR spectrum. Thus these complexes can be used as good precursors for the preparation of sulfide materials.

$$[MoS_4]^{2-} \xrightarrow[\text{excess}]{H^+} MoS_3 \downarrow \qquad (4.14)$$
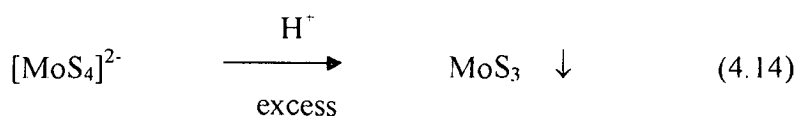
The reaction of an ammonical solution of organic ammonium tetrathiomolybdate with an aqueous solution of [Ni(en)$_3$]Cl$_2$.2H$_2$O in 1:1 stoichiometry resulted in the formation of the previously reported [Ni(en)$_3$][MoS$_4$][75] in quantitative yields. Müller and coworkers have shown that the reaction of aqueous Ni(II) with [MS$_4$]$^{2-}$ (M=Mo, W) in a 1:2 mole ratio, in the presence of an organic cation like (PPh$_4$)$^+$ leads to the formation of the bis tetrathiometalato complex of Ni(II) namely (PPh$_4$)$_2$[Ni(MS$_4$)$_2$], wherein the thiometalate functions as a bidentate ligand [48]. However, the use of a coordinatively saturated Ni complex like [Ni(en)$_3$]$^{2+}$ results in the formation of the complex [Ni(en)$_3$][MoS$_4$] where [MoS$_4$]$^{2-}$ functions as a dianion. This can also indicates that [MoS$_4$]$^{2-}$ is a weaker ligand as compared to en for Ni(II). [Ni(en)$_3$][MoS$_4$] is highly insoluble and unlike other organic ammonium tetrathiomolybdates, does not dissolve in ammonia or excess organic amine. The high insoluble nature of [Ni(en)$_3$][MoS$_4$] in many solvents constitutes a method for the convenient estimation of Mo content of [MoS$_4$]$^{2-}$ in variety of a organic ammonium tetrathiomolybdates. The high insoluble nature of [Ni(en)$_3$][MoS$_4$] seems to be the driving force for the formation of this product even under solvothermal conditions [66]. The Mo content of several new and earlier reported ammonium tetrathiomolybdate complexes can be estimated by reacting the ammonical solutions of [MoS$_4$]$^{2-}$ complexes with an aqueous solution of [Ni(en)$_3$]Cl$_2$.2H$_2$O in 1:1 stoichiometry. For example, an aqueous ammonical solution of (enH$_2$)[MoS$_4$] (pH = 11.5) on reaction with an aqueous solution of [Ni(en)$_3$]Cl$_2$.2H$_2$O (pH = 11.26) resulted in the quantitative formation of [Ni(en)$_3$][MoS$_4$]. Due to lack of solubility of benzyltriethylammonium and cetyltrimethyl ammonium tetrathiomolybdate in aqueous medium, their reaction with aqueous [Ni(en)$_3$]Cl$_2$.2H$_2$O were carried out in CH$_3$CN. The formation of [Ni(en)$_3$][MoS$_4$] in aqueous as well as in non aqueous solvents indicates the generality of this method. The gravimetric estimation of Mo as Pb[MoO$_4$] and S as BaSO$_4$ [210] is well known. The methods described previously for the estimation of Mo and S involve several steps thus making them very cumbersome. Instead the method developed in the present work is rapid and simple as addition of [Ni(en)$_3$]Cl$_2$.2H$_2$O to [MoS$_4$]$^{2-}$ solution results in the quantitative formation of [Ni(en)$_3$][MoS$_4$]. The analytical data for tetrathiomolybdates obtained by using this method is presented in Table 4.2.1. These values add credence to the proposed formulas based on C,H,N and S analytical data.

Table 4.2.1 Analytical data for tetrathiomolybdates

Compound	Mol. Formula	% MoS$_4$ found	% MoS$_4$ calc.
(NH$_4$)$_2$[MoS$_4$]	H$_8$N$_2$MoS$_4$	85.85	86.23
(Et$_2$NH$_2$)$_2$[MoS$_4$]	C$_8$H$_{24}$N$_2$MoS$_4$	59.88	60.18
(piperidium)$_2$[MoS$_4$]	C$_{10}$H$_{24}$N$_2$MoS$_4$	55.05	56.54
(trienH$_2$)[MoS$_4$]	C$_6$H$_{20}$N$_4$MoS$_4$	59.90	60.19
(1,4-bnH$_2$)[MoS$_4$]	C$_4$H$_{14}$N$_2$MoS$_4$	70.67	71.31
(1,6-hxnH$_2$)[MoS$_4$]	C$_6$H$_{18}$N$_2$MoS$_4$	63.35	65.47
(1,4-dmpH$_2$)[MoS$_4$]	C$_6$H$_{16}$N$_2$MoS$_4$	65.40	65.86
(dabcoH)$_2$[MoS$_4$]	C$_{12}$H$_{26}$N$_4$MoS$_4$	49.75	49.75
(1,2-pnH$_2$)[MoS$_4$]	C$_3$H$_{12}$N$_2$MoS$_4$	72.90	74.64
(enH$_2$)[MoS$_4$]	C$_2$H$_{10}$N$_2$MoS$_4$	77.33	78.31
(1,3-pnH$_2$)[MoS$_4$]	C$_3$H$_{12}$N$_2$MoS$_4$	74.59	74.64
(tmenH$_2$)[MoS$_4$]	C$_6$H$_{18}$N$_2$MoS$_4$	65.07	65.47
(dienH$_2$)[MoS$_4$]	C$_4$H$_{15}$N$_3$MoS$_4$	67.76	68.06
(pipH$_2$)[MoS$_4$]	C$_4$H$_{12}$N$_2$MoS$_4$	71.37	71.77
(trenH$_2$)[MoS$_4$]·H$_2$O	C$_6$H$_{22}$N$_4$OMoS$_4$	57.40	57.42
(trenH$_2$)[MoS$_4$]	C$_6$H$_{20}$N$_4$MoS$_4$	59.50	60.19
[(PhCH$_2$)N(C$_2$H$_5$)$_3$]$_2$[MoS$_4$]	C$_{26}$H$_{14}$N$_2$MoS$_4$	36.62	36.82
[(CTA)]$_2$[MoS$_4$]	C$_{38}$H$_{84}$N$_2$MoS$_4$	28.06	28.26

Thus the new method described here in is rapid and convenient for the estimation of [MoS$_4$] content in tetrathiomolybdate complexes. The complexes like (trienH$_2$)[MoS$_4$], (trenH$_2$)[MoS$_4$]·H$_2$O are derived from the isomeric polyamines trien and tren having four N atoms each. The correct formulation of these complexes has been achieved by use of above method. Thus based on analytical data, it can be predicted that out of four N atoms in the above polyamines, only two N atoms are protonated while other two are free. The method works well for formulation of other complexes like (dienH$_2$)[MS$_4$], which contains three N atoms out of which two are protonated. The use of organic diamines in base promoted cation exchange reaction results in the formation of diprotonated ammonium cations, except dabco and trans-1,2-cn. However in case of cyclic diamine like dabco, it is singly protonated. Out of

two N atoms, only one N atom is protonated. The correct formulation of the complex was arrived as $(dabcoH)_2[MoS_4]$ based on the analytical data obtained by using this method. If dabco is diprotonated, then the formula of the complex would have been $(dabcoH_2)[MoS_4]$. The expected % $[MoS_4]$ in $(dabcoH_2)[MoS_4]$ is 65.46 % is different from that of the observed % $[MoS_4]$ (45.75 %). However the observed % $[MoS_4]$ of 45.75 % is in good agreement with the expected value (45.75 %) for $(dabcoH)_2[MoS_4]$. Thus an important conclusion, which has been drawn from this method, is that the reactivity of soluble tetrathiomolybdates with the aqueous solution containing $[Ni(en)_3]^{2+}$ ions to form quantittave highly insoluble $[Ni(en)_3][MoS_4]$ can be used to formulate new complexes containinig $[MoS_4]$ core. The reactivity characteristics of a few of the $[WS_4]^{2-}$ complexes with $[Ni(en)_3]Cl_2.2H_2O$ has been also studied and analytical data is presented in Table 4.2.2.

Table 4.2.2 Analytical data for tetrathiotungstates

Compound	Mol. Formula	% WS$_4$	
		found	calc.
$(NH_4)_2[WS_4]$	$H_8N_2WS_4$	88.99	89.65
$(enH_2)[WS_4]$	$C_2H_{10}N_2WS_4$	82.28	83.39
$(1,3-pnH_2)[WS_4]$	$C_3H_{12}N_2WS_4$	79.33	80.38
$(1,2-pnH_2)[WS_4]$	$C_3H_{12}N_2WS_4$	77.96	80.38
$(tmenH_2)[WS_4]$	$C_6H_{18}N_2WS_4$	72.59	72.52
$(dienH_2)[WS_4]$	$C_4H_{15}N_3WS_4$	74.0	74.79
$(pipH_2)[WS_4]$	$C_4H_{12}N_2WS_4$	75.97	78.06
$(1,4-dmpH_2)[WS_4]$	$C_6H_{16}N_2WS_4$	72.50	72.86
$(1,4-bnH_2)[WS_4]$	$C_4H_{14}N_2WS_4$	76.59	77.58
$(trienH_2)[WS_4]$	$C_6H_{20}N_4WS_4$	59.90	60.19
$(dabcoH)_2[WS_4]$	$C_{12}H_{26}N_4WS_4$	57.92	57.96

The reaction of an aqueous ammonical solution of tetrathiotungstate complexes with an aqueous of $[Ni(en)_3]Cl_2.2H_2O$ resulted in the formation of the insoluble yellow $[Ni(en)_3][WS_4]$ complex. The correct formulation of the complex like $(dabcoH)_2[WS_4]$ explains credibility of the method in W-S chemistry. The

experimental % [WS$_4$] for (dabcoH)$_2$[WS$_4$] is 57.96 % which is in good agreement with the observed percentage of 57.92 %. The reaction between [Ni(en)$_3$]Cl$_2$.2H$_2$O and [MS$_4$]$^{2-}$ is shown below:

$$[MS_4]^{2-} \text{(aq or org)} + [Ni(en)_3]^{2+} \text{(aq)} \longrightarrow [Ni(en)_3][MS_4] \downarrow \quad (4.15)$$
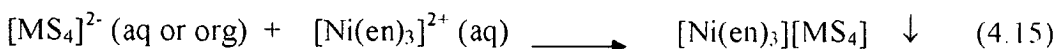
Both [Ni(en)$_3$][MoS$_4$] and [Ni(en)$_3$][WS$_4$] were characterized by elemental analysis, IR-Raman spectroscopy and X-ray powder diffractometry. The IR spectra of [Ni(en)$_3$][MoS$_4$] and [Ni(en)$_3$][WS$_4$] are similar indicating that the two complexes are isostructural. The IR spectra of two complexes are presented in Fig 4.2.1. In the middle IR region, several intense bands can be assigned to presence of en moiety in both the complexes. The sharp bands around 3300 cm^{-1} in the N-H region reveal that the organic amine en is free unlike en in (enH$_2$)[MoS$_4$] which becomes broad at around 3000 cm^{-1}. The characteristic asymmetric stretching vibration (ν_3) for Mo=S band in [Ni(en)$_3$][MoS$_4$] occurs at 471 cm^{-1} while W=S band in [Ni(en)$_3$][WS$_4$] is observed at 457 cm^{-1}. The X-ray powder diffractograms of two complexes [Ni(en)$_3$][MoS$_4$] and [Ni(en)$_3$][WS$_4$] are identical exhibiting intense sharp peaks adds further credence for the isostructural nature of these complexes. The X-ray powder pattern of [Ni(en)$_3$][MoS$_4$] is presented in the Fig. 4.2.2. Ni-Mo and Ni-W sulfide catalysts synthesized by decomposition of Ni-impregnated thiometalates and their HDS activity have been recently reported in the literature [37]. In this context the above two complexes readily obtained by reacting [Ni(en)$_3$]Cl$_2$.2H$_2$O with corresponding [MoS$_4$]$^{2-}$ and [WS$_4$]$^{2-}$ can serve as good precursors for synthesis of Ni-Mo and Ni-W-S catalysts.

The reactivity of Cu(II) with [MoS$_4$]$^{2-}$ complexes is becoming an intense area of research in clinical and biological sciences. The ammonium tetrathiomolybdate interacts with copper and has been recently employed to reduce excess copper in patients with Wilson disease [157-158]. The reaction between Cu (II) and (NH$_4$)$_2$[MS$_4$] has been reported to form polymeric [NH$_4$CuMS$_4$]$_n$ complexes [135]. Here Cu (II) is reduced by an aqueous solution of (NH$_4$)$_2$[MS$_4$] to Cu (I). In this context, to understated the effect of organic amines in reduction of Cu (II) to Cu(I) and also due to the biological applications of tetrathiometalates, the reactions of
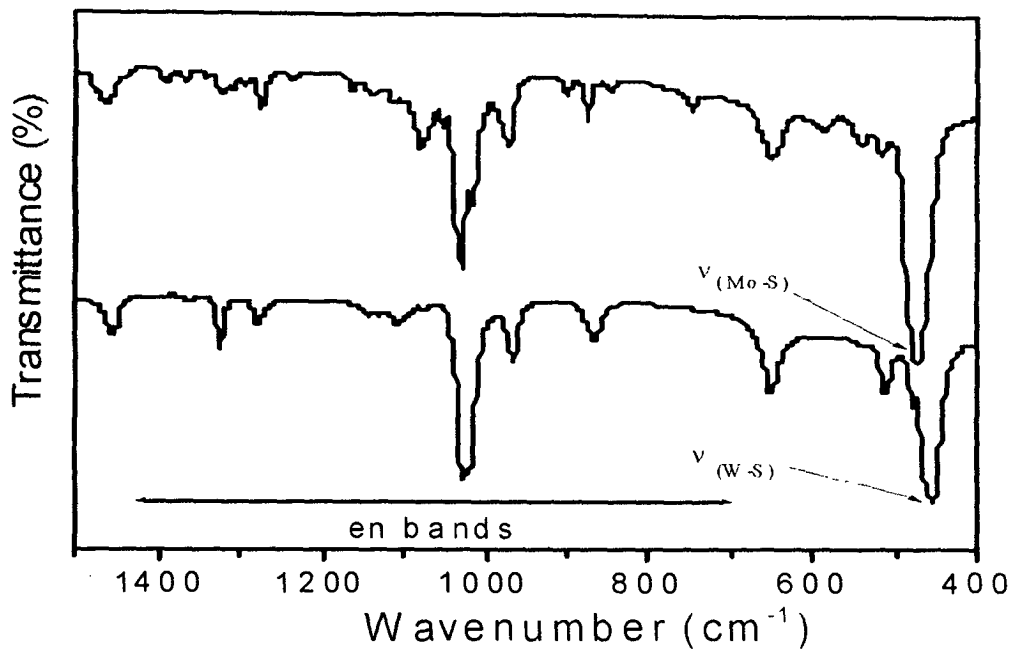
Fig. 4.2.1 IR spectra (a) [Ni(en)$_3$][MoS$_4$] (b) [Ni(en)$_3$][WS$_4$]
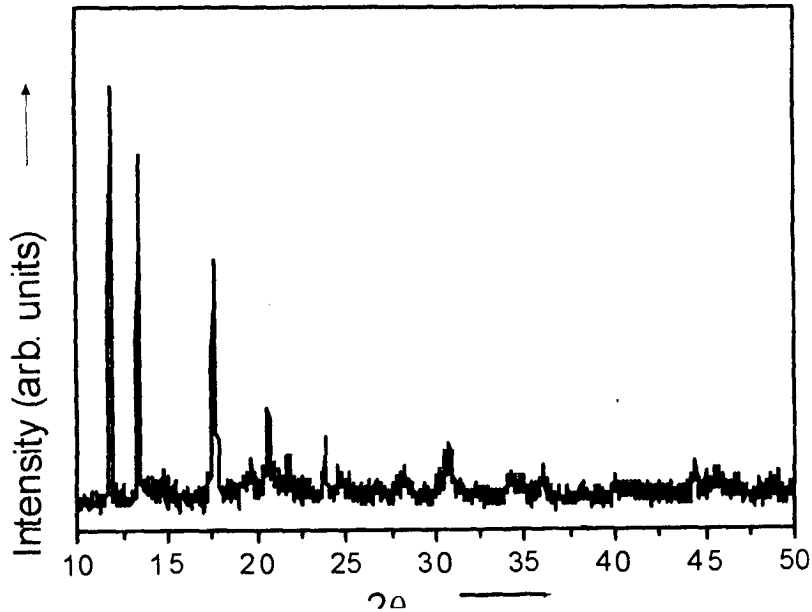
Fig. 4.2.2 XRD powder pattern of [Ni(en)$_3$][MoS$_4$]

Cu(II) with $(NH_4)_2[MoS_4]$ and $(NH_4)_2[WS_4]$ in the presence of organic diamine such as en has been investigated in the present work. The reaction of Cu (II) salt like copper sulfate pentahydrate with excess of en results in formation of dark blue en coordinated $[Cu(en)_2]^{2+}$ complex. The subsequent addition of aqueous solution of $(NH_4)_2[MoS_4]$ or $(NH_4)_2[WS_4]$ to the alkaline solution results in formation of corresponding heterometallic complexes namely $[Cu(en)_2][MoS_4]$ (red) or $[Cu(en)_2][WS_4]$ (yellow) complexes. The formation of Cu(II) complexes can be shown as below.

$$[Cu(en)_2]^{2+} + (NH_4)_2[MS_4] \rightarrow [Cu(en)_2][MS_4] \downarrow \qquad (4.16)$$
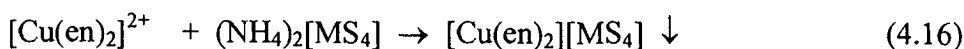
The absence of metal source Cu(II) in this reaction results in the formation of **1** and **2** as discussed in chapter 3. Both $[Cu(en)_2][MoS_4]$ and $[Cu(en)_2][WS_4]$ complexes obtained by reacting $(NH_4)_2[MS_4]$ with Cu (II) in 1: 1 (1Cu: 1MS$_4$) (M=Mo or W) are characterized by IR-Raman, electron spin resonance spectroscopy and X-ray diffractometry. The IR spectra of $[Cu(en)_2][MoS_4]$ and $[Cu(en)_2][WS_4]$ are presented in Fig 4.2.3. The spectra of both the complexes are similar indicating that both are isostructural. The several intense bands in the middle IR region can be assigned to the organic en molecules. The sharp intense signal at around 3277 cm^{-1} in $[Cu(en)_2][MoS_4]$ and at 3283 cm^{-1} in $[Cu(en)_2][WS_4]$ can be assigned to the N-H vibration of coordinated en. The presence of $[MoS_4]$ core in $[Cu(en)_2][MoS_4]$ is evidenced from the appearance of the characteristic asymmetric vibration (v_3) for Mo=S bond which occurs at 467 cm^{-1}. For $[Cu(en)_2][WS_4]$, the characteristic W=S asymmetric vibration (v_3) occurs at 453 cm^{-1} indicating the presence of $[WS_4]^{2-}$ dianion. The spectroscopic data for $[Cu(en)_2][MS_4]$ is given in Table 4.2.3 The isostructural nature of these complexes gets further credence from X-ray powder patterns depicted in Fig 4.2.4. The ESR spectra of the complexes suggest that Cu in both the complexes is in II oxidation state and is not reduced by thiometalate to Cu (I) in presence of en. Similarly the reaction of $[Cu(NH_3)_4]^{2+}$, with aqueous solution of $(NH_4)_2[MS_4]$ (M = Mo or W) in 1:1 stoichiometric ratio resulted in the formation fine crystalline powders of $[Cu(NH_3)_4][MoS_4]$ and $[Cu(NH_3)_4][WS_4]$ complexes. For $[Cu(NH_3)_4][MoS_4]$, the characteristic asymmetric vibration (v_3) occurs at 458 cm^{-1} while for $[Cu(NH_3)_4][WS_4]$, this signal is observed at 451 cm^{-1}.
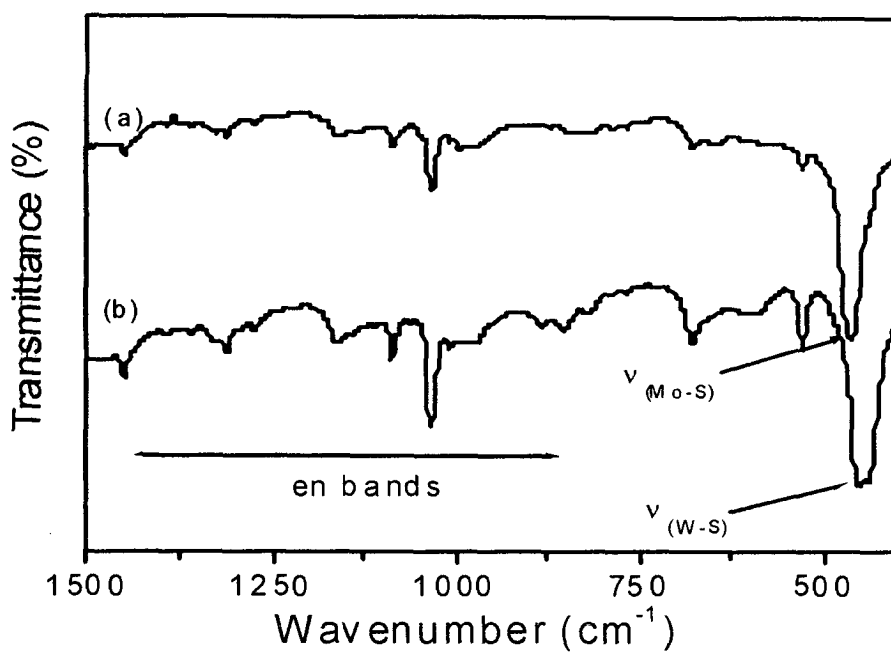
Fig. 4.2.3 IR spectra of (a) $[Cu(en)_2][MoS_4]$ and (b) $[Cu(en)_2][WS_4]$
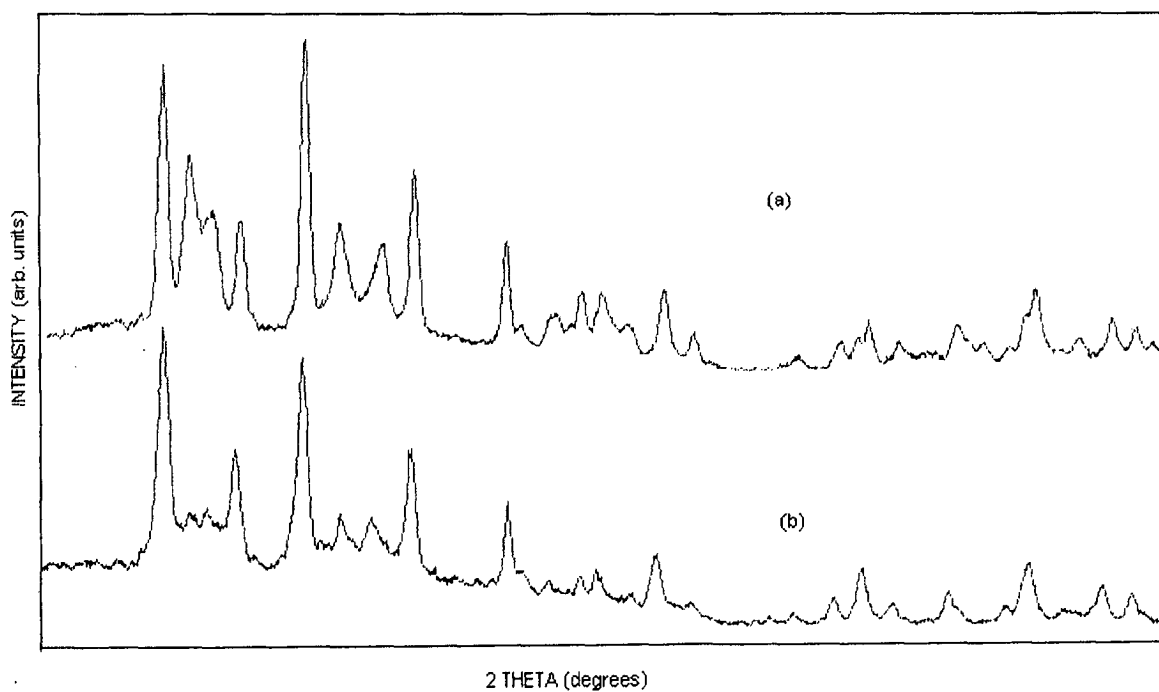
Fig. 4.2.4 XRD powder patterns of (a) $[Cu(en)_2][MoS_4]$ and (b) $[Cu(en)_2][WS_4]$

4.2.3 Yield and spectroscopic data for heterometallic tetrathiometalates

Compound	Yield (%)	IR bands (in cm^{-1})	Raman Bands (in cm^{-1})
[Ni(en)$_3$][MoS$_4$]	99	3293, 3252, 3145, 2929, 2880, 1586, 1464, 1258, 1080, 1030, 974, 876, 652, 518, 478 (v_3)	474, 456, 172.
[Ni(en)$_3$][WS$_4$]	98	3294, 3240, 3137, 2928, 2876, 1564, 1457, 1325, 1280, 1108, 1027, 967, 868, 653, 514, 457 (v_3).	481, 467, 178
[Cu(en)$_2$][MoS$_4$]	84	3277, 3214, 1564, 1312, 1159, 1087, 1033, 677, 467 (v_3)	455, 444, 257, 221, 185
[Cu(en)$_2$][WS$_4$]	88	3283, 3196, 15 65, 1322, 1452, 1312, 1159, 1088, 1035, 970, 858, 679, 602, 453 (v_3)	467, 258, 221, 186, 154, 88
[Cu(NH$_3$)$_4$][MoS$_4$]	89	3165, 1391, 1109, 898, 458(v_3)	-
[Cu(NH$_3$)$_4$][WS$_4$]	90	3167, 1393, 1109, 891, 451(v_3)	-
[Zn(en)$_3$][MoS$_4$]	90	3292, 3243, 3127, 2929, 2875, 1560, 1462, 1328, 1279, 1107, 1003, 954, 855, 630, 468 (v_3)	-
[Zn(en)$_3$][WS$_4$]	92	3298, 3292, 3244, 3126, 2927, 2875, 1560, 1462, 1327, 1278, 1107, 1004, 962, 630, 455 (v_3)	-

To understand the reactivity of Cu(II) with tetrathiometalates in the presence of organic amines, the reactions of [Cu(en)$_2$]$^{2+}$ and (NH$_4$)$_2$[MoS$_4$] has been investigated and summarized in Scheme VIII. On addition of an aqueous solution of [MoS$_4$]$^{2-}$ to a complex ion [Cu(en)$_2$]$^{2+}$ in 2:1 mole ratio, resulted in the formation of water insoluble complex [Cu(en)$_2$][MoS$_4$] and unreacted (NH$_4$)$_2$[MoS$_4$]. The addition of an aqueous solution of [Ni(en)$_3$]Cl$_2$.H$_2$O (1 mmol) resulted in the quantitative formation of insoluble orange red [Ni(en)$_3$][MoS$_4$] complex. Further the reaction between [Cu(en)$_2$]$^{2+}$ and (NH$_4$)$_2$[MoS$_4$] in 2:1 mole ratio resulted only in formation of one mole of red insoluble [Cu(en)$_2$][MoS$_4$] suggesting that one mole of [Cu(en)$_2$]$^{2+}$ has remained unreacted. On addition of another mole of (NH$_4$)$_2$[MoS$_4$] to unreacted [Cu(en)$_2$]$^{2+}$ in the above mixture, resulted in formation of [Cu(en)$_2$][MoS$_4$]. Thus the reaction of between [Cu(en)$_2$]$^{2+}$ and (NH$_4$)$_2$[MoS$_4$] takes place only in 1:1 mole ratio and results in the formation of the insoluble [Cu(en)$_2$][MoS$_4$] complex.

$(NH_4)Cu[MoS_4]$

$\uparrow$

Cu^{2+}

$\frac{1}{2}[Cu(en)_2][MoS_4] + \frac{1}{2}(NH_4)_2[MoS_4]$ $\xleftarrow{\frac{1}{2}[Cu(en)_2]^{2+}}$ $\boxed{(NH_4)_2[MoS_4]}$ $[Cu(en)_2]^{2+}$

$\downarrow \frac{1}{2}[Ni(en)_3]Cl_2 \cdot 2H_2O$ $\qquad 2[Cu(en)_2]^{2+}$ $\qquad\qquad [Cu(en)_2][MoS_4]$

$\frac{1}{2}[Ni(en)_3][MoS_4]$ $\qquad\qquad$ $\downarrow (NH_4)_2[MoS_4]$ $\nearrow$

$\qquad\qquad\qquad$ $[Cu(en)_2][MoS_4] + [Cu(en)_2]^{2+}$
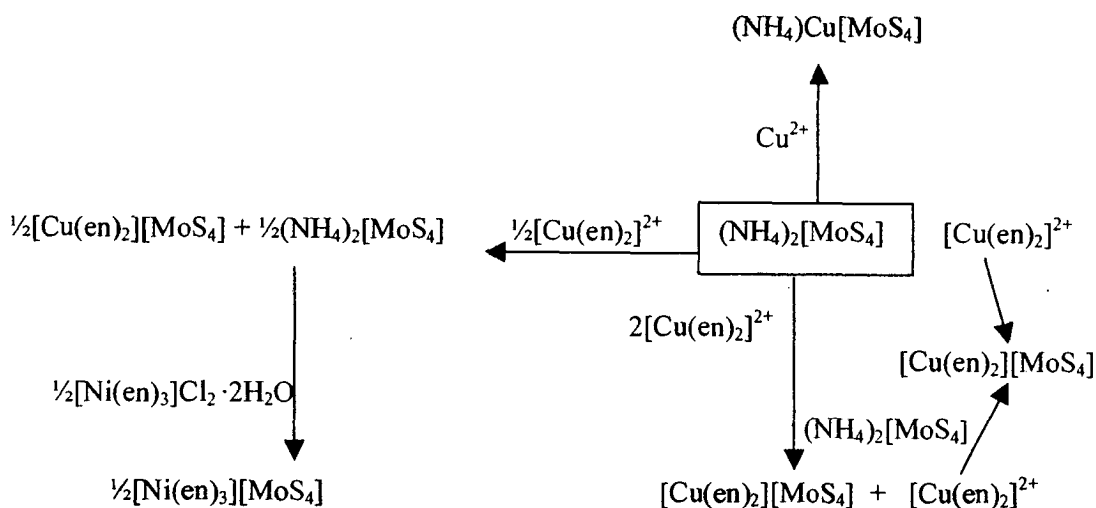
Scheme VIII

The reactivity of $(NH_4)_2[MoS_4]$ with other divalent metal ion such as Zn(II) in presence of an organic amine en has been also investigated. The reaction between aqueous solution of $(NH_4)_2[MoS_4]$ and Zn (II) salt in presence en results in the formation of insoluble orange red $[Zn(en)_3][MoS_4]$ while $(NH_4)_2[WS_4]$ under identical conditions forms the yellow complex $[Zn(en)_3][WS_4]$ as shown below:

$$[Zn(en)_3]^{2+} + (NH_4)_2[MS_4] \rightarrow [Zn(en)_3][MS_4] \qquad (4.17)$$
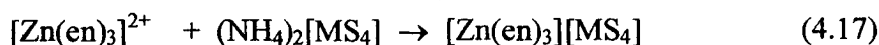
The complexes have been characterized by IR spectroscopy, which gave the preliminary evidence for the presence of $[MS_4]$ core (M=Mo, W) in these complexes. The spectroscopic data for Zn (II) complexes is in Table 4.2.3.

4.3 Single crystal X-ray diffractometry

Intensity data of tetrathiomolybdate, tetrathiotungstate and chromates were collected on different instruments. The structures were solved with direct methods using SHELXS-97 [211] and refinement was carried out against F^2 using SHELXS-97 [212]. All non-hydrogen atoms were refined using anisotropic displacement parameters. The hydrogen atoms were located in difference map but positioned with idealized geometry and refined using the riding model with fixed isotropic displacement parameters. The technical details of data acquisition and some selected refinement results for the complexes structurally characterized in this work are summarized in APPENDIX-II. Some of the structures have been already been published and their CCDC numbers are also given. The compounds crystallize in different space groups as shown below (Table 4.3.1).

Table 4.3.1 Crystal systems and space groups of tetrathiometalates

Organic ammonium [WS$_4$]		Crystal system and Space group	Organic ammonium [MoS$_4$]	
(enH$_2$)[WS$_4$]	**2**	Orthorhombic P2$_1$2$_1$2$_1$	(enH$_2$)[MoS$_4$]	**1**
(N-Me-enH$_2$)[WS$_4$]	**4**	Orthorhombic, P2$_1$2$_1$2$_1$	(N-Me-enH$_2$)[MoS$_4$]	**3**
(tmenH$_2$)[WS$_4$]	**6**	Monoclinic P2$_1$/n	(tmenH$_2$)[MoS$_4$]	**5**
(1,3-pnH$_2$)[WS$_4$]	**8**	Monoclinic P2$_1$/c,	(1,3-pnH$_2$)[MoS$_4$]	**7**
(N,N-dm-1,3-pnH$_2$)[WS$_4$]	**10**	Monoclinic P2$_1$/n	-	
(1,4-bnH$_2$)[WS$_4$]	**12**	Triclinic, P$\bar{1}$	(1,4-bnH$_2$)[MoS$_4$]	**11**
(dienH$_2$)[WS$_4$]	**14**	Orthorhombic Pmmn	(dienH$_2$)[MoS$_4$]	**13**
(dipnH$_2$)[WS$_4$]	**16**	Orthorhombic Pca2$_1$	(dipnH$_2$)[MoS$_4$]	**15**
(trenH$_2$)[WS$_4$]·H$_2$O	**18**	Monoclinic P2$_1$/c	(trenH$_2$)[MoS$_4$]·H$_2$O	**17**
(pipH$_2$)[WS$_4$]	**22**	Monoclinic P2$_1$/c	(pipH$_2$)[MoS$_4$]	**21**
(1,4-dmpH$_2$)[WS$_4$]	**24**	Orthorhombic Pbca	-	
-		Monoclinic C2/c	(2-pipH-1-etNH$_3$)[MoS$_4$]·½ H$_2$O	**27**
(trans-1,2-cnH)$_2$[WS$_4$]	**28**	Monoclinic C2/c	-	
(mipaH)$_2$[WS$_4$]	**29**	Monoclinic C2/c	-	

The crystal structures of all the complexes can be described as consisting of tetrahedral $[MoS_4]^{2-}$ or $[WS_4]^{2-}$ anions which are linked to the organic ammonium cations via weak hydrogen bonding interactions in the form of N-H...S bonds. The average Mo-S bond distances in all the complexes range from 2.179 to 2.187 Å while the W-S bond distances range from 2.185 to 2.1954 Å. The S-M-S bond angles in all the complexes are close to the tetrahedral values and are observed in the range 107-110^0. The N-H...S distances range between 2.348 to 2.567 Å in the investigated tetrathiomolybdates and while the N-H...S distances range from 2.31 to 2.67 Å in tetrathiotungstates. It is observed that an organic ammonium tetrathiomolybdate is isostructural with the corresponding tetrathiotungstate

4.3.1 Crystal structure of complexes 2 - 6

The complex $(enH_2)[WS_4]$ 2 [84] crystallizes in the orthorhombic $P2_12_12_1$ space group with unit cell parameters $a = 8.6401$ (4) Å, $b = 9.3228$ (5) Å, $c = 11.8281$ (7) Å The crystal structure of 2 consists of $(enH_2)^{2+}$ cations and $[WS_4]^{2-}$ dianions as depicted in Fig 4.3.1. Complex 2 is isostructural to the earlier reported 1 [75]. The substitution of Mo by W has resulted in a slight increase in the unit cell volume as unit cell volume for $(enH_2)[WS_4]$ is 952.75 (9) Å^3 and for $(enH_2)[MoS_4]$ is 938.7 (9) Å^3. The slight increase in unit cell volume can be explained on the basis of the larger size of W. The lattice parameters show very small increase in a, b and c values compared to the Mo analogue ($a = 8.582$ Å, $b = 9.276$ (5) Å, $c = 11.792$ (5) Å. The S-W-S angles in $(enH_2)[WS_4]$ range between 108.77 (7) to 110.08 ^{0} indicating slight distortion of the WS$_4$ tetrahedron (Table 4.3.2). The average S-W-S bond angle is 109.47 ^{0}. W-S bond distances vary from 2.1851 (14) to 2.1943 (6) Å with a mean W-S bond distance of 2.1893 Å. In 2, nine short H-bonding contacts ranging from 2.43 to 3.00 Å between the S atom of $[WS_4]^{2-}$ anion and H atom of $(enH_2)^{2+}$ cation are observed (Table 4.3.3). The crystal-packing diagram of 2 showing the three-dimensional hydrogen-bonding network is displayed in Fig 4.3.2. In complex 2, $[WS_4]^{2-}$ rods run along the crystallographic 'c' axis while $(enH_2)^{2+}$ are sliding along 'a' axis. In this network, each $[WS_4]^{2-}$ anion is surrounded by five $(enH_2)^{2+}$ cations while each $(enH_2)^{2+}$ is surrounded by four $[WS_4]^{2-}$ anions (Fig. 4.3.3). Atom S3 is 2.1943 (13) Å from central atom W and is involved in three short contacts with H atom of $(enH_2)^{2+}$ cation. One of the N-H...S distance is equal to sum of the van der
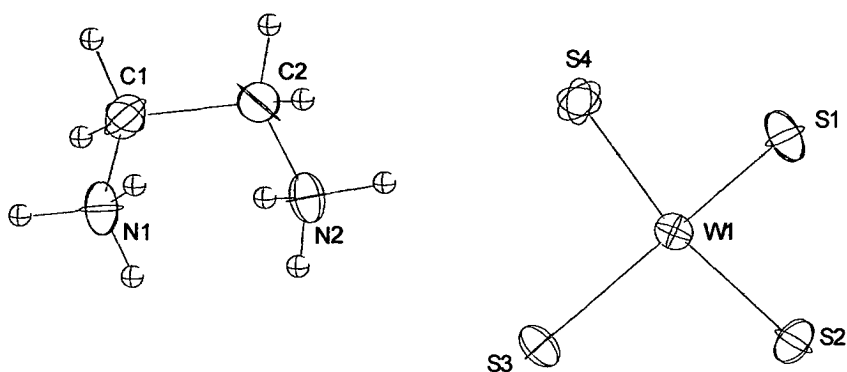
Fig. 4.3.1 Crystal structure of (enH$_2$)[WS$_4$] **2** with labeling and displacement ellipsoids drawn at the 50% probability level.

Fig. 4.3.2 Three dimensional hydrogen bonding network in (enH$_2$)[WS$_4$] **2** with view along 'c' axis (hydrogen bonding is shown as dashed lines). Colour codes; H purple, C black, W grey, S yellow, N blue.

Table 4.3.2 Selected geometric parameters (Å, °) for (enH₂)[WS₄] **2**

W(1)-S(4)	2.1851 (14)	N(1)-C(1)	1.483 (8)
W(1)-S(1)	2.1927 (14)	C(2)-N(2)	1.468 (8)
W(1)-S(2)	2.1852 (13)	C(1)-C(2)	1.500 (9)
W(1)-S(3)	2.1943 (13)		
S(4)-W(1)-S(2)	109.23 (6)	S(4)-W(1)-S(3)	109.78 (6)
S(4)-W(1)-S(1)	108.66 (7)	S(2)-W(1)-S(3)	109.60 (6)
S(2)-W(1)-S(1)	109.46 (6)	S(1)-Mo(1)-S(3)	110.08 (6)
N(1)-C(1)-C(2)	112.8 (5)	N(2)-C(2)-C(1)	113.3 (5)

Table 4.3.3 Hydrogen-bonding geometry (Å, °) for (enH₂)[WS₄] **2**

D-H...A	d(D-H)	d(H...A)	d(D...A)	<DHA	Symmetry code
N1-H1...S4	0.890	2.48	3.274	149.4	3/2 −x, 2-y, 1/2+z
N1-H1...S2	0.890	3.00	3.478	115.3	3/2 −x, 2-y, 1/2+z
N1-H2...S1	0.890	2.44	3.300	161.4	1+x, y, z
N1-H3...S2	0.890	2.69	3.370	134.1	1/2+x, 3/2-y, 1-z
N1-H3...S3	0.890	2.80	3.558	143.6	1/2+x, 3/2-y, 1-z
N2-H1...S4	0.890	2.47	3.254	146.5	
N2-H1...S3	0.890	2.85	3.424	123.8	
N2-H2...S1	0.890	2.43	3.301	165.5	1/2-x, 2-y,1/2+z,
N2-H3...S3	0.890	2.55	3.385	157.1	1/2+x, 3/2-y, 1-z

D = Donor; A = Acceptor

Waals radii of S and H atoms (3.00 Å) while the remaining are all less than 3.00 Å [213]. The difference Δ between the shortest and longest W-S bond distance is 0.0092 Å.

Complex **4** crystallizes in the non-centrosymmetric space group $P2_12_12_1$ [88] with all atoms in general positions (Fig 4.3.4). The geometric parameters of **4** are in good agreement with those in other tetrathiotungstates like e.g. $(enH_2)[WS_4]$ **2** [84]. The WS_4 tetrahedron is slightly distorted and the W-S bonds vary from 2.1727(15) to 2.2064(14) Å (average: 2.1919 Å) (Table 4.3.4). Two of the bonds are shorter while the other two are longer than the average value. This feature can be explained based on the strength and number of S···H bonding interactions. The resulting hydrogen bonding network is shown in Fig 4.3.5. Seven S···H contacts ranging from 2.308 to 2.915 Å (Table 4.3.5) are observed in **4**, less than the nine contacts in **2** (range: 2.43 to 3.0 Å), which can be attributed to the replacement of one H atom bound to N2 by a CH_3 group. All the S...H distances in **4** are shorter than 3.00 Å the sum of the van der Waals radii of S and H [213] and six of them are shorter by about 0.30 Å indicating strong interactions. The S(1), S(3) and S(4) atoms have two short contacts each while S(2) has only one such contact. The single short contact with a relatively long S···H distance of 2.685 Å is accompanied by a small N-H-S angle (134.57°) and may explain the shortest W-S2 bond of 2.1727(15) Å. In contrast, the two shortest S···H separations (2.308 and 2.383 Å) accompanied by the largest N-H···S angles (163.91 and 161.91°) can account for the longest W-S(1) distance of 2.2064(14) Å. The intermediate W-S bond lengths of 2.1850 and 2.2037 Å can be similarly explained based on the strengths of the H-bonding interactions. The difference between the longest and the shortest W-S bond Δ is 0.0337 Å and is considerably larger than the difference observed in $(enH_2)[WS_4]$ **2** (0.0092). This feature indicates that the further alkylation of an organic diamine can increase the distortion of the WS_4 tetrahedron.

The structure of compound of $(N-Me-enH_2)[MoS_4]$ **3** can be explained similarly as for its W analogue. Compound **3** is composed of tetrahedral $[MoS_4]^{2-}$ dianions and $(N-Me-enH_2)^{2+}$ cations (Fig 4.3.6). The MoS_4 tetrahedron is moderately distorted as seen from S-Mo-S bond angles, which range between 108.36 (6) and 110.65 (5)° (Table 4.3.6). The Mo-S distances vary from 2.1635 (14) to 2.2014 (12) Å
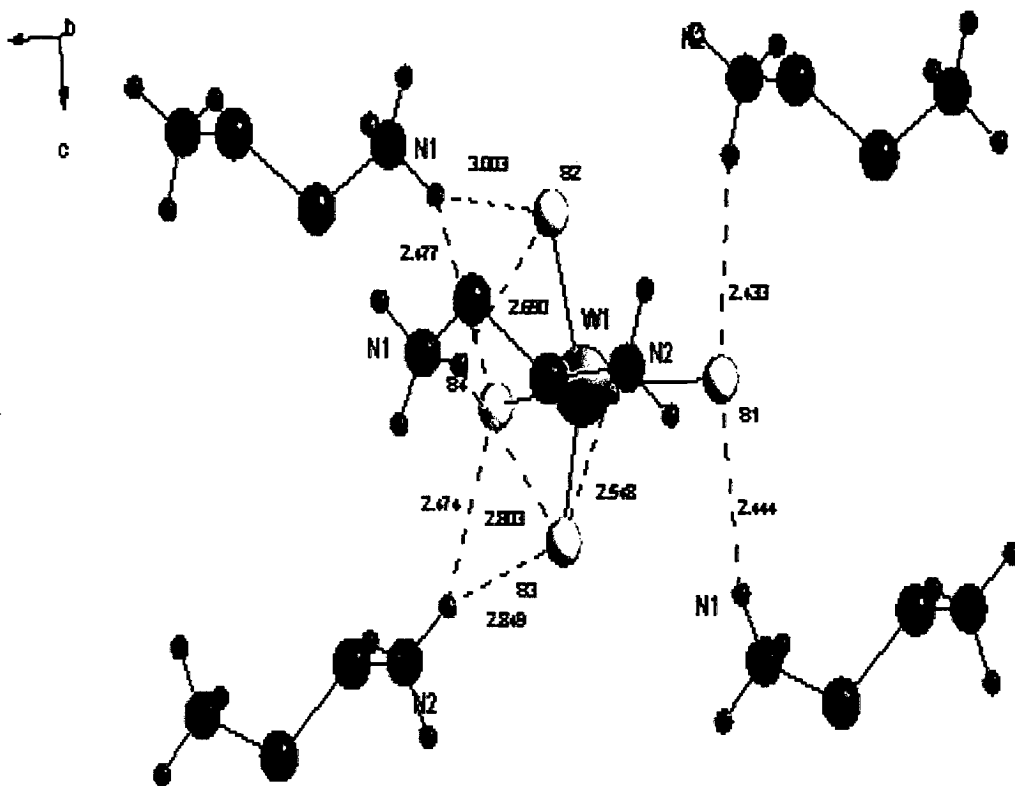
Fig. 4.3.3 Hydrogen bond labels in (enH₂)[WS₄] **2** (each anion is surrounded by five cations) Colour codes; H purple, C black, W grey, S yellow, N blue. H atoms attached to carbon are omitted for clarity.

Fig. 4.3.4 Crystal structure of (N-Me-enH₂)[WS₄] **4** with labeling and displacement ellipsoids drawn at the 50% probability level.

Fig. 4.3.5 Crystal structure of (N-Me-enH₂)[WS₄] **4** with view along 'c' axis (hydrogen bonding is shown as dashed lines). Colour codes; H purple, C black, W grey, S yellow, N blue.

Table 4.3.4   Selected geometric parameters (Å, °) for (N-Me-enH$_2$)[WS$_4$] **4**

W(1)-S(2)	2.1727 (15)	N(1)-C(1)	1.476 (8)
W(1)-S(4)	2.1850 (14)	C(1)-C(2)	1.513 (9)
W(1)-S(3)	2.2037 (15)	C(2)-N(2)	1.475 (8)
W(1)-S(1)	2.2064 (14)	N(2)-C(3)	1.501 (8)
S(2)-W(1)-S(4)	110.64 (6)	S(2)-W(1)-S(1)	109.27 (6)
S(2)-W(1)-S(3)	108.28 (6)	S(4)-W(1)-S(1)	108.97 (6)
S(4)-W(1)-S(3)	109.73 (6)	S(3)-W(1)-S(1)	109.93 (6)
N(1)-C(1)-C(2)	110.2 (5)	C(2)-N(2)-C(3)	111.7 (6)
N(2)-C(2)-C(1)	110.6 (5)		

Table 4.3.5 Hydrogen-bonding geometry (Å, °) for (N-Me-enH$_2$)[WS$_4$] **4**

D-H...A	d(D-H)	d(H...A)	d(D...A)	<DHA	Symmetry code
N1-H1...S1	0.940	2.383	3.290	161.91	x-1/2, -y+3/2, -z+1
N1-H1...S4	0.940	2.915	3.404	113.75	x-1/2, -y+3/2, -z+1
N1-H2...S4	0.940	2.650	3.376	134.46	
N1-H2...S2	0.940	2.685	3.411	134.57	
N1-H3...S3	0.940	2.536	3.259	133.99	-x+1/2, -y+1, z-1/2
N2-H1...S3	0.940	2.388	3.198	144.18	x+1/2, -y+3/2, -z+1
N2-H2...S1	0.940	2.308	3.222	163.91	-x+3/2, -y+1, z-1/2

D = Donor; A = Acceptor

with a mean bond distance of 2.183Å. All the structural parameters of the $[MoS_4]^{2-}$ anion in **3** are in good agreement with those of the (enH$_2$)[MoS$_4$] **1** [75]. The elongation of Mo-S bond distances in **3** can be attributed to the observed eight short intermolecular hydrogen bonding interactions (N-H...S) which are spread over the range 2.362 to 3.003 Å between tetrahedral $[MoS_4]^{2-}$ dianions and (MeenH$_2$)$^{2+}$ cations (Table 4.3.7). The difference Δ between the longest and shortest Mo-S bond length in **3** is 0.0379 Å and is larger than 0.0111 Å that observed in earlier reported **1** indicating that the further alkylation of en can increase the considerable distortion of the MoS$_4$ tetrahedron.

The crystal structure of the complex (tmenH$_2$)[MoS$_4$] **5** [79], consists of tetrahedral $[MoS_4]^{2-}$ dianions and (tmenH$_2$)$^{2+}$ dications (Fig 4.3.7). All C-C and C-N bond distances are in good agreement with those reported in compounds containing (tmenH$_2$)$^{2+}$ [214]. The S-Mo-S bond angles are nearly identical with values ranging from 109.08(3) to 109.72(3)° pointing to a very small distortion form ideal tetrahedral geometry. The Mo-S bond distances vary from 2.1694(8) to 2.1983(8) Å with an average of 2.1838 Å (Table 4.3.8). Here the Mo-S2 bond distance of 2.1983(8) Å is considerably longer than the average Mo-S bond length of 2.1838. The organic cation (tmenH$_2$)$^{2+}$ and $[MoS_4]^{2-}$ are linked to each other through weak hydrogen bonding interactions. The organic cation in compound **5** carries a single H atom and three alkyl groups on each N. In view of the fewer number of H atoms in this compound, only four short intermolecular contacts are observed (Fig 4.3.8). The $[MoS_4]^{2-}$ anions run along the 'b' axis. The S2 atom is involved in two short contacts while the S1 and S3 atoms make one relatively short contact each (Table 4.3.9). No S4···H contact is observed. The N-H···S bond angles range from 129.62 and 143.82° with the larger values found for S2···H. It is well documented that short S···H distances that are accompanied by large N-H···S angles yield the strongest H bonds. Therefore, the interpretation of the differing Mo-S bond lengths is straightforward. The shortest Mo-S bond is found to the S4 atom (2.1694(8) Å) which has no S4···H bond. Furthermore, S2 has two contacts with N-H···S2 angles around 140° that weaken the Mo-S interaction to yield the longest Mo-S bond of 2.1983(8) Å. Intermediate Mo-S distances are observed to S1 and S3 with one S···H contact each and N-H···S angles

Table 4.3.6 Selected geometric parameters (Å, °) for (N-Me-enH₂)[MoS₄] **3**

Mo(1)-S(2)	2.1635 (14)	N(1)-C(1)	1.490 (6)
Mo(1)-S(4)	2.1798 (14)	C(1)-C(2)	1.501 (7)
Mo(1)-S(3)	2.1997 (13)	C(2)-N(2)	1.472 (6)
Mo(1)-S(1)	2.2014 (12)	N(2)-C(3)	1.488 (7)
S(2)-Mo(1)-S(4)	110.65 (5)	S(2)-Mo(1)-S(1)	109.37 (6)
S(2)-Mo(1)-S(3)	108.36 (6)	S(4)-Mo(1)-S(1)	108.91 (5)
S(4)-Mo(1)-S(3)	109.78 (6)	S(3)-Mo(1)-S(1)	109.76 (5)
N(1)-C(1)-C(2)	109.8 (4)	C(2)-N(2)-C(3)	112.5 (4)
N(2)-C(2)-C(1)	111.3 (4)		

Table 4.3.7 Hydrogen-bonding geometry (Å, °) for (N-Me-enH₂)[MoS₄] **3**

| D-H...A	d(D-H)	d(H...A)	d(D...A)	<DHA	Symmetry code
N1-H1...S3	0.890	2.418	3.254	156.56	-x+3/2, -y+1, z+1/2
N1-H2...S4	0.890	2.663	3.368	136.84	
N1-H2...S2	0.890	2.746	3.411	132.57	
N1-H3...S1	0.890	2.442	3.280	157.13	x+1/2, -y+1/2, -z+1
N1-H3...S4	0.890	2.868	3.388	118.84	x+1/2, -y+1/2, -z+1
N2-H1...S3	0.900	2.362	3.190	152.89	x-1/2, -y+1/2, -z+1
N2-H2...S1	0.900	2.377	3.225	157.12	-x+1/2, -y+1, z+1/2
N2-H2...S2	0.900	3.003	3.500	116.55	-x+1/2, -y+1, z+1/2

D = Donor; A = Acceptor
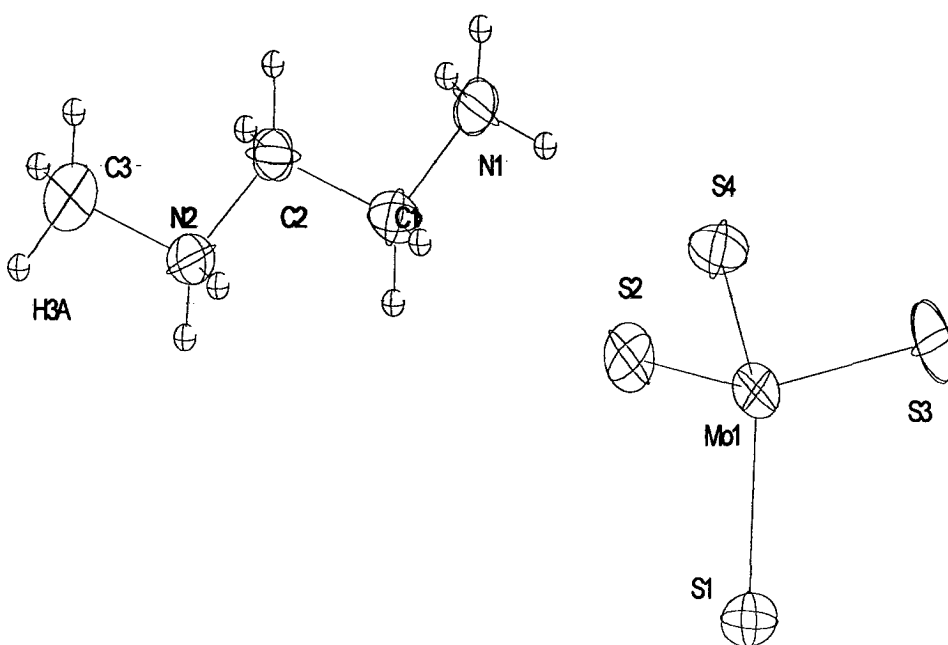
Fig. 4.3.6 Crystal structure of (N-Me-enH$_2$)[MoS$_4$] **3** with labeling and displacement ellipsoids drawn at the 50% probability level.
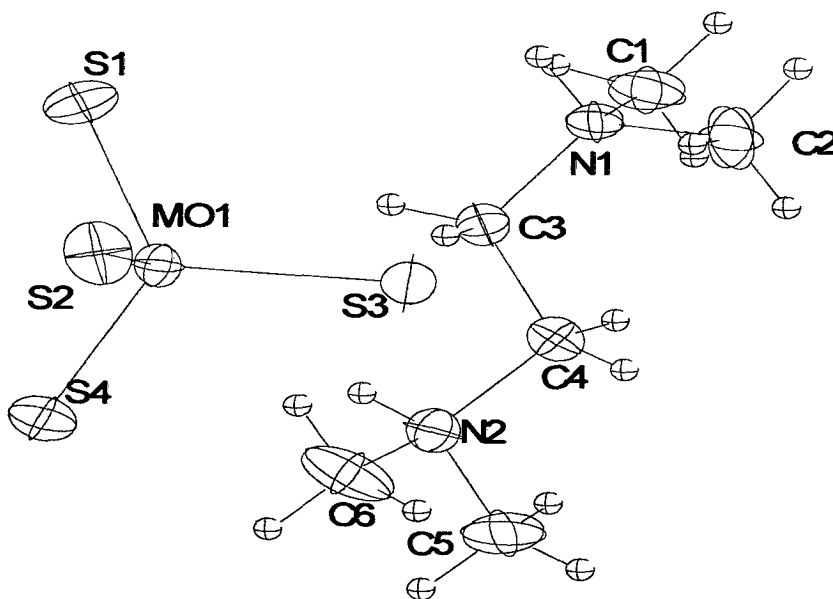
Fig. 4.3.7 Crystal structure of (tmenH$_2$)[MoS$_4$] **5** with labeling and displacement ellipsoids drawn at the 50% probability level.
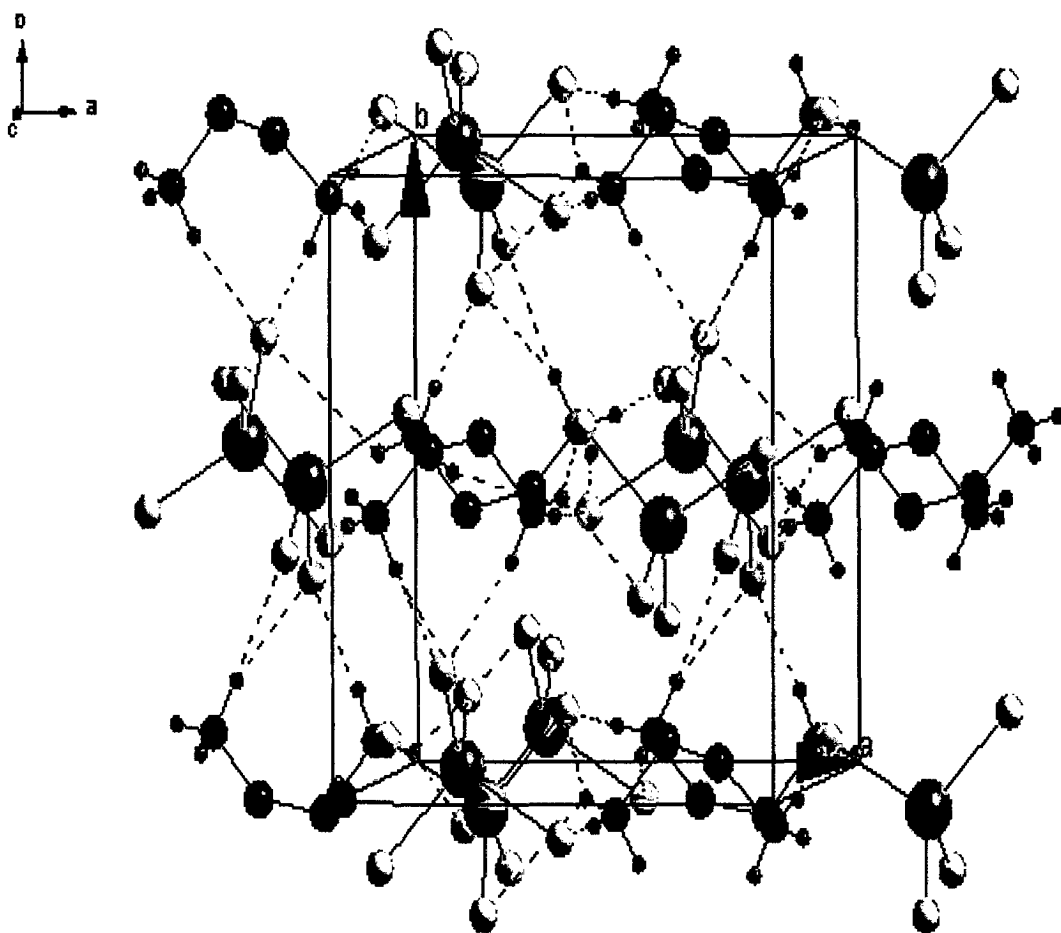
Table 4.3.8 Selected geometric parameters (Å, °) for (tmenH$_2$)[MoS$_4$] **5**

Mo(1)-S(4)	2.1694 (8)	C(1)-N(1)	1.498 (3)
Mo(1)-S(3)	2.1805 (7)	C(2)-N(1)	1.491(3)
Mo(1)-S(1)	2.1870 (7)	N(1)-C(3)	1.497 (3)
Mo(1)-S(2)	2.1983 (8)	C(3)-C(4)	1.511 (4)
C(4)-N(2)	1.497 (3)	N(2)-C(5)	1.485 (3)
N(2)-C(6)	1.488 (3)		
S(4)- Mo(1) -S(3)	109.69 (3)	S(4)- Mo(1) -S(1)	109.59 (3)
S(3)- Mo(1) -S(1)	109.08 (3)	S(4)- Mo(1) -S(2)	109.72 (3)
S(3)- Mo(1) -S(2)	109.57 (3)	S(1)- Mo(1) -S(2)	109.18 (3)
C(2)- N(1) -C(3)	113.3 (2)	C(2)- N(1) –C(1)	111.4 (2)
C(3)- N(1) –C(1)	113.0 (2)	N(1)-C(3)-C(4)	112.1 (2)
N(2)-C(4)-C(3)	111.1 (2)	C(5)-N(2)-C(6)	110.9 (2)
C(5)-N(2)-C(4)	110.6 (2)	C(6)-N(2)-C(4)	112.9 (2)

Table 4.3.9 Hydrogen-bonding geometry (Å, °) for (tmenH$_2$)[MoS$_4$] **5**

D-H...A	d(D-H)	d(H...A)	d(D...A)	<DHA	Symmetry code
N1-H1⋯S1	0.910	2.567	3.267	134.21	
N1-H1⋯S2	0.910	2.757	3.504	140.09	
N2-H1⋯S3	0.910	2.740	3.394	129.62	−x+1, -y+1, -z+1
N2-H1⋯S2	0.910	2.776	3.551	143.82	−x+1, -y+1, -z+1

D = Donor; A = Acceptor

significantly smaller than 140°. In the complex **5**, each [MoS$_4$]$^{2-}$ anion is surrounded by two (tmenH$_2$)$^{2+}$ cations.

Complex (tmenH$_2$)[WS$_4$] **6** [85] is isostructural to its Mo analogue **5**. The crystal structure of **6** is composed of discrete [WS$_4$]$^{2-}$ danions and (tmenH$_2$)$^{2+}$ cations as displayed in Fig 4.3.9. The substitution of Mo by W in **6** has resulted in a slight increase in its volume. The volume for **6** is 1391.5 (2) Å^3 while that of its Mo analogue is 1384.08 (19) Å^3. The S-W-S bond angles are nearly identical with values ranging from 109.13 (5) to 109.85 (6)° with an average bond angle of 109.47° while W-S bond lengths vary from 2.1772 (13) to 2.1995 (13) Å with an average of bond length of 2.1891 Å (Table 4.3.10). Interestingly the longest W-S3 distance of 2.1995 (13) Å is nearly the same as the longest Mo-S distance of 2.1983 (8) found in its Mo analogue. Only four short intermolecular N-H...S contacts are observed in **6** (Table 4.3.11). S3 atom of [WS$_4$]$^{2-}$ involved in two short contacts, S1 and S4 have only one such contact. Interestingly S2 is not involved in any of the four intermolecular contacts. This feature is responsible for short W-S2 bond distance of 2.1771 (13) Å and long W-S3 bond distance of 2.1995 (13) Å. The N-H...S angles in **6** ranges from 131 to 143°. The resulting hydrogen bonded network is shown in Fig. 4.3.10. In both the complexes **5** and **6**, all four S...H distances are less than the sum of the van der Waals radii of S and H [213]. The difference between the shortest and longest W-S bond Δ is 0.0223 and is more 0.0092 in (enH$_2$)[WS$_4$] **2** [84]. This can be attributed to the further alkylation of amine in **6** as compared to en.

4.3.2 Crystal structure description for (1,3-pnH$_2$)[MoS$_4$] **7**, (1,3-pnH$_2$)[WS$_4$] **8** and (N,N'-dm-1,3-pnH$_2$)[WS$_4$] **10**

The crystal structures of three complexes namely (1,3-pnH$_2$)[MoS$_4$] **7** [79], (1,3-pnH$_2$)[WS$_4$] **8** [85] and (N,N'-dm-1,3-pnH$_2$)[WS$_4$] **10** which contain 1,3-pn moiety are discussed together in this section. Both the complexes **7** and **8** are isostructural [79,85]. The structure of (1,3-pnH$_2$)[MoS$_4$] **7** consists of (1,3-pnH$_2$)$^{2+}$ dications and tetrahedral [MoS$_4$]$^{2-}$ dianions (Fig 4.3.11). The C-C and C-N bond lengths are in good agreement with those reported for compounds containing similar cations [215]. The [MoS$_4$] tetrahedron is slightly distorted with S-Mo-S angles
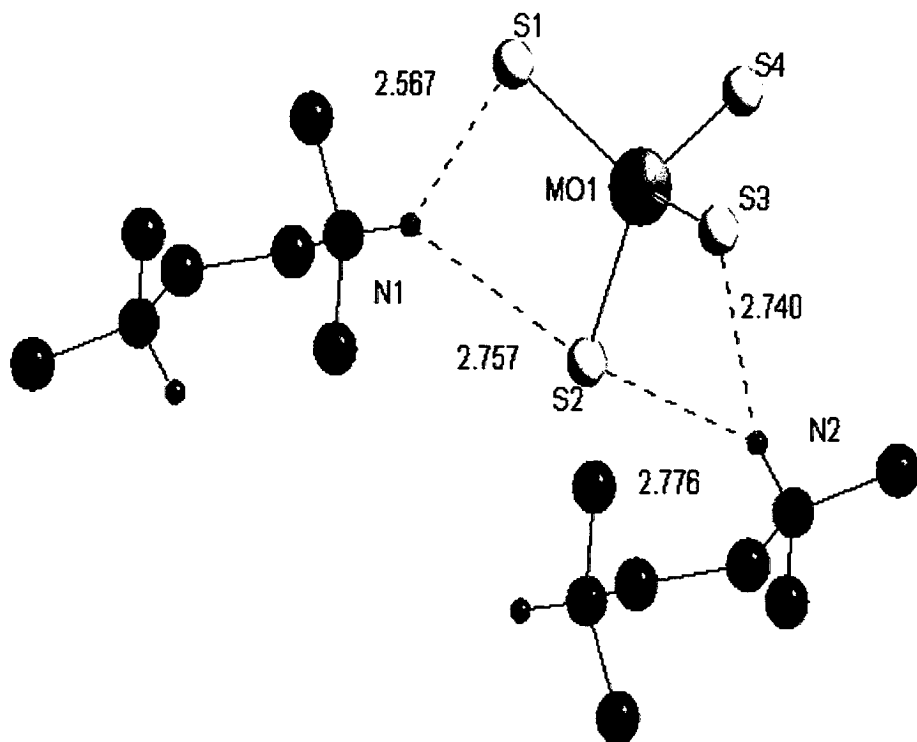
Fig. 4.3.8 Hydrogen bond labels in (tmenH$_2$)[MoS$_4$] **5**. Colour codes; H purple, C black, Mo grey, S yellow, N blue. H atoms attached to carbon are omitted for clarity.
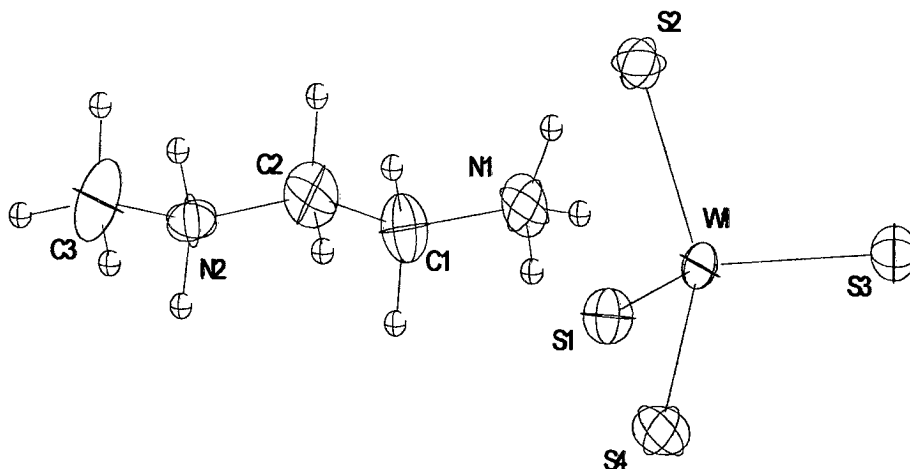

Fig. 4.3.9 Crystal structure of (tmenH$_2$)[WS$_4$] **6** with labeling and displacement ellipsoids drawn at the 50% probability level.
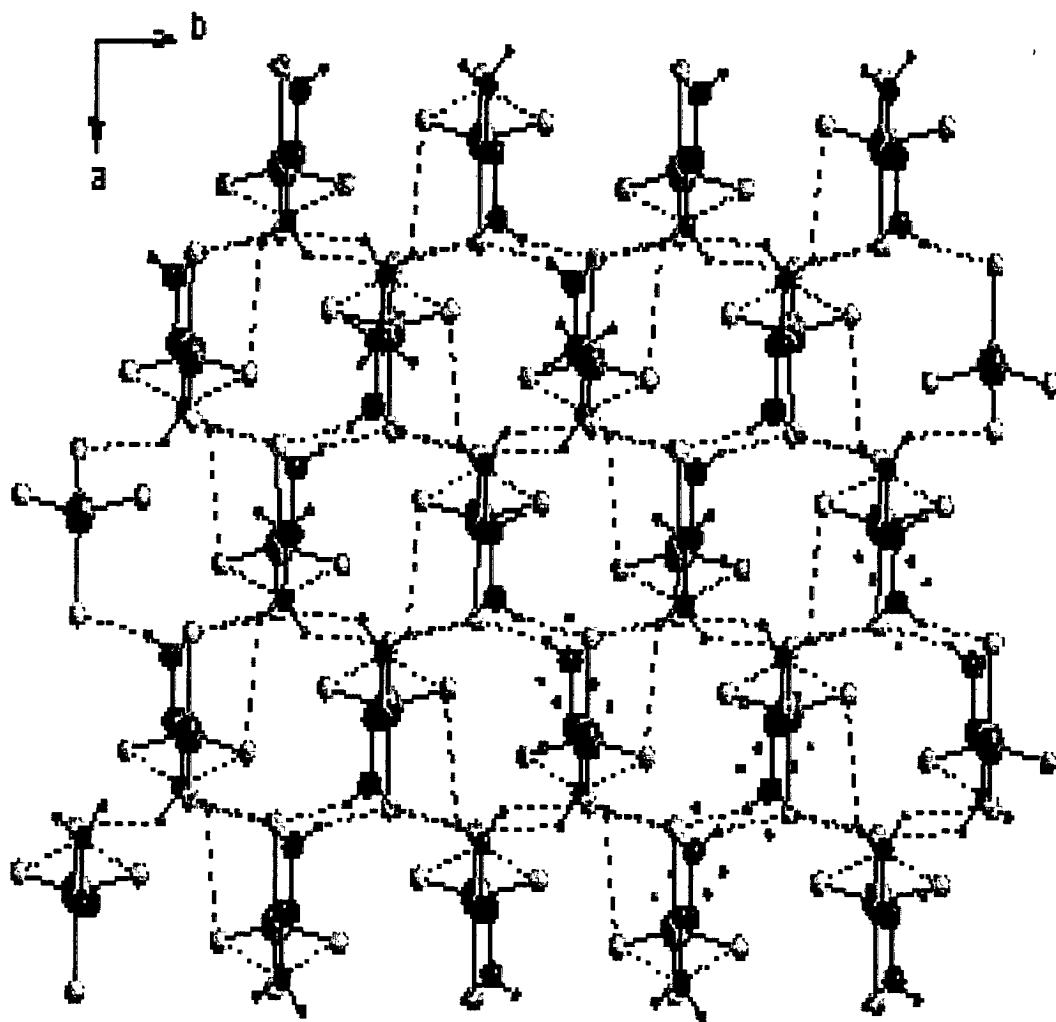
Table 4.3.10 Selected geometric parameters (Å, °) for (tmenH₂)[WS₄] **6**

W(1)-S(2)	2.1772 (13)	C(2)-N(1)	1.490 (6)
W(1)-S(1)	2.1864 (13)	N(1)-C(3)	1.502 (6)
W(1)-S(4)	2.1932 (13)	C(3)-C(4)	1.526 (6)
W(1)-S(3)	2.1995 (13)	N(2)-C(6)	1.487 (6)
C(1)-N(1)	1.485 (7)	N(2)-C(5)	1.492 (7)
S(2)-W(1 -S(1)	109.77 (5)	S(2)-W(1)-S(3)	109.85 (6)
S(2)-W(1)-S(4)	109.49 (5)	S(1)-W(1 -S(3)	109.45 (5)
S(1)-W(1) -S(4)	109.14 (5)	S(4)-W(1) -S(3)	109.13 (5)
C(1)-N(1)-C(1)	110.9 (5)	N(2)-C(4)–C(3)	112.1 (4)
C(1)-N(1)–C(3)	112.9 (4)	C(6)-N(2)-C(5)	111.7 (4)
C(2)-N(1)-C(3)	110.1 (4)	C(6)-N(2)-C(4)	113.4 (4)
N(1)-C(3)-C(4)	110.9 (4)	C(5)-N(2)-C(4)	112.9 (4)

Table 4.3.11 Hydrogen-bonding geometry (Å, °) for (tmenH₂)[WS₄] **6**

D-H...A	d(D-H)	d(H...A)	d(D...A)	<DHA	Symmetry code
N1-H1⋯S1	0.910	2.724	3.387	130.54	
N1-H1⋯S3	0.910	2.802	3.570	142.89	
N2-H1⋯S4	0.910	2.558	3.266	135.10	1–x, 1-y, -z
N2-H1⋯S3	0.910	2.790	3.533	139.59	1–x, 1-y, -z

D = Donor; A = Acceptor

Fig. 4.3.10 Crystal structure of (tmenH₂)[WS₄] **6** with view along 'c' axis (hydrogen bonding is shown as dashed lines). Colour codes; H purple, C black, W grey, S yellow, N blue.
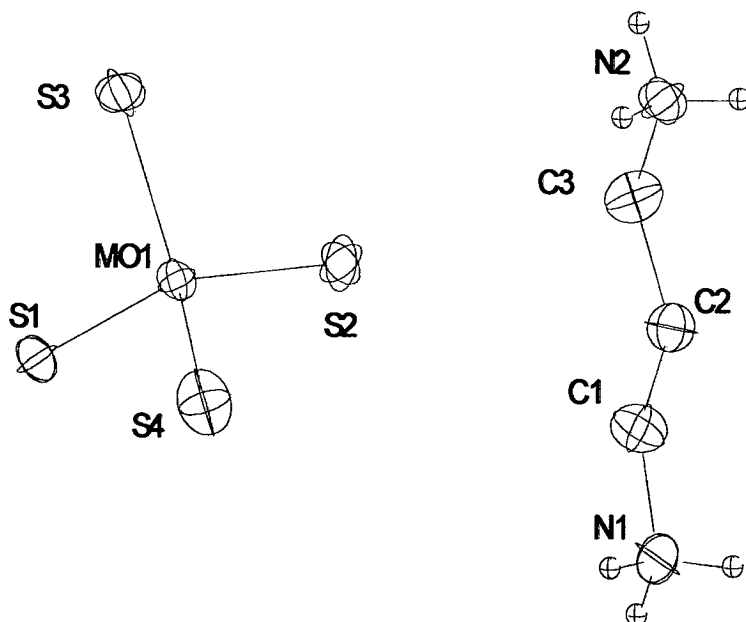

Fig. 4.3.11 Crystal structure of (1,3-pnH₂)[MoS₄] **7** with labeling and displacement ellipsoids drawn at the 50% probability level.

between 108.16(3) and 110.43(3)°. The Mo-S bond lengths range from 2.1699(8) to 2.1882(7) Å with an average of 2.1815 Å. The selected bond lengths and bond angles for $\underline{7}$ are listed in Table 4.3.12. In all ten short intermolecular contacts between the S atoms of $[MoS_4]^{2-}$ and the H atoms of the $(1,3\text{-}pnH_2)^{2+}$ dication ranging from 2.494 to 2.880 Å are observed (Table 4.3.13). In this compound the $(1,3\text{-}pnH_2)^{2+}$ dications and tetrahedral $[MoS_4]^{2-}$ dianions are connected via weak H-bonds. The labeling scheme for H-bonding interactions in $(1,3\text{-}pnH_2)[MoS_4]$ $\underline{7}$ is shown in Fig 4.3.12 The atoms S1 and S3 make three contacts each while the S2 and S4 atoms have two short contacts each. Interestingly, the S3 atom has three contacts at relatively long distances compared to the shortest distance of 2.509 Å made by S1 with the H atom bound to N. The N-H···S bond angles ranging from 117.26 to 162.97° indicate different degrees of S···H bond strengths. The Mo-S3 distance of 2.1699(8) Å is the shortest Mo-S bond and the S3 atom shows the longest S··H separations with the smallest N-H···S angles. Hence, the lengthening of Mo-S bond distances can be attributed to the strength of the H-bonding interactions. In the three dimensional network of $\underline{7}$, the $[MoS_4]^{2-}$ anions run along the 'b' axis and occupy the channels between the surrounding anions (Fig. 4.3.13). Each of the $[MoS_4]^{2-}$ is surrounded by five $(1,3\text{-}pnH_2)^{2+}$ cations which are connected via the observed ten N-H...S contacts which are shorter that the sum of Van der Waals radii of S and H (3.00 Å) [213].

The complex $(1,3\text{-}pnH_2)[WS_4]$ $\underline{8}$ [85] is composed of discrete $(1,3\text{-}pnH_2)^{2+}$ dications and $[WS_4]^{2-}$ anions (Fig 4.3.14). The substitution of Mo by W in $\underline{7}$ has resulted in a slight increase in the unit cell volume as unit cell volume for $\underline{7}$ is 1073.5 (5) Å^3 and that for $\underline{8}$ (1060.2 (1) Å^3). The WS_4 tetrahedron is slightly distorted, with S-W-S bond angles ranging between 108.04 (5) and 110.37 (5)^0 (Table 4.3.14). The W-S bond lengths vary from 2.1798 (12) to 2.1946 (10) Å with an average bond length of 2.1903. The weak intermolecular interactions between H atoms of the $(1,3\text{-}pnH_2)^{2+}$ cation and S atoms of the $[WS_4]^{2-}$ dianion give rise to a three dimensional network in $\underline{8}$ (Fig 4.3.15). The differing W-S bond distances can be due to the different number and strengths of hydrogen bonding contacts between the H atoms attached to the N atoms of the cation and the S atoms of $[WS_4]^{2-}$ anion. In all, seven short intermolecular S...H contacts are observed with N...S distances ranging from 3.3777 (4) to 3.458 (4) Å and N-H...S angles ranging from 124 to 169° in $\underline{8}$ (Table 4.3.15). Atom S3 has one short contact, while the other S atoms have two short
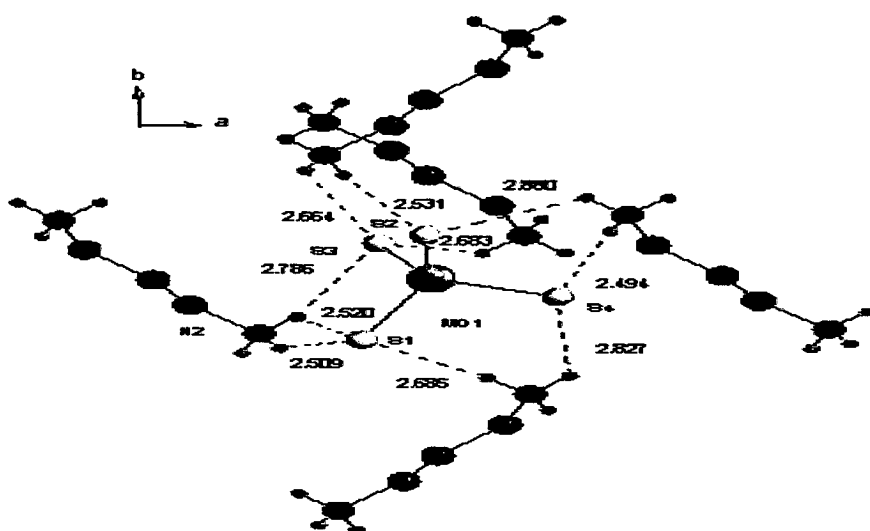
Fig. 4.3.12 Hydrogen bond labels in (1,3-pnH₂)[MoS₄] **7**. Colour codes; H purple, C black, Mo grey, S yellow, N blue. H atoms attached to carbon are omitted for clarity.
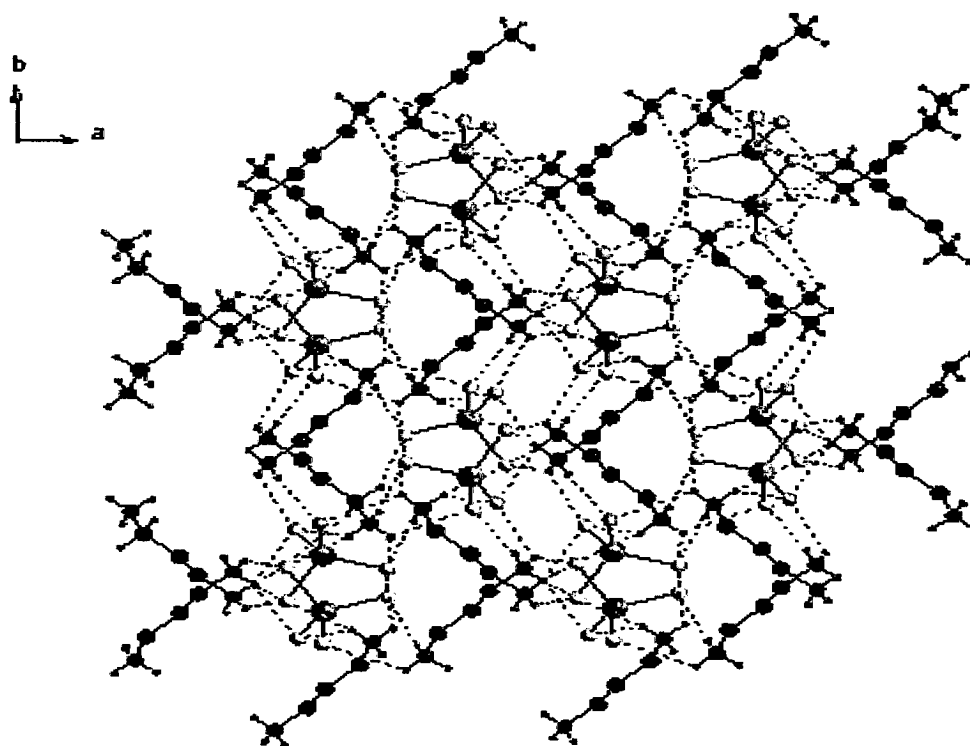
Fig. 4.3.13 Crystal structure of (1,3-pnH₂)[MoS₄] **7** with view along 'c' axis (hydrogen bonding is shown as dashed lines). Colour codes; H purple, C black, Mo grey, S yellow, N blue.

Fig. 4.3.14 Crystal structure of (1,3-pnH$_2$)[WS$_4$] **8** with labeling and displacement ellipsoids drawn at the 50% probability level.

Fig. 4.3.15 Three dimensional hydrogen bonding network in (1,3-pnH$_2$)[WS$_4$] **8** with view along 'a' axis (hydrogen bonding is shown as dashed lines). Colour codes; H purple, C black, W grey, S yellow, N blue.

Table 4.3.12 Selected geometric parameters (Å, °) for (1,3-pnH$_2$)[MoS$_4$] 7

Mo(1)-S(3)	2.1699 (8)	N(1)-C(1)	1.486 (4)
Mo(1)-S(4)	2.1821 (8)	C(1)-C(2)	1.509 (4)
Mo(1)-S(2)	2.1859 (7)	C(2)-C(3)	1.504 (4)
Mo(1)-S(1)	2.1882 (7)	C(3)-N(2)	1.476 (4)
S(3)- Mo(1) -S(4)	110.08 (4)	S(3)- Mo(1) -S(2)	109.27 (3)
S(4)- Mo(1) -S(2)	110.43 (3)	S(3)- Mo(1) -S(1)	108.16 (3)
S(4)- Mo(1) -S(1)	109.40 (3)	S(2)- Mo(1) -S(1)	109.47 (3)
N(1)- C(1) -C(2)	111.2 (3)	C(3)- C(2) -C(1)	111.8 (3)
N(2)- C(3) –C(2)	110.9 (3)		

Table 4.3.13 Hydrogen-bonding geometry (Å, °) for (1,3-pnH$_2$)[MoS$_4$] 7

D-H...A	d(D-H)	d(H...A)	d(D...A)	<DHA	Symmetry code
N1-H1...S4	0.890	2.827	3.454	128.74	–x+1, -y+1, -z+1
N1-H1...S2	0.890	2.880	3.382	117.26	x, -y+1/2, z-1/2;
N1-H2...S4	0.890	2.494	3.347	160.72	x, -y+1/2, z-1/2;
N1-H3...S3	0.890	2.683	3.330	130.42	–x+1, y+1/2, -z+1/2
N1-H3...S1	0.890	2.685	3.369	134.52	–x+1, -y+1, -z+1
N2-H1...S1	0.890	2.509	3.273	144.20	x+1, -y+1/2, z+1/2
N2-H1...S3	0.890	2.664	3.231	122.51	–x+1, -y, -z+1
N2-H2...S1	0.890	2.520	3.277	143.30	x+1, y, z
N2-H2...S3	0.890	2.786	3.416	128.95	x+1, -y+1/2, z+1/2
N2-H3...S2	0.890	2.531	3.392	162.97	–x+1, -y, -z+1

D = Donor; A = Acceptor

Table 4..3.14 Selected geometric parameters (Å, °) for (1,3-pnH₂)[WS₄] **8**

W(1)-S(3)	2.1798 (12)	N(1)-C(1)	1.492 (5)
W(1)-S(4)	2.1931 (12)	C(1)-C(2)	1.508 (6)
W(1)-S(2)	2.1936 (10)	C(2)-C(3)	1.517 (6)
W(1)-S(1)	2.1946 (10)	C(3)-N(2)	1.485 (6)
S(3)- W(1) -S(4)	110.22 (6)	S(3)- W(1) -S(1)	108.04 (5)
S(3)- W(1) -S(2)	109.26 (4)	S(4)- W(1) -S(1)	109.33 (5)
S(4)- W(1) -S(2)	110.37 (5)	S(2)- W(1) -S(1)	109.57 (4)
N(1)- C(1) -C(2)	110.4 (3)	N(2)- C(3) -C(2)	111.0 (4)
C(1)- C(2) –C(3)	111.2 (4)		

Table 4.3.15 Hydrogen-bonding geometry (Å, °) for (1,3-pnH₂)[WS₄] **8**

D-H...A	d(D-H)	d(H...A)	d(D...A)	<DHA	Symmetry code
N1-H1...S1	0.890	2.442	3.284	157.94	1-x, 1-y, 1-z
N1-H1...S3	0.890	2.939	3.430	116.5	1-x, 1/2+y, 3/2-z
N1-H2...S1	0.890	2.432	3.277	158.82	1-x, 1/2+y, 3/2-z
N1-H3...S2	0.890	2.530	3.407	168.54	x, 1+y, z
N2-H1...S4	0.890	2.579	3.357	146.43	–x, 1/2+y, 1/2-z
N2-H1...S2	0.890	2.812	3.394	124.28	–x, 1/2+y, 1/2-z
N2-H2...S4	0.890	2.609	3.458	169.96	
N2-H3...S3	0.890	2.473	3.335	163.25	x, 1/2-y, z-1/2
N2-H3...S1	0.890	2.952	3.377	111.13	

D = Donor; A = Acceptor

contacts each. The W-S bond lengths tend to be longer when the S...H contacts are shorter and N-H...S angles are more linear. Each [WS$_4$]$^{2-}$ anion is surrounded by five cations which are connected via observed nine N-H...S contacts. All the nine H...S distances in **8** are less than sum of van der Waals radii of S and H [213].

(N,N'-dm-1,3-pnH$_2$)[WS$_4$] **10** [88] differs from **7** and **8**, in that contains (N,N'-dm-1,3-pnH$_2$)$^{2+}$ cations unlike (1,3-pnH$_2$)$^{2+}$ in **7** and **8**. Complex **10** crystallizes in space group P2$_1$/n and its structure consists tetrahedral [WS$_4$]$^{2-}$ dianions and (N,N'-dm-1,3-pnH$_2$)$^{2+}$ counter cations (Fig 4.3.16). All C-C and C-N bond lengths are in good with those reported in compounds containing similar cations [216]. The [WS$_4$]$^{2-}$ tetrahedron is slightly distorted (W-S bonds: 2.1771(14) - 2.1992(12) Å, average: 2.1931 Å) and the geometric parameters are comparable to that in (1,3-pnH$_2$)[WS$_4$] **10** [85]. Three of the W-S bonds are longer than the mean value while the fourth W-S bond is shorter (Table 4.3.16). The elongation of the three W-S bonds is accompanied by short N-H···S contacts ranging from 2.424 to 2.960 Å (Table 4.3.17) and all these distances are shorter than the sum of the van der Waals radii of S and H. The extended H bonding network is depicted in Fig 4.3.17. The S···H distances are comparable to those in the related complex (1,3-pnH$_2$)[WS$_4$] (2.43 to 2.81 Å). S(2) has three S···H contacts, S(1) two and S(3)/S(4) each have one such interaction. The W-S(4) bond is very short at 2.1771(14) Å which may be induced by the weak S···H interaction (2.96 Å) and the small N-H···S(4) angle of 131.21°. Also the W-S(3) bond of 2.1980 Å can be explained on the basis of a single S···H contact at 2.479 Å and the N-H···S angle of 154.59°. The W-S(1) distance of 2.1992(12) Å is the longest bond and is associated with the shortest S···H separation (2.424 Å) and the largest N-H···S angle of 175.62°. Although S(2) has three S···H contacts the W-S(2) distance is slightly shorter than W-S(1), which can be explained on the basis of two longer S···H separations with smaller N-H···S angles. The value for Δ is 0.0221 Å and is larger than that observed for (1,3-pnH$_2$)[WS$_4$] (0.0148 Å) [85] indicating the role of the methyl groups to enhance the distortion of the WS$_4$ tetrahedron.
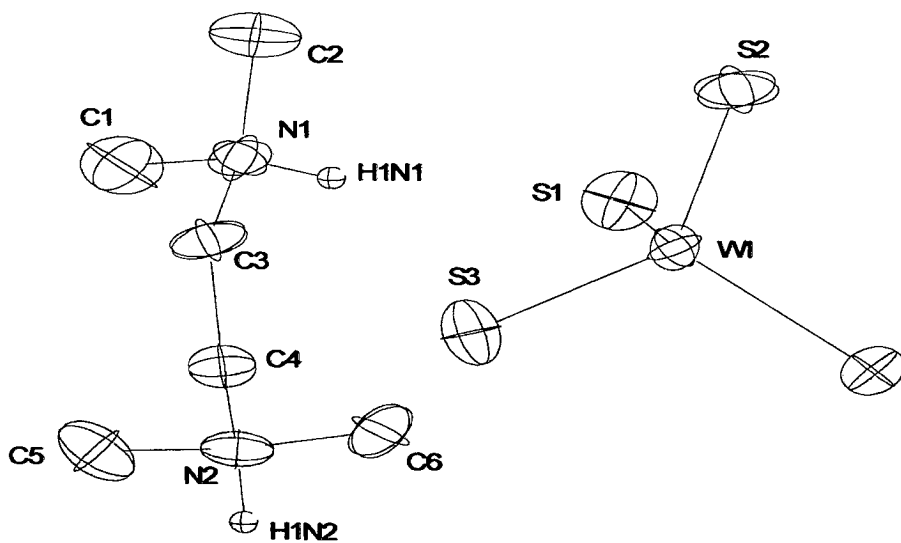
Fig. 4.3.16 Crystal structure of (N,N'-dm-1,3-pnH₂)[WS₄] **10** with labeling and displacement ellipsoids drawn at the 50% probability level.
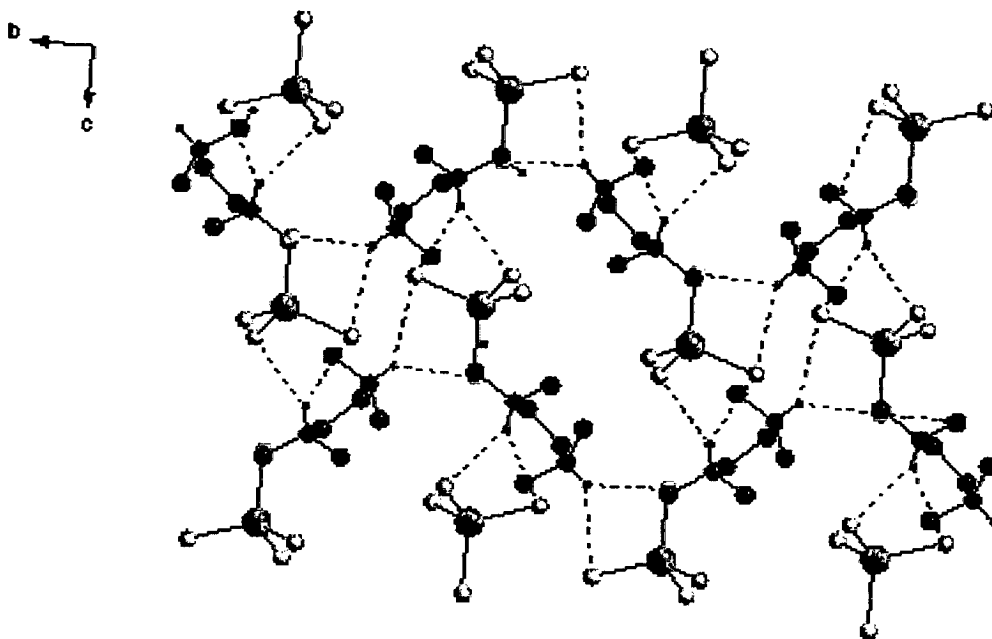

Fig. 4.3.17 Crystal structure of (N,N'-dm-1,3-pnH₂)[WS₄] **10** with view along 'a' axis (hydrogen bonding is shown as dashed lines). Colour codes; H purple, C black, W grey, S yellow, N blue.

Table 4.3.16 Selected geometric parameters (Å, °) for (N,N'-dm-1,3-pnH$_2$)[WS$_4$] **10**

W(1)-S(4)	2.1771 (14)	N(1)-C(2)	1.462 (7)
W(1)-S(3)	2.1980 (15)	C(2)-C(3)	1.520 (7)
W(1)-S(2)	2.1982 (12)	C(3)-C(4)	1.496 (9)
W(1)-S(1)	2.1992 (12)	C(4)-N(2)	1.503 (8)
C(1)-N(1)	1.468 (7)	N(2)-C(5)	1.466 (8)
S(4)-W(1)-S(3)	109.26 (7)	S(4)-W(1)-S(1)	109.60 (6)
S(4)-W(1)-S(2)	109.93 (6)	S(3)-W(1)-S(1)	109.64 (6)
S(3)-W(1)-S(2)	109.09 (6)	S(2)-W(1)-S(1)	109.30 (5)
C(2)-N(1)-C(1)	115.0 (5)	C(4)-C(3)-C(2)	113.7 (5)
N(1)-C(2)-C(3)	109.9 (4)	C(3)-C(4)-N(2)	114.2 (5)
		C(5)-N(2)-C(4)	117.3 (5)

Table 4.3.17 Hydrogen-bonding geometry (Å, °) for (N,.N'-dm-1,3-pnH$_2$)[WS$_4$] **10**

D-H...A	d(D-H)	d(H...A)	d(D...A)	<DHA	Symmetry code
N1-H1...S3	0.900	2.479	3.314	154.59	x-1, y, z
N1-H1...S2	0.900	2.895	3.458	122.12	x-1, y, z
N1-H2...S1	0.900	2.424	3.322	175.62	
N2-H1...S2	0.900	2.556	3.351	147.70	-x+3/2, y+1/2, -z+3/2
N2-H1...S4	0.900	2.960	3.617	131.21	-x+3/2, y+1/2, -z+3/2
N2-H2...S1	0.900	2.596	3.390	147.56	x-1/2, -y+1/2, z-1/2
N2-H2...S2	0.900	2.811	3.431	127.23	x-1/2, -y+1/2, z-1/2

D = Donor; A = Acceptor

(1,4-bnH$_2$)[WS$_4$] **12** [88] crystallizes in the triclinic space group P1̄. The asymmetric unit contains two crystallographically independent cations which are located on centres of inversion (Fig.4.5.18). Its structure is built up of discrete (1,4-bnH$_2$)$^{2+}$ cations and tetrahedral [WS$_4$]$^{2-}$ anions connected to each other via hydrogen bonding interactions (Fig 4.3.19). Bond lengths and angles of (1,4-bnH$_2$)$^{2+}$ (Table 4.3.18) are in good agreement with data for (1,4-bnH$_2$)[CrO$_4$] [201]. The WS$_4$ tetrahedron is moderately distorted and W-S bonds vary from 2.1799(8) Å to 2.2030(8) Å (average: 2.1918) (Table 4.3.18), being comparable with values in other tetrathiotungstates. Two W-S bonds are longer and the other two are comparatively shorter than the mean W-S distance. Nine S···H distances (range: 2.387 - 3.002 Å) (Table 4.3.19) are observed and six of these are shorter than the sum of the S and H van der Waals radii by about 0.35 Å. S(1) and S(4) are involved in three short S···H bonds while S(2) has two such short contacts. As in the other compounds the longest W-S bond (W-S(2): 2.2030) is found for the shortest S···H contacts (S(2)···H: 2.387 and 2.473 Å) accompanied by large N-H···S angles (164.97 and 159.66°). Despite the fact that S(4) exhibits three short contacts (range: 2.388 to 2.654 Å) the W-S(4) bond is shorter than W-S(2). An explanation is that one of the interactions is weak due to the smaller N-H···S angle of 135.47°. Although S(1) has three hydrogen bonds the W-S(1) bond is the shortest (2.1799 Å) which may be caused by the relatively long S···H distances (2.720 - 3.002 Å) and small N-H···S angles (Table 4.3.19) indicating weak interactions. The single short S···H contact (2.578 Å) accompanied by a N-H···S angle of 156.11° observed for S(3) which is shorter than any of the three S(1)···H contacts can account for the slightly longer W-S(3) bond length of 2.1820(10) Å. The value for Δ is 0.0231 Å which may be responsible for the appearance of a broad W-S vibration in the IR spectrum.

The crystal structure of (1,4-bnH$_2$)[MoS$_4$] **11** consists of discrete (1,4-bnH$_2$)$^{2+}$ cations and tetrahedral [MoS$_4$]$^{2-}$ dianions (Fig 4.3.20). The C-C and C-N bond lengths in **11** are in good agreement with those reported in compounds containing similar cation [201]. There are two crystallographically independent (1,4-bnH$_2$)$^{2+}$ dications in the asymmetric unit, both of which are located on a centre of inversion,

Fig. 4.3.18 Crystal structure of (1,4-bnH₂)[WS₄] **12** with labeling and displacement ellipsoids drawn at the 50% probability level.

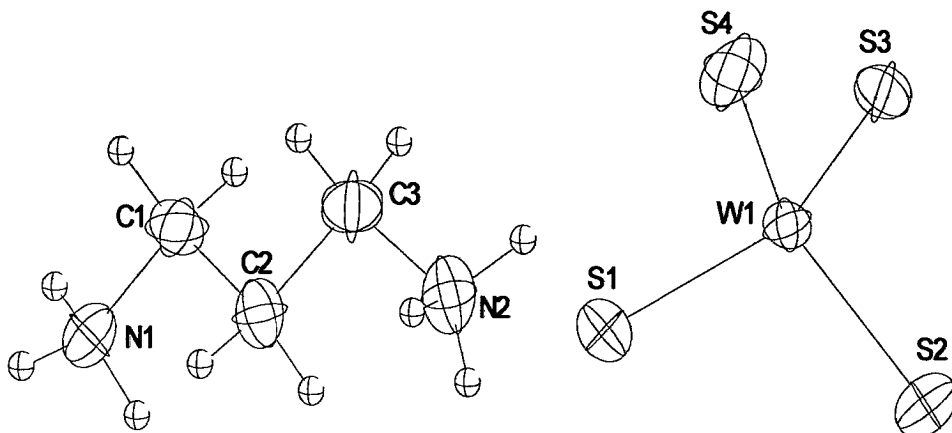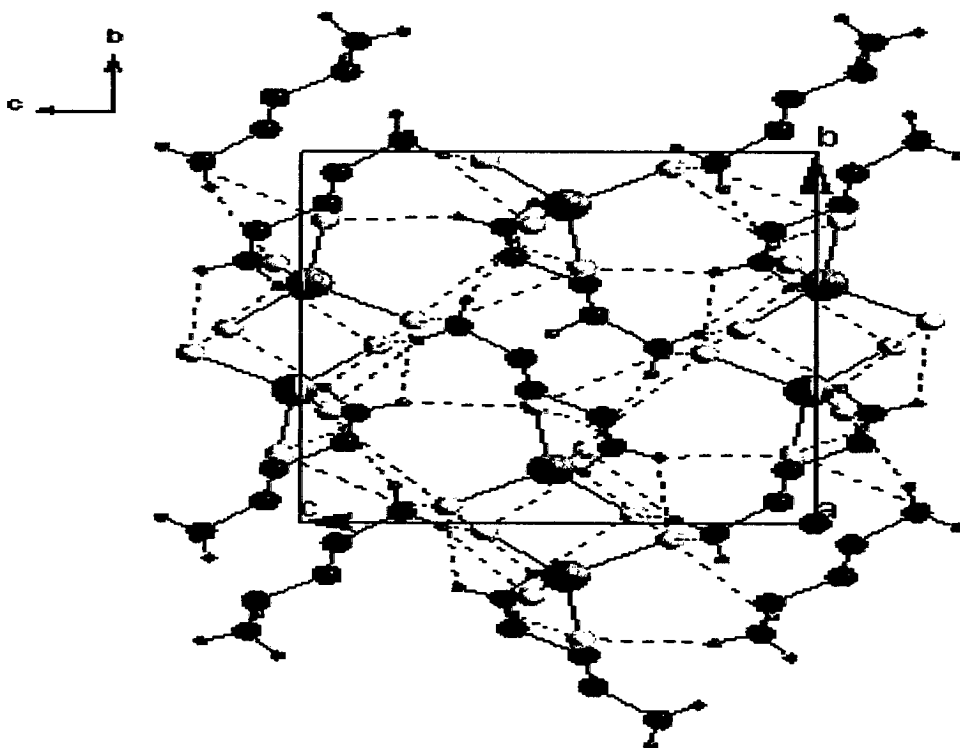Fig. 4.3.19 Three dimensional hydrogen bonding network in (1,4-bnH₂)[WS₄] **12** with view along 'c' axis (hydrogen bonding is shown as dashed lines). Colour codes; H purple, C black, W grey, S yellow, N blue.

Table 4.3.18 Selected geometric parameters (Å, °) for (1,4-bnH$_2$)[WS$_4$] **12**

W(1)-S(1)	2.1799 (8)	C(2)-C(2A)	1.516 (6)
W(1)-S(3)	2.1820 (10)	C(3)-C(4)	1.483 (5)
W(1)-S(4)	2.2024 (9)	C(1)-C(2)	1.514 (4)
W(1)-S(2)	2.2030 (8)	N(2)-C(3)	1.482 (4)
N(1)-C(1)	1.486 (4)	C(4)-C (4A)	1.514 (6)
S(1)-W(1)-S(3)	109.70 (4)	S(1)-W(1)-S(4)	108.63 (4)
S(3)-W(1)-S(4)	109.91 (4)	S(1)-W(1)-S(2)	109.49 (3)
S(3)-W(1)-S(2)	109.09 (3)	S(4)-W(1)-Ś(2)	110.01 (4)
N(1)-C(1)-C(2)	111.8 (3)	C(1)-C(2)-C(2A)	113.4 (4)
N(2)-C(3)-C(4)	112.7 (3)	C(3)-C(4)-C(4A)	112.6 (4)

Table 4.3.19 Hydrogen-bonding geometry (Å, °) for (1,4-bnH$_2$)[WS$_4$] **12**

D-H...A	d(D-H)	d(H...A)	d(D...A)	<DHA	Symmetry code
N1-H1A...S4	0.890	2.444	3.304	162.48	-x+1, -y+1, -z+2
N1-H1B...S3	0.890	2.578	3.411	156.11	-x+2,-y+1, -z+2
N1-H1B...S1	0.890	2.938	3.469	119.91	-x+2,-y+1, -z+2
N1-H1C...S2	0.890	2.473	3.322	159.66	
N2-H2A...S4	0.890	2.388	3.278	179.02	-x+1, -y+1, -z+1
N2-H2B...S2	0.890	2.387	3.255	164.97	-x+2, -y+1, -z+1
N2-H2B...S1	0.890	3.002	3.426	111.18	-x+2, -y+1, -z+1
N2-H2C...S4	0.890	2.654	3.347	135.47	
N2-H2C...S1	0.890	2.720	3.419	136.31	

D = Donor; A = Acceptor

while the anions are located in general positions. The MoS_4 tetrahedron is moderately distorted with S-Mo-S bond angles between 108.56(3) and 110.28(4)° with a mean bond angle of 109.47°. The Mo-S bond distances vary between 2.1749(8) Å and 2.1992(7) Å with an average Mo-S bond distance of 2.1814 (Table 4.3.20) and are comparable with those in other tetrathiomolybdates. Three of the Mo-S bonds are shorter and the other one is comparatively longer than the mean Mo-S distance of 2.1814 Å. $(1,4-bnH_2)^{2+}$ dications and $[MoS_4]^{2-}$ dianions are connected via N-H...S interactions forming an extended three dimensional network (Fig 4.3.21). In all, nine S...H contacts ranging from 2.348 to 2.992 Å are observed (Table 4.3.21). The H-bonding interactions run along the 'c' axis forming chains. The H-bonding labels for **11** are displayed in Fig 4.3.22. The other structural features in **11** can be explained similarly as in **12**. The difference between the longest and the shortest Mo-S bond Δ is 0.0243 Å and is relatively more than of that 0.0111 in $(enH_2)[MoS_4]$ [75].

4.3.4 Crystal structure of (dienH₂)[MoS₄] 13 and (dienH₂)[WS₄] 14

The crystal structure of $(dienH_2)[MoS_4]$ has been reported earlier in the monoclinic *Pn* space group [77]. The structure of $(dienH_2)[MoS_4]$ **13** is investigated and the structure can be better described in the higher symmetry orthorhombic space group *Pmmn*. Complex **13** crystallizes with unit cell parameters $a = 11.5279$ (10) Å, $b = 7.1941(4)$ Å, $c = 7.5474$ (5) Å, $V = 625.9$ (2) Å^3 and Z = 2. Complex $(dienH_2)[WS_4]$ **14** is isostructural to complex **13**. The crystal structure of **13** is composed of $(dienH_2)^{2+}$ and $[MoS_4]^{2-}$ dianions (Fig 4.3.23). The selected bond lengths and bond angles for **13** are listed in Table 4.3.22. Four of the S-Mo-S bond angles are identical at 109.38 (3)° the other two being 109.08 (7) and 110.21 (7)°, thus indicating a very small deviation from ideal tetrahedral geometry. **13** exhibits two short Mo-S distances of 2.169 (2) Å and two long Mo-S distances of 2.191 (1) Å with an average Mo-S bond length of 2.180 Å. The lengthening of the Mo-S bond distances can be explained in terms of short hydrogen bonding contacts between the H atoms attached to the N of the cation and the S atom of the anion. The H-bonding network in **13** is two dimensional and runs along 'a' axis in a zigazag fashion by connecting $(dienH_2)^{2+}$ cations and $[MoS_4]^{2-}$ anions (Fig 4.3.24). The $[MoS_4]^{2-}$ rods are running along 'b' axis. The alternating layers are parallel to 'ac' plane when viewed along 'b' axis. In complex **13**, three short intermolecular contacts between the S atoms of $[MoS_4]^{2-}$ and

96

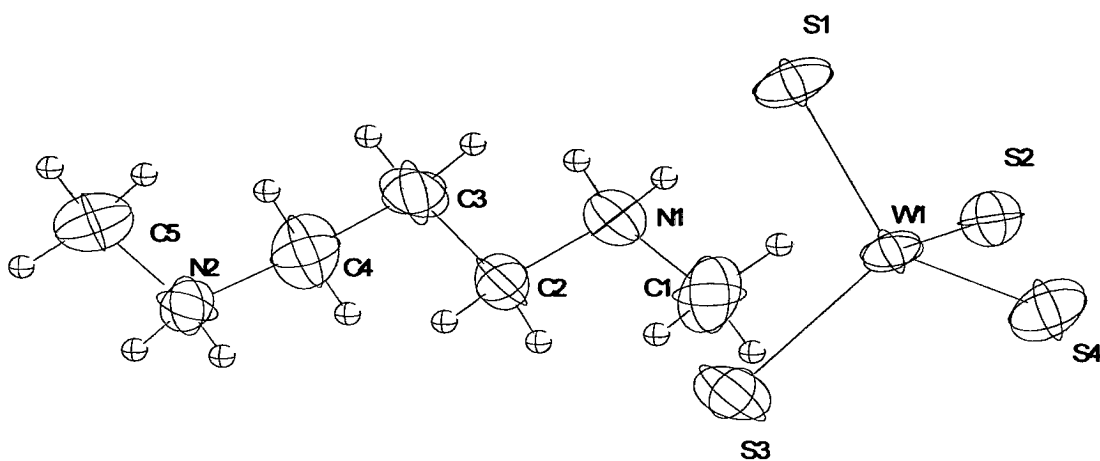Fig. 4.3.20 Crystal structure of (1,4-bnH$_2$)[MoS$_4$] **11** with labeling and displacement ellipsoids drawn at the 50% probability level.

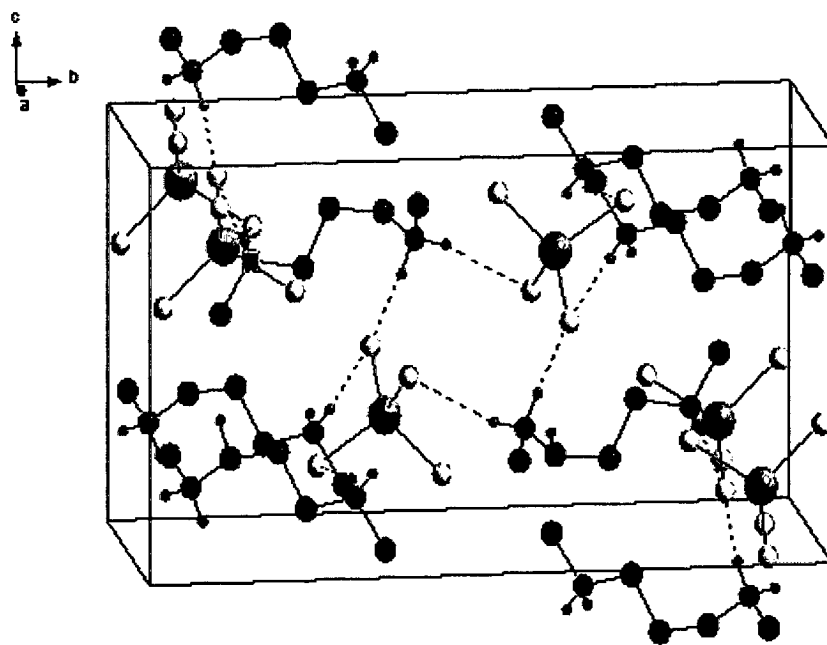Fig. 4.3.21 Hydrogen bonding network in (1,4-bnH$_2$)[MoS$_4$] **11** with view along 'c' axis (hydrogen bonding is shown as dashed lines). Colour codes; H purple, C black, W grey, S yellow, N blue.

Fig. 4.3.22 Hydrogen bond labels in (1,4-bnH$_2$)[MoS$_4$] **11**. Colour codes; H purple, C black, Mo grey, S yellow, N blue. H atoms attached to carbon are omitted for clarity.

Fig. 4.3.23 Crystal structure of (dienH$_2$)[MoS$_4$] **13** with labeling and displacement ellipsoids drawn at the 50% probability level.

Table 4.3.20 Selected geometric parameters (Å, °) for (1,4-bnH₂)[MoS₄] **11**

Mo(1)-S(1)	2.1749 (8)	C(2)-C(2)#1	1.503 (5)
Mo(1)-S(3)	2.1765(8)	C(3)-C(4)	1.486 (4)
Mo(1)-S(4)	2.1750(8)	C(1)-C(2)	1.518 (3)
Mo(1)-S(2)	2.1992(7)	N(2)-C(3)	1.472 (4)
N(1)-C(1)	1.485 (3)	C(4)-C(4)#2	1.504 (5)
S(1)-Mo(1)-S(4)	108.56(3)	S(1)-Mo(1)-S(3)	109.58(3)
S(4)-Mo(1)-S(3)	110.28(3)	S(1)-Mo(1)-S(2)	109.41(3)
S(4)-Mo(1)-S(2)	109.87(3)	S(3)-Mo(1)-S(2)	109.14(3)
N(1)-C(1)-C(2)	111.8(2)	C(2)#1-C(2)-C(1)	113.0(3)
N(2)-C(3)-C(4)	113.0(3)	C(3)-C(4)-C(4)#2	112.5(3)

Table 4.3.21 Hydrogen-bonding geometry (Å, °) for (1,4-bnH₂)[MoS₄] **11**

D-H...A	d(D-H)	d(H...A)	d(D...A)	<DHA	Symmetry code
N1-H1A...S4	0.890	2.386	3.263	168.19	-x+1, -y+1, -z+2
N1-H1B...S3	0.890	2.550	3.410	162.60	-x+2,-y+1, -z+2
N1-H1B...S1	0.890	2.986	3.448	114.26	-x+2,-y+1, -z+2
N1-H1C...S2	0.890	2.482	3.297	152.52	
N2-H2A...S4	0.890	2.348	3.238	177.99	-x+1, -y+1, -z+1
N2-H2B...S2	0.890	2.372	3.240	165.14	-x+2, -y+1, -z+1
N2-H2B...S1	0.890	2.992	3.423	111.72	-x+2, -y+1, -z+1
N2-H2C...S4	0.890	2.625	3.324	136.04	
N2-H2C...S1	0.890	2.718	3.417	136.23	

D = Donor; A = Acceptor

the H atoms of the $(dienH_2)^{2+}$ dication ranging from 2.541 to 2.940 Å are observed (Table 4.3.23). The atom S1 makes two short contacts with the H atoms of the $(dienH_2)^{2+}$ dication while S2 makes a single contact with the H atom of the organic dication. The N-H...S bond angles ranging from 135.65 to 151.73° are also indicative of H-bonding. The Δ value of 0.0020 in **13** is almost double than that observed in $(enH_2)[MoS_4]$ indicating more distortion of MS_4 in **13**.

Complex $(dienH_2)[WS_4]$ **14**, is isostructural with **13** and its structure is composed of $(dienH_2)^{2+}$ and $[WS_4]^{2-}$ dianions (Fig 4.3.25). The substitution of Mo by W in this case has resulted in an overall increase in the unit cell volume (V= 627.50 (9) Å). $[WS_4]^{2-}$ anion is surrounded by four $(dienH_2)^{2+}$ cations which are connected via observed weak N-H...S interactions (Fig 4.3.26). In complex **14**, the four S-W-S bond angles are identical at 109.4 (1)° while the other two being 109.2 (1) and 110.1 (1)°, thus indicating a very small deviation from ideal tetrahedral geometry (Table 4.3.24). Complex **14** exhibits two short W-S distances of 2.172 (1) Å and two long W-S distances of 2.189 (1) Å, with an average W-S bond length of 2.185 Å. The lengthening of the W-S bond can be explained based on the short contacts between the S atoms of W and H atoms of N. (Table 4.3.25). The longest W-S bond distance of 2.189 (1) Å observed in **14** is slightly shorter than the longest W-S bond lengths of 2.1943 (13) Å observed in **2**. The difference between the shortest and the longest W-S bond lengths in **14** is 0.017 Å indicating that a slight distortion of the WS_4 tetrahedron. In both **13** and **14**, S...H distances are shorter than the sum of the van der Waals radii of S and H [213].

4.3.5 Crystal structure description for $(dpnH_2)[MoS_4]$ **15** and $(dpnH_2)[WS_4]$ **16**

Compound **16** contains discrete diprotonated dipn cations and $[WS_4]^{2-}$ anions (Fig.4.3.27) with all atoms being located on general positions. The WS_4 tetrahedron is slightly distorted (S-W-S angles: 108.90(6)° - 110.23(5)°; average: 109.47°). The W-S bond lengths vary from 2.188(2) to 2.2053(12) Å with a mean W-S bond length of 2.195 Å (Table 4.3.26). The geometric parameters are in close agreement with those for other organic ammonium tetrathiotungstates. Extended H-bonding interactions produces a three-dimensional network (Fig.4.3.28.) The cations and $[WS_4]^{2-}$ anions are stacked in rods along [001] to form a pseudo-hexagonal array. Along [100] and
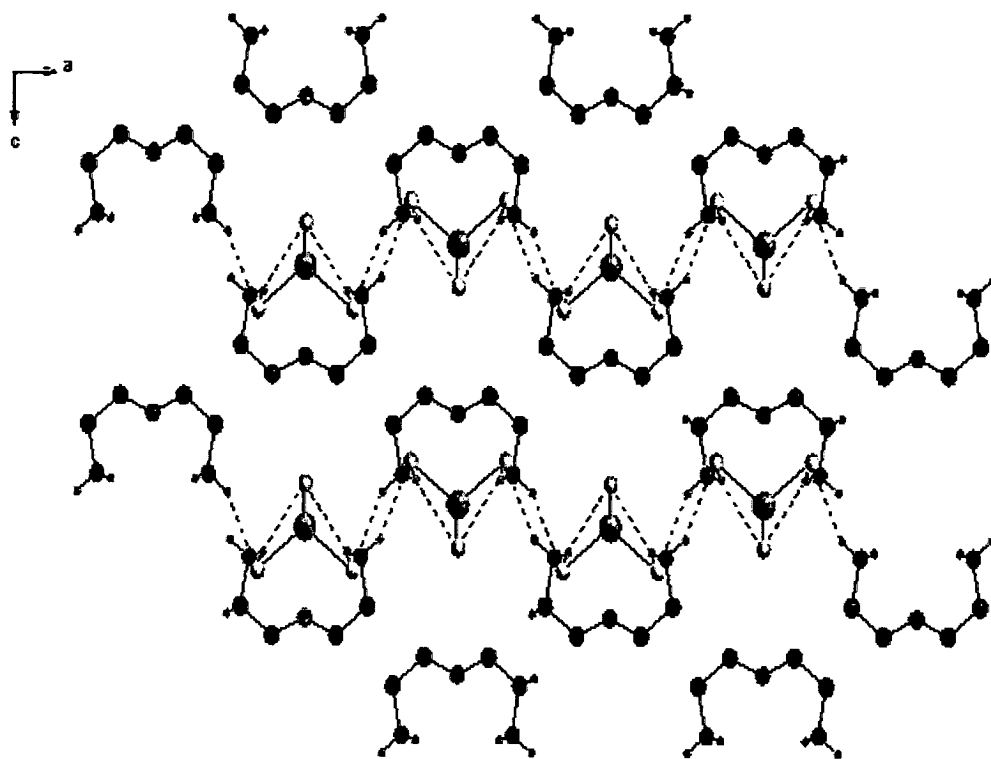
Fig. 4.3.24 Hydrogen bonding network in (dienH$_2$)[MoS$_4$] **13** with view along 'b' axis (hydrogen bonding is shown as dashed lines). Colour codes; H purple, C black, Mo grey, S yellow, N blue.
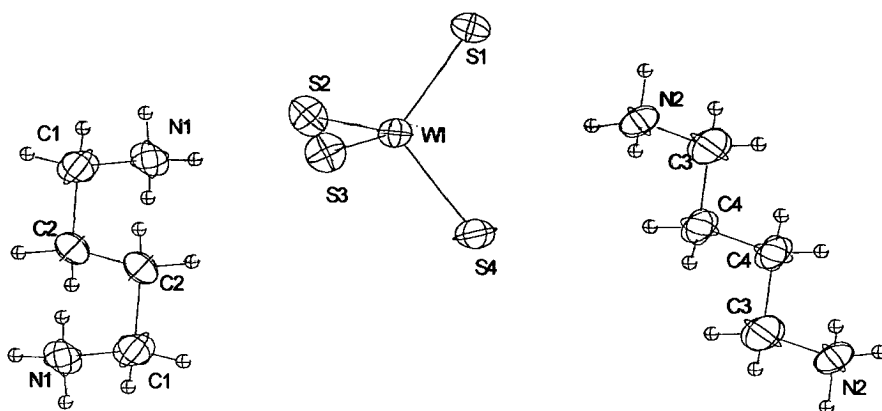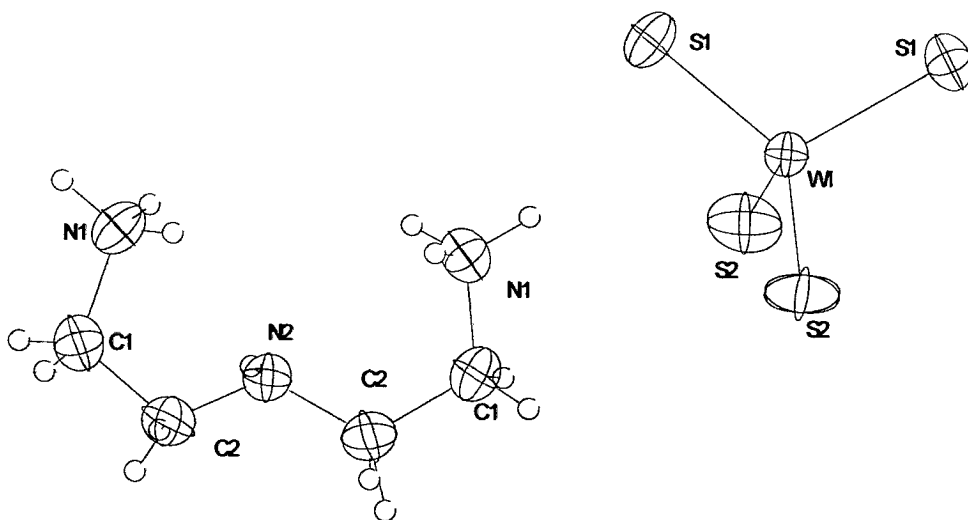

Fig. 4.3.25 Crystal structure of (dienH$_2$)[[WS$_4$] **14** with labeling and displacement ellipsoids drawn at the 50% probability level.
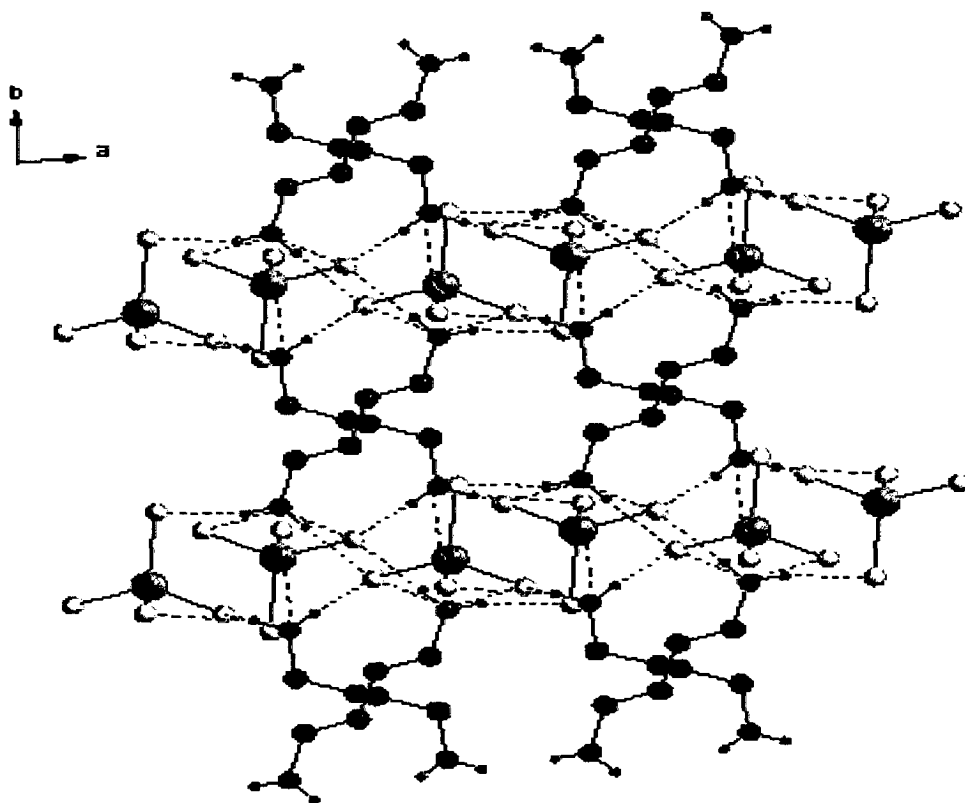
Table 4.3.22 Selected geometric parameters (Å, °) for (dienH$_2$)[MoS$_4$] **13**

Mo(1)-S(2A)	2.169 (2)	N(1)-C(1)	1.453 (6)
Mo(1)-S(2)	2.169 (2)	C(2)-N(2)	1.373 (6)
Mo(1)-S(1)	2.191 (1)	N(2)-C(2A)	1.373 (6)
Mo(1)-S(1A)	2.191 (1)	C(1)-C(2)	1.458 (7)
		C(2)-N(2A)	1.373 (6)
S(2A)-Mo(1)-S(2)	109.08 (7)	S(1)-Mo(1)-S(1A)	110.21 (7)
S(2A)-Mo(1)-S(1)	109.38 (2)	N(1)-C(1)-C(2)	113.3 (4)
S(2)-Mo(1)-S(1)	109.38 (3)	N(2)-C(2)-C(1)	120.5 (4)
S(2A)-Mo(1)-S(1A)	109.38 (3)	N(2A)-C(2)-C(1)	120.5 (4)
S(2)-Mo(1)-S(1A)	109.38 (2)	C(2)-N(2)-C(2A)	124.2 (6)

Table 4.3.23 Hydrogen-bonding geometry (Å, °) for (dienH$_2$)[MoS$_4$] **13**

D-H...A	d(D-H)	d(H...A)	d(D...A)	<D-HA	Symmetry code
N1-H1...S1	0.890	2.541	3.351	151.73	
N1-H2...S2	0.890	2.778	3.508	140.27	x-1/2,y+1/2,-z+1
N1-H2...S1	0.890	2.940	3.631	135.65	-x+1, -y+1, -z+1

D = Donor; A = Acceptor

Table 4.3.24 Selected geometric parameters (Å, °) for (dienH₂)[WS₄] **14**

W(1)-S(2A)	2.172 (1)	N(1)-C(1)	1.456 (5)
W(1)-S(2)	2.172 (1)	C(1)-C(2)	1.456 (6)
W(1)-S(1)	2.189 (1)	C(2)-N(2)	1.382 (5)
W(1)-S(1A)	2.189 (1)	C(2)-N(2A)	1.382 (5)
		N(2)-C(2A)	1.382 (5)
S(2A)-W(1)-S(2)	109.2 (1)	S(1)-W(1)-S(1A)	110.1 (1)
S(2A)-W(1)-S(1)	109.4 (1)	N(1)-C(1)-C(2)	113.6 (3)
S(2)-W(1)-S(1)	109.4 (1)	N(1)-C(2)-C(1)	119.9 (4)
S(2A)-W(1)-S(1A)	109.4 (1)	N(2A)-C(2)-C(1)	119.9 (4)
S(2)-W(1)-S(1A)	109.4 (1)	C(2)-N(2)-C(2A)	122.9 (5)

Table 4.3.25 Hydrogen-bonding geometry (Å, °) for (dienH₂)[WS₄] **14**

D-H...A	d(D-H)	d(H...A)	d(D...A)	<D-HA	Symmetry code
N1-H1...S1	0.890	2.531	3.344	152.13	
N1-H2...S2	0.890	2.765	3.500	140.74	x-1/2,y+1/2,-z+1
N1-H2...S1	0.890	2.968	3.657	135.61	-x+1, -y+1, -z+1

D = Donor; A = Acceptor
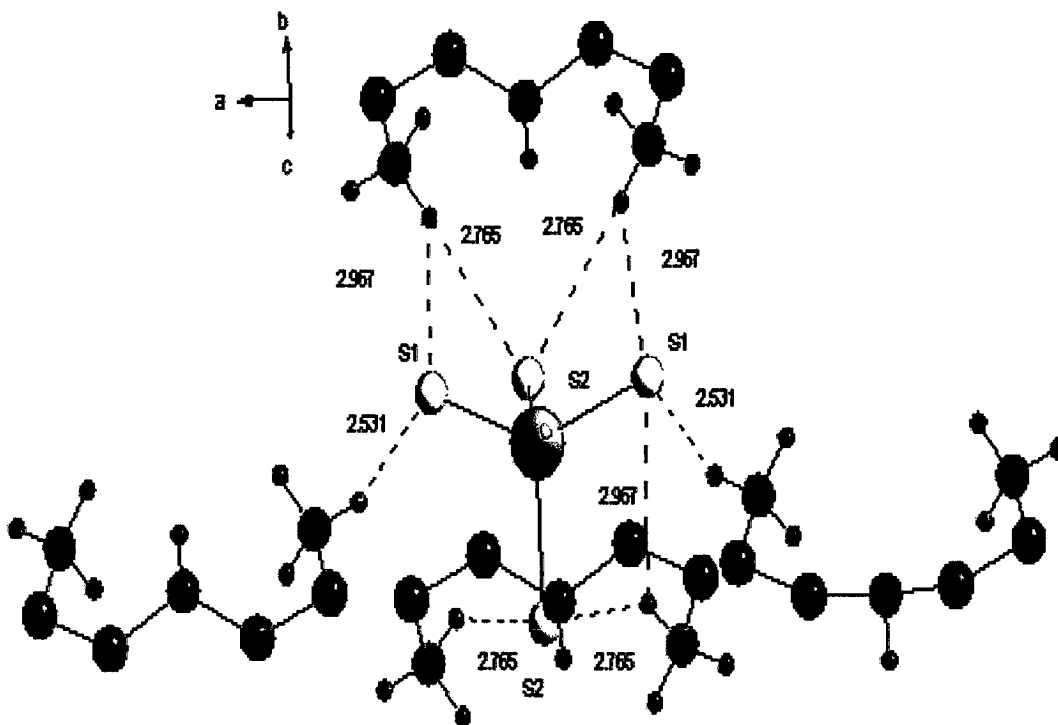
Fig. 4.3.26 Hydrogen bond labels in $(dienH_2)[WS_4]$ **14**. Colour codes; H purple, C black, W grey, S yellow, N blue. H atoms attached to carbon are omitted for clarity.
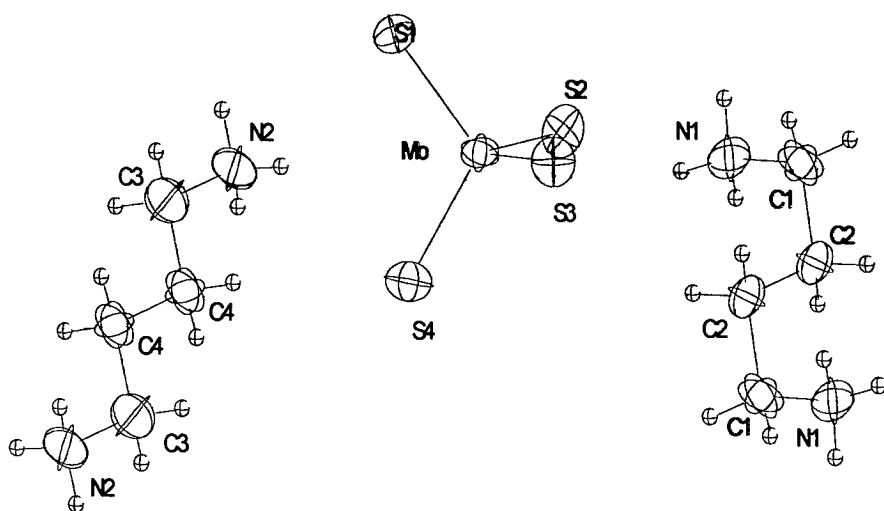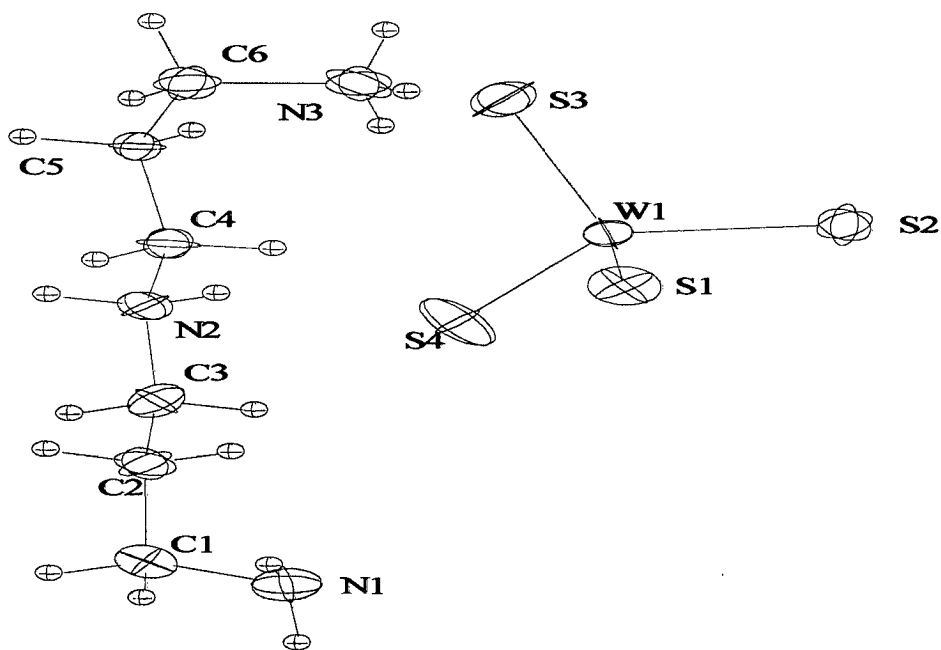

Fig. 4.3.27 Crystal structure of $(dipnH_2)[[WS_4]$ **16** with labeling and displacement ellipsoids drawn at the 50% probability level.

[010] cations and anions alternate. In the (010) plane a layer like arrangement is found with the anions being located in the pockets formed by three neighboring cations. A very short N3-H...N1 contact at 1.896 Å links the cations into a chain along the c axis. Every anion is surrounded by four different cations and eight short S...H distances ranging from 2.532 to 2.958 Å (Table 4.3.27) indicate weak S...H bonding. It has been observed that the W-S bond lengths tend to be longer when the S...H contacts are shorter and the N-H...S angles are less acute. In **16** the shortest S...H contact of 2.532 Å is accompanied by the shortest W-S3 bond. The difference between the longest and shortest W-S bond Δ in **2** is 0.0173 Å and is quite less compared to the Δ value observed earlier for (pipH$_2$)[WS$_4$]**24** (0.0385).

Compound **15** is isostructural to its W analogue and contains discrete diprotonated dipn cations and [MoS$_4$]$^{2-}$ anions (Fig. 4.3.29) with all atoms being located on general positions. The WS$_4$ tetrahedron is slightly distorted (S-W-S angles: 108. 97 (5) to 110.33 (4)°; average: 109.47°). The Mo-S bond lengths vary from 2.1717(13) to 2.1903(9) Å with a mean Mo-S bond length of 2.182 Å (Table 4.3.28). The dipn cations and [MoS$_4$]$^{2-}$ anions are connected via weak hydrogen bonding interactions (Table 4.3.29) which leads to extended three-dimensional network. Other structural features in **15** can be explained similarly as in **16**. The difference between the longest and shortest Mo-S bond Δ in **15** is 0.0189 Å and is quite less compared to the Δ value observed earlier for (pipH$_2$)[MoS$_4$] (0.0431).

4.3.6 Crystal structure description for (trenH$_2$)[MS$_4$]·H$_2$O [M = Mo **17**, W **18**

The two complexes (trenH$_2$)[MoS$_4$]·H$_2$O **17** [83] and (trenH$_2$)[WS$_4$]·H$_2$O **18** [87] are isostructural and crystallize in the monoclinic P2$_1$/C space group. (trenH$_2$)[MS$_4$]·H$_2$O complexes are the first examples of structurally characterized hydrated tetrathiometalates. The unit cell parameters for **17** (Mol. Wt = 390.47) are a = 11.470 (2) Å, b = 11.793 (2) Å, c = 12.483 (2) Å, α = γ = 90° β = 111.63 (1), V = 1569.5 (4) Å^3, Z = 4, D$_c$ = 1.652 g.cm^{-3}. The crystal structure of (trenH$_2$)[MoS$_4$]·H$_2$O consists of diprotonated tren cations, [MoS$_4$]$^{2-}$ anions and crystal water (Fig 4.3.30). Only two of the four N atoms in tren are protonated while the tertiary atom N(1) as well as one of the primary amino group N(4) are not protonated. All interatomic distances and angles in the tren cation are in agreement with the data reported for
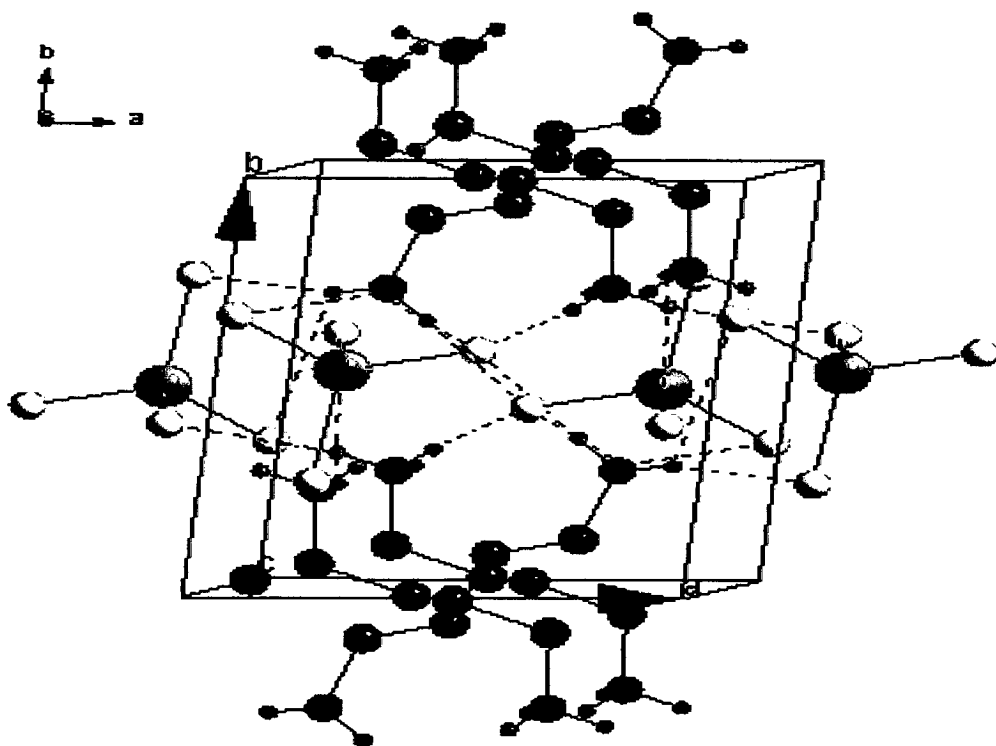
Fig. 4.3.28. Hydrogen bonding network in (dipnH$_2$)[WS$_4$] **16** with view along 'b' axis (hydrogen bonding is shown as dashed lines). Colour codes; H purple, C black, W grey,yellow, N blue.
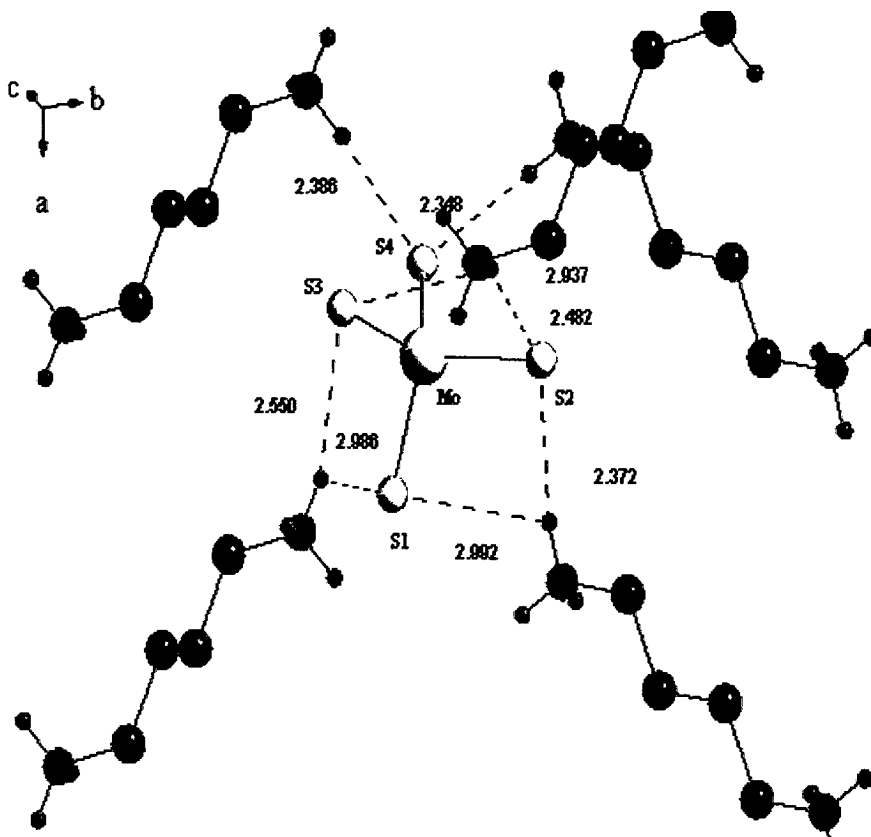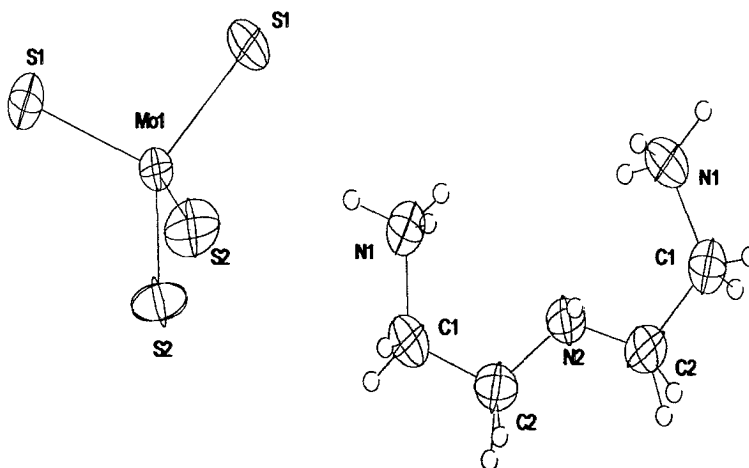

Fig. 4.3.29 Crystal structure of (dipnH$_2$)[[MoS$_4$] **15** with labeling and displacement ellipsoids drawn at the 50% probability level.

Table 4.3.26 Selected geometric parameters (Å, °) for (dipnH₂)[WS₄] **16**

W(1)-S(3)	2.1882 (22)	C(2)-C(3)	1.539 (9)
W(1)-S(2)	2.1935 (13)	C(3)-N(2)	1.479 (8)
W(1)-S(4)	2.1950 (21)	N(2)-C(4)	1.512 (8)
W(1)-S(1)	2.2053 (12)	C(4)-C(5)	1.514 (8)
N(1)-C(1)	1.481 (7)	C(5)-C(6)	1.515 (8)
C(1)-C(2)	1.510 (8)	C(6)-N(3)	1.482 (7)
S(3)-W(1)-S(2)	108.90 (7)	S(3)-W(1)-S(1)	109.40 (8)
S(3)-W(1)-S(4)	109.21 (8)	S(2)-W(1)-S(1)	110.23 (5)
S(2)-W(1)-S(4)	109.83 (9)	S(4)-W(1)-S(1)	109.25 (7)
N(1)-C(1)-C(2)	111.8 (5)	C(3)-N(2)-C(4)	111.7 (4)
C(1)-C(2)-C(3)	112.1 (5)	N(2)-C(4)-C(5)	112.4 (5)
N(2)-C(3)-C(2)	111.4 (5)	C(4)-C(5)-C(6)	112.0 (5)
		N(3)-C(6)-C(5)	113.0 (5)

Table 4.3.27 Hydrogen-bonding geometry (Å, °) for (dipnH₂)[WS₄] **16**

D-H...A	d(D-H)	d(H...A)	d(D...A)	<DHA	Symmetry code
N1-H2...S2	0.890	2.779	3.587	151.73	-x+3/2, y-1, z+1/2
N1-H2...S3	0.890	2.806	3.361	121.76	-x+3/2, y-1, z+1/2
N2-H1...S4	0.900	2.639	3.494	159.08	
N2-H2...S2	0.900	2.660	3.401	140.20	x-1/2, -y+1, z
N2-H2...S1	0.900	2.741	3.446	135.98	x-1/2, -y+1, z
N3-H1...S3	0.890	2.532	3.408	167.95	
N3-H2...S1	0.890	2.675	3.470	149.35	-x+3/2, y, z-1/2
N3-H2...S4	0.890	2.958	3.534	124.07	-x+3/2, y, z-1/2
N3-H3...N1	0.890	1.899	2.768	165.06	-x+3/2, y, z-1/2

D = Donor; A = Acceptor

Table 4.3.28 Selected geometric parameters (Å, °) for (dipnH$_2$)[MoS$_4$] **15**

Mo(1)-S(1)	2.1717 (13)	C(2)-C(3)	1.505 (6)
Mo(1)-S(3)	2.1810 (10)	C(3)-N(2)	1.489 (5)
Mo(1)-S(4)	2.1844 (14)	N(2)-C(4)	1.502 (6)
Mo(1)-S(2)	2.1903 (9)	C(4)-C(5)	1.522 (6)
N(1)-C(1)	1.460 (5)	C(5)-C(6)	1.508 (6)
C(1)-C(2)	1.529 (6)	C(6)-N(3)	1.480 (5)
S(1)-Mo(1)-S(3)	108.97 (5)	S(1)-Mo(1)-S(2)	109.72 (5)
S(1)-Mo(1)-S(4)	109.30 (6)	S(3)-Mo(1)-S(2)	110.33 (4)
S(3)-Mo(1)-S(4)	109.44 (5)	S(4)-Mo(1)-S(2)	109.07 (5)
N(1)-C(1)-C(2)	111.7 (3)	N(2)-C(4)-C(5)	111.7 (3)
C(3)-C(2)-C(1)	112.0 (3)	C(6)-C(5)-C(4)	111.8 (3)
N(2)-C(3)-C(2)	111.4 (3)	N(3)-C(6)-C(5)	112.6 (3)

Table 4.3.29 Hydrogen-bonding geometry (Å, °) for (dipnH$_2$)[MoS$_4$] **15**

D-H...A	d(D-H)	d(H...A)	d(D...A)	<DHA	Symmetry code
N1-H2...S3	0.890	2.759	3.563	150.77	-x+1, -y+2, z-1/2
N1-H2...S1	0.890	2.768	3.345	123.78	-x+1, -y+2, z-1/2
N2-H1...S3	0.900	2.645	3.384	140.06	
N2-H1...S2	0.900	2.711	3.415	135.78	
N2-H2...S4	0.900	2.627	3.479	158.30	x-1/2, -y+1, z
N3-H1...N1	0.890	1.864	2.752	175.07	-x+1/2, y, z+1/2
N3H2...S2	0.890	2.648	3.451	150.60	-x+1, -y+1, z+1/2
N3-H2...S4	0.890	2.890	3.510	128.08	-x+1, -y+1, z+1/2
N3-H3...S1	0.890	2.553	3.401	159.37	x-1/2, -y+1, z

D = Donor; A = Acceptor

complexes containing the tren moiety. In $(trenH_2)[MoS_4]\cdot H_2O$ **17**, the $[MoS_4]$ tetrahedron is distorted with S-Mo-S angles between 107.89(2) and 110.97(2)° and Mo-S bond lengths from 2.1670(5) to 2.1951(5) Å, with a mean Mo-S distance of 2.1846 Å (Table 4.3.30). In **17**, short S⋯H contacts are observed between the organic cation and the anion (Table 4.3.31), and the crystal water is also involved in two H⋯S(1) interactions. Due to the presence of crystal water, a five membered ring (H atoms are omitted) is formed (Fig 4.3.31). The resulting H bonding network is depicted in Fig. 4.3.32. The S⋯H contacts range from 2.458 to 3.019 Å and are shorter than those (2.55 to 3.02 Å) reported for $(NH_4)_2[MoS_4]$ [179]. The shortest Mo-S bond length of 2.1670(5) Å is observed for S(3), which has only one contact to a H atom at a distance of 2.929 Å. The analysis of the situation for S(1) and S(4) shows some interesting trends. The atom S(4) has two H atoms at distances 2.623 and 2.530 Å with corresponding angles of 153.12 and 169.34° and the longest Mo-S bond length of 2.1951(5) Å. On the other hand, S(1) has four interactions with H atoms, two with H atoms of the ammonium groups and two with H atoms of the water molecule. The two former are very weak (2.936 Å, angle: 120.06°; 3.019 Å, 128.29°) while the latter two interactions are significantly stronger (2.499 Å, 161.38°; 2.586 Å, 169.33°). The resulting Mo-S(1) bond of 2.1856(5) Å is surprisingly short as one would expect that this bond is at least as long as the Mo-S(4) bond. One possible explanation may be that despite the short S(1)⋯H distances to the H atoms of the water molecule the interactions are weaker than with H atoms bound to N with S⋯H separations of comparable lengths. Finally, S(2) has two short contacts, and the Mo-S(2) bond amounts to 2.1905(5) Å. The N⋯S distances range from 3.219 to 3.465 Å. The difference Δ between the longest and the shortest Mo-S bond distances in $(trenH_2)[MoS_4]\cdot H_2O$ is 0.0281 Å.

The crystal structure of $(trenH_2)[WS_4]\cdot H_2O$ **18** [87] contains diprotonated $(trenH_2)^{2+}$ cation and tetrahedral $[WS_4]^{2-}$ dianions and crystal water (Fig 4..3.33). The substitution of Mo by W in **17** leads to an increase in unit cell volume (1569.5 (4) Å^3 for the Mo complex) due to the larger size of W(VI). In the case of **18**, the $[WS_4]$ tetrahedron is distorted with S-W-S angles between 108.09(3) and 110.90(3)° and W-S bond lengths from 2.1739 (6) to 2.1997 (6) Å, with a mean W-S distance of 2.1904 Å (Table 4.3.32). Three of the W-S bonds are longer than the average W-S distance of
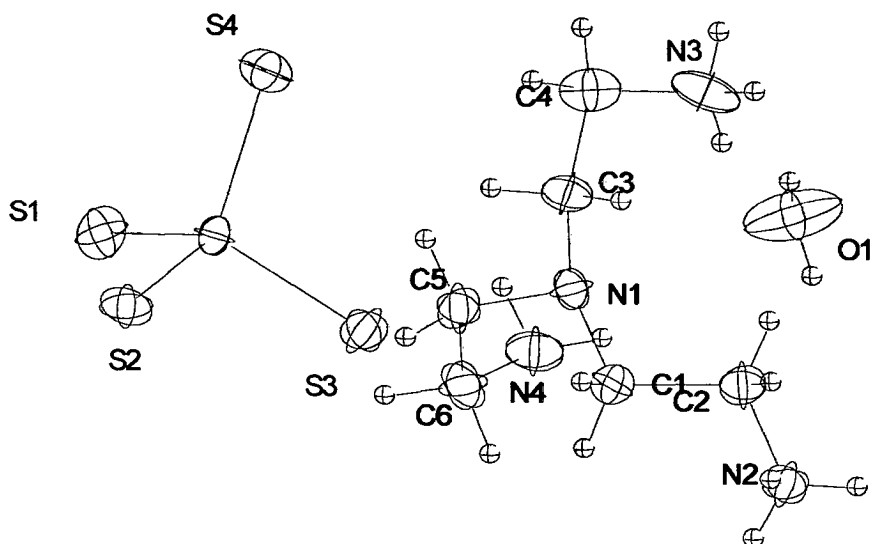
Fig. 4.3.30 Crystal structure of (trenH₂)[[MoS₄]·H₂O **17** with labeling and displacement ellipsoids drawn at the 50% probability level.
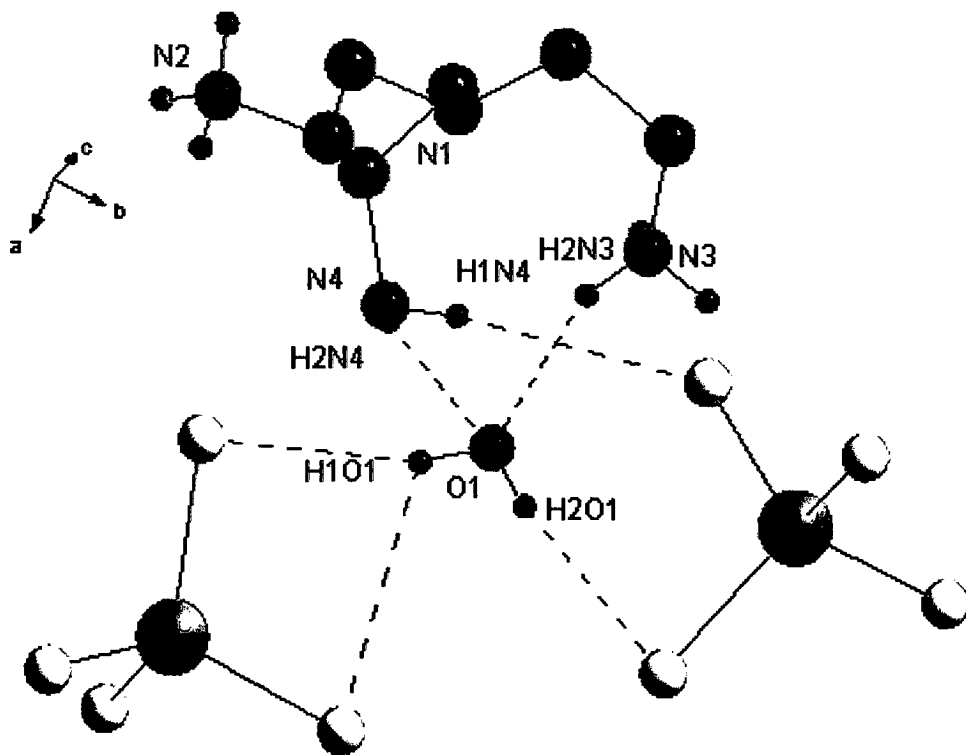
Fig. 4.3.31 Five membered ring with S, O, N and Mo in (trenH₂)[[MoS₄]·H₂O **17**. Colour codes; H purple, C black, Mo grey, S yellow, N blue. H atoms attached to carbon and in the ring are omitted for clarity.
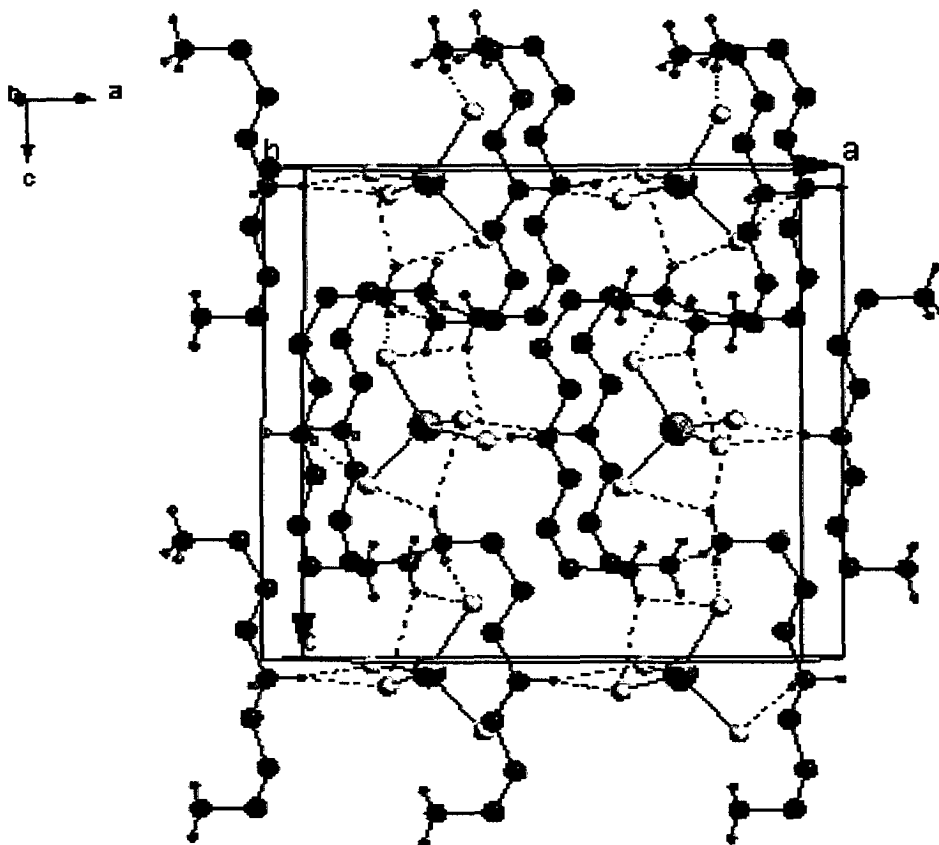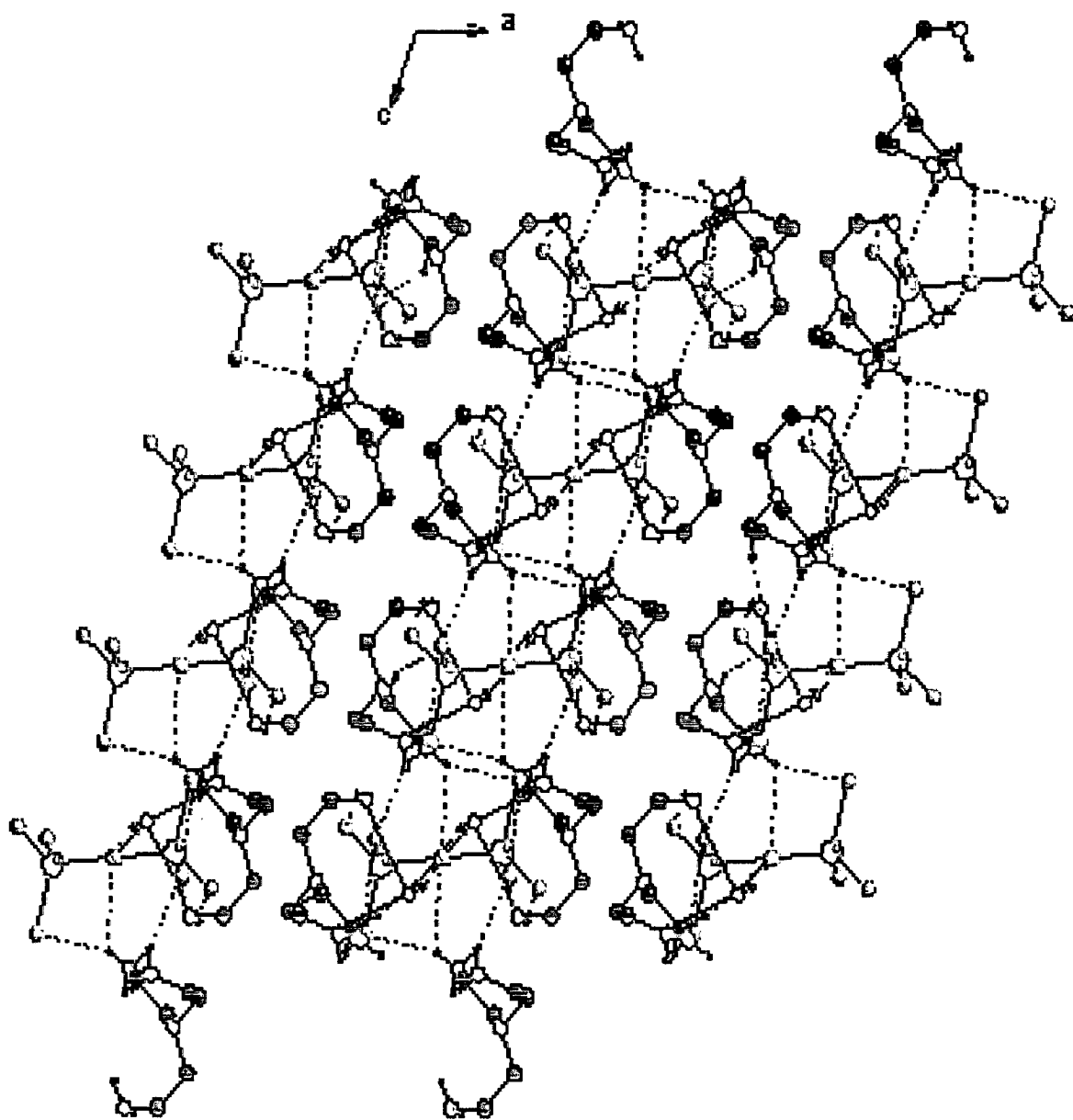
Fig. 4.3.32. Hydrogen bonding network in (trenH$_2$)[[MoS$_4$]·H$_2$O **17** with view along 'c' axis (hydrogen bonding is shown as dashed lines). Colour codes; H purple, C black, Mo grey, S yellow, N blue. H atoms attached to carbon are omitted for clarity.
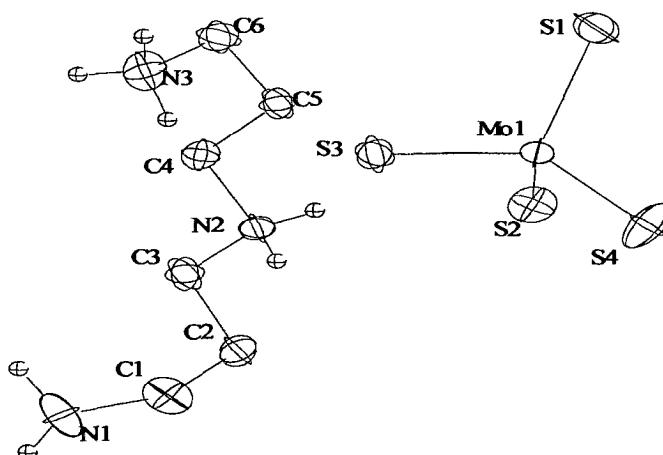
Table 4.3.30 Selected geometric parameters (Å, °) for (trenH$_2$)[MoS$_4$]· H$_2$O **17**

Mo(1)-S(3)	2.1670 (5)	C(3)-N(1)	1.4710 (19)
Mo(1)-S(2)	2.1905 (5)	C(5)-N(1)	1.4729 (19)
Mo(1)-S(1)	2.1856 (5)	N(2)-C(2)	1.4862 (20)
Mo(1)-S(4)	2.1951 (5)	N(3)-C(4)	1.4732 (25)
C(1)-N(1)	1.4653 (19)	N(4)-C(6)	1.4594 (23)
S(3)-Mo(1)-S(1)	107.89 (2)	S(3)-Mo(1)-S(2)	110.97 (2)
S(1)-Mo(1)-S(2)	109.79 (2)	S(3)-Mo(1)-S(4)	109.79 (2)
S(1)-Mo(1)-S(4)	109.71 (2)	S(2)-Mo(1)-S(4)	108.68 (2)
C(3)-N(1)-C(1)	111.13 (12)	C(4)-C(3)-N(1)	112.02 (13)
C(5)-N(1)-C(1)	112.15 (12)	C(4)-C(3)-N(3)	110.73 (14)
C(5)-N(1)-C(3)	110.52 (12)	C(5)-C(6)-N(1)	113.25 (13)
C(2)-C(1)-N(1)	110.60 (12)	C(6)-C(5)-N(4)	116.03 (14)
C(1)-C(2)-N(2)	110.48 (13)		

Table 4.3.31 Hydrogen-bonding geometry (Å, °) for (trenH$_2$)[MoS$_4$].H$_2$O **17**

D-H...A	d(D-H)	d(H...A)	d(D...A)	<DHA	Symmetry code
N1-H1···S2	0.860	2.583	3.396	158.03	x+1, -y+1/2, z+1/2
N1-H1···S1	0.860	2.936	3.448	120.06	x+1, -y+1/2, z+1/2
N2-H2···S4	0.860	2.530	3.379	169.34	−x+1, y-1/2, -z+1/2
N2-H2···S2	0.860	2.992	3.386	110.12	−x+1, y-1/2, -z+1/2
N2-H3···N4	0.860	1.946	2.805	177.06	x, -y+1/2, z+1/2
N3-H1···S4	0.860	2.623	3.413	153.12	−x+1, -y+1,-z+1
N3-H2···O1	0.860	1.985	2.797	157.11	
N3-H3···S2	0.860	2.458	3.313	172.51	-x+1, y+1/2, -z+1/2
N4-H1···S3	0.890	2.929	3.715	148.18	-x+1, y+1/2, -z+1/2
N4-H2···S1	0.890	3.019	3.638	128.29	x+1, y, z
O1-H1O1··S1	0.820	2.499	3.286	161.38	x+1, y, z
O1-H2O1··S1	0.820	2.586	3.395	169.33	−x+1, y+1/2, -z+1/2

D = Donor; A = Acceptor

2.1893 Å reported for **2**. In (trenH$_2$)[WS$_4$]·H$_2$O short S···H contacts are observed between the organic cation and the anion (Table 4.3.33), and the crystal water is also involved in two H···S(1) interactions. These structural features can be explained as described earlier in complex **17**. The difference Δ between the longest and the shortest W-S bond distances in (trenH$_2$)[WS$_4$]·H$_2$O **18** is 0.0158 Å. In both **17** and **18**, the cations, anions and crystal water are in the direction of crystallographic 'c' axis in (101) plane (Fig 4.3.34). The crystal waters, occupy the channels between the alternating layers of cations along 'c' axis. In both 17 and 18, out of eight N-H...S distances, one of the contacts is longer than the sum of the van der Waals radii of S and H [213].

4.3.7 Crystal structure description for (pipH$_2$)[MoS$_4$] **21**, (pipH$_2$)[WS$_4$] **22**, (1,-4-dmpH$_2$)[WS$_4$] **24** and (2-pip-1-EtNH$_3$)[MoS$_4$]·½ H$_2$O **27**

All the four complexes namely (pipH$_2$)[MoS$_4$] **21** [83], (pipH$_2$)[WS$_4$] **22** [87], (1,-4-dmpH$_2$)[WS$_4$] **24** and (2-pipH-1-EtNH$_3$)[MoS$_4$]·½ H$_2$O **27** which contains pip are discussed under this section. In complexes **21**, **22** and **24** both N atoms of the cyclic amine pip are protonated, while in **27** only one of the N of pip is protonated and the other is linked to an ethylammonium group. Complexes **21** and **22** are isostructural and crystallize in the monoclinic P2$_1$/c space group. The crystal structure of **21** is composed of (pipH$_2$)$^{2+}$ cation and tetrahedral [MoS$_4$]$^{2-}$ anion (Fig 4.3.35). The structure of (pipH$_2$)[MoS$_4$] which was reported earlier [217] has been redetermined, because the quality of the earlier structural data was poor. The cyclic organic cation adopts the chair form and the C-C and C-N bond lengths and bond angles are in good agreement with those reported for other complexes containing the same cation [218,219]. The [MoS$_4$] tetrahedron is distorted with S-Mo-S angles between 108.66(3) and 110.04(3)°. The Mo-S bond distances vary from 2.1683(8) to 2.2114(8) Å, with a mean Mo-S bond length of 2.1872 Å (Table 4.3.34). Although the geometric parameters of **21** are in agreement with those in other thiomolybdates, two of the Mo-S bond distances are longer, while the other two distances are shorter than the average Mo-S bond length of 2.177(6) Å reported for (Et$_4$N)$_2$[MoS$_4$] [178]. The elongation of Mo-S bond distances can be attributed to the observed short hydrogen bonding contacts (2.379 to 2.884 Å) between the cation and anion (Table 4.3.35).
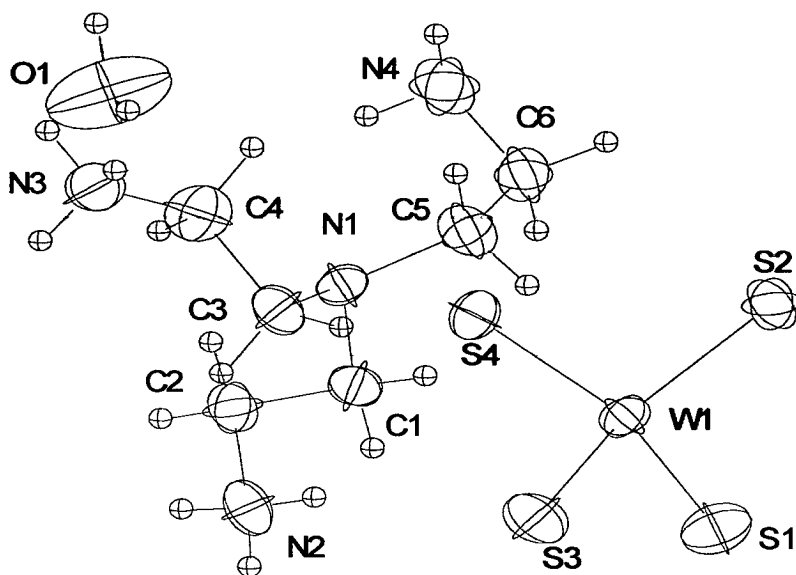
Fig. 4.3.33 Crystal structure of (trenH₂)[[WS₄]·H₂O **18** with labeling and displacement ellipsoids drawn at the 50% probability level.
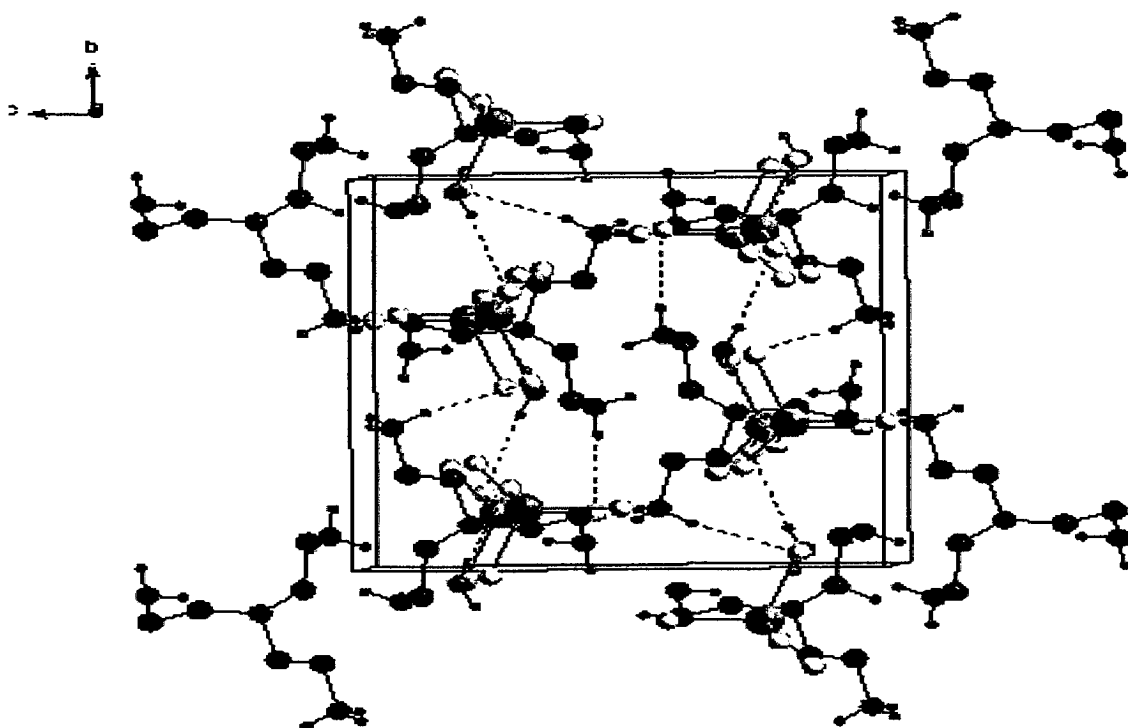
Fig. 4.3.34. Hydrogen bonding network in (trenH₂)[[WS₄]·H₂O **18** with view along 'c' axis (hydrogen bonding is shown as dashed lines). Colour codes; H purple, C black, W grey, S yellow, N blue. H atoms attached to carbon are omitted for clarity

Table 4.3.32 Selected geometric parameters (Å, °) for (trenH$_2$)[WS$_4$] · H$_2$O **18**

W(1)-S(3)	2.1739 (6)	C(1)-C(2)	1.512 (3)
W(1)-S(1)	2.1925 (7)	C(2)-N(2)	1.489 (3)
W(1)-S(2)	2.1954 (6)	C(3)-C(4)	1.505 (3)
W(1)-S(4)	2.1997 (6)	C(4)-N(3)	1.477 (4)
N(1)-C(1)	1.470 (3)	C(5)-C(6)	1.521 (3)
N(1)-C(5)	1.471 (3)	C(6)-N(4)	1.458 (3)
N(1)-C(3)	1.475 (3)		
S(3)- W(1) -S(1)	108.09 (3)	C(5)-N(1)-C(3)	110.58 (18)
S(3)- W(1) -S(2)	110.90 (3)	N(1)-C(1)-C(2)	110.60 (17)
S(1)- W(1) -S(2)	109.68 (3)	N(2)-C(2)-C(1)	110.52 (18)
S(3)- W(1) -S(4)	109.80 (3)	N(1)-C(3)-C(4)	111.97 (19)
S(1)- W(1) -S(4)	109.63 (3)	N(3)-C(4)-C(3)	110.6 (2)
S(2)- W(1) -S(4)	108.73 (2)	N(1)-C(5)-C(6)	113.7 (2)
C(1)- N(1) -C(5)	111.93 (18)	N(4)-C(6)-C(5)	116.0 (2)
C(1)- N(1) –C(3)	110.98 (17)		

Table 4.3.33 Hydrogen-bonding geometry (Å, °) for (trenH$_2$)[WS$_4$] · H$_2$O **18**

D-H...A	d(D-H)	D(H...A)	d(D...A)	<DHA	Symmetry code
N2-H1...S2	0.861	2.590	3.405	158.17	x+1, -y+1/2, z+1/2
N2-H1...S1	0.861	2.946	3.457	119.97	x+1, -y+1/2, z+1/2
N2-H2...S4	0.862	2.536	3.387	169.24	–x+1, y-1/2, -z+1/2
N2-H2...S2	0.862	2.994	3.388	110.07	–x+1, y-1/2, -z+1/2
N2-H3...N4	0.862	1.946	2.807	176.84	x, -y+1/2, z+1/2
N3-H1...S4	0.862	2.634	3.424	152.95	–x+1, -y+1,-z+1
N3-H2...O1	0.862	1.983	2.797	156.99	
N3-H3...S2	0.861	2.462	3.318	172.65	-x+1, y+1/2, -z+1/2
N4-H1...S3	0.891	2.939	3.727	148.28	-x+1, y+1/2, -z+1/2
N4-H2...S1	0.892	3.015	3.636	128.32	x+1, y, z
O1-H1...S1	0.822	2.500	3.289	161.20	x+1, y, z
O1-H2...S1	0.822	2.596	3.407	169.28	–x+1, y+1/2, -z+1/2

D = Donor; A = Acceptor

Table 4.3.34 Selected geometric parameters (Å, °) for (pipH$_2$)[MoS$_4$] **21**

Mo(1)-S(4)	2.1683 (8)	C(1)-C(2)	1.512 (4)
Mo(1)-S(3)	2.2004 (7)	N(2)-C(3)	1.487 (4)
Mo(1)-S(1)	2.1687 (8)	N(1)-C(4)	1.481 (4)
Mo(1)-S(2)	2.2114 (8)	C(2)-N(2)	1.485 (4)
N(1)-C(1)	1.479 (4)	C(3)-C(4)	1.515 (4)
S(4)-Mo(1)-S(1)	110.48 (3)	S(4)-Mo(1)-S(3)	109.71 (3)
S(1)-Mo(1)-S(3)	108.66 (3)	S(4)-Mo(1)-S(2)	110.04 (3)
S(1)-Mo(1)-S(2)	108.71 (3)	S(3)-Mo(1)-S(2)	109.21 (3)
C(1)-N(1)-C(4)	112.0 (2)	N(1)-C(1)-C(2)	110.6 (2)
N(2)-C(2)-C(1)	110.5 (2)	C(2)-N(2)-C(3)	111.8 (2)
N(2)-C(3)-C(4)	110.2 (2)	N(1)-C(4)-C(3)	110.2 (2)

Table 4.3.35 Hydrogen-bonding geometry (Å, °) for (pipH$_2$)[MoS$_4$] **21**

D-H...A	d(D-H)	d(H...A)	d(D...A)	<DHA	Symmetry code
N1-H1A...S2	0.900	2.561	3.298	139.62	
N1-H1A...S1	0.900	2.648	3.303	130.33	
N1-H1B...S2	0.900	2.379	3.260	166.21	$x, -y+1/2, z+1/2$
N2-H2C...S3	0.900	2.465	3.219	141.50	$x-1, -y+1/2, z+1/2$
N2-H2C...S4	0.900	2.884	3.465	123.65	$x-1, -y+1/2, z+1/2$
N2-H2D...S3	0.900	2.454	3.255	162.91	$x-1, y, z$
N2-H2D...S1	0.900	2.819	3.274	112.72	$x-1, y, z$

D = Donor; A = Acceptor

These details were not given in the earlier report [217]. This results in an extended two-dimensional network as shown in Fig 4.3.36. Each $(pipH_2)^{2+}$ cation is surrounded by four $[WS_4]^{2-}$ anions and every $[WS_4]^{2-}$ anion is surrounded by four cations. Both cations and anions are held together by hydrogen bonds which many of which run along 'c' axis in a zigzag fashion (Fig 4.3.37). The S···H distances in **21** are shorter than the S···H distances of 2.55 to 3.02 Å reported for $(NH_4)_2[MoS_4]$ [176]. The atoms S(1,2,3) have two S···H contacts and S(4) has one such interaction. This feature is responsible for the very short Mo-S(4) distance of 2.1683 Å. The small D-H···A bond angle of 123.65° together with the longest S···H distance of 2.884 Å observed for S(4) indicates a very weak interaction. The shortest S···H distance of 2.379 Å is accompanied by the largest D-H···A angle which can explain the long Mo-S(2) bond of 2.2114(8) Å. The intermediate Mo-S bond lengths can be similarly explained based on the strengths of the H-bonding interactions. The Mo-S(2) distance of 2.2114(8) Å in is one of the longest Mo-S bond lengths reported so far, for tetrathiomolybdate complexes. It is also noted that the difference between the longest and the shortest Mo-S bond distances of 0.0431 Å is very large. This is responsible for the appearance of a split Mo-S vibration in the IR spectrum (*vide infra*).

The structure of $(pipH_2)[WS_4]$ **22** [87] consists of $(pipH_2)^{2+}$ cation and $[WS_4]^{2-}$ anion (Fig 4.3.38). The substitution of Mo by W in **21** has resulted in a very slight increase in the unit cell volume (unit cell volume of the Mo complex is 1101.7 (2) Å^3). The [WS_4] tetrahedron is moderately distorted with S-W-S angles between 108.57(3) and 110.49(3)°. The W-S bond distances vary from 2.1762(7) to 2.2147(7) Å, with a mean W-S bond length of 2.1937 Å (Table 4.3.36). Two of the W-S bond distances in **22** are longer, while the other two distances are shorter at around 2.1762 (7) Å. The elongation of W-S bond distances can be attributed to the observed seven short hydrogen bonding contacts (2.389 to 2.881 Å) between the cation and anion (Table 4.3.37).
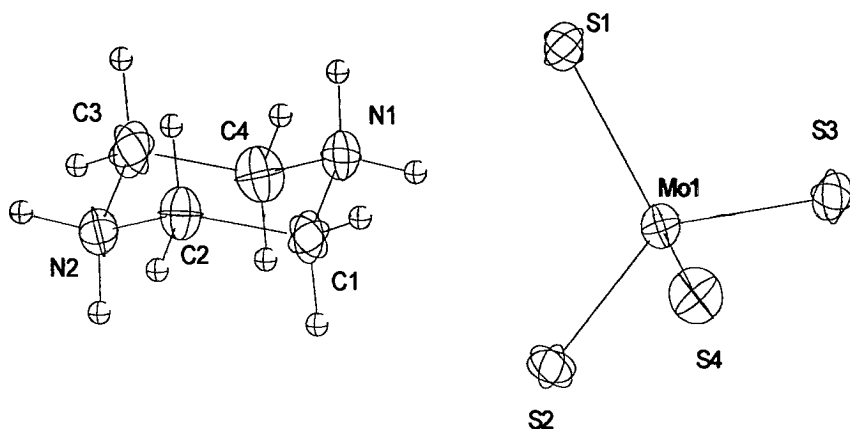
Fig. 4.3.35 Crystal structure of (pipH₂)[[MoS₄] **21** with labeling and displacement ellipsoids drawn at the 50% probability level.

Fig. 4.3.36 Hydrogen bonding network in (pipH₂)[[MoS₄] **21** with view along 'b' axis (hydrogen bonding is shown as dashed lines). Colour codes; H purple, C black, Mo grey, S yellow, N blue. H atoms attached to carbon are omitted for clarity.

Fig. 4.3.37 Crystal packing of $(pipH_2)^{2+}$ and $[MoS_4]^{2-}$ in $(pipH_2)[[MoS_4]$ **21** via zigzag hydrogen bonding network which run along 'c' axis (hydrogen bonding is shown as dashed lines). Colour codes; H purple, C black, Mo grey, S yellow, N blue. H atoms attached to carbon are omitted.
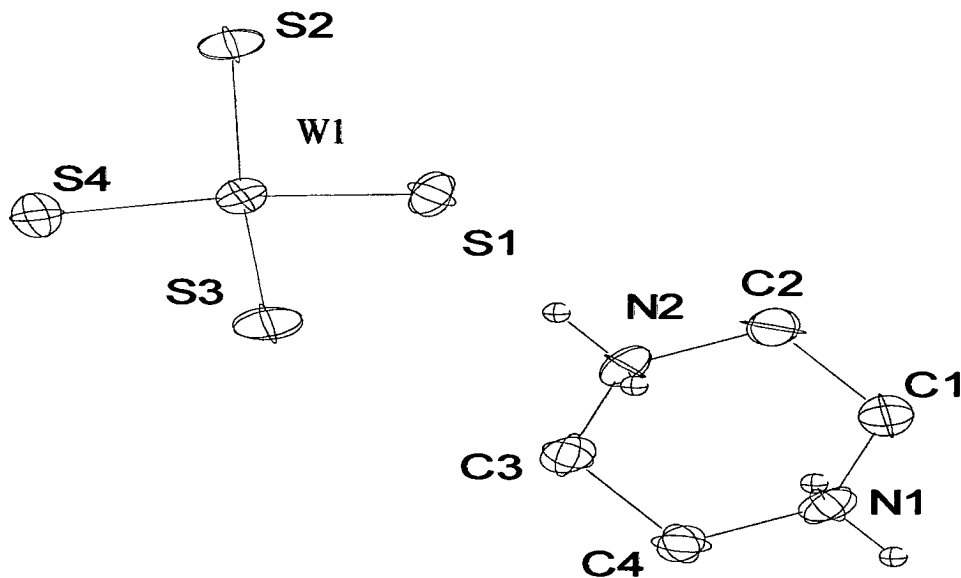
Fig. 4.3.38 Crystal structure of $(pipH_2)[[WS_4]$ **22** with labeling and displacement ellipsoids drawn at the 50% probability level.

Table 4.3.36 Selected geometric parameters (Å, °) for (pipH₂)[WS₄] **22**

W(1)-S(3)	2.1762 (7)	N(1)-C(4)	1.492 (4)
W(1)-S(4)	2.1797 (7)	C(1)-C(2)	1.510 (4)
W(1)-S(1)	2.2042 (7)	C(2)-N(2)	1.502 (4)
W(1)-S(2)	2.2147 (7)	N(2)-C(3)	1.479 (4)
N(1)-C(1)	1.485 (4)	C(3)-C(4)	1.510 (3)
S(3)- W(1) -S(4)	110.49(3)	C(1)-N(1)-C(4)	111.6 (2)
S(3)- W(1) -S(1)	109.67 (3)	N(1)-C(1)-C(2)	110.7 (2)
S(4)- W(1) -S(1)	108.57 (3)	N(2)-C(2)-C(1)	110.0 (2)
S(3)- W(1) -S(2)	110.12 (3)	C(3)-N(2)-C(2)	112.1 (2)
S(4)- W(1) -S(2)	108.75 (3)	N(2)-C(3)-C(4)	110.3 (2)
S(1)- W(1) -S(2)	109.20 (3)	N(1)-C(4)-C(3)	110.3 (2)

Table 4.3.37 Hydrogen-bonding geometry (Å, °) for (pipH₂)[WS₄] **22**

D-H...A	d(D-H)	d(H...A)	d(D...A)	<DHA	Symmetry code
N1-H1...S2	0.900	2.389	3.272	166.67	
N1-H1...S2	0.900	2.587	3.318	138.85	x, -y+1/2, z-1/2
N1-H2...S4	0.900	2.638	3.299	130.95	x, -y+1/2, z-1/2
N2-H1...S1	0.900	2.486	3.234	140.83	x-1, y, z
N2-H1...S3	0.900	2.881	3.470	124.33	x-1, y, z
N2-H2...S1	0.900	2.458	3.331	163.71	x-1, -y+1/2, z-1/2
N2-H2...S4	0.900	2.841	3.287	112.07	x-1, -y+1/2, z-1/2

D = Donor; A = Acceptor

The diagram showing the hydrogen bonding scheme and coordination of $[WS_4]^{2-}$ anion in **22** is displayed in Fig 4.3.39. The S···H distances are shorter than the S···H distances of 2.432 to 3.003 Å observed in the related complex **2**. The atoms S(1,2,4) have two S···H contacts and S(3) has one such interaction. This feature is responsible for the very short W-S(3) distance of 2.1762 (7) Å. The small D-H···A bond angle of 124.33° together with the longest S···H distance of 2.881 Å observed for S(3) indicates a very weak interaction. The shortest S···H distance of 2.389 Å is accompanied by the largest D-H···A angle which can explain the long W-S(2) bond of 2.2147 (7) Å. The W-S(2) distance of 2.2147 (7) Å in **22** is one of the longest W-S bonds in tetrathiotungstates. It is to be noted that the difference between the longest and the shortest W-S bond distances of 0.0385 Å in **22** is very large when compared with other tetrathiotungstates discussed above. This is probably responsible for the appearance of a split W-S vibration in the IR spectrum.

The structure of $(1,4-dmpH_2)[WS_4]$ **24** [86] contains discrete $(1,4-dmpH_2)^{2+}$ cations and $[WS_4]^{2-}$ (Fig 4.3.40). There are two crystallographically independent 1,4-dimethylpiperazinium dications in the asymmetric unit, both of which are located around a centre of inversion, while the anions are located in general positions. The bond lengths and bond angles of the $(1,4-dmpH_2)^{2+}$ dication are in good agreement with those reported for compounds containing similar cations [220]. There is a slight distortion of $[WS_4]$ tetrahedron with the S-W-S angles ranging between 108.32 (3) and 111.67 (4) with average S-W-S bond angle of 109.46 ° (Table 4.3.38). The W-S bond distances range from 2.1781 (8) to 2.2136 (8) Å. All the structural parameters are in good agreement with those for other complexes containing the $[WS_4]^{2-}$ moiety. In **24** the $(1,4-dmpH_2)^{2+}$ cations are connected to $[WS_4]^{2-}$ dianion via hydrogen bonding between the S atoms of $[WS_4]^{2-}$ anion and the H atoms bound to donor nitrogen atoms of cation. The two dimensional packing of cations and anions via hydrogen bonding network is depicted in Fig 4.3.41. As a result of intermolecular H-bonding interactions, layers are formed which are parallel to (010) plane. All the $[WS_4]^{2-}$ are running along the crystallographic 'b' axis while the hydrogen bonding interactions are along the 'a' axis running in a zigzag fashion. Detailed analysis of hydrogen bonding pattern indicates that the differing nature of W-S bond distances can be attributed to the different numbers and strengths of N-H...S interactions. In
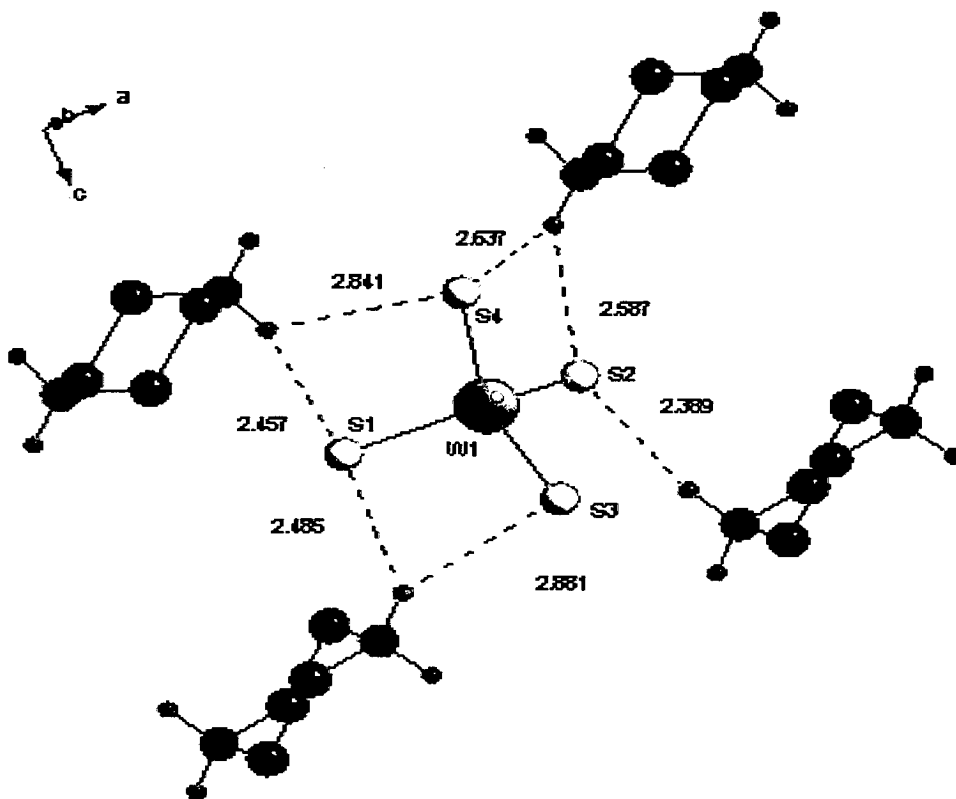
Fig. 4.3.39 Hydrogen bond labels in (pipH$_2$)[WS$_4$] **22**. Colour codes; H purple, C black, W grey, S yellow, N blue. H atoms attached to carbon are omitted for clarity.
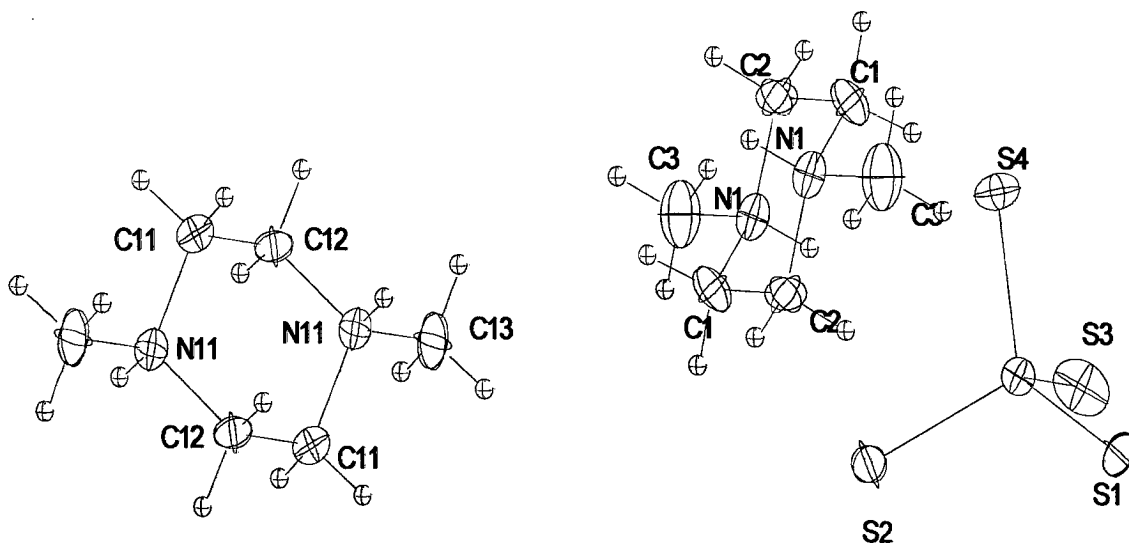

Fig. 4.3.40 Crystal structure of (1,4-dmpH$_2$)[[WS$_4$] **24** with labeling and displacement ellipsoids drawn at the 50% probability level.

all, four short intermolecular S...H contacts are observed in **24** (Fig 4.3.42), with N...S distances ranging from 3.347 (3) to 3.489 (2) Å (Table 4.3.39). Atoms S1 and S2 are involved in making a single contact with H atoms bound to donor N of cation while S4 has two short contacts. The shortest W-S distance of 2.1781 (8) Å is observed for S3, which is not involved any of the four hydrogen-bonding interactions. Although atom S4 has two short contacts with an average N...S distance of 3.4785 Å, they are relatively long compared to the shortest distance, 3.374 Å between S2 and N1. This observation suggests that a short hydrogen bond influences the W-S distances more strongly than two medium long H...S contacts and therefore may explain why W-S2 is longer than W-S4. The longer W-S2 bond distance is accompanied with the shortest intermolecular hydrogen bonding interaction with bond separation 2.64 Å and smallest <DHA angle of 135 °. The longest W-S distance of 2.2136 Å is shorter than that observed in **22** (2.2147 Å). The difference between longest and shortest W-S bon lengths in **24** is 0.0355 and is again shorter than 0.0385 observed in **22**.

The crystal structure of (2-pipH-1-EtNH$_3$)[MoS$_4$]·½H$_2$O **27** consists of (2-pipH-1-EtNH$_3$)$^{2+}$ cations, [MoS$_4$]$^{2-}$ dianions and half lattice water molecule (Fig 4.3.43). In this case, although (2-pip-1-EtNH$_2$) is a triamine, only two N atoms are protonated. The secondary N of pip and primary N of ethylamine are protonated while the tertiary N of pip is not protonated. It crystallizes in the monoclinic C2/c space group with unit cell parameters, a = 24.451(3) Å, b = 7.1150(10) Å, c = 17.864(2) Å, β = 115.030(10)°, V = 2815.9(6) Å^3 and Z = 8. The selected bond angles and bond lengths are listed in Table 4.5.17. The S-Mo-S bond angles vary between 110.34 (3) and 108.51 (3) ° (Table 4.3.40). In 27, the cyclic amine adopts the chair form. The Mo-S distances range from 2.1703 (7) to 2.2005 (8) Å with mean Mo-S bond distance of 2.183 Å. The difference between the longest and the shortest Mo-S bond distance is 0.0302 Å. Two of the Mo-S bond distances are shorter than the average Mo-S bond length of 2.177 (6) Å in (Et$_4$N)$_2$[MoS$_4$]. The cation, anion, and crystal water in **27** are connected via six N-H...S short contacts, a N-H...O contact and a O-H...S contact which leads to an extended three dimensional network structure. The cyclic amine which adopts a chair form and [WS$_4$]$^{2-}$ anion rods are parallel to the crystallographic 'ac' plane and run in the direction of 'c' axis (Fig 4.3.44). The N-H...S distances range between 2.451 and 2.999 Å with <DHA
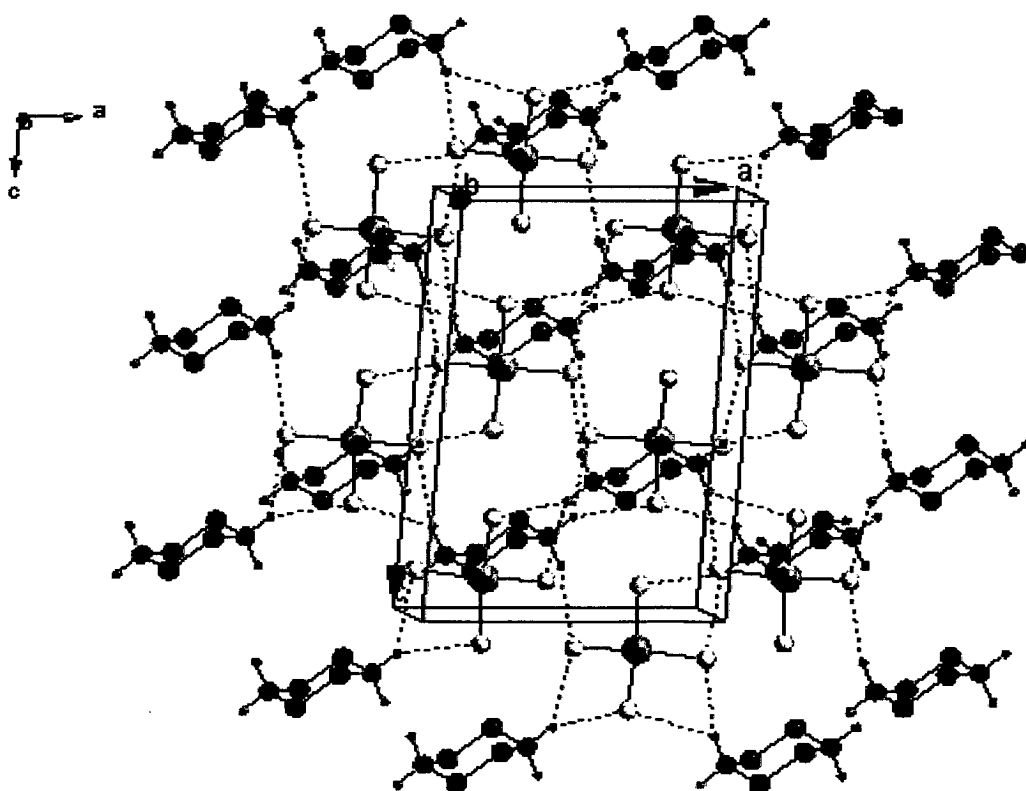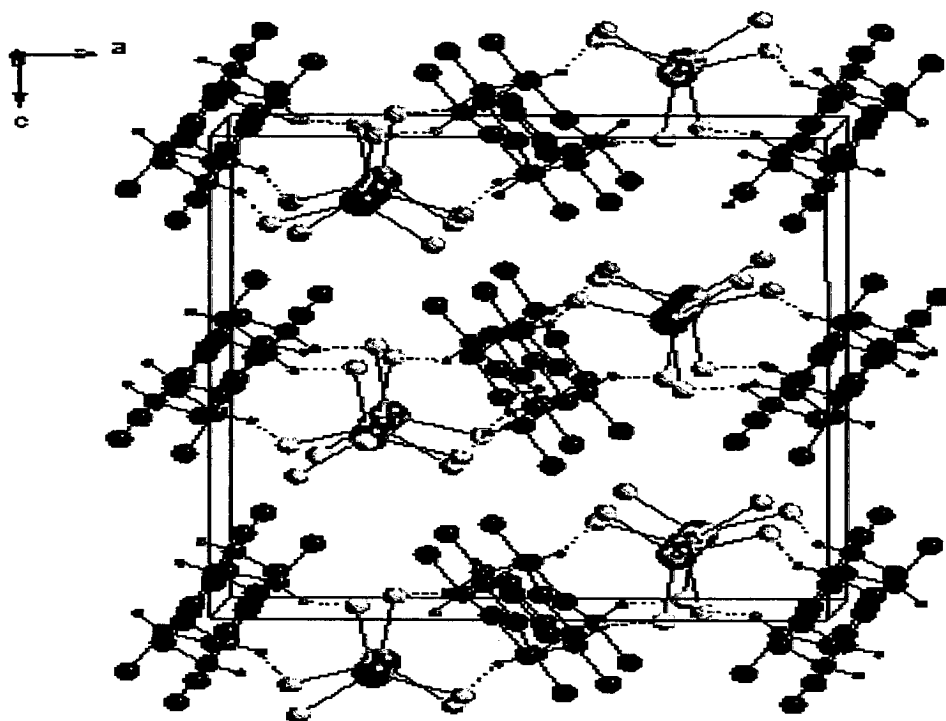
Fig. 4.3.41 Hydrogen bonding network in $(1,4\text{-dmpH}_2)[[WS_4]$ **24** with view along 'b' axis (hydrogen bonding is shown as dashed lines). Colour codes; H purple, C black, W grey, S yellow, N blue. H atoms attached to carbon are omitted.
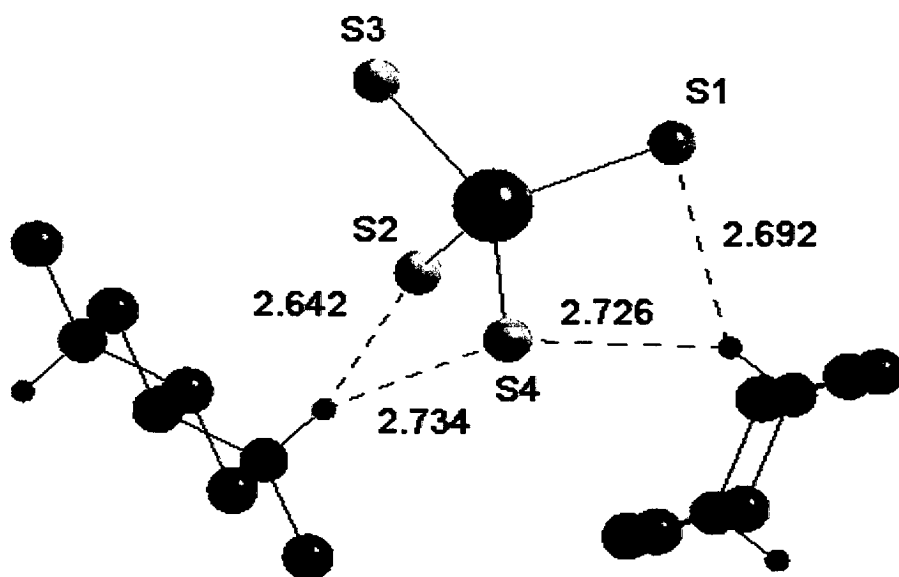
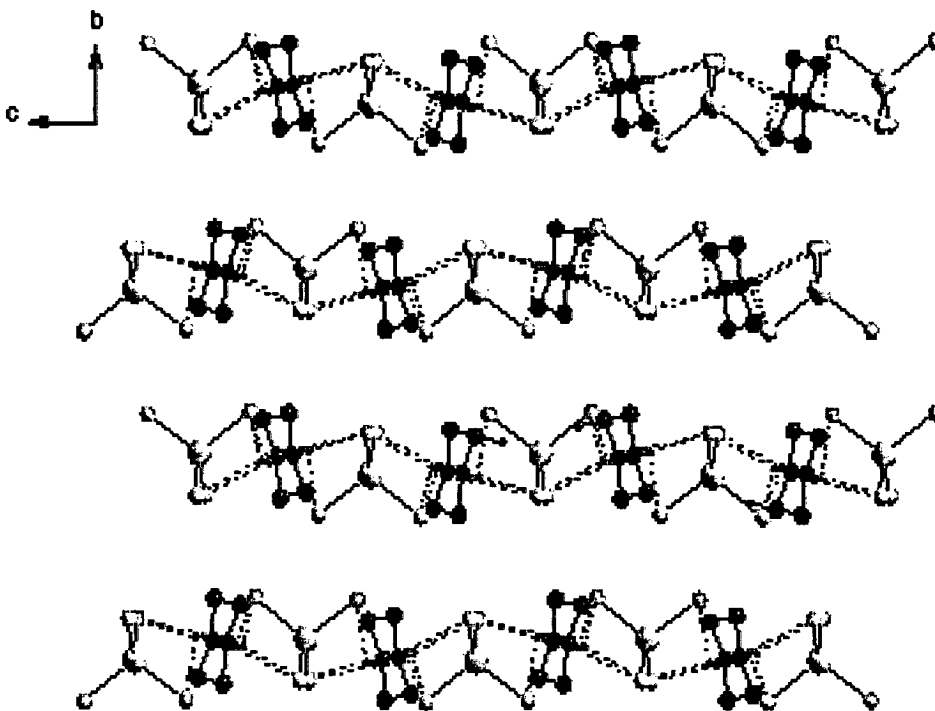Fig. 4.3.42 Hydrogen bond labels in $(1,4\text{-dmpH}_2)[WS_4]$ **24**. Colour codes; H purple, C black, W grey, S yellow, N blue. H atoms attached to carbon are omitted.

Table 4.3.38 Selected geometric parameters (Å, °) for (1,4-dmpH$_2$)[WS$_4$] **24**

W(1)-S(3)	2.1781 (8)	C(1)-C(2)	1.514 (5)
W(1)-S(1)	2.1866 (7)	C(2)-N(1)^i	1.495 (4)
W(1)-S(4)	2.1988 (12)	N(11)-C(13)	1.499 (4)
W(1)-S(2)	2.2136 (8)	N(11)-C(12)^{ii}	1.500 (4)
N(1)-C(3)	1.491 (4)	N(11)-C(11)	1.502 (4)
N(1)-C(2)^i	1.495 (4)	C(11)-C(12)	1.512 (5)
N(1)-C(1)	1.497 (4)	C(11)-N(11)^{ii}	1.500 (4)
S(3)-W(1)-S(1)	111.67 (3)	S(3)-W(1)-S(2)	110.88 (4)
S(3)-W(1)-S(4)	108.48 (3)	S(1)-W(1)-S(2)	108.94 (3)
S(1)-W(1)-S(4)	108.46 (6)	S(4)-W(1)-S(2)	108.32 (3)
C(3)-N(1)-C(2)^i	111.4 (3)	C(13)-N(11)-C(12)^{ii}	111.1 (2)
C(3)-N(1)-C(1)	110.8 (3)	C(13)-N(11)-C(11)	111.1 (3)
C(2)^i-N(1)-C(1)	110.4 (2)	C(12)^{ii}-N(11)-C(11)	110.4 (2)
N(1)-C(1)-C(2)	111.5 (2)	N(11)-C(11)-C(12)	110.7 (3)
N(1)^i-C2(1)-C(1)	110.3 (3)	N(11)^{ii}-C(12)-C(11)	111.3 (2)

Symmetry code: (i)1-x, 1-y, 1-z; (ii) 1-x, 1-y, -z

Table 4.3.39 Hydrogen-bonding geometry (Å, °) for (1,4-dmpH$_2$)[WS$_4$] **24**

D-H...A	d(D-H)	d(H...A)	d(D...A)	<DHA	Symmetry code
N1-H1...S2	0.91	2.641	3.347	134.99	
N1-H1...S4	0.91	2.734	3.489	141.11	
N11-H11...S1^{iii}	0.91	2.692	3.427	138.53	1/2+x, y, 1/2-z
N11-H11...S4^{iii}	0.91	2.727	3.468	139.38	1/2+x, y, 1/2-z

D = Donor; A = Acceptor

Fig. 4.3.43 Crystal structure of (2-pipH-1-EtNH₃)[MoS₄]·½H₂O **27** with labeling and displacement ellipsoids drawn at the 50% probability level.

Fig. 4.3.44 Hydrogen bonding network in 2-pipH-1-EtNH₃)[MoS₄]·½H₂O **27** with view along 'b' axis (hydrogen bonding is shown as dashed lines). Colour codes; H purple, C black, Mo grey, S yellow, N blue. H atoms attached to carbon are omitted.

ranging between 122.33 and 161.85 ° (Table 4.3.41). S1 is involved in two N-H...S contacts, S2 has three such contacts, S3 has one contact and interestingly S4 is not at all involved in any of the N-H...S interactions. However S4 has one O-H...S contact that arises from the interaction between crystal water and $[WS_4]^{2-}$ anion. S1 has two short contacts of 2.558 and 2.714 Å while S2 is involved in longest S...H distance of 2.999 Å. The other two contacts of S2 with distances 2.529 and 2.706 are relatively shorter. The shortest S...H contact of 2.451 Å is accompanied with S3. All the six S...H distances are shorter than the sum of van der Waals radii of S and [213] atoms indicating that these contacts are relatively stronger.

4.3.8. Crystal structure of (trans-1,2-cnH)₂[WS₄] **28**

The asymmetric unit of compound **28** contains discrete monoprotonated cation of *trans*-1,2-cn, which adopts a chair confirmation, and the $[WS_4]^{2-}$ anion (Fig 4.3.45). The WS₄ tetrahedron is moderately distorted with S-W-S angles ranging between 108.04 (6)° and 110.89 (5)° with an average value of 109.47°. The W-S bond lengths vary from 2.1874(11) to 2.1978 (10) Å with a mean W-S bond length of 2.1926 Å (Table 4.3.42). The geometric parameters of **28** are in good agreement with those for other organic ammonium tetrathiotungstates like (enH₂)[WS₄] **2** [84] and (1,3-pnH₂)[WS₄] [85]. Two of the bond lengths are shorter while the other two are longer than the average W-S bond length of 2.1926 Å. This feature can be explained based on the strength and number of H-bonding interactions between the organic cation and the $[WS_4]^{2-}$ anion. As a result of the H-bonding interactions the cations and anions in **28** are organized in a rod-like manner along [100] with the ammonium groups of the organic cations always pointing towards the S atoms of the anion. Hence, the sequence along this direction is ···$[WS_4]^{2-}$ - *trans*-1,2-cn - *trans*-1,2-cn - $[WS_4]^{2-}$ ···. The special arrangement of the constituents may be viewed as layers within the (001) plane. Along [010] and [001] the anions and cations each form individual stacks. Each anion is surrounded by six cations and 5 short S...H contacts ranging from 2.675 to 2.969 Å (Table 4.3.43) are observed. The shortest S...H contact of 2.675 Å and another at 2.769 Å observed for S1 can explain the elongation of the W-S1 bond. Although three S...H contacts are observed for S2, the W-S2 bond is relatively shorter at 2.1874(11) Å. This can be attributed to the longer S...H distances as well as the smaller values of the N-H...S angles. In addition, a very short N-H...N contact at

Table 4.3.40 Selected geometric parameters (Å, °) for (2-pipH-1-EtNH₃)[MoS₄]· ½H₂O **27**

Mo(1)-S(4)	2.1703 (7)	N(1)-C(1)	1.469 (3)
Mo(1)-S(3)	2.1750 (7)	C(1)-C(2)	1.503 (4)
Mo(1)-S(2)	2.1884 (7)	C(2)-N(2)	1.485 (3)
Mo(1)-S(1)	2.2005 (8)	N(2)-C(3)	1.488 (3)
N(1)-C(4)	1.457 (3)	C(3)-C(4)	1.513 (4)
N(1)-C(5)	1.460 (3)	C(5)-C(6)	1.511 (4)
		C(6)-N(3)	1.476 (4)
S(4)-Mo(1)-S(3)	109.43 (3)	S(4)-Mo(1)-S(1)	108.51(3)
S(4)-Mo(1)-S(2)	110.34 (3	S(3)-Mo(1)-S(1)	110.29(3)
S(3)-Mo(1)-S(2)	108.82 (3)	S(2)-Mo(1)-S(1)	109.45 (3)
C(4)-N(1)-C(5)	111.9 (2)	C(2)-N(2)-C(3)	110.45 (19)
C(4)-N(1)-C(1)	109.69 (19)	N(2)-C(3)-C(4)	109.9 (2)
C(5)-N(1)-C(1)	110.2 (2)	N(1)-C(4)-C(3)	111.1 (2)
N(1)-C(1)-C(2)	110.3 (2)	N(1)-C(5)-C(6)	111.6 (2)
N(2)-C(2)-C(1)	109.9 (2)	N(3)-C(6)-C(5)	110.5 (2)

Table 4.3.41 Hydrogen-bonding geometry (Å, °) for (2-pipH-1-EtNH₃)[MoS₄]· ½H₂O **27**

D-H...A	d(D-H)	d(H...A)	d(D...A)	<DHA	Symmetry code
N1-H1...O1	0.900	2.349	3.064	136.29	
N1-H1...S2	0.900	2.706	3.445	140.07	-x+3/2, y+1/2, z+3/2
N2-H2...S3	0.900	2.451	3.282	153.64	x-1/2, y+1/2, z
N2-H2...S2	0.900	2.999	3.562	122.33	x-1/2, y+1/2, z
N3-H3...S2	0.890	2.529	3.320	148.39	-x+3/2, -y+1/2, z+1
N3H3...S1	0.890	2.558	3.415	161.85	
N3-H3...S1	0.890	2.714	3.378	132.31	-x+3/2, -y+3/2, -z+1
O1-H1...S4	0.820	2.670	3.443	157.88	x-1/2, y-1/2, z

D = Donor; A = Acceptor

Table 4.3.42 Selected geometric parameters (Å, °) for (trans-1,2-cnH)₂[WS₄] **28**

W(1)-S(2)	2.1874 (11)	C(1)-C(2)	1.526 (6)
W(1)-S(2A)	2.1874 (11)	C(1)-C(6)	1.527 (5)
W(1)-S(1A)	2.1978 (10)	C(2)-C(3)	1.522 (7)
W(1)-S(1)	2.1978 (10)	C(3)-C(4)	1.512 (8)
N(1)-C(1)	1.509 (5)	C(4)-C(5)	1.519 (8)
N(2)-C(6)	1.470 (6)	C(5)-C(6)	1.539 (6)
S(2)-W(1)-S(2A)	108.33 (7)	S(2)-W(1)-S(1)	109.35 (4)
S(2)-W(1)-S(1A)	110.89 (5)	S(2A)-W(1)-S(1)	110.89 (5)
S(2A)-W(1)-S(1A)	109.35 (4)	S(1A)-W(1)-S(1)	108.04 (6)
N(1)-C(1)-C(2)	110.3 (3)	C(3)-C(4)-C(5)	110.5 (4)
N(1)-C(1)-C(6)	109.8 (3)	C(4)-C(5)-C(6)	111.3 (4)
C(2)-C(1)-C(6)	111.7 (4)	N(2)-C(6)-C(1)	110.0 (3)
C(3)-C(2)-C(1)	111.5 (4)	N(2)-C(6)-C(5)	114.4 (4)
C(4)-C(3)-C(2)	110.8 (4)	C(1)-C(6)-C(5)	109.5 (3)

Table 4.3.43 Hydrogen-bonding geometry (Å, °) for (trans-1,2-cnH)₂[WS₄] **28**

D-H...A	d(D-H)	d(H...A)	d(D...A)	<DHA	Symmetry code
N1-H1...S1	0.890	2.769	3.596	155.19	-x+1, -y+1, -z
N1-H1...S2	0.890	2.872	3.472	126.10	-x+1, -y+1, -z
N1-H2...N2	0.890	2.029	2.911	171.02	-x+1, y, -z+1/2
N1-H3...S1	0.890	2.675	3.538	163.69	-x+1, y-1, -z+1/2
N2-H1...S2	0.890	2.969	3.786	153.47	
N2-H2...S2	0.890	2.741	3.433	135.58	x, -y+1, z+1/2

D = Donor; A = Acceptor

2.029 Å is observed which joins the cations to form pairs. The crystal packing diagram of the resulting hydrogen bonding network in **28** is shown in (Fig 4.3.46). The difference between the longest and shortest W-S bond Δ in **28** is 0.0104 Å and is indicative of little distortion. This value is much less compared to the Δ value for (pipH$_2$)[WS$_4$] **22** (0.0385 Å).

4.3.9 Crystal structure description for (mipaH)$_2$[WS$_4$] **29**

Compound **29** crystallizes in space group C2/c and consists of (mipaH)$^+$ cations and [WS$_4$]$^{2-}$ anions (Fig. 4.3.47). The amine group in **29** is protonated and functions as a monocation. The S-W-S angles indicate a small distortion of the tetrahedron. The W-S bond lengths vary from 2.1792(13) to 2.2126(12) Å with an average of 2.1940 Å (Table 4.3.44). The pattern of W-S bond lengths shows two shorter and two longer bonds than the average value. The reason for the elongation of W-S(4) is that S(4) has three strong H bonds (Table 4.3.45) which weaken the bond to W. On the other hand, W-S(2) is the shortest bond because S(2) has only two weak contacts to H atoms and one S(2)$\cdots$H is very long and has a remarkably low angle of 110.77° (Table 4.3.45). The cations and anions are linked via nine N-H$\cdots$S interactions (Fig 4: 3.48) and all the S...H distances are shorter than the sum of the van der Waals radii of S and H. S(4) is involved in three hydrogen bonds, while S(1), S(2) and S(3) have two such contacts each. It is to be noted that the value for Δ = 0.0334 Å is large and can explain the distortion of the [WS$_4$] tetrahedron as well as the observed IR spectrum. The cations and anions are arranged in a layer like fashion with the anions and cations alternating along the 'a' axis (Fig. 4.5.53).

The structural parameters of several tetrathiomolybdates are presented in Table 4.3.46. This has been made with a view to understand the importance of the H-bonding interactions in the elongation of the Mo-S bond lengths. In all the complexes [MoS$_4$] tetrahedron is slightly distorted as seen from range of Mo-S bond distances and S-Mo-S bond angles (Table 4.3.46). The isolation and structural characterization of [MoS$_4$]$^{2-}$ with different cations ranging from (enH$_2$)$^{2+}$, (N-Me-enH$_2$)$^{2+}$, (1,3-pnH$_2$)$^{2+}$, (1,4-bnH$_2$)$^{2+}$, (dienH$_2$), (trenH$_2$)$^{2+}$, (pipH$_2$)$^{2+}$, etc. indicates the flexibility of [MoS$_4$] tetrahedron to exist in different structural environments. In all these complexes the average value of the S-W-S bond angles is very close to the tetrahedral
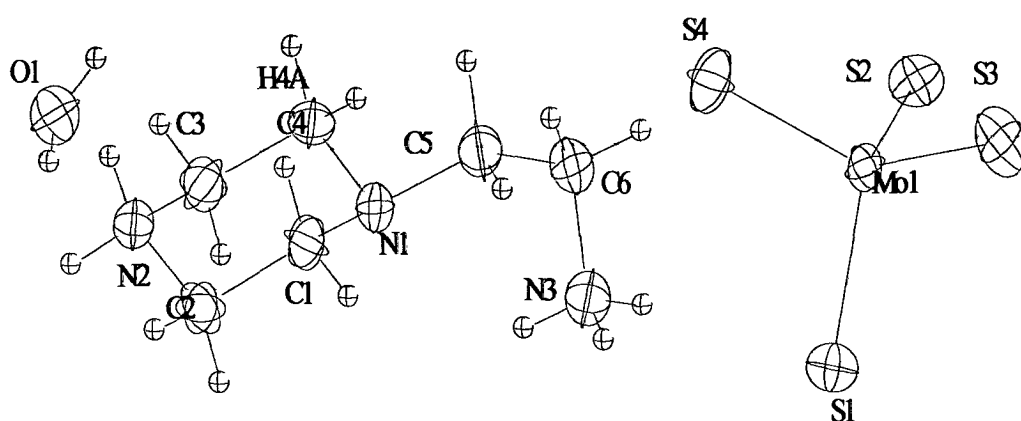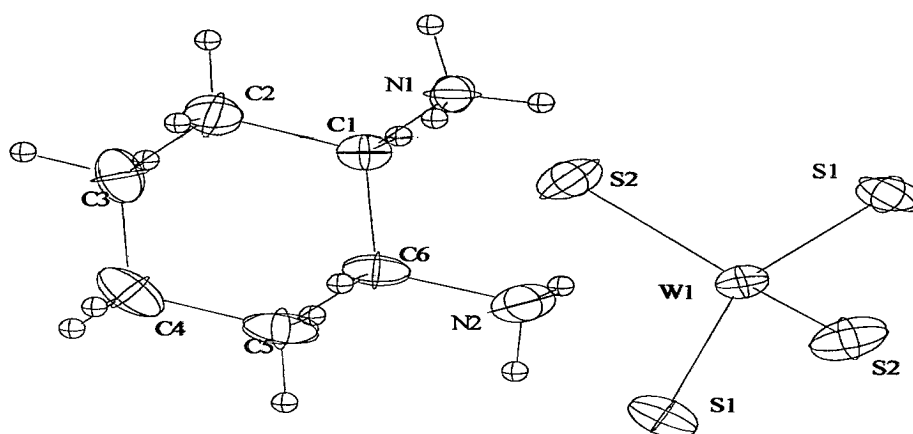
Fig. 4.3.45 Crystal structure of (trans-1,2-cnH)$_2$[WS$_4$] **28** with labeling and displacement ellipsoids drawn at the 50% probability level.
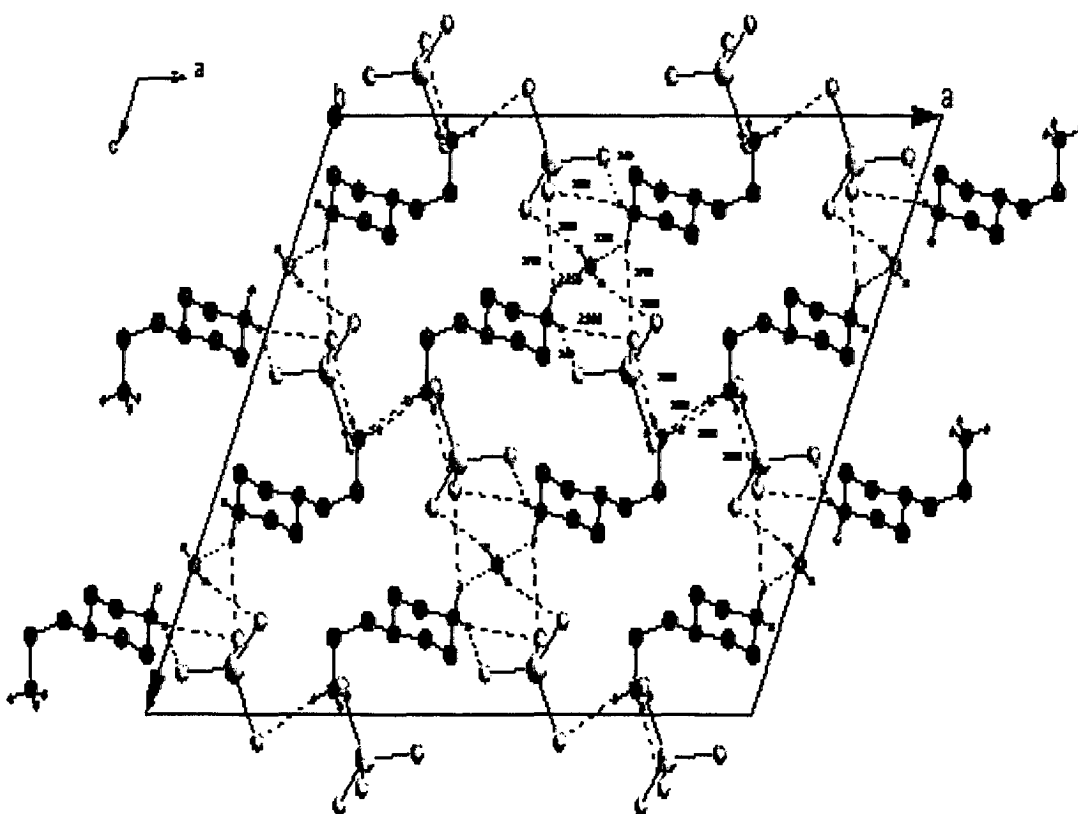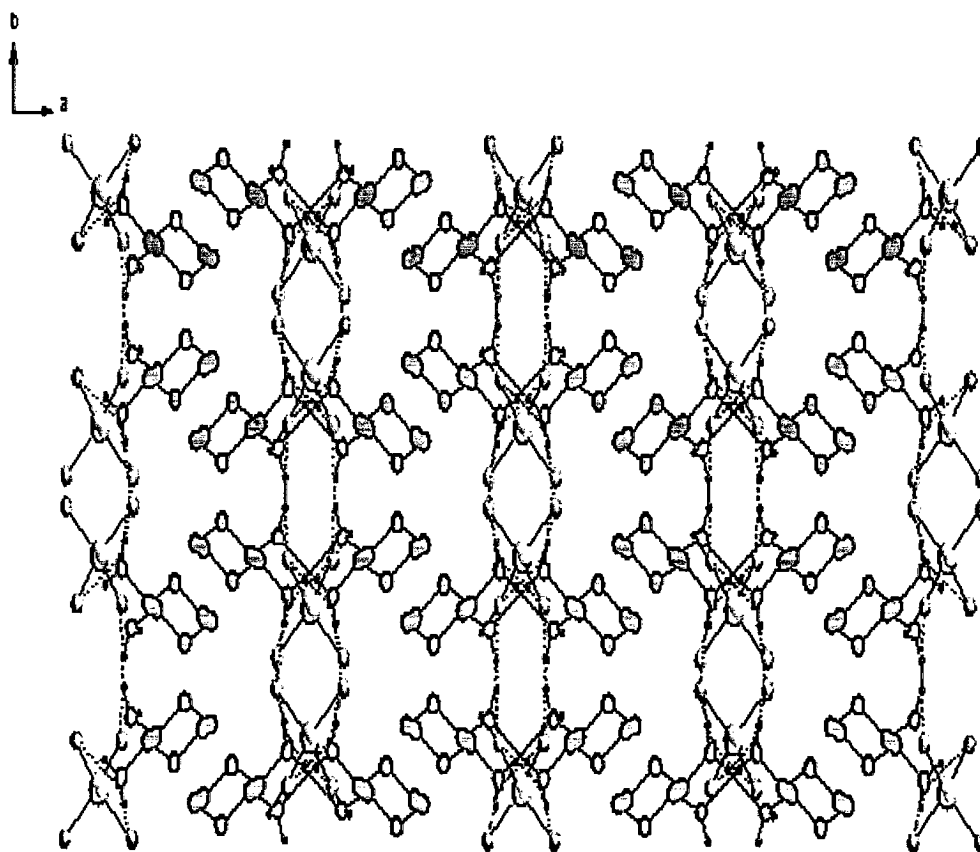

Fig. 4.3.46 Hydrogen bonding network in (trans-1,2-cnH)$_2$[WS$_4$] **28** with view along 'c' axis (hydrogen bonding is shown as dashed lines). Colour codes; H purple, C black, W grey, S yellow, N blue. H atoms attached to carbon are omitted
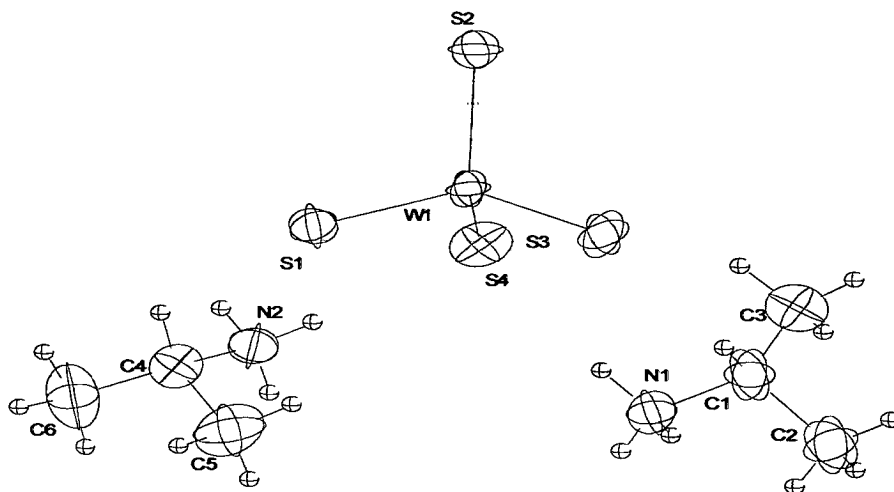
Fig. 4.3.47 Crystal structure of (mipaH)$_2$[WS$_4$] **29** with labeling and displacement ellipsoids drawn at the 50% probability level.
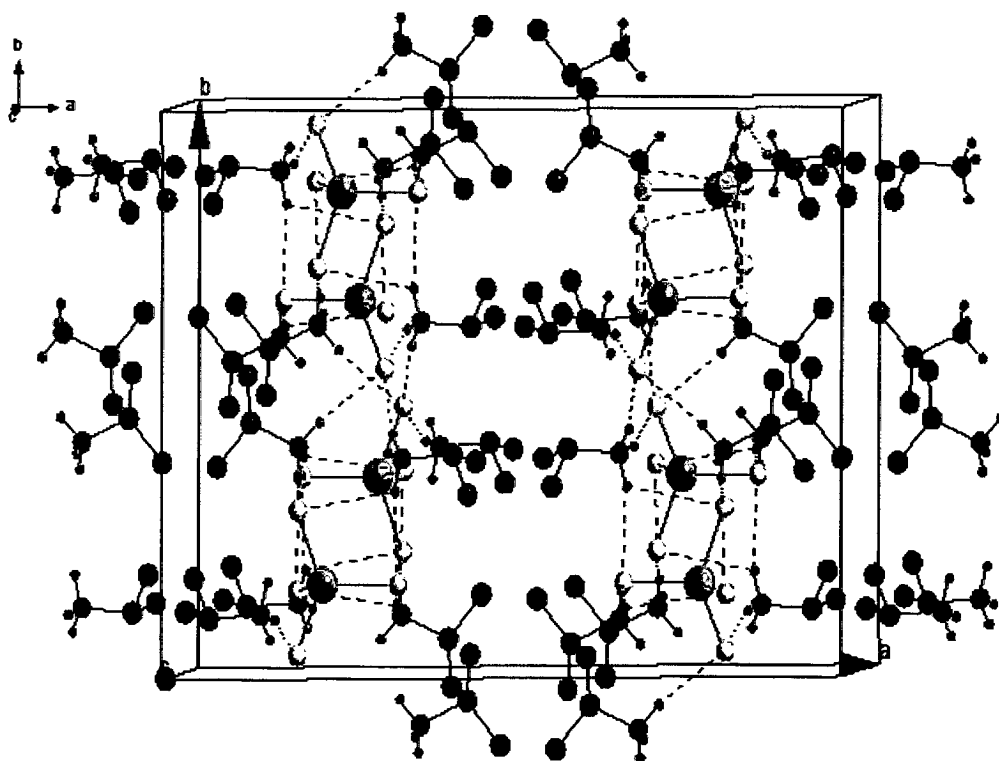
Fig. 4.3.48 Hydrogen bonding network in (mipaH)$_2$[WS$_4$] **29** with view along 'b' axis (hydrogen bonding is shown as dashed lines). Colour codes; H purple, C black, W grey, S yellow, N blue. H atoms attached to carbon are omitted.

Table 4.3.44 Selected geometric parameters (Å, °) for (mipaH)$_2$[WS$_4$] **29**

W(1)-S(2)	2.1792 (13)	C(1)-C(3)	1.465 (10)
W(1)-S(3)	2.1805 (12)	C(1)-C(2)	1.514 (9)
W(1)-S(1)	2.2038 (14)	N(2)-C(4)	1.501 (7)
W(1)-S(4)	2.2126 (12)	C(4)-C(6)	1.497 (8)
N(1)-C(1)	1.497 (7)	C(4)-C(5)	1.510 (8)
S(2)-W(1)-S(3)	109.28 (5)	S(2)-W(1)-S(4)	108.88 (5)
S(2)-W(1)-S(1)	109.28 (6)	S(3)-W(1)-S(4)	110.03 (5)
S(3)-W(1)-S(1)	109.30 (5)	S(1)-W(1)-S(4)	110.05 (6)
C(3)-C(1)-N(1)	109.7 (6)	C(6)-C(4)-N(2)	107.4 (5)

Table 4.3.45 Hydrogen-bonding geometry (Å, °) for (mipaH)$_2$[WS$_4$] **29**

D-H...A	d(D-H)	d(H...A)	d(D...A)	<DHA	Symmetry code
N1-H1...S4	0.890	2.490	3.355	164.11	
N1-H2...S4	0.890	2.555	3.424	165.66	x, -y+1, z-1/2
N1-H3...S1	0.890	2.612	3.473	163.21	-x+1/2, -y+3/2, -z+1
N1-H3...S3	0.890	2.882	3.349	114.34	-x+1/2, -y+3/2, -z+1
N2-H1...S3	0.890	2.675	3.439	144.52	-x+1/2, y-1/2, -z+3/2
N2-H1...S2	0.890	2.885	3.571	135.05	-x+1/2, y-1/2, -z+3/2
N2-H2...S4	0.890	2.468	3.348	169.86	
N2-H3...S1	0.890	2.561	3.438	168.64	x, -y+1, z-1/2
N2-H3...S2	0.890	2.981	3.400	110.77	x, -y+1, z-1/2

D = Donor; A = Acceptor

Table 4.3.46 Comparative structural data for tetrathiomolybdates

Compound	S-Mo-S (av) in °	Mo-S (long) in Å	Mo-S (short) in Å	Δ in Å	Mo-S (av.) in Å	S...H Short in Å	Ref.
[Mn(dien)$_2$][MoS$_4$]	109.47	2.1765	2.1765	0	2.1765	2.70	70
[Ni(en)$_3$][MoS$_4$]	109.46	2.186	2.1766	0.0094	2.189	2.653	66
(enH$_2$)[MoS$_4$]	109.47	2.1846	2.1735	0.0111	2.179	-	75
(NEt$_4$)$_2$[MoS$_4$]	109.47	2.183	2.169	0.014	2.176	-	178
Rb$_2$[MoS$_4$]	109.36	2.1917	2.1782	0.0135	2.182	-	63
(NH$_4$)$_2$[MoS$_4$]	109.47	2.186	2.171	0.015	2.178	-	179
(NH$_4$)$_2$[MoS$_4$]	109.47	2.2057	2.18251	0.0232	2.189	2.555	176
[(prop)$_4$N]$_2$[MoS$_4$]	109.47	2.193	2.175	0.018	2.185	-	79
(1,3-pnH$_2$)[MoS$_4$]	109.47	2.1882	2.1699	0.0183	2.181	2.494	79
(dipnH$_2$)[MoS$_4$]	109.47	2.1903	2.1717	0.0186	2.182	2.553	This work
(dienH$_2$)MoS$_4$	109.47	2.191	2.169	0.0220	2.180	2.541	This work
(1,4-bnH$_2$)[MoS$_4$]	109.47	2.1992	2.1749	0.0243	2.181	2.348	This work
K$_2$[MoS$_4$]	109.45	2.200	2.1757	0.0243	2.182	-	61
[Co$_2$(tren)$_3$](MoS$_4$)$_2$	-	2.190	2.163	0.027	2.180	2.542	68
(trenH$_2$)[MoS$_4$].H$_2$O	109.50	2.1951	2.1670	0.0281	2.185	2.458	83
(tmenH$_2$)[MoS$_4$]	109.47	2.1983	2.1694	0.0289	2.184	2.567	79
(2-pipH-1-EtNH$_3$)-[MoS$_4$]·½H$_2$O	109.47	2.2005	2.1703	0.0302	2.183	-	This work
(N-MeenH$_2$)[MoS$_4$]	109.47	2.2014	2.1635	0.0379	2.186	2.362	This work
(pipH$_2$)[MoS$_4$]	109.47	2.2114	2.1683	0.0431	2.187	2.379	131

134

tetrahedral value. All the complexes exhibit cation-anion interactions in the form of S...Rb as in $Rb_2[MoS_4]$ [63] or S...H as in all the other complexes. The compounds $(trenH_2)[MoS_4].H_2O$ **17** and $(2-pipH-1-EtNH_3)[MoS_4]\cdot\frac{1}{2}H_2O$ **27** exhibits S...H-O interactions in addition to S...H-N. In $(Et_4N)_2[MoS_4]$ [178] no S...H interactions are possible. The average value of the Mo-S distance ranges from 2.175 Å in $(Et_4N)_2[MoS_4]$ to 2.1898 Å in $[Ni(en)_3][MoS_4]$ [66]. In all the complexes the longest Mo-S distance varies from 2.1846 Å in $(enH_2)[MoS_4]$ [75] to 2.2114 Å in $(pipH_2)[MoS_4]$ [83]. The mean Rb...S distance in $Rb_2[MoS_4]$ [63] has been reported to be 3.568 Å. It is also to be noted that the difference between the longest and the shortest Mo-S bond distances in all the complexes ranges from of 0.0094 Å $[Ni(en)_3][MoS_4]$ to 0.0431 Å in $(pipH_2)[MoS_4]$. In the two structurally characterized alkali metal tetrathiomolybdate complexes namely $K_2[MoS_4]$ [61] and $Rb_2[MoS_4]$ [63], the difference between the longest and the shortest Mo-S distances are 0.0243 and 0.0135 Å respectively. Among all the complexes listed in Table 4.3.46, $(pipH_2)[MoS_4]$ **21** [83] shows the longest Mo-S distance of 2.2114 Å as well as the maximum Δ value of 0.0431 Å and also the shortest S...H contact. The average N...S distance in $(pipH_2)[MoS_4]$ complex is relatively short at 3.306 Å as compared to 3.60 Å in $[Mn(dien)_2][MoS_4]$ [70] or 3.43 Å in $(tmenH_2)[MoS_4]$ [79]. It appears that the difference between the longest and shortest Mo-S distances is an important factor and this difference can probably be taken as a measure of the distortion of the MoS_4 tetrahedron. In the present work it is interesting to note that, in tetrathiomolybdate complexes, when the difference between the longest and the shortest Mo-S distances is more than 0.03 Å, the effect of such a distortion is clearly evidenced in the IR spectra, which exhibit a split of the asymmetric stretching of the Mo-S vibration (*vide infra*). The compounds **27**, **3** and **21**, where Δ values are more than 0.03 Å exhibit a splitting of the Mo-S vibration indicating that in these compounds theMS_4 tetrahedron is distorted.

A comparative study of the structural parameters of several known tetrathiotungstates (Table 4.3.47) has been made with a view to understand the importance of the S...H bonding interactions to induce the elongation of the W-S bond lengths. The isolation and structural characterization of $[WS_4]^{2-}$ with different cations ranging from $(NH_4)^+$, Rb^+, $[Ni(tren)_2]^{2+}$, $(enH_2)^{2+}$, $(pipH_2)^{2+}$, $(N-Me-enH_2)^{2+}$ etc.

Table 4.3.47 Comparative structural parameters of tetrathiotungstates

Compound	S-W-S (av) in Å	W-S (long) in Å	W-S (short) in Å	Δ in Å	W-S (av.) in Å	S...H Short in Å	N...S (av.) in Å	Ref.
(enH$_2$)[WS$_4$]	109.47	2.1943	2.1851	0.0092	2.1893	2.43	3.37	84
(trans-1,2-cnH)$_2$[WS$_4$]	109.47	2.1978	2.1874	0.0104	2.1940	2.67	3.56	This work
(1,3-pnH$_2$)[WS$_4$]	109.47	2.1946	2.1798	0.0148	2.1903	2.43	3.36	85
(dienH$_2$)[WS$_4$]	109.48	2.189	2.172	0.0170	2.189	2.53	3.50	This work
(dipnH$_2$)[WS$_4$]	109.47	2.2053	2.188	0.0173	2.1954	2.53	3.46	This work
(N,N'-dm-1,3-pnH$_2$)[WS$_4$]	109.47	2.1992	2.1771	0.0221	2.1931	2.42	3.41	88
(tmenH$_2$)[WS$_4$]	109.47	2.1995	2.1772	0.0223	2.1891	2.56	3.44	85
(1,4-bnH$_2$)[WS$_4$]	109.47	2.2030	2.1799	0.0231	2.1918	2.39	3.36	88
(NH$_4$)$_2$[WS$_4$]	109.42	2.2090	2.1856	0.0234	2.1905	2.57	3.47	177
(trenH$_2$)[WS$_4$].H$_2$O	109.47	2.1997	2.1739	0.0258	2.1904	2.46	3.47	87
(mipaH)$_2$[WS$_4$]	109.47	2.2126	2.1792	0.0334	2.1940	2.47	3.42	88
(N-Me-enH$_2$)[WS$_4$]	109.47	2.2064	2.1727	0.0337	2.1919	2.31	3.31	88
Rb$_2$[WS$_4$]	109.46	2.2053	2.1710	0.0343	2.1878	-	-	64
(1,4-dmpH$_2$)[WS$_4$]	109.46	2.2136	2.1781	0.0355	2.1943	2.64	3.43	86
(pipH$_2$)[WS$_4$]	109.47	2.2147	2.1762	0.0385	2.1937	2.39	3.31	87
[Ni(tren)$_2$][WS$_4$]	109.47	2.2122	2.1580	0.0542	2.1872	2.73	3.56	67

136

indicates the flexibility of the tetrathiotungstate ion to exist in different structural environments. In all these compounds the average value of the S-W-S angles is very close to the ideal tetrahedral value. All complexes listed in Table 4.3.46 exhibit cation-anion interactions in the form of S···Rb as in $Rb_2[WS_4]$ [64] or S···H-N as in all the other compounds. In $Rb_2[WS_4]$ the mean Rb···S distance has been reported to be 3.5466 Å. The average value of the W-S distance ranges from 2.189 Å in $(dienH_2)[WS_4]$ **14** to 2.1954 Å in $(dipnH_2)[WS_4]$ **16**. It is also noted that the difference between the longest and the shortest W-S bond ranges from of 0.0092 Å in $(enH_2)[WS_4]$ [84] to 0.0542 in $[Ni(tren)_2][WS_4]$ [69]. The compound $[Ni(tren)_2][WS_4]$ is different compared with the organic ammonium tetrathiotungstates because it shows the shortest W-S distance of 2.1580 Å and also the maximum $\Delta = 0.0542$, even though the shortest S···H contact is observed for this complex with a distance of 2.73 Å. It is to be noted that in $[Ni(tren)_2][WS_4]$ the N atom of tren is not protonated unlike in the organic ammonium compounds but linked to Ni(II). This indicates that the strengths of the N-H···S contacts in $[Ni(tren)_2][WS_4]$ are probably different from those in the organic ammonium tetrathiotungstates. In the organic ammonium tetrathiotungstate complexes and the fully protonated $(NH_4)_2[WS_4]$ complex, the longest W-S bond lengths scatter in a very small range from 2.2147 in $(pipH_2)[WS_4]$ **22** [87] to 2.189 in $(dienH_2)[WS_4]$ **14**. Furthermore, the shortest S···H contacts in all organic ammonium tetrathiotungstates are in a very narrow range of 2.31 in **4** to 2.64 Å in $(1,4-dmpH_2)[WS_4]$ **24** [86] The shortest S···H distance of 2.31 Å in **4** is observed for the H atom attached to N which carries two alkyl groups indicating the importance of steric features for the structural distortion. It appears that the difference between the longest and shortest W-S distances is an important factor and this difference can probably be taken as a measure of the distortion of the WS_4 tetrahedron. The compounds **29**, **4**, **24** and **22**, where Δ values are more than 0.0330 Å exhibit a splitting of the W-S vibration indicating that in these compounds the WS_4 tetrahedron is distorted.

4.3.10 Crystal structure of (dbtmen)Br₂ · 2H₂O 30

(dbtmen)Br$_2$·2H$_2$O was isolated by reacting tmen in CH$_3$CN with benzyl bromide. The crystals of X-ray quality were obtained by recrystallization from water. The crystal of (dbtmen)Br$_2$·2H$_2$O were isolated by reacting tmen in CH$_3$CN with benzyl bromide. (dbtmen)Br$_2$·2H$_2$O crystallizes in the triclinic space group P$\bar{1}$ with unit cell parameters a = 8.6672 (6)Å, b = 11.7046 (8) Å, c = 11.7731 (8) Å, α = 76.988 (8)°, β = 88.978 (8) °, γ = 76.198 (8) ° and V 1129.26 (13) Å^3. The crystal structure consists of free organic cation (dbtmen)$^{2+}$ and two bromide anions which are connected to crystal waters via weak H-bonding interactions (O-H...Br) as shown in Fig 4.3.49. Both N are not involved in any H-bond formation. This is as expected as both N are fully alkylated. The H-bonding network in (dbtmen)Br$_2$·2H$_2$O is presented in Fig 4.3.50. The selected bond lengths and bond angles in (dbtmen)Br$_2$ · 2H$_2$O are listed in Table 4.3.48 while the hydrogen bonding interactions which exits between the crystal waters and bromides anions are listed Table 4.3.49.

4.3.11 Crystal structures of (enH₂)[CrO₄] 33 and (enH₂)[Cr₂O₇] 34

The oxochromate 33 crystallizes in the orthorhombic space group P2$_1$2$_1$2$_1$ and is isostructural with the reported (enH$_2$)$^{2+}$ salts like (enH$_2$)[MS$_4$] (M$'$=Mo, W) [75, 84]. The substitution of Mo or W by Cr and the substitution of S by O in ethylenediammonium chromate has resulted in a decrease in the unit cell dimensions a, b, c and a consequent reduction in the unit volume. The unit cell volumes of the Mo and W complexes are 938.7 (9) and 952.75 (9) Å^3 respectively. The structure of complex 33 consists of tetrahedral dinegative tetraoxochromate anions hydrogen bonded to the ethylenediammonium dications [221]. The same compound has also been crystallized by a different synthetic procedure and its structure subsequently reported in the same space group by Chebbi and Driss [222]. The ellipsoid plot of the [CrO$_4$]$^{2-}$ anion in ethylenediammonium chromate is shown in Fig 4.3.51 and selected bond lengths and bond angles for ethylenediammonium chromate are listed in Table 4.3.50. The Cr(VI) ion is tetracoordinated by four oxygen atoms. The tetrahedral environment is distorted as evidenced by the O-Cr-O bond angles with values ranging from 107.71(6)° to 111.02(7)°. The Cr-O bond lengths range from 1.619(1) Å to 1.691 (1) Å. All structural parameters are in good agreement with those reported for other organic diammonium chromates like 1,4-butanediammonium chromate [201], 2,2-
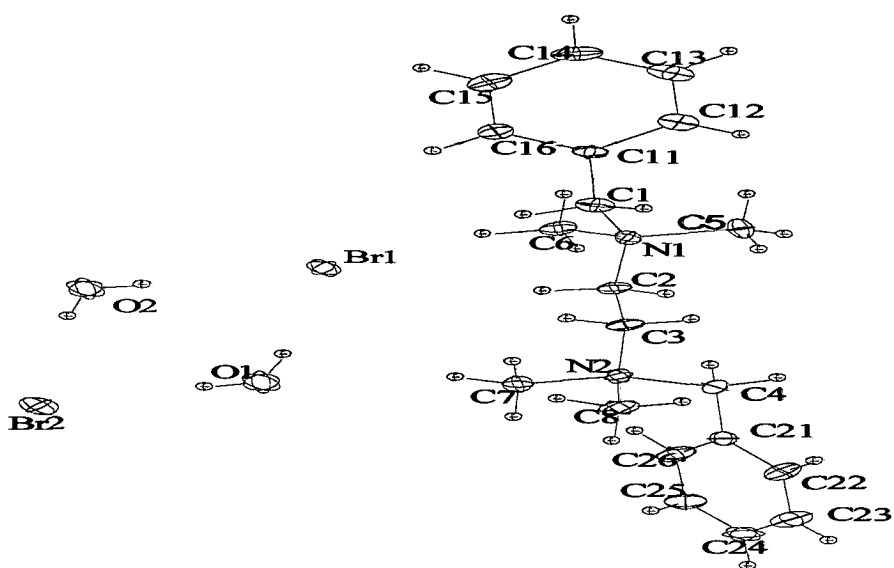
Fig. 4.3.49 Crystal structure of (dbtmen)Br$_2$.2H$_2$O **30** with labeling and displacement ellipsoids drawn at the 50% probability level

Fig. 4.3.50 Crystal structure of (dbtmen)Br$_2$.2H$_2$O **30** with view along 'b' axis (hydrogen bonding is shown as dashed lines). Colour codes; H purple, C black, N blue. H atoms attached to carbon are omitted.

139

Table 4.3.48 Selected geometric parameters (Å, °) for (dbtmen)Br$_2$·2H$_2$O **30**

C(1)-C(11)	1.513 (3)	C(11)-C(12)	1.396 (3)
C(1)-N(1)	1.540 (3)	C(12)-C(13)	1.400 (3)
N(1)-C(6)	1.500 (3)	C(13)-C(14)	1.379 (4)
N(1)-C(5)	1.502 (2)	C(14)-C(15)	1.387 (4)
N(1)-C(2)	1.517 (2)	C(15)-C(16)	1.394 (3)
C(2)-C(3)	1.530 (3)	C(21)-C(26)	1.391 (3)
C(3)-N(2)	1.517 (2)	C(21)-C (22)	1.400 (3)
N(2)-C(7)	1.506 (3)	C(22)-C (23)	1.393 (3)
N(2)-C(8)	1.506 (3)	C(23)-C (24)	1.378 (4)
N(2)-C(4)	1.528 (3)	C(26)-C(25)	1.391 (3)
C(4)-C(21)	1.511 (3)	C(24)-C(25)	1.394 (4)
C(11)-C(16)	1.392 (3)		
C(11)-C(1)-N(1)	114.10 (17)	C(16)-C(11)-C(12)	119.51 (19)
C(6)-N(1)-C(5)	109.56 (17)	C(16)-C(11)-C(1)	119.78 (19)
C(6)-N(1)-C(2)	110.85 (15)	C(12)-C(11)-C(1)	120.6 (2)
C(5)-N(1)-C(2)	110.38 (16)	C(11)-C(12)-C(13)	119.7 (2)
C(6)-N(1)-C(1)	110.41 (16)	C(14)-C(13)-C(12)	120.1 (2)
C(5)-N(1)-C(1)	110.32 (16)	C(13)-C(14)-C(15)	120.5 (2)
C(2)-N(1)-C(1)	105.26 (15)	C(14)-C(15)-C(16)	119.7 (2)
N(1)-C(2)-C(3)	112.09 (17)	C(11)-C(16)-C(15)	120.4 (2)
N(2)-C(3)-C(2)	112.69 (17)	C(26)-C(21)-C(22)	119.06 (19)
C(7)-N(2)-C(8)	108.49 (16)	C(26)-C(21)-C(4)	120.97 (19)
C(7)-N(2)-C(3)	110.46 (15)	C(22)-C(21)-C(4)	119.9 (2)
C(8)-N(2)-C(3)	106.02 (17)	C(23)-C(22)-C(21)	120.1 (2)
C(7)-N(2)-C(4)	111.53 (17)	C(24)-C(23)-C(22)	120.4 (2)
C(8)-N(2)-C(4)	110.58 (15)	C(25)-C(26)-C(21)	120.6 (2)
C(3)-N(2)-C(4)	109.63 (15)	C(23)-C(24)-C(25)	119.9 (2)
C(21)-C(4)-N(2)	114.27 (16)	C(26)-C(25)-C(24)	119.9 (2)

dimethyl-1,3,-propane-diammonium chromate [199]. The Cr-O1 bond length of 1.691(1) Å is considerably longer than the other three Cr-O distances and Cr-O distance of 1.667 Å reported for the (1,4-bnH$_2$)[CrO$_4$] chromate. The lengthening can be attributed to H bonding interactions. The O1 atom is involved in three short contacts to the H atoms of the organic dication (Table 4.3.51). In total, seven short contacts between the O atoms and the H atoms ranging from 1.897 to 2.597 Å are observed. O1 makes three short contacts while O3 is involved in two short contacts. The O2 and O4 atoms each have a single contact to a H of the cation. To the best of our knowledge, the O⋯H distance of 1.897 Å found in this complex is one of the shortest H-bonding distance observed in organic diammonium chromates. Interestingly, the shortest Cr-O bond of 1.619 Å is observed for Cr-O4 and the distance between O4 and H3 attached to N1 is the longest separation. In addition, the angle N1-H3⋯O4 of 111.12° indicates a very weak N⋯H interaction. Thus the lengthening of the Cr-O1 bond can be attributed to H-bonding interactions between the H atoms and the O atoms. The O⋯H network of (enH$_2$)[CrO$_4$] is presented in Fig 4.3.52. As expected the O⋯H distances of the order of 2.0 Å are much shorter than the S⋯H distances observed in (enH$_2$)[WS$_4$] and other thiomolybdate containing organic cations. The crystal structure of ethylenediammonium dichromate showing cation and anion is displayed in Fig 4.3.53. The structure consists of [Cr$_2$O$_7$]$^{2-}$ anions, which are H-bonded to the organic dication. The O-Cr-O bond angles are very close to the tetrahedral values ranging from 107.45(8)° to 110.75(8)°. The Cr-O (terminal) bond distances range from 1.6075(15) to 1.6236(14) Å (Table 4.3.52). As expected the Cr-O2 (bridging) bond length is significantly longer and amounts to 1.7767(9) Å. It is noted that a Cr-O(terminal) bond distance of 1.61(1) Å and Cr-O(bridging) distance of 1.78(1) Å has been reported for β-Na$_2$Cr$_2$O$_7$ [190]. The dichromate anions exhibit several H bonds to the organic dication. The Cr-O3 distance is considerably longer (1.6236 (14) Å) than the other Cr-O bond lengths. This lengthening can be again explained on the basis of different O⋯H bonding interactions. A total of five short contacts between the O atoms and the H atoms of (enH$_2$)$^{2+}$ ranging from 1.946 to 2.500 Å are observed. O3 has three short contacts while O1 and O4 are involved in only one contact (Table 4.3.53). This feature explains the lengthening of the Cr-O3 bond as compared to the Cr-O4 and Cr-O1 bonds. The O⋯H distances in ethylenediammonium dichromate are longer compared to the corresponding chromate

Table 4.3.49 Hydrogen-bonding geometry (Å, °) for (dbtmen)Br₂·2H₂O **30**

D-H...A	d(D-H)	d(H...A)	d(D...A)	<DHA	Symmetry code
O1-H1...Br1	0.840	2.528	3.359	170.23	
O1-H2...Br2	0.840	2.498	3.337	176.31	x, y, z-1
O2-H1...Br2	0.840	2.497	3.329	170.61	
O2-H2...Br1	0.840	2.472	3.306	171.77	x, y, z+1

D = Donor; A = Acceptor

Table 4.3.50 Selected geometric parameters (Å, °) for (enH₂)[CrO₄] **33**

Cr(1)-O(4)	1.619 (1)	N(1)-C(1)	1.483 (2)
Cr(1)-O(2)	1.633 (1)	C(1)-C(2)	1.517 (2)
Cr(1)-O(3)	1.663 (1)	C(2)-N(2)	1.479 (2)
Cr(1)-O(1)	1.691 (1)		
O(4)-Cr(1)-O(2)	111.02 (7)	O(4)-Cr(1)-O(3)	110.97 (7)
O(2)-Cr(1)-O(3)	109.56 (6)	O(4)-Cr(1)-O(1)	107.71 (6)
O(2)-Cr(1)-O(1)	108.98 (5)	O(3)-Cr(1)-O(1)	108.52 (5)
N(1)-C(1)-C(2)	108.99 (10)	N(2)-C(2)-C(1)	110.52 (10)

Table 4.3.51 Hydrogen-bonding geometry (Å, °) for (enH₂)[CrO₄] **33**

| D-H...A	d(D-H)	d(H...A)	d(D...A)	<D-H...A	Symmetry code
N1-H1...O3	0.890	1.901	2.783	170.93	x-1/2, -y+3/2, -z+2
N1-H2...O1	0.890	1.897	2.784	174.01	-x+1, y-1/2, -z+3/2
N1-H3...O1	0.890	1.972	2.856	172.39	-x+3/2, -y+2, z+1/2
N1-H3...O4	0.890	2.597	3.034	111.12	-x+3/2, -y+2, z+1/2
N2-H1...O3	0.890	1.898	2.777	168.88	-x+3/2, -y+1, z+1/2
N2-H2...O1	0.890	1.909	2.796	174.25	x+1/2, -y+3/2, -z+2
N2-H3...O2	0.890	1.930	2.806	167.75	-x+2, y-1/2, -z+3/2

D = Donor; A = Acceptor
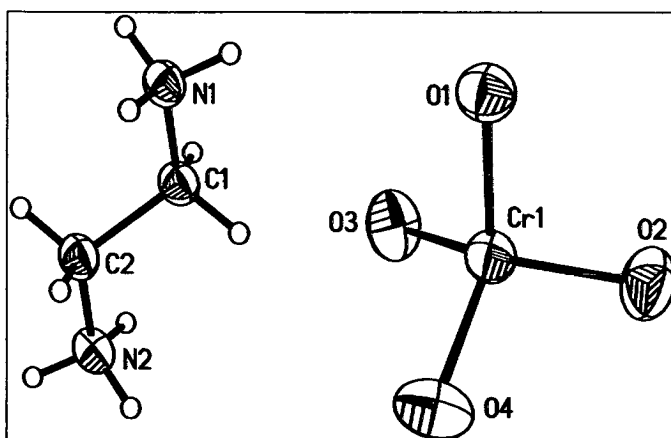
Fig. 4.3.51 Crystal structure of (enH₂)[CrO₄] **33** with labeling and displacement ellipsoids drawn at the 50% probability level.
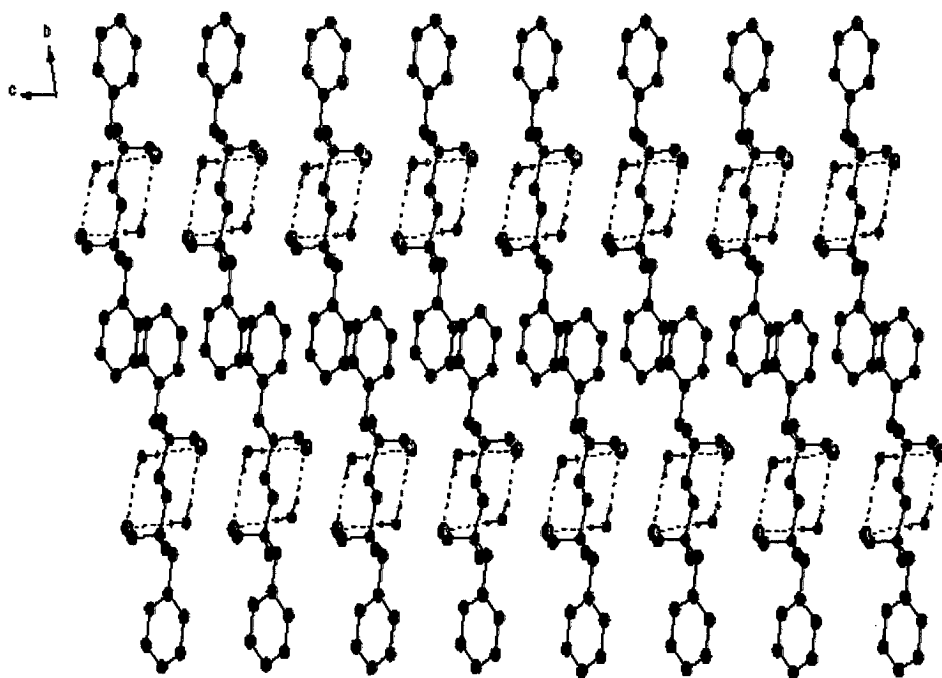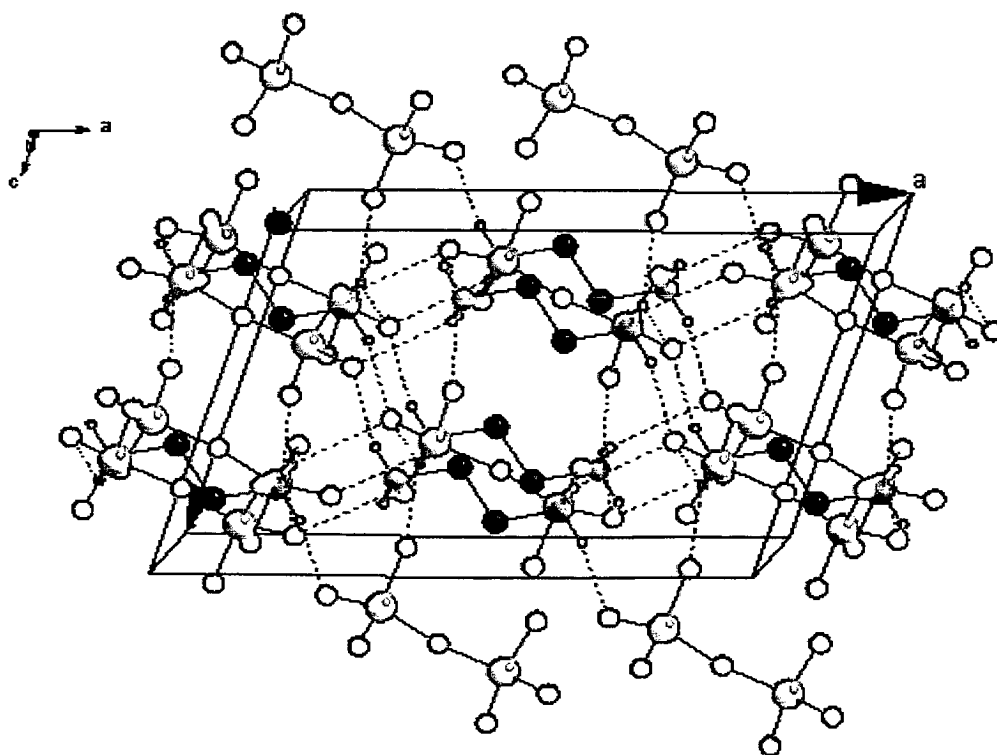

Fig. 4.3.52 Hydrogen bonding network in (enH₂)[CrO₄] **33** with view along 'b' axis (hydrogen bonding is shown as dashed lines). Colour codes; H purple, C black, N blue, Cr grey. H atoms attached to carbon are omitted

Table 4.3.52 Selected geometric parameters (Å, °) for (enH$_2$)[Cr$_2$O$_7$] **34**

Cr(1)-O(4)	1.6075 (15)	Cr(1)-O(2)	1.7767 (9)
Cr(1)-O(1)	1.6173 (15)	N(1)-C(1)	1.487 (2)
Cr(1)-O(3)	1.6236 (14)	C(1)-C(1A)	1.508 (3)
O(2)-Cr(1A)	1.7767 (9)		
O(4)-Cr(1)-O(1)	109.40 (9)	O(4)-Cr(1)-O(3)	110.99 (8)
O(1)-Cr(1)-O(3)	110.75 (8)	O(4)-Cr(1)-O(2)	109.68 (7)
O(1)-Cr(1)-O(2)	108.52 (7)	O(3)-Cr(1)-O(2)	107.45 (8)
Cr(1A)-O(2)-Cr(1)	124.19 (11)	N(1)-C(1)-C(1A)	110.43 (17)

Table 4.3.53 Hydrogen-bonding geometry (Å, °) for (enH$_2$)[Cr$_2$O$_7$] **34**

D-H...A	d (D-H)	d (H...A)	d(D...A)	<D-H...A	Symmetry Code
N1-H1A...O4	0.890	2.091	2.896	149.93	-x+1/2, y-1/2, -z+1/2
N1-H1A...O3	0.890	2.500	2.985	114.80	-x+1/2, -y+1/2, -z+1
N1-H1B...O3	0.890	1.946	2.800	160.45	
N1-H1C...O1	0.890	2.068	2.881	151.28	-x+1/2, -y+3/2, -z+1
N1-H1C...O3	0.890	2.460	3.031	122.37	x, -y+1, z-1/2

D = Donor; A = Acceptor

salt. In Fig 4.3.54 the resulting hydrogen bonded network is displayed. It is to noted that the observed unit cell parameters and geometric parameters of **34** are in excellent agreement with those for the same complex isolated by a different synthetic route, i. e. a synthesis in a HF medium [198].
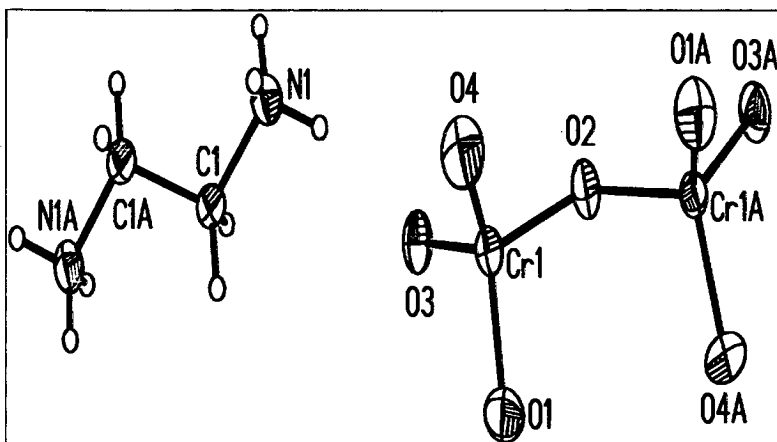
Fig. 4.3.53 Crystal structure of (enH$_2$)[Cr$_2$O$_7$] **34** with labeling and displacement ellipsoids drawn at the 50% probability level.
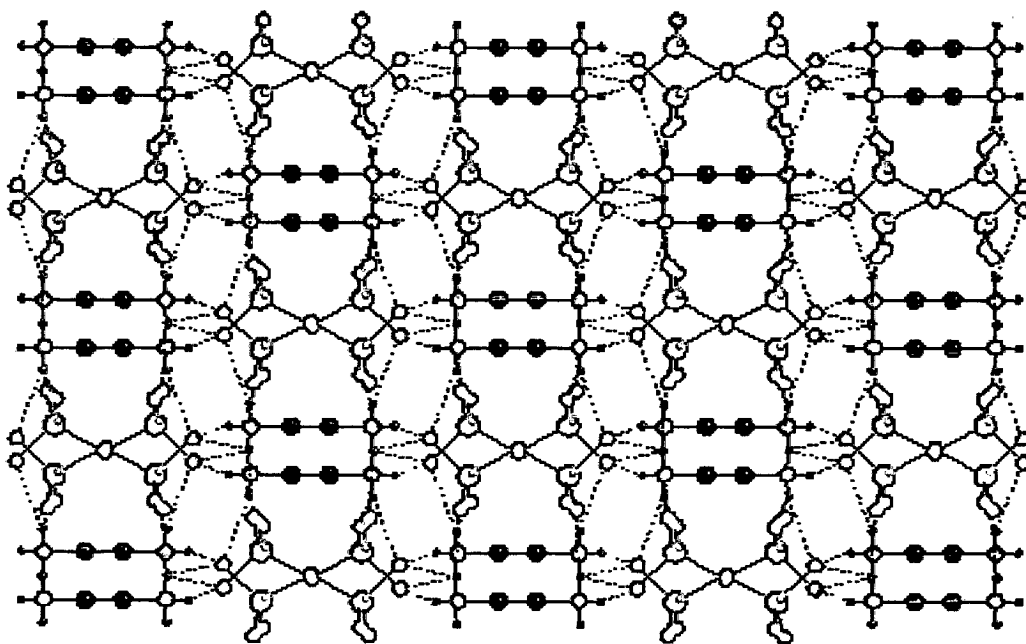
Fig. 4.3.54 An extended hydrogen bonding network in (enH$_2$)[Cr$_2$O$_7$] **34** with view along 'b' axis (hydrogen bonding is shown as dashed lines). Colour codes; O red, H purple, C black, N blue, Cr grey. H atoms attached to carbon are omitted.

4.4 Spectroscopic Characterization

4.4.1 Vibrational spectra

All the new organic ammonium tetrathiometalates prepared in this work have been characterized by the use of vibrational spectroscopy viz IR and Raman. The details of the sample preparation and instrumentation used have been given in the earlier chapter. The IR and Raman spectral data of all the complexes synthesized in the present work are collected in Table 4.4.1. The IR spectrum of tetrathiomolybdate and its corresponding W are identical excepting that the signals below 500 cm^{-1} in the W compound are shifted to lower energies. All the complexes exhibit several signals in the mid IR region indicating the presence of the organic moiety in the complexes. The hydrated complexes like $(trenH_2)[MS_4] \cdot H_2O$ exhibit the characteristic O-H stretching vibration at around 3440 cm^{-1}. The N-H vibrations in almost all the complexes are observed at around 3000 cm^{-1} unlike in the free amines where these signals occur at higher energies. The lowering of the N-H vibrations in the complexes can be attributed to the presence of the amine in the form of organic ammonium cation and also due to the weak H-bonding interactions (*vide supra*) in the complexes between the anion and cation. The signals due to the vibrations of the tetrathiometalates are observed in the lower energy region i.e below 500 cm^{-1}. It is well documented in the literature that for the free tetrahedral $[MS_4]^{2-}$ (M = Mo,W) anion four normal modes of vibrations $\nu_1(A_1)$, $\nu_2(E)$, $\nu_3(F_2)$, and $\nu_4(F_2)$ are expected [176]. Of these ν_3 and ν_4 are IR active while all four bands are Raman active. The asymmetric stretching vibration (ν_3) for all the tetrathiomolybdates are observed at around 475 cm^{-1} while the tetrathiotungstates exhibit this vibration (ν_3) at around 455 cm^{-1}. The symmetric stretching vibration (ν_1) is observed as an intense signal in the Raman spectra of the complexes at around 450 cm^{-1} for tetrathiomolybdates and ~475 cm^{-1} for tetrathiotungstates. All these vibrations have been observed in the synthesized complexes. The degenerate stretching vibrations ν_2 and ν_4 occurs at around 180 cm^{-1} (see Table 4.4.1) and the assignments are made based on reported values [176]. When the symmetry is lowered from Td to C_{3v} or C_{2v} the bands are split and all the vibrations are both IR and Raman active.

Table 4.4.1 IR and Raman spectroscopic data for tetrathiometalates

Compound	IR bands cm^{-1}	Raman bands cm^{-1}
(enH$_2$)[MoS$_4$] **1**	2965 (br), 1567, 1532, 1458, 1432, 1306, 1113, 1075, 1024, 964, 886, 804, 668, 473(ν_3), 202(ν_4), 156, 148, 125	480(ν_3),452(ν_1), 352, 191(ν_4), 178(ν_2)
(enH$_2$)[WS$_4$] **2**	3027 (br), 1570, 1528, 1442, 1429, 1324, 1297, 1121, 1297,1121, 1081, 1024, 952, 865, 805, 477 (ν_1), 452 (ν_3), 213, 183 (ν_4), 146, 121	475(ν_1), 464(ν_3), 352, 195(ν_4), 183, 118
(N-MeenH$_2$)[MoS$_4$] **3**	3046, 2955, 2727, 1441, 1115, 1025, 935, 766, 473 (ν_3), 460(ν_2), 448(ν_1), 433, 254, 166, 131, 99	475 (ν_3), 458 (ν_3), 449(ν_1), 412, 202(ν_4), 185(ν_2), 170
(N-MeenH$_2$)[WS$_4$] **4**	3059, 2961, 2740, 1454, 1116, 1026, 935, 766, 483, 471(ν_1), 450(ν_3), 257, 183(ν_4), 158, 126	480 (ν_1), 473, 454 (ν_3), 450, 444, 412, 200, 181(ν_2), 169
(tmenH$_2$)[MoS$_4$] **5**	2982, 1439, 1405, 1319, 1189, 964, 840, 782, 479 (ν_3), 452(ν_2), 196(ν_4), 126, 102	484(ν_3), 468(ν_2), 453 (ν_1), 183(ν_2), 173
(tmenH$_2$)[WS$_4$] **6**	3009 (br), 1464, 1321, 965, 783, 479 (ν_1), 452 (ν_3), 249, 189 (ν_4), 151,122,88	479(ν_1), 464(ν_2), 456(ν_2), 193(ν_4), 173

Compound	IR bands cm^{-1}	Raman bands cm^{-1}
(1,3-pnH$_2$)[MoS$_4$] **7**	3006 (br), 1544, 1451, 1398, 1305, 1202, 1097, 943, 751, 484 (ν_3), 475(ν_3), 455(ν_1), 207 (ν_4), 175, 116	484, 470, 453 (ν_1), 197, 187(ν_4), 171
(1,3-pnH$_2$)[WS$_4$] **8**	3048 (br), 1561, 1482, 1401, 1327, 1204, 1098, 935, 752, 483(ν_1), 472(ν_3), 211, 170 (ν_2), 115	479(ν_1), 453(ν_3), 196(ν_2), 173
(N, N'-dm-1,3-pnH$_2$)[MoS$_4$] **9**	2995, 2768, 1515, 1450, 1432, 1017, 801, 736, 488, 482(ν_3), 464(ν_3), 450(ν_1), 232, 144, 96	482(ν_3), 472(ν_3), 464(ν_3), 451(ν_1), 190(ν_4), 180
(N,N'-dm-1,3-pnH$_2$)[WS$_4$] **10**	3006, 2775, 1561, 1487, 1461, 1432, 1123, 1068, 1040, 1013, 1007, 973, 865, 800, 743, 479(ν_1), 454(ν_3), 189(ν_4)	479(, 468, 457, 416, 295, 197(ν_4), 188, 175
(1,4-bnH$_2$)[MoS$_4$] **11**	3004, 1564, 1549, 1464, 1435, 1322, 1254, 1086, 1018, 909, 859, 808, 733, 478(ν_3), 460(ν_1)	472(ν_3), 464(ν_3), 450(ν_1), 189(ν_4)
(1,4-bnH$_2$)[WS$_4$] **12**	3004, 2903, 1567, 1466, 1436, 1378, 1323, 1255, 1086, 1017, 908, 858, 733, 498, 480(ν_1), 446(ν_3), 214, 188(ν_4), 150, 112, 96, 88	478(ν_2), 448(ν_3), 187(ν_4)
(dienH$_2$)[MoS$_4$] **13**	3257, 3054 (br), 1568, 1540, 1504, 1464, 1459, 1365, 1345, 1311, 1283, 1257, 1188, 1177, 1088, 1054, 1027, 987, 959, 932, 866, 838, 818, 797, 770, 676, 495, 464(ν_3), 427, 320, 283, 204 (ν_4), 185(ν_2), 171, 141, 125, 92	491, 479(ν_3), 469(ν_3), 451(ν_1), 192(ν_4), 182
(dienH$_2$)[WS$_4$] **14**	3243, 3054 (br), 1563, 1547, 1513, 1458, 1365, 1297, 1279, 1257, 1203, 1162, 1122, 1107, 1094, 1026, 980, 959, 933, 866, 824, 797, 789, 770, 750, 627, 479 (ν_1), 464 (ν_3), 443, 357, 324, 243, 185 (ν_4), 99	481(ν_1), 460(ν_3), 359, 188(ν_4)

Compound	IR bands cm^{-1}	Raman bands cm^{-1}
(dipnH$_2$)[MoS$_4$] **15**	3272, 3228, 2998, 1575, 1519, 1461, 1380, 1284, 1083, 989, 755, 477(ν_3), 219, 262, 194	475(ν_3), 453(ν_1), 189(ν_4), 178
(dipnH$_2$)[WS$_4$] **16**	3275, 3235, 2993, 1573, 1518, 1460, 1420, 1380, 1284, 1208, 1083, 1040, 989, 922, 868, 823, 755, 478(ν_1), 461(ν_3)	477(ν_1), 458(ν_3) 188
(trenH$_2$)[MoS$_4$]·H$_2$O **17**	3462 (br), 3328(w), 3277 (w), 3072, 3004, 2924, 2829, 1601, 1569, 1513, 1464, 1345, 1295, 1115, 1071, 1007, 963, 857, 755, 487(ν_3), 467(ν_3), 450(ν_1), 357, 344, 248, 215, 203(ν_4), 185(ν_2), 132, 101	474(ν_3), 453(ν_1), 181(ν_4), 94
(trenH$_2$)[WS$_4$]·H$_2$O **18**	3471, 3330, 3278, 3084, 3009, 2886, 2829, 1601, 1569, 1513, 1478, 1345, 1295, 1142, 1086, 1007, 963, 857, 754, 481 (ν_1), 454(ν_3), 357, 344, 247, 218, 203, 185(ν_4), 133, 101	480(ν_1), 467(ν_3), 459(ν_3),179(ν_2)
(pipH$_2$)[MoS$_4$] **21**	3000 (br), 1544, 1440, 1371, 1297, 1186, 1079, 910, 862, 655, 556, 479(ν_3), 465(ν_3), 445(ν_1), 336, 267, 200(ν_4), 133, 93	478(ν_3), 469(ν_3), 448(ν_1), 438, 199(ν_4), 184(ν_2), 175
(pipH$_2$)[WS$_4$] **22**	2989, 2928, 2752, 2668, 1510, 1425, 1400, 1371, 1298, 1186, 1079, 909, 862, 556, 473(ν_1), 454(ν_3), 441(ν_3), 267, 201(ν_4), 191(ν_4), 125, 92	480(ν_1), 460(ν_2), 451(ν_3), 438, 380, 203(ν_4), 183(ν_4)
(1,4-dmpH$_2$)[MoS$_4$] **23**	2964, 2776, 1664, 1444, 1350, 1124, 1056, 1004, 962, 941, 883, 841, 757, 684, 605, 474(ν_3), 469(ν_3) (ν_3), 448(ν_1)	
(1,4-dmpH$_2$)[WS$_4$] **24**	3007 (br), 1551, 1475, 1087, 1018, 909, 734, 498, 470(ν_1), 457(ν_3), 218, 188(ν_4), 150, 113, 93	477(ν_1), 448(ν_3), 186(ν_4), 154
(dabcoH)$_2$[MoS$_4$] **25**	2959, 2806, 2648, 1468, 1366, 1174, 1051, 1000, 842, 782, 593, 474(ν_3), 412, 202(ν_4)	472(ν_3), 451(ν_1), 413, 179(ν_4)

Compound	IR bands cm^{-1}	Raman bands cm^{-1}
(dabcoH)$_2$[WS$_4$] **26**	2982, 2811, 2652, 1470, 1383, 1320, 1178, 1052, 1001, 874, 783, 618, 530, 458(ν_3), 412, 177(ν_4)	475(ν_1), 457 (ν_3), 413, 179(ν_4)
(2-pipH-1-EtNH$_3$)[MoS$_4$]·½H$_2$O **27**	3434, 3162, 3981, 2950, 1635, 1608, 1553, 1451, 1267, 1172, 1094, 1067, 993, 902, 509, 475(ν_3), 451(ν_1), 435, 363, 335, 279, 227, 202(ν_4), 173, 139, 105, 88	477(ν_3), 466(ν_3), 451(ν_1), 189(ν_4), 179, 172, 110
(trans-1,2-cnH)$_2$[WS$_4$] **28**	3309, 3239, 3094, 2939, 2856, 1581, 1498, 1443, 1398, 1229, 1126, 1002, 965, 847, 583, 521, 482(ν_1), 465(ν_3), 429, 409, 329, 286, 214, 136, 102	481(ν_1), 464(ν_3), 193(ν_4), 178, 168
(mipaH)$_2$[WS$_4$] **29**	3050, 2772, 2661, 2562, 2433, 1577, 1458, 1366, 1201, 1155, 975, 933, 476(ν_1), 442(ν_3), 379, 193(ν_4), 122	483(ν_1), 458(ν_3), 399, 188(ν_4)

The IR spectra of $(enH_2)Cl_2$, $(enH_2)[MoS_4]$ $\underline{1}$ and $(enH_2)[WS_4]$ $\underline{2}$ are displayed in Fig 4.4.1. The middle region of the IR spectra of all the three complexes exhibit several vibrations that can be assigned to the vibrations of the $(enH_2)^{2+}$ moiety. The IR spectra of complexes $\underline{1}$ and $\underline{2}$ are identical excepting that the signals below 500 cm^{-1} of the $[WS_4]^{2-}$ complex are shifted to lower energies as compared to that of $(enH_2)[MoS_4]$ $\underline{1}$. The identical nature of the IR spectra is also indicative of the isostructural nature of both the compounds as evidenced by the structural studies (*vide supra*). The N-H vibration occurs as a broad band at around 3000 cm^{-1}. The broadening and shifting of N-H region to the lower frequency values in $\underline{2}$ can be attributed to the diprotonated nature of $(enH_2)^{2+}$ cation as well as (N-H...S) between the organic cation and the $[WS_4]^{2-}$ anion in $\underline{2}$. The asymmetric vibration (v_3) occurs at 473 cm^{-1} in $\underline{1}$ while in $\underline{2}$ this is observed at 452 cm^{-1} in the IR spectra. The symmetric stretching vibration (v_1) is observed as an intense signal at 475 cm^{-1} in the Raman spectrum of $\underline{2}$ (Fig 4.4.2). The signals at 195 and 183 cm^{-1} in the Raman spectrum can be assigned to the degenerate (v_2) and (v_4) vibrations.

The IR and Raman spectra of $(N\text{-}Me\text{-}enH_2)[MoS_4]$ $\underline{3}$ and $(N\text{-}Me\text{-}enH_2)[WS_4]$ $\underline{4}$ are depicted in Fig 4.4.3 and Fig. 4.4.4 respectively. The IR spectra of both complexes are nearly identical as observed earlier. In $\underline{3}$ the intense signal centered around 460 cm^{-1} appears broad with a shoulder at 473 cm^{-1} with a further band at 448 cm^{-1}. The appearance of a broad Mo-S vibration split in $\underline{3}$ indicates the considerable distortion of $[MoS_4]$ tetrahedron, which has also been observed in the X-ray studies. It is to be noted that the Δ value observed for this compound is 0.0379 Å. In the case of the W analogue whose Δ value is 0.0337 Å the splitting of the v_3 vibration is clearly evident. The other bands can be assigned as mentioned for $(enH_2)[WS_4]$ $\underline{2}$.

The IR spectra of three complexes viz $(tmenH_2)Cl_2$, $(tmenH_2)[MoS_4]$ $\underline{5}$ and $(tmenH_2)[WS_4]$ $\underline{6}$ containing the $(tmenH_2)^{2+}$ cation are presented in Fig 4.4.5. The central part of IR spectra of all three complexes, which reveal strong and sharp bands are identical indicating the presence of the organic moiety. It is to be noted that no bands are observed below 500 cm^{-1} in the IR spectrum of $(tmenH_2)Cl_2$ (Fig 4.4.5a). However IR spectra of $\underline{5}$ and $\underline{6}$ as displayed in Fig 4.4.5(b) and Fig 4.4.5(c) show
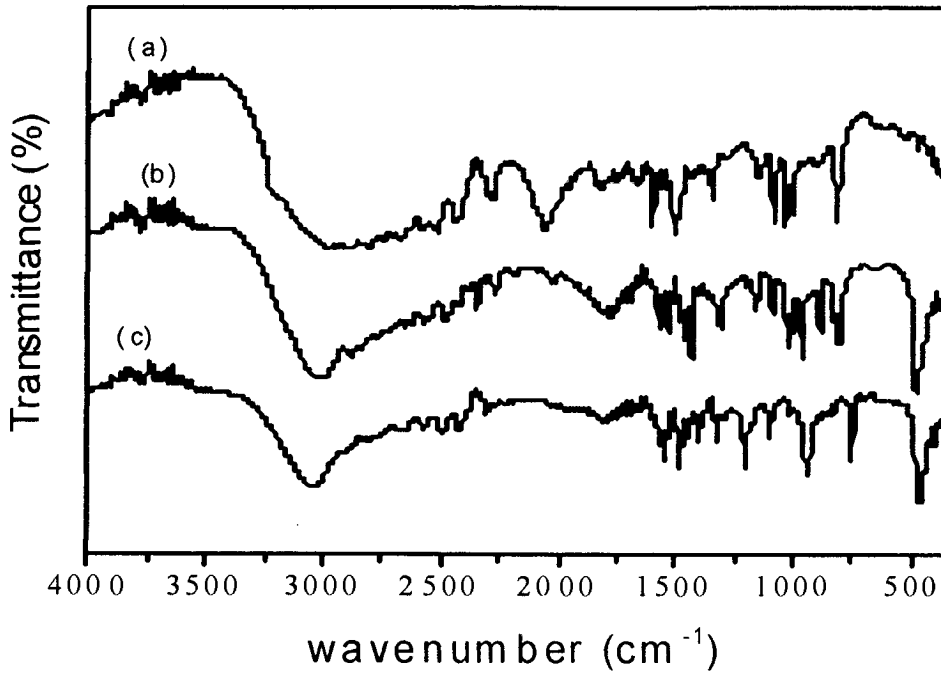
Fig. 4.4.1 IR spectra of (a) (enH$_2$)Cl$_2$ (b) (enH$_2$)[MoS$_4$] **1** (c) (enH$_2$)[WS$_4$] **2**
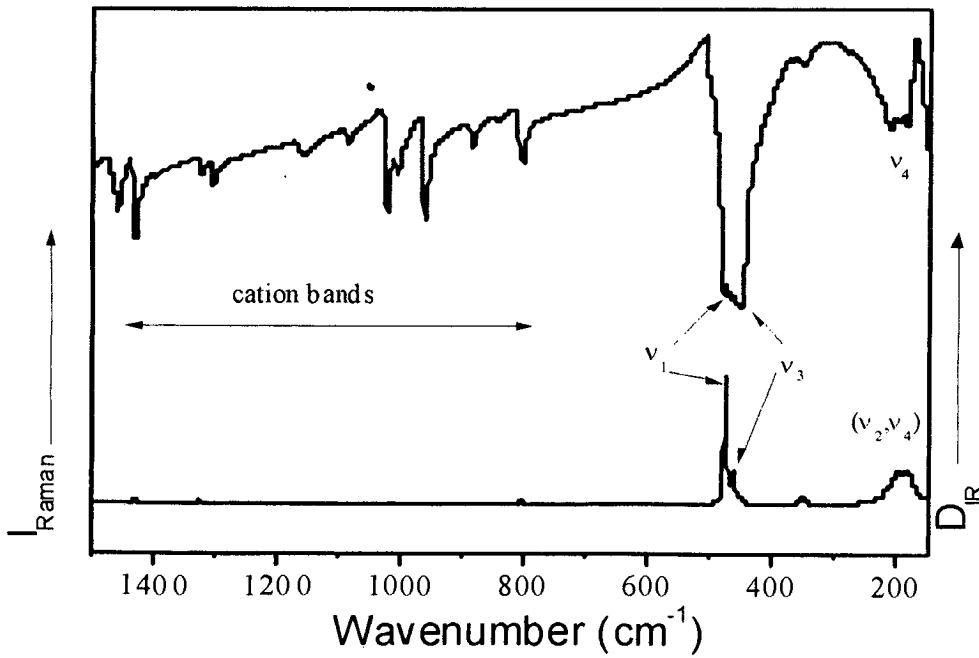
Fig. 4.4.2 IR-Raman spectra (enH$_2$)[WS$_4$] **2**
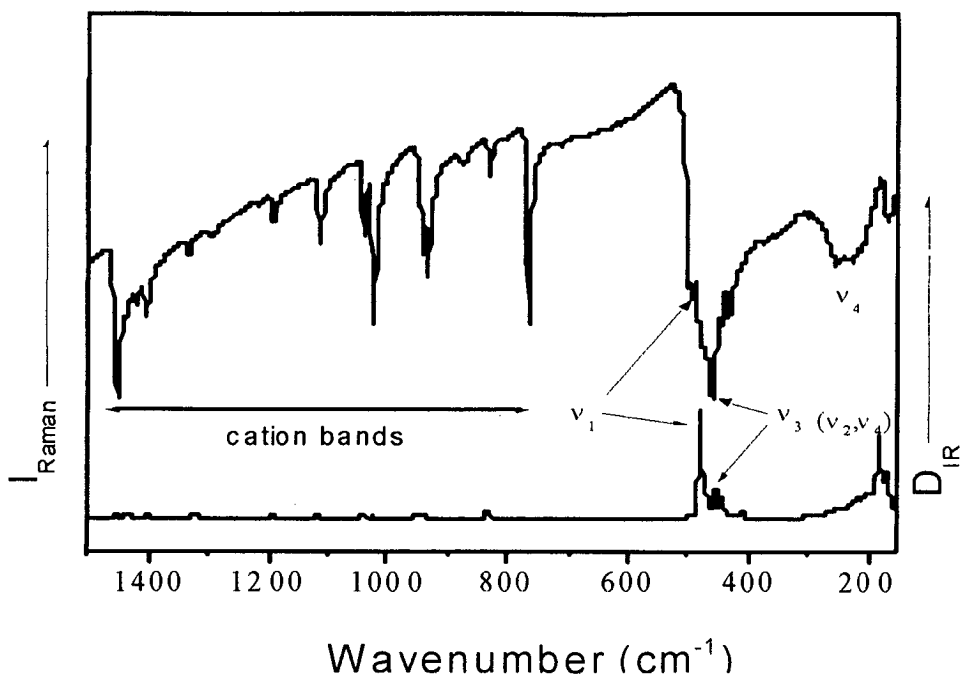
Fig. 4.4.3 Raman and IR spectra of (N-Me-enH$_2$)[MoS$_4$] **3**
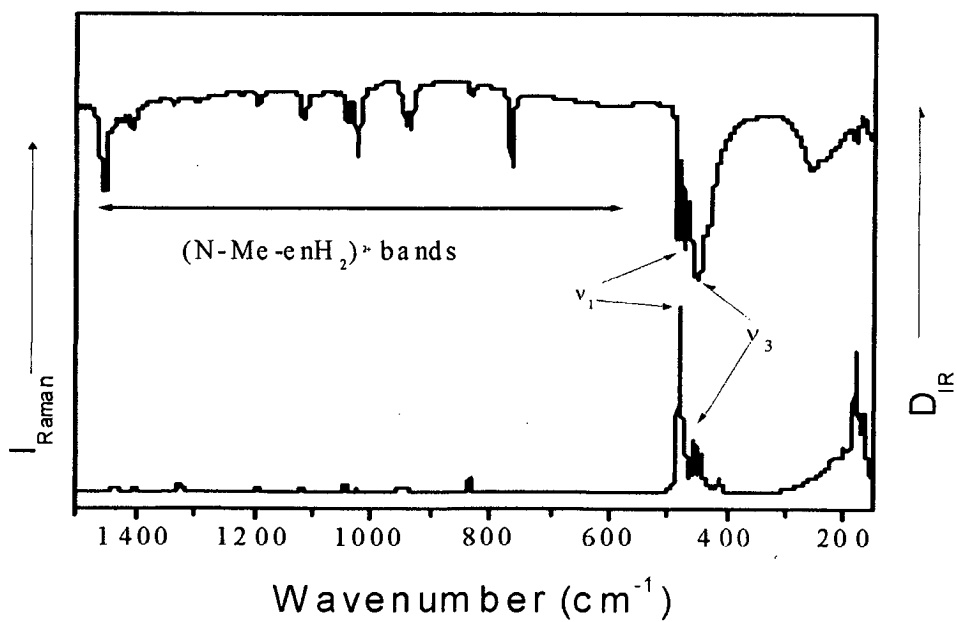
Fig. 4.4.4 Raman and IR spectra of (N-Me-enH$_2$)[WS$_4$] **4**

strong signals below 500 cm^{-1} and these signals can be assigned for the vibrations of the thiometalate anions. The strong signal at 479 cm^{-1} in the IR spectrum of **5** can be assigned the (v_3) vibration of the Mo=S bond while the weak band at 197 cm^{-1} can be assigned to (v_4). The Raman spectrum of **5** shows an intense signal at 453 cm^{-1} due the symmetric stretching vibration (v_1) while strong band at around 173 cm^{-1} is assignable to (v_2). The IR and Raman bands for (tmenH$_2$)[WS$_4$] can be explained similarly.

The IR spectra of (1,3-pnH$_2$)Cl$_2$, (1,3-pnH$_2$)[MoS$_4$] **7** and (1,3-pnH$_2$)[WS$_4$] **8** are presented in Fig 4.4.6. The identical intense and sharp bands in middle IR region indicate the common organic moiety in all three salts. The broadening and shifting of N-H region to lower wave numbers in the IR spectra of all three complexes can be due to the weak hydrogen bonding interactions in the complexes. The IR spectrum of **7** exhibits a strong signal at 484 cm^{-1} that can be assigned to the triply degenerate asymmetric stretching vibration (v_3) of the Mo=S bond while the weak band at 207 cm^{-1} can be assigned to the (v_4). The Raman spectrum of **7** shows an intense signal at 453 cm^{-1} assignable to symmetric stretching vibration (v_1) while the strong band at around 170 cm^{-1} is assignable to (v_2). The IR-Raman spectra of corresponding W analogue **8** are presented in Fig 4.4.7. This spectrum can be explained in a similar way as for the corresponding Mo analogue. The IR spectra of complexes **7** and **8** are identical excepting that the signals below 500 cm^{-1} of the [WS$_4$]$^{2-}$ anion are shifted to lower energies as compared that of **7**. The IR-Raman spectra of the complexes **10** and **11** which contains (N,N'-dm-1,3-pnH$_2$) cation can be explained similarly. The IR-Raman spectral data for complexes **12** to **16** in the Table 4.3.1 can be explained similarly.

The IR spectra of two tren complexes viz (trenH$_2$)[MoS$_4$]·H$_2$O **17** and (trenH$_2$)[WS$_4$]·H$_2$O **18** are presented in Fig 4.4.8(a & b). The identical nature of the two spectra indicates that both the complexes are isostructural. This isostructural nature of (trenH$_2$)[MoS$_4$]·H$_2$O **17** and its W analogue (trenH$_2$)[WS$_4$]·H$_2$O **18** gets further credence from the X-ray powder diffractometry. Several bands in the mid IR region can be assigned to the absorption of (trenH$_2$)$^{2+}$ cations. Both complexes contain crystal waters as evidenced from the appearance of strong signals at ~3462 and 3471
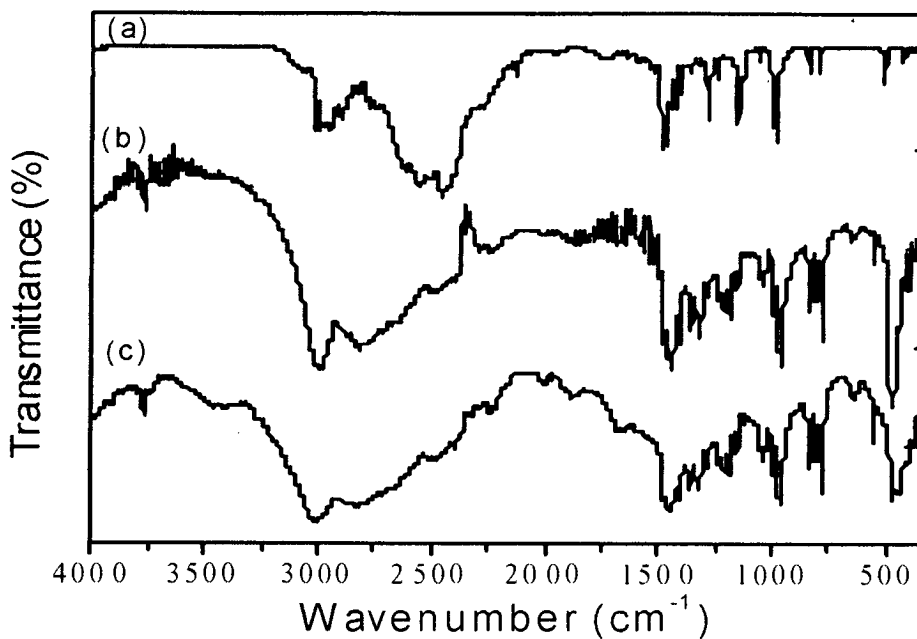
Fig 4.4.5. Infra red spectra of (a) (tmenH$_2$)Cl$_2$ (b) (tmenH$_2$)[MoS$_4$] **5** (c) (tmenH$_2$)[WS$_4$] **6**
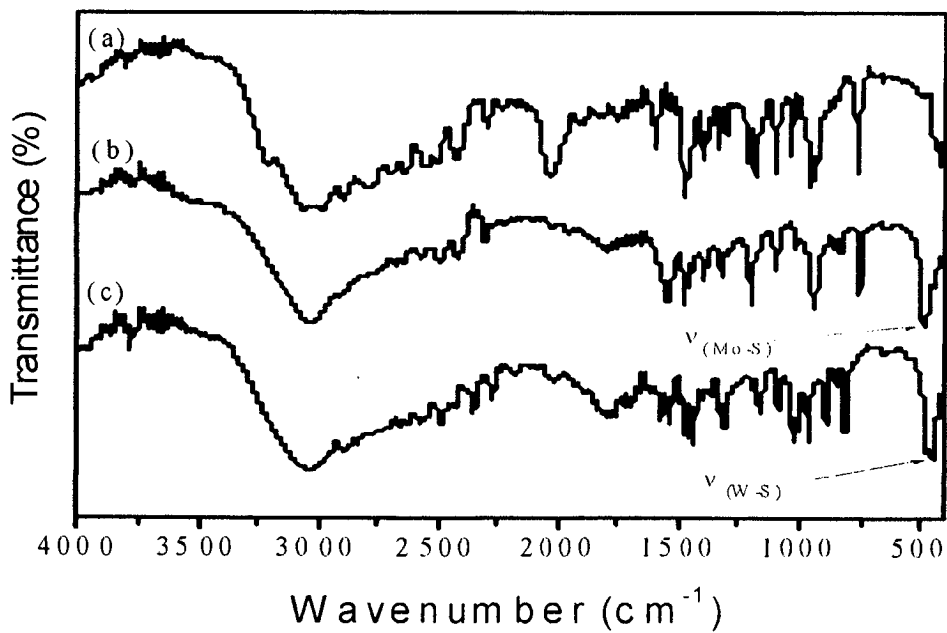
Fig.4.4.6. Infra red spectra of (a)(1,3-pnH$_2$)Cl$_2$ (b) (1,3-pnH$_2$)[MoS$_4$] **7** (c) (1,3-pnH$_2$)[WS$_4$] **8**
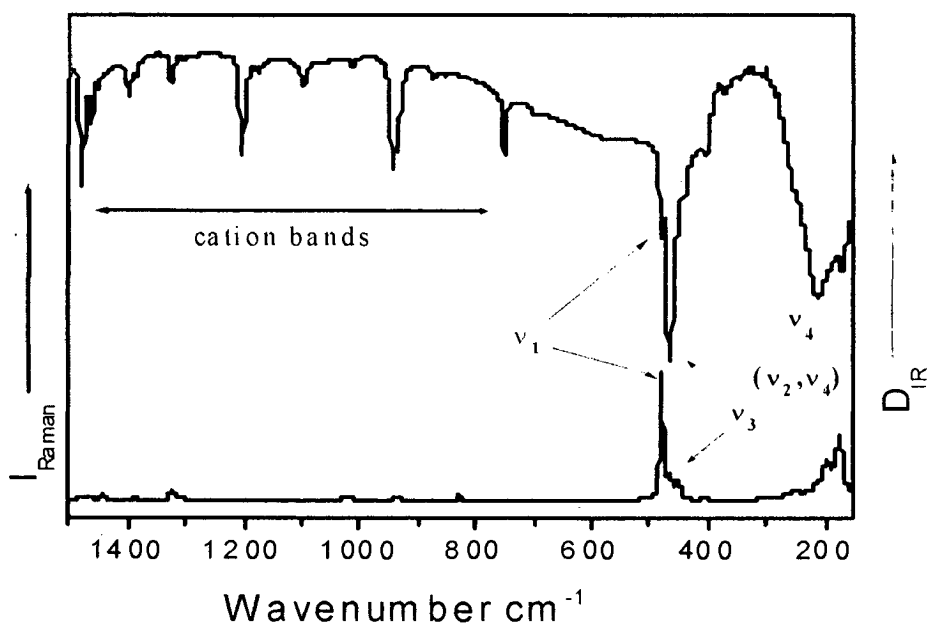
Fig. 4.4.7 IR and Raman spectra of (1,3-pnH$_2$)[WS$_4$] $\underline{\mathbf{8}}$
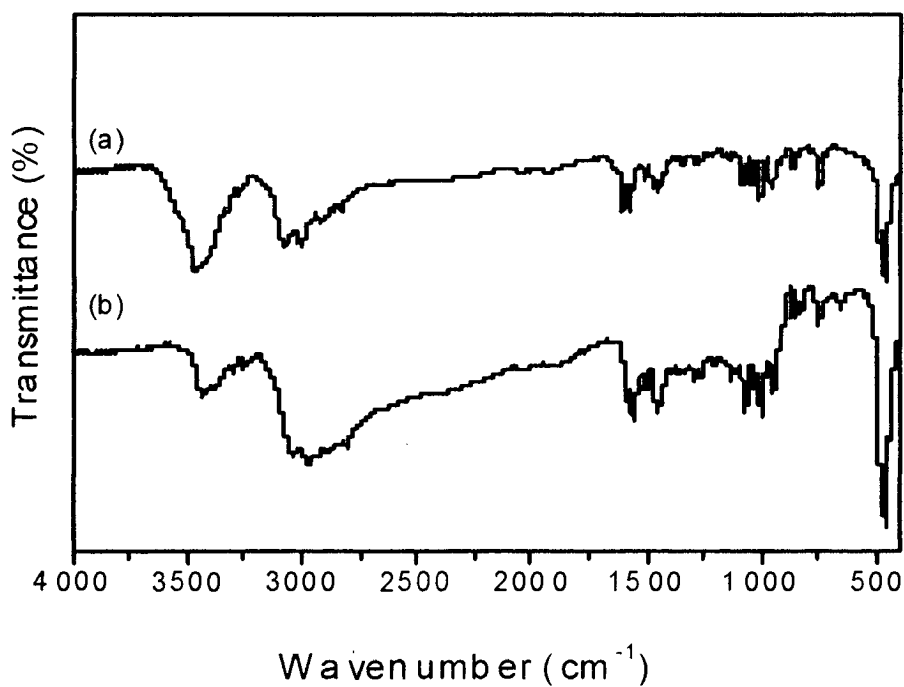
Fig. 4.4.8 IR spectra of (a) (trenH$_2$)[MoS$_4$]·H$_2$O $\underline{\mathbf{17}}$ and (b) (trenH$_2$)[WS$_4$]·H$_2$O $\underline{\mathbf{18}}$

cm^{-1} which can be assigned to the O-H stretching vibration of the crystal water in __17__ (Fig. 4.4.8a) and __18__ (Fig. 4.4.8b). For __17__, ν_{N-H} occurs at around 3072 and 3004 cm^{-1} while in the case of its W analogue __18__ the N-H stretching vibrations appear at around at 3084 and 3009 cm^{-1}. The shift to lower wave numbers compared to the free amine can be attributed to the H-bonding interactions (N-H···S) between the organic cation (trenH$_2$)$^{2+}$ and the [MS$_4$]$^{2-}$ (M = Mo, W) anion. IR-Raman spectra of __17__ are displayed in Fig 4.4.9. The IR absorption bands located at around 487 and 467 cm^{-1} can be assigned to the triply degenerate asymmetric vibration (ν_3) with a very weak shoulder at 450 cm^{-1} due to the symmetric vibration (ν_1). The appearance of band at 450 cm^{-1} indicates the slight distortion of [MoS$_4$] tetrahedron in __17__. The assignment of the 450 cm^{-1} band for the symmetric stretching vibration gains credence from the observation of an intense signal in the Raman spectrum at 453 cm^{-1}. The weak signal at 474 cm^{-1} in the Raman spectrum can be assigned to the (ν_3) vibration while the signal at 181 cm^{-1} is due to the degenerate (ν_2) and (ν_4) modes. The Raman and IR spectra of __18__ are represented in Fig 4.4.10. The IR absorptions at 481 and 454 cm^{-1} can be assigned to (ν_1) and vibrations (ν_3). The signal at 454 cm^{-1} is not clearly split even though it appears quite broad indicating the distortion of the anion is less pronounced. The assignment of the signal for (ν_1) at 454 cm^{-1} gains credence from the observation of an intense signal in the Raman spectrum at 459 cm^{-1}. The weak signal at 480 cm^{-1} in the Raman spectrum can be assigned to the (ν_3) vibration while the signal at 179 cm^{-1} is due to the degenerate (ν_2) and (ν_4) vibrations of the [WS$_4$]$^{2-}$.

The IR spectra of (pipH$_2$)Cl$_2$.2H$_2$O, (pipH$_2$)[MoS$_4$] __21__ and (pipH$_2$)[WS$_4$] __22__ are depicted in Fig 4.4.11. Several bands in the central part of the three IR spectra indicates the presence (pipH$_2$)$^{2+}$ in these compounds. In all the complexes the N-H region is broad at around 3000 cm^{-1} compared to the N-H vibration of pip, which exhibits sharp signals in the region 3400-3300 cm^{-1}. The shift to lower wave numbers compared to the free amine can be attributed to the H-bonding interactions (N-H···S) between the (pipH$_2$)$^{2+}$ cations and the tetrathiomolybdate anion. It is interesting to note that the triply degenerate asymmetric stretching vibration (ν_3) of the Mo=S bond in __21__ is split and appears as a doublet at 479 and 465 cm^{-1} with a further band around 445 cm^{-1} (Fig. 4.4.11b). The observed extra signals cannot be assigned to the vibrations of the organic cation (pipH$_2$)$^{2+}$ in view of the fact that no strong signals are
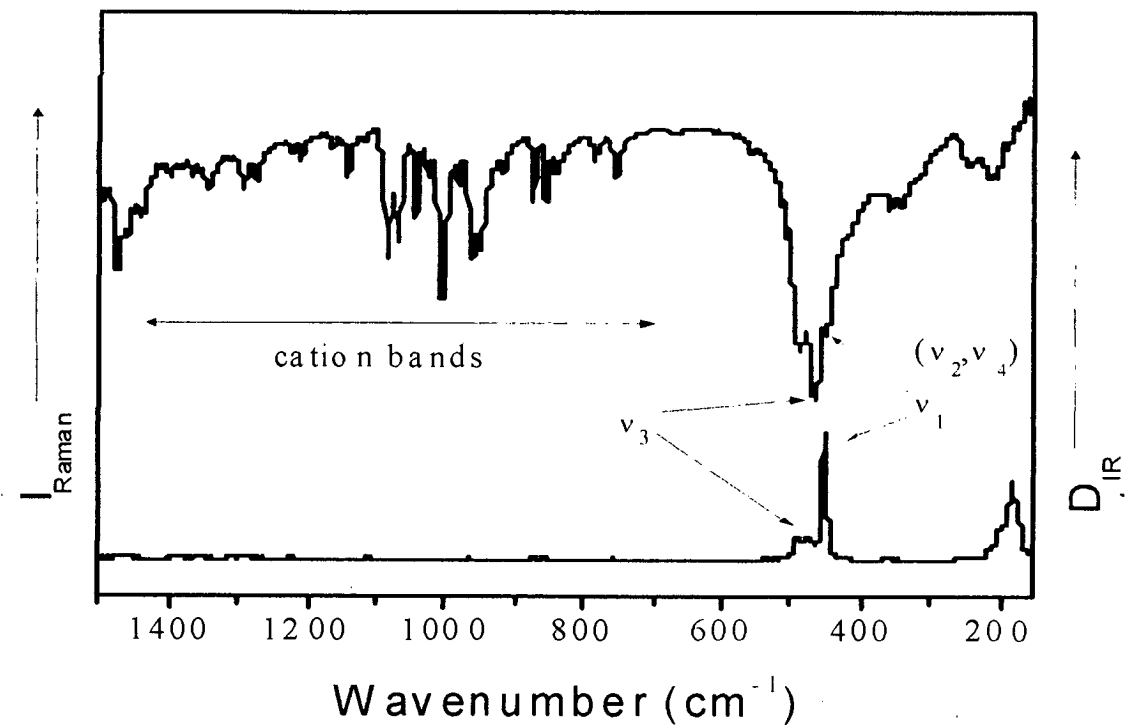
Fig 4.4.9 Raman and IR spectra of (trenH$_2$)[MoS$_4$] · H$_2$O **17**
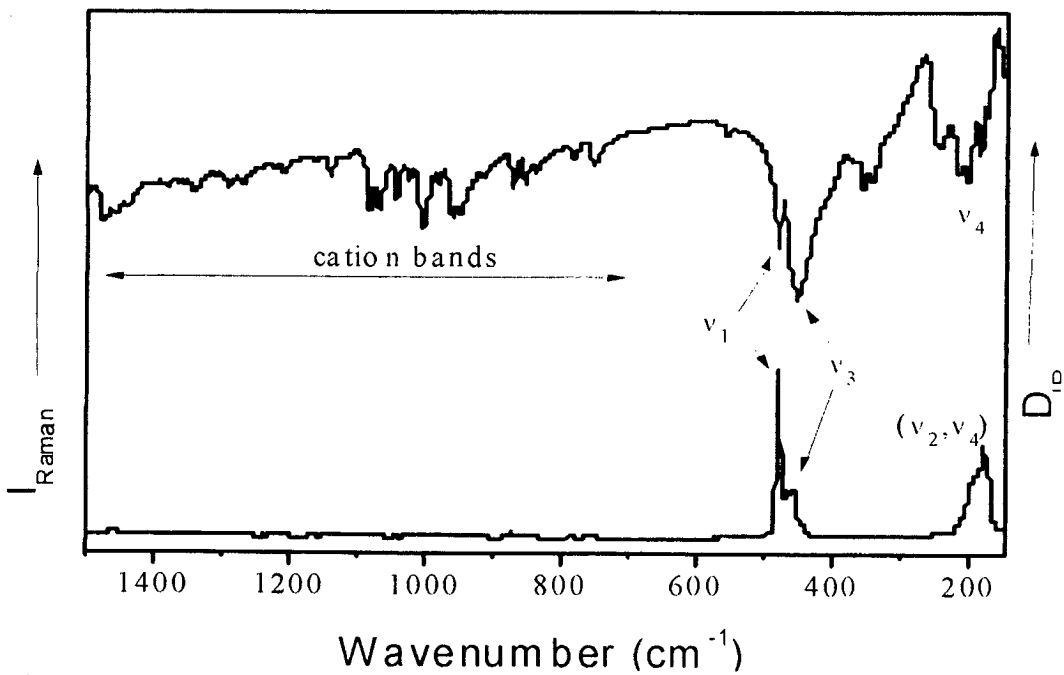
Fig. 4.4.10 Raman and IR spectra of (trenH$_2$)[WS$_4$]· H$_2$O **18**

observed for (pipH$_2$)Cl$_2$ below 500 cm^{-1} as seen from Fig 4.4.11a. Hence these features indicate considerable distortion of the [MoS$_4$] tetrahedron and can be explained by the lowering in symmetry, which is responsible for the symmetric stretching vibration (v_1) of the Mo=S bond at 445 cm^{-1} to appear as a medium intensity band. The distortion was also observed in the X-ray investigations in the form of the largest Δ value 0.0431 Å in this complex. The assignment of the 445 cm^{-1} band for the symmetric stretching vibration gains credence form the observation of an intense signal in the Raman spectrum of **21** at 448 cm^{-1}. IR spectrum of **22** is depicted in Fig 4.4.11c and a Fig.4.4.12. The IR spectrum of **22** exhibits a broad N-H vibration at around 3000 cm^{-1}. The shift to lower wave numbers compared to the free amine can be again explained by similar arguments as in the case of **21**. The IR spectra of **21** and **22** are identical excepting that the signals below 500 cm^{-1} of the [WS$_4$]$^{2-}$ anion are shifted to lower energies. The IR-Raman spectra of a few organic ammonium tetrathiometalates are displayed in **Appendix II**.

The solid-state IR spectra of the complexes (enH$_2$)[CrO$_4$] **33** and (enH$_2$)[Cr$_2$O$_7$] **34** exhibit several signals indicating the presence of the organic dication. The broad absorption signal at 2970-2365 cm^{-1} in **33** can be assigned to C-H and N-H stretching vibrations. This signal is quite broad compared to the signal observed in other ethylenediammonium salts like **1** and **2** discussed earlier and occurs at lower energies. This feature is indicative of H-bonding interactions and the broadness of the signal indicates that the H-bonding interactions are stronger in the tetraoxochromate compared to tetrathiometalates. The broad signal observed at 3063–2512 cm^{-1} in (enH$_2$)[Cr$_2$O$_7$] can be assigned to the N-H and C-H stretching vibrations. The strong signals observed at 924 and 835 cm-1 in (enH$_2$)[CrO$_4$] can be assigned to Cr-O vibrations while all the other signals can be attributed to the organic ethylenediammonium counter cation. The bands observed at 930 and 878 cm^{-1} for the dichromate complex (enH$_2$)[Cr$_2$O$_7$] can be assigned to the asymmetric and symmetric Cr-O stretching vibrations and are in good agreement with the reported values of the same compound prepared in a HF medium [198]. The IR spectra of (enH$_2$)Cl$_2$, (enH$_2$)[CrO$_4$] and (enH$_2$)[Cr$_2$O$_7$] are displayed in Fig. 4.4.13.
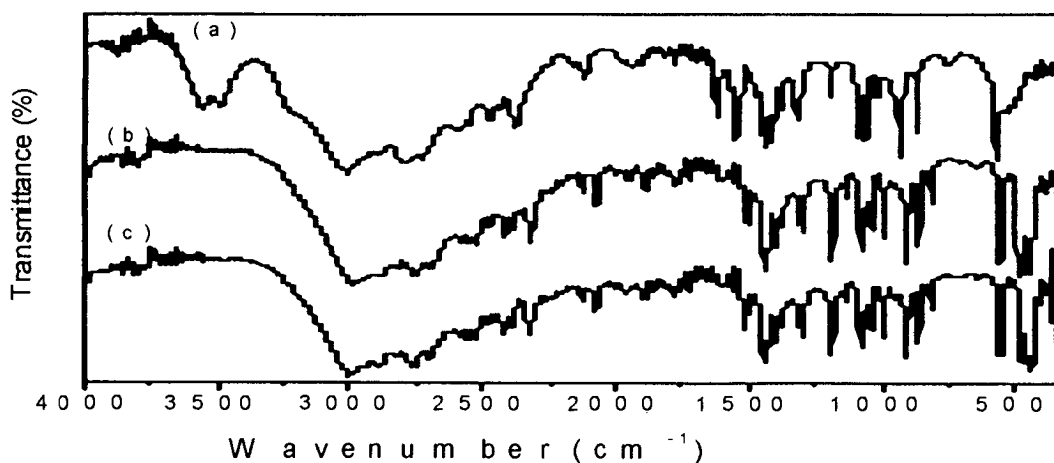
Fig. 4.4.11 IR spectra of (a) $(pipH_2)Cl_2.2H_2O$, (b) $(pipH_2)[MoS_4]$ **21**, (c) $(pipH_2)[WS_4]$ **22**
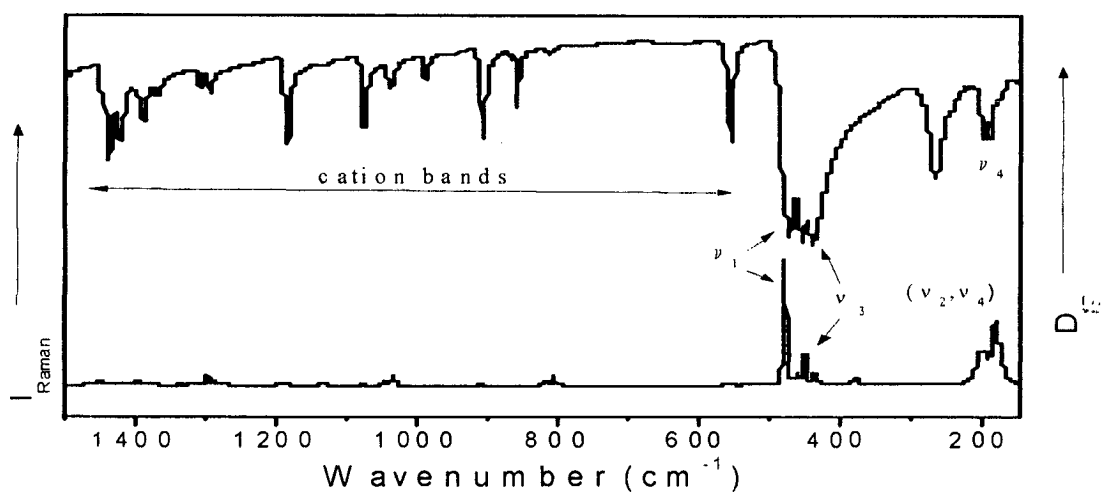
Fig. 4.4.12 Raman and IR spectra of $(pipH_2)[WS_4]$ **22**
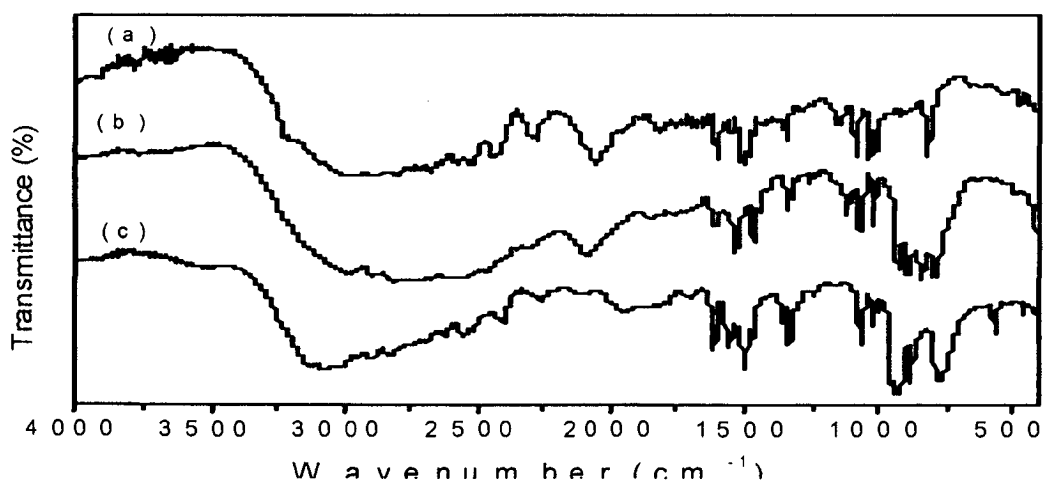
Fig. 4.4.13 IR spectra of (a) $(enH_2)Cl_2$, (b) $(enH_2)[CrO_4]$ **33**, (c) $(enH_2)[Cr_2O_7]$ **34**

161

4.4.2 UV-Visible Spectroscopy

The organic ammonium tetrathiometalates $[MS_4]^{2-}$ (M = Mo, W) and oxochromates synthesized in this work have been characterized by UV-Visible spectroscopy. The electronic spectra of all new tetrathiomolybdates and tetrathiotungstates have been recorded in dilute aqueous ammonia. For tetrathiomolybdates, intense bands were observed at around 468, 317 and 241 nm while for tetrathiotungstates these signals are observed at around 393, 277 and 221 nm (Table 4.4.2). The peak positions observed in all tetrathiometalates are almost identical within experimental error to the corresponding ammonium or tetraethylammonium salts [50]. These intense electronic bands can be assigned to the charge transfer transitions of the tetrahedral $[MS_4]^{2-}$ chromophores. UV-Visible spectrum of oxochromates namely $(enH_2)[CrO_4]$ **33** and $(enH_2)[Cr_2O_7]$ **34** were recorded in water. The electronic spectrum of $(enH_2)[CrO_4]$ in H_2O exhibits two bands at 373, 270 nm while $(enH_2)[Cr_2O_7]$ in H_2O absorbs at 353 and 260 nm. These bands can be assigned to the charge transfer transitions of $[CrO_4]^{2-}$ and $[Cr_2O_7]^{2-}$ in. Representative UV-Vis spectra of the complexes containing $[MoS_4]^{2-}$, $[WS_4]^{2-}$, $[CrO_4]^{2-}$ and $[Cr_2O_7]^{2-}$ chromophores are depicted in Fig. 4.4.14.

4.4.3. NMR spectroscopy

In the present work, a few new complexes have been investigated by ^1H NMR and ^{13}C NMR. The purpose behind this study is to confirm the presence of the organic moiety in the new complexes ^{13}C DEPT technique has also been used for identification of different $-CH_2$ and $-CH_3$ groups in few of the complexes. The ^1H NMR spectral data for organic ammonium salts of tetrathiometalates is presented in Table 4.4.2. The ^{13}C NMR and ^{13}C DEPT spectral data for a few compounds are presented in Table 4.4.3.

The ^1H NMR spectrum of $(enH_2)[WS_4]$ **2** in DMSO-d_6 exhibits a sharp singlet at δ = 3.04 ppm. This signal can be attributed to the resonance of the equivalent methylene protons of en. The broad signal due to the ammonium protons is observed at 7.77 ppm. The corresponding Mo analogue $(enH_2)[MoS_4]$ **1** exhibits signals at 3.05 and 7.80 ppm. The ^1H NMR spectrum of $(N-Me-enH_2)[MoS_4]$ **3** in DMSO-d_6, exhibits three signals at δ=2.59 (s, 3H), δ=3.12 (t, 2H, J=5.18 Hz) and δ=3.09 (t, 2H, J=5.08

162

Table 4.4.2 ^{1}H NMR and UV-visible data for tetrathiometalates

Compound	^{1}H NMR (δ in ppm) DMSO-d_6	λ_{max} in nm (ε_{max} in mol^{-1}.l.cm^{-1})
(enH$_2$)[MoS$_4$] **1**	3.05 (s, 2 H), 7.80 (br, -NH$_3$)	466, 316, 240
(enH$_2$)[WS$_4$] **2**	3.039(s, 2 H), 7.771(br,-NH$_3$)	393 (15452), 277 (18528) 221 (17340)
(N-MeenH$_2$)[MoS$_4$] **3**	2.59 (s, 3H), 3.12 (t, 2H, J=5.18 Hz), 3.09 (t, 2H, J=5.08 Hz)	468(110752), 317(10928), 245(11020)
(N-MeenH$_2$)[WS$_4$] **4**	2.32 (s, 3H), 2.69 (t, 2H, J=5.9 Hz), 2.79 (t, 2H, J=3.1 Hz)	393 (15841), 278(22929), 216(28277)
(tmenH$_2$)[MoS$_4$] **5**	3.40 (s, 4H), 2.80 (s, 12H) in D$_2$O	468(7024), 317(10038), 241(15334)
(tmenH$_2$)[WS$_4$] **6**	-	393(15076), 277(18221), 221(17090)
(1,3-pnH$_2$)[MoS$_4$] **7**	1.85 (p, 2H, J=7.5 Hz), 2.88 (t, 4H, J=7.5 Hz), 7.60 (br, -NH$_3$)	468(8755), 317(14020), 241(21490)
(1,3-pnH$_2$)[WS$_4$] **8**	-	393(14489), 277 (16619), 220(16154)
(N,N'-dm-1,3-pnH$_2$)[WS$_4$] **10**	1.91 (p, 2H, J=7.5 Hz), 2.55 (s, 3H), 2.96 (t, 4H, J=7.6 Hz)	393(15689), 278 (22934), 216(31462)
(1,4-bnH$_2$)[WS$_4$] **12**	1.52 (s, 2H), 2.74 (s, 2H)	393(13333), 278(18400), 214(22311)
(dienH$_2$)[MoS$_4$] **13**	2.82 (t, 2H, J = 5.4 Hz), 2.66 (t, J = 5.5Hz), 6.72 (br, -NH$_3$) 2.79 (t, 2H, J = 5.55), 2.63 (t, 2H, J = 5.4 Hz) in DMSO-d_6+ D$_2$O	468(14260), 317(18107), 240(19951)
(dienH$_2$)[WS$_4$] **14**	2.83 (t, 2H, J = 5.7 Hz), 2.67 (t, 2H, J = 5.55 Hz)	393(15858), 280(17459), 220(19244)
(dipnH$_2$)[MoS$_4$] **15**	1.65 (p, 2H, J=7.2 Hz), 2.57 (t, 2H, J=6.7), 2.81 (t, 2H, J=7.3)	468(12891), 317(17069), 241(21345)
(dipnH$_2$)[WS$_4$] **16**	-	393(12441), 277 (18114), 217(21122)
(trenH$_2$)[WS$_4$]·H$_2$O **18**	2.55 (t, 2H, J = 6 Hz), 2.82 (t, 2H, J = 5.5Hz)	393(16360), 277(22460), 221(23800).
(pipH$_2$)[MoS$_4$] **21**	3.32 (s, 2H)	468(3524), 317(5108), 241(6057)

Compound	^{1}H NMR (δ in ppm) DMSO-d_6	λ_{max} in nm (ε_{max} in mol^{-1}.l.cm^{-1})
(pipH$_2$)[WS$_4$] **22**	3.25 (s, 2H)	393 (14800), 277 (18900), 221 (18600)
(1,4-dmpH$_2$)[WS$_4$] **24**	-	393 (15293), 277 (17048), 220 (16473)
(2-pipH-1-EtNH$_3$)[MoS$_4$] **27**	2.57 (t, 4H, J=4.92 Hz), 3.07 (t, 4H, J=5.04 Hz), 2.89 (t, 2H, J=5.98 Hz), 2.40 (t, 2H, J=.6.0 Hz)	468(11246), 317(13470), 239(13663)
(trans-1,2-cn)	-	393(18437), 277(23802), 211(24375)
(mipaH)$_2$[WS$_4$] **29**	3.2 (m,1H, J=6.4 Hz), 1.09 (d, 6 H, J= 6.9 Hz)	393 (16740), 277 (22573), 211 (26480)

Table 4.4.3 ^{13}C NMR and DEPT spectral data for tetrathiometalates

Compound Name	^{13}C NMR (ppm) in DMSO-d$_6$	^{13}C DEPT in DMSO-d$_6$
(tmenH$_2$)[MoS$_4$] **5**	43.75, 52.29	-
(N,N'-dm-1,3-pnH$_2$)[WS$_4$]**10**	22.95, 33.36, 46.33	22.99, 33.39, 46.36
(dipnH$_2$)[MoS$_4$] **15**	27.25, 38.59, 46.56	27.26, 38.59, 46.57
(2-pipH-1-EtNH$_3$)[MoS$_4$]·½H$_2$O **27**	36.59,44.04,50.02, 54.31	36.59, 44.06, 50.04, 54.32
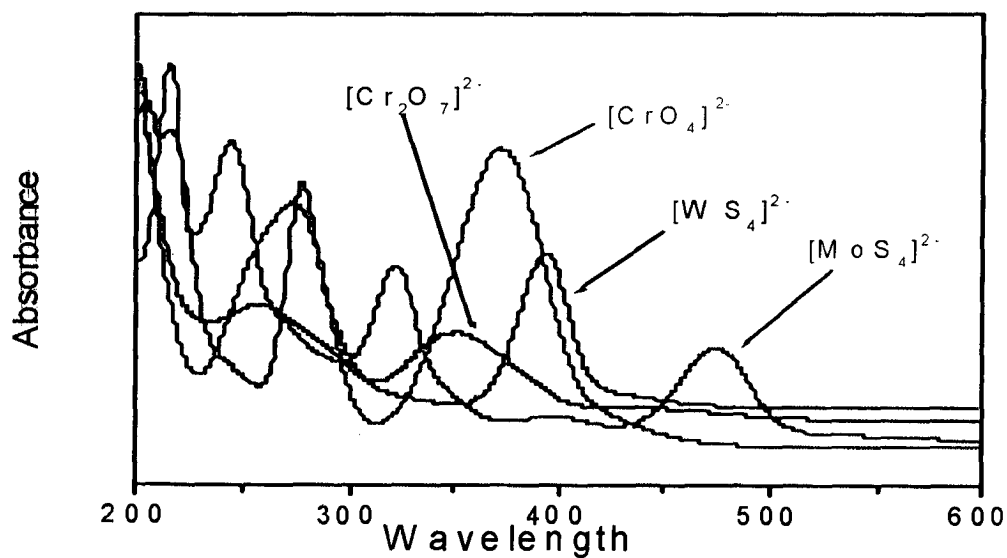
Fig. 4.4.14 UV-Visible spectra of (a) [MoS$_4$]$^{2-}$, (b) [WS$_4$]$^{2-}$, (c) [CrO$_4$]$^{2-}$ and (d) [Cr$_2$O$_7$]$^{2-}$ complexes

Hz) which are assigned to the resonance of the three types of protons on C3, C2 and C1. In the ^{1}H NMR spectrum of (N-Me-enH$_2$)[WS$_4$] **4** in DMSO-d_6, the three signals at δ =2.32, δ = 2.69 (J=5.9 Hz) and δ = 2.79 (J = 3.09 Hz) observed in **4** can be assigned to the resonance of the protons on carbon C3, C2 and C1 respectively. The PMR spectrum of (tmenH$_2$)[MoS$_4$] **5** exhibit two singlets at δ = 3.39 and δ = 2.80 ppm respectively in D$_2$O. Based on the reported spectrum of (tmenH$_2$)[Cr$_2$O$_7$] [208], which absorbs at δ = 3.8 ppm (s, 4H) and δ = 3.11 ppm (s, 12H) in D$_2$O as well as the integration of the signals, the resonance at δ = 3.39 ppm can be assigned to the equivalent methylene protons. A signal at δ =2.80 ppm can be attributed to the methyl protons. The up field shifting of the resonances in **5** as compared to the dichromate complex can be explained based on the differing nature of the anions. The ^{13}C NMR spectrum of **5** exhibits two signals at 52.29 and 43.75 ppm indicating the presence of two different carbon atoms in **5** (Table 4.4.3)

The ^{1}H NMR spectrum of (1,3-pnH$_2$)[MoS$_4$] **7** in DMSO-d$_6$ exhibits three signals at δ = 1.85 (J=7.5 Hz), δ = 2.88 (J=7.5Hz) and δ = 7.60 ppm (Fig 4.4.15). The observed chemical shifts and the coupling constants are as expected for 1,3-pn. The quintet at δ = 1.85 ppm can be assigned to the resonance of the protons on the central carbon (C2), while the triplet observed at δ = 2.88 ppm originates from the resonance of the equivalent protons on C1 and C3. The broad resonance at δ = 7.60 ppm can be assigned to the absorption due to the ammonium protons. The PMR spectrum of (N,N'-dm-1,3-pnH$_2$)[WS$_4$] DMSO-d$_6$ exhibits three signals a singlet, triplet and quintet at δ = 2.56, δ = 2.97 and δ= 1.91 ppm respectively. The quintet at δ = 1.91 ppm can be assigned to the absorption of the protons on the central carbon (C3), while the triplet observed at δ = 2.97 ppm originates from the resonance of protons on two equivalent –CH$_2$ groups (C2 and C4). A singlet observed at δ= 2.56 ppm is due to the six protons of two equivalent terminal methyl groups (C1 and C5). These signals are in good agreement with signals observed in the PMR spectrum of **7**. The signal due to the ammonium protons is not observed indicating a very rapid exchange of these protons with the trace amounts of water in DMSO-d6. ^{13}C NMR and ^{13}C DEPT spectra of (N,N'-dm-1,3-pnH$_2$)[WS$_4$] **10** have been recorded in DMSO-d_6. The appearance of three signals at 22.95 (C3), 33.36 (C1 and C5) and 46.33 ppm (C2 and C4) in ^{13}C NMR spectrum of **10** reveals the presence of three carbons in different

environments. ^{13}C DEPT spectrum of **10** exhibit three signals at 22.99, 33.39 and 46.36 ppm which can be attributed to the $-CH_2(C3)$, $-CH_3(C1)$ and C5) and $-CH_2$ (C2 and C4) group. The ^1H NMR spectrum of $(1,4-bnH_2)[WS_4]$ **12** in DMSO-d_6 exhibits two signals at $\delta = 1.52$ and $\delta = 2.74$ ppm which are assigned to the equivalent protons on and the symmetry related carbons (C2 and C2A) and (C1 and C1A) respectively.

The ^1H NMR spectrum of $(dienH_2)[MoS_4]$ **13** exhibits two triplets at $\delta= 2.82$ (J = 5.4 Hz) and $\delta= 2.66$ (J = 5.5 Hz) ppm in DMSO-d_6 which can be assigned to the equivalent methylene protons (C1 and C1A) and (C2 and C2A) respectively. The signal at $\delta = 6.72$ ppm can be attributed to the ammonium protons. The same spectrum when recorded after adding D_2O exhibits two triplets at $\delta = 2.79$ (J = 5.5 Hz) and $\delta = 2.63$ (J = 5.4 Hz) ppm. The signal due to the ammonium protons disappears due to the rapid exchange of these protons with D_2O. The ^1H NMR spectrum of $(dienH_2)[WS_4]$ **14** can be explained similarly (Fig 4.4.16). The two triplets at $\delta= 2.83$ (J = 5.7 Hz) and $\delta = 2.67$ (J = 5.5 Hz) ppm in DMSO-d_6 can be assigned to the resonances of protons on C1 and C2. The signal due ammonium protons is not observed due the rapid exchange of these protons with the trace amounts of water in DMSO-d_6.

The PMR spectrum of $(dipnH_2)[MoS_4]$ **15** in DMSO-d_6 exhibits three signals a quintet at 1.65 (2H, J = 7.2 Hz) and two triplets at $\delta = 2.57$ (2H, J = 6.7) and 2.81 ppm (t, 2H, J = 7.3) (Fig 4.4.17). A quintet at $\delta = 1.65$ ppm can be assigned to the resonance of the protons on equivalent methylene groups (C2 and C5), while the triplet observed at $\delta=2.57$ ppm originates from the resonance of protons on C1 which is attached to the free -NH_2 group. A second triplet observed at $\delta = 2.81$ ppm is due to the six protons of three equivalent methyelene groups (C3, C4 and C6) which are directly attached to the quaternary N atoms. In the ^{13}C NMR spectrum of **15** the three distinct resonances are observed at 27.25, 38.59 and 46.56 ppm. The signal at 27.25 ppm can be assigned to the equivalent C2 and C5, while a sharp line at 38.59 ppm is due to C1. The third signal at 46.56 ppm can be attributed to the identical C2, C4 and C6. ^{13}C DEPT spectrum of $(dipnH_2)[MoS_4]$ exhibits three signals at 27.26, 38.59 and 46.57 ppm indicating three different $-CH_2$ methylene groups.
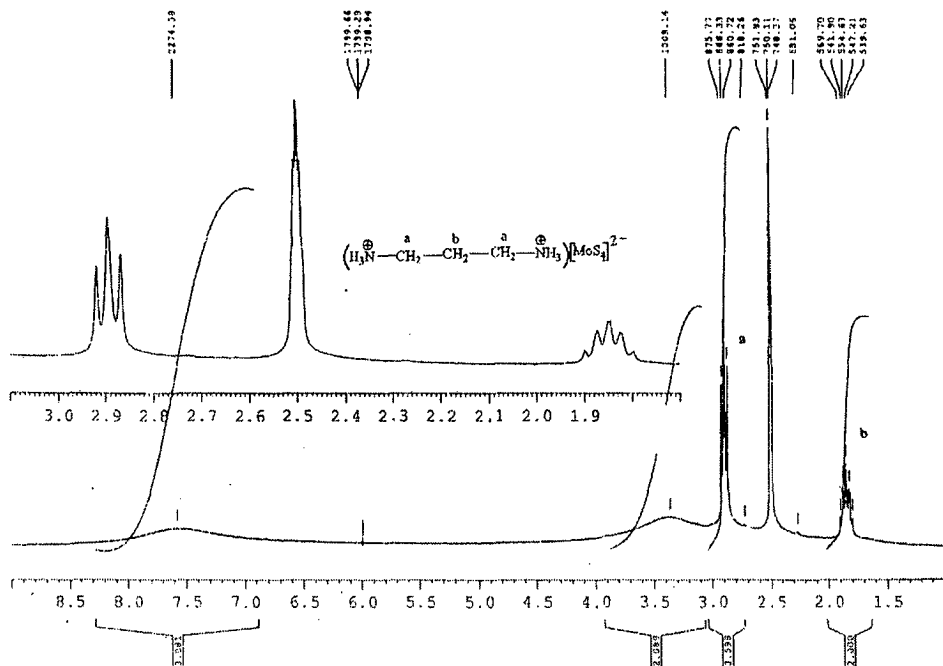
Fig 4.4.15 ^{1}H NMR spectra of (1,3-pnH$_2$)[MoS$_4$] **7** in DMSO-d_6
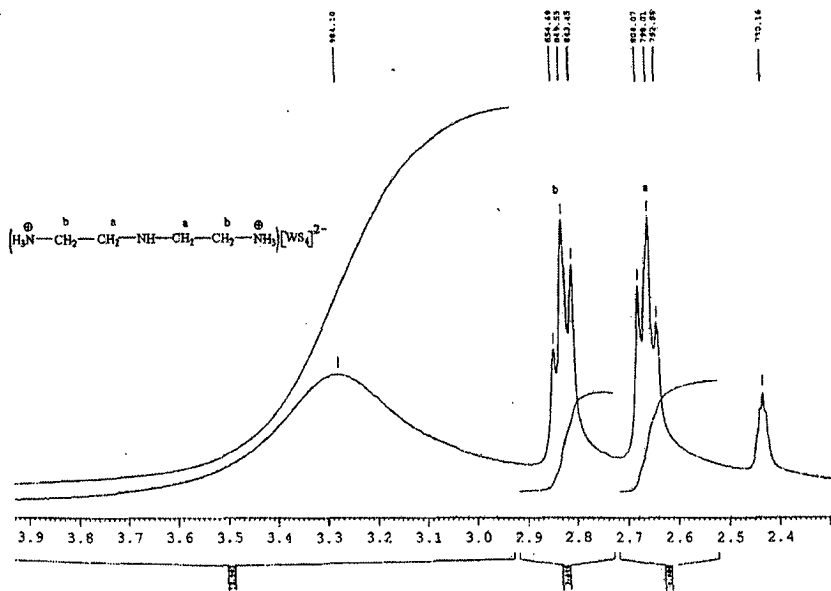
Fig 4.4.16 ^{1}H NMR spectra of (dienH$_2$)[WS$_4$] **14** in DMSO-d_6

The PMR spectrum of (trenH$_2$)[WS$_4$]· H$_2$O **17** in DMSO-d$_6$ exhibits two triplet at δ = 2.55 (J = 6 Hz) and δ = 2.82 (J = 5.5Hz) respectively. The analytical data of this complex indicates that two of the four N atoms in tren are protonated. In the ^{1}H NMR spectrum of **17**, two triplets, one each for the equivalent -CH$_2$ groups (C1, C3 and C5) directly bonded to N1 and the other for the remaining three -CH$_2$ groups (C2, C4 and C6) are observed in **17** as expected for the free unprotonated tren. Although the reason for the magnetic equivalence observed in **17** is not very clear, such a phenomenon has been reported in the related complex (trienH$_2$)[MoS$_4$] (trien=triethylenetetraammine) [76]. The PMR spectrum of (pipH$_2$)[MoS$_4$] **21** in DMSO-d$_6$ exhibits a sharp singlet at δ = 3.32 ppm which can be assigned due to the resonance of the equivalent methylene protons of pip. The ^{1}H NMR spectrum of the W analogue (pipH$_2$)[WS$_4$] **22** in DMSO-d$_6$ exhibits a sharp singlet at δ = 3.25 ppm due to the resonance of the equivalent –CH$_2$ protons of cyclic piperazine.

The ^{1}H NMR spectrum of (2-pipH-1-EtNH$_3$)[MoS$_4$] · ½H$_2$O **27** exhibits four intense signals that can be assigned to the resonances of protons of four different types of methylene groups (Fig. 4.4.18). Four triplets are observed at δ = 2.57 (t, 4H, J = 4.92 Hz), δ = 3.07 (t, 4H, J = 5.04 Hz), δ = 2.89 (t, 2H, J = 5.98 Hz) and δ = 2.40 (t, 2H, J = 6.0 Hz). The triplet at δ = 2.40 can be assigned to the resonance of the four equivalent protons on C1 and C4 which are attached to the unprotonated N1 atom while the triplet at δ = 2.57 ppm can be attributed to the resonance of two protons on C5 atom. The other two triplets at δ = 3.07 (t, 4H, J = 5.04 Hz), δ = 2.89 (t, 2H, J = 5.98 Hz) originate from the protons on C6 and (C2 and C3) respectively which are attached to the protonated nitrogen atoms N3 and N2. ^{13}C NMR and ^{13}C DEPT spectra of **27** are displayed in Fig. 4.4.19. ^{13}C NMR spectrum of **27** exhibits four distinct signals at 36.59, 44.04, 50.02 and 54.31 ppm which can be assigned to four carbons in different environments. The presence of four different –CH$_2$ groups in this compound has been identified by ^{13}C DEPT spectrum, which exhibits four signals 36.59, 44.06, 50.04 and 54.32. The PMR spectrum of (mipaH)$_2$[WS$_4$] **29** exhibit a doublet at δ = 1.09 (J = 6.9 Hz) and a multiplet at δ= 3.20 ppm (J=6.45 Hz). The doublet can be attributed to the resonance of six equivalent protons of the two methyl groups while the multiplet originates from the single proton on the central carbon atom.

168
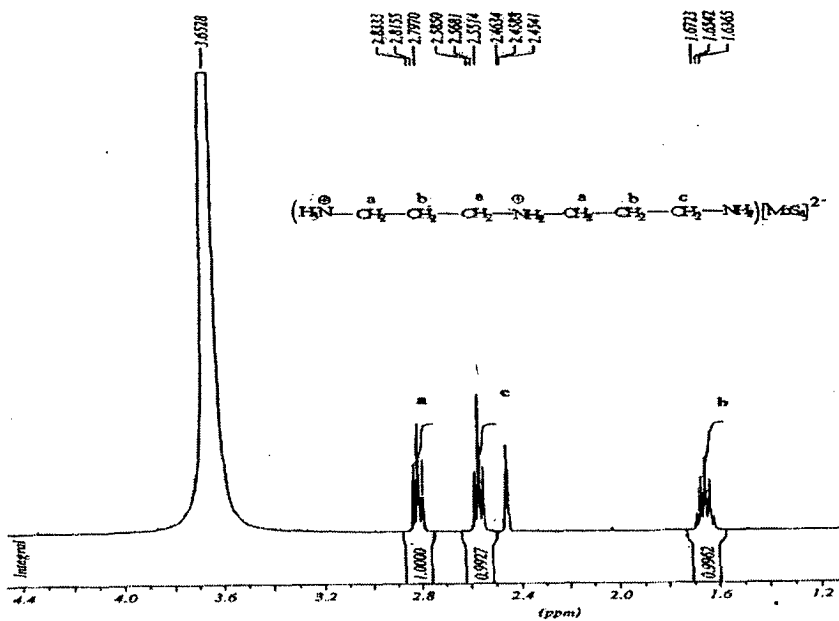
Fig 4.4.17 ^{1}H NMR spectra of (dipnH$_2$)[WS$_4$] **15** in DMSO-d_6
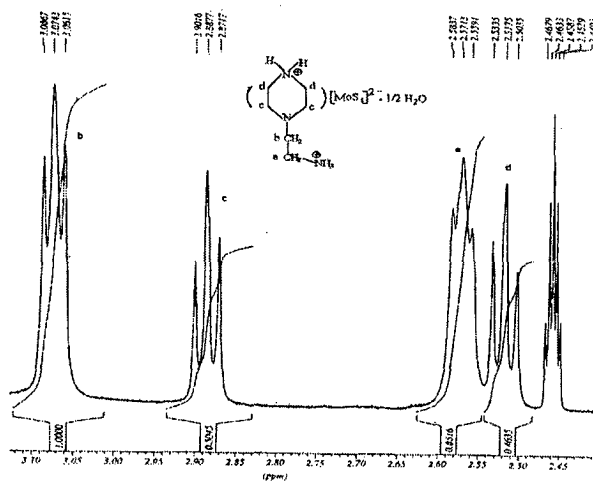
Fig 4.4.18 ^{1}H NMR spectra of (2-pipH-1-EtNH$_3$)MoS$_4$·½H$_2$O **27** in DMSO-d_6

169
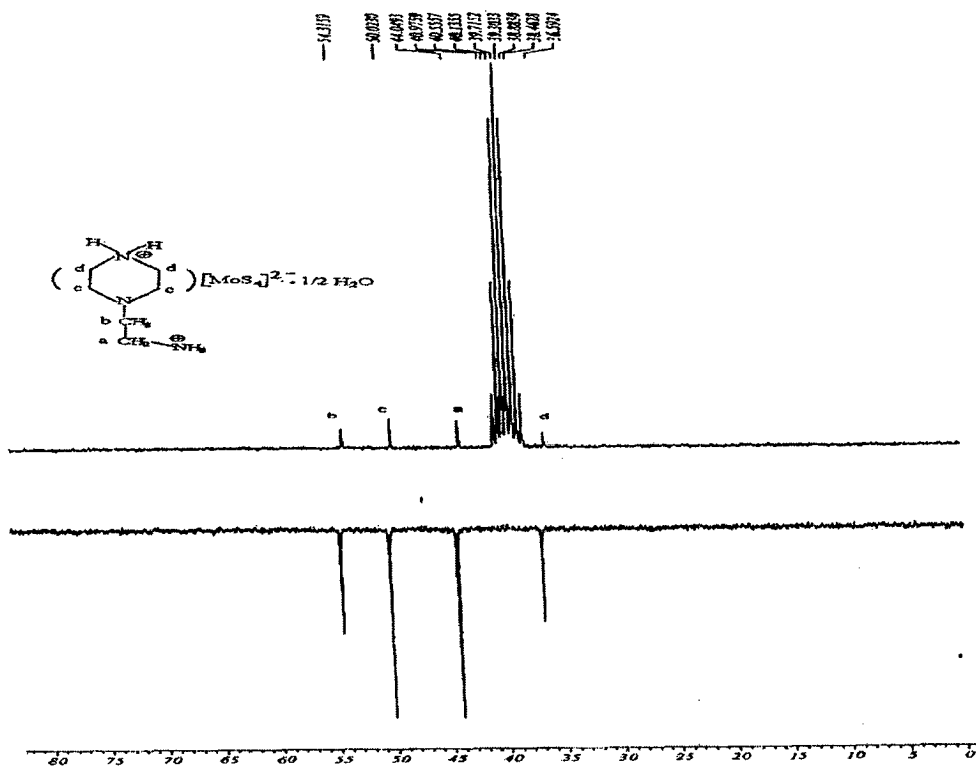
Fig 4.4.19 ^{13}C NMR and DEPT spectra of (2-pipH-1-EtNH$_3$)MoS$_4$·½H$_2$O **27** in DMSO-d_6

The spectral data for two oxochromates $(enH_2)[CrO_4]$ (Fig. 4.4.20) **33** and $(enH_2)[Cr_2O_7]$ **34** are presented in Table 4.4.4. The high field ^1H NMR spectra of complexes **33** and **34** are very similar. Both **33** and **34** exhibit sharp singlet resonances in D_2O at $\delta = 3.16$ and $\delta = 3.24$ ppm and these signals can be readily assigned to the two methylene groups. The signal due to the ammonium protons are not observed in both cases in D_2O, which can be attributed to the rapid exchange of these protons. However, in DMSO-d_6 the resonances due to both types of protons are observable. One of these signals is broad and the addition of D_2O results in the disappearance of this broad signal. The broad signal is assigned to the resonance of the protons bound to N. The resonance due to the N-H protons in **33** is observed at $\delta = 3.43$ ppm while the signal for the protons bound to N in **34** occurs at (7.78 ppm). Interestingly in two other $(enH_2)^{2+}$ salts the resonance of the proton bound to N is observed at around $\delta = 8$ ppm. The reason for the upfield shifting of the $-NH_3$ signal in $(enH_2)[CrO_4]$ is not very clear. The spectroscopic data for chromates is presented in Table 4.4.4.

4.4.4 Highly Insoluble tetrathiometalates

Infra red spectroscopy and X-ray powder diffractometry techniques have been used as an unambiguous tool for identification of the isostructural nature of few of the organic ammonium salts of tetrathiometalate which could not be investigated by X-ray crystal studies. The reaction of $(dbtmen)Br_2 \cdot 2H_2O$ **30** with ammonium salts of tetrathiomolybdate or tetrathiotungstate in 1:1 mole ratio forms the highly insoluble organic ammonium salts namely $(dbtmen)[MoS_4]$ **31** and $(dbtmen)[WS_4]$ **32**. The complexes are highly insoluble in almost all common solvents. Both complexes have been characterized by elemental analysis, IR-Raman spectroscopy and X-ray powder diffractometry. Based on the elemental analysis the two complexes **31** and **32** have been formulated as $C_{20}H_{30}MoS_4$ and $C_{20}H_{30}WS_4$. The analytical and spectral data for the above three complexes given in Table 4.4.5. The central part of IR spectra of both the complexes exhibit several intense bands which can be assigned to $(dbtmen)^{2+}$ cation . The IR spectrum of **31** exhibits a strong signal at 475 cm^{-1} which can be readily assigned to the asymmetric stretching vibration (v_3) of Mo=S bond. In the complex **32**, the asymmetric stretching vibration (v_3) occurs at 457 cm^{-1}. Interestingly

171
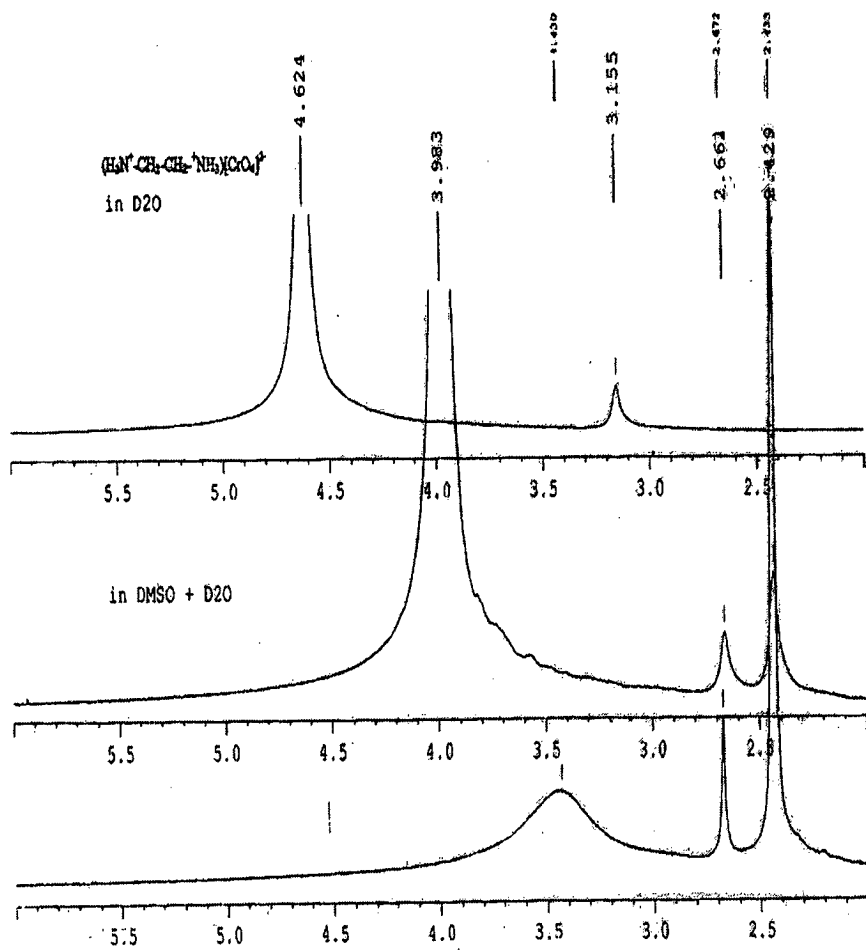
Fig 4.4.20 ^{1}H NMR spectrum of $(enH_2)[CrO_4]$

Table 4.4.4 Infra red, UV-Visible and ^{1}H NMR spectroscopic data for (enH$_2$)[CrO$_4$] **33** and (enH$_2$)[Cr$_2$O$_7$] **34**

Compound	IR bands in cm^{-1}	λ_{max} in nm (ε_{max} in mol^{-1}.l.cm^{-1})	δ in ppm		
			DMSO-*d6*	D$_2$O	DMSO-*d6* + D$_2$O
(enH$_2$)[CrO$_4$] **33**	2971-2365(br), 2081(w), 1607(m), 1526(m), 1466(m), 1412(w), 1327(w), 1256(w), 1098(m), 1067(m), 1021(s), 924(s), 801(br), 777(m)	373(2500) 270(2480)	2.672 (s,-CH$_2$) 3.430 (br,-NH$_3$)	3.155 (s, -CH$_2$)	2.661 (s, -CH$_2$)
(enH$_2$)[Cr$_2$O$_7$] **34**	3063–2512(br), 1615(m), 1556(m), 1501(m), 1470(m), 1360(m), 1333(w), 1065(m), 1022(m), 930(s), 878(m), 787(w)	353(2770) 260(3700)	3.064 (s, -CH$_2$) 7.777 (br, -NH$_3$)	3.235 (s, -CH$_2$) --	3.068 (s, -CH$_2$) --

Table 4.4.5 IR and Raman spectroscopic data for highly insoluble tetrathiometalates

Compound Name	Analytical Data (%)	IR bands cm^{-1}	Raman bands cm^{-1}		
(dbtmen)Br$_2$.2H$_2$O	C 48.63 (48.57), H 7.01 (6.95), N 5.68 (5.67)	3463, 3394, 3228, 3021, 1616, 1486, 1473, 1453, 1393, 1353, 1214, 1087, 1033, 996, 960, 947, 920, 893, 864, 783, 744, 727, 713, 580, 513, 4817, 447	-		
(dbtmen)[MoS$_4$]	C 45.09 (45.95) H 5.61 (5.80), N 5.30 (5.36) S 23.31 (24.54	2982, 1458, 1216, 1155, 997, 865, 787, 730, 475 (v_3)	483, 183, 111	468, 174,	454, 169,
(dbtmen)[WS$_4$]	C 38.50 (39.33) H 4.81 (4.96) N 4.52 (4.59) S 19.49 (21.01)	2984, 1445, 1355, 1217, 1155, 997, 864, 786, 730, 706, 619, 584, 457 (v_3)	484, 453, 110	479, 180,	469, 171,

no split of M-S band is observed in these complexes indicating probably very less distortion of $[MS_4]^{2-}$ (M = Mo, W) tetrahedron compared to other organic ammonium salts discussed earlier. As both the N atoms of (dbtmen)$^{2-}$ are fully alkylated, H-bonding interaction features are not possible in these compounds. The Raman spectra of both the complexes exhibit all the four bands viz $v_1(A1)$, $v_2(E)$, $v_3(F2)$, and $v_4(F2)$ which are expected for the free tetrahedral $[MS_4]^{2-}$ (M=Mo,W) anion. The spectral data and analytical data for **30**, **31** and **32** are presented in Table 4.4.4. The IR spectra of two complexes are identical indicating that both of them are isostructural Fig. 4.4.21. The isostructural nature of these complexes gets further credence from the data of X-ray powder diffraction studies of these complexes. All the intense peaks in powder patterns of the both complexes are very similar indicating their isostructural nature (Fig 4.4.22). The IR-Raman spectra of **31** and **32** are displayed in Appendix-II.

The complexes (dabcoH)$_2$[MoS$_4$] **25** and (dabcoH)$_2$|WS$_4$| **26** which contain the bicyclic diamine have been isolated in good yields. Both the complexes have been synthesized by using the diamine dabco. As explained earlier, in these complexes the organic cyclic diamine dabco is monoprotonated unlike other diamines such as pip, 1,4-dmp in (pipH$_2$)[MS$_4$], and (1,4-dmp)|WS$_4$| which are diprotonated. The IR spectra of both **25** and **26** are identical as most of the peaks have the same energies except in the region of 450-500 cm^{-1}. This is due to the presence of different anions in (dabcoH)$_2$[MoS$_4$] **25** and (dabcoH)$_2$[WS$_4$] **26**. The characteristic asymmetric vibration for Mo=S bond in the IR spectrum of **25** is observed at 474 cm^{-1} while for **26** this vibration, occurs at 458 cm^{-1}. The remaining signals in the mid IR spectra can be considered to originate from (dabcoH)$^+$ cations. The IR spectra of **25** and **26** are displayed in Fig 4.4.23. The isostructural nature of the two complexes can be further inferred from X-ray powder patterns (Fig. 4.4.24).

4.4.5 Reversible hydration studies

In the present investigation, IR spectroscopy and X-ray powder difractometry has been also used as a tool for monitoring of dehydration-rehydration process in (trenH$_2$)[MoS$_4$]·H$_2$O **17** and (trenH$_2$)|WS$_4$|·H$_2$O **18**. The IR spectra displayed in Fig
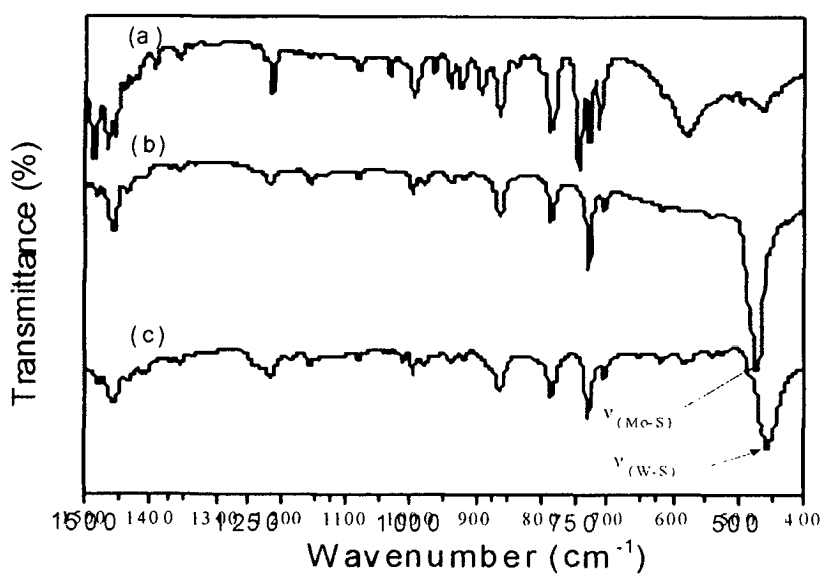
Fig. 4.4.21 IR spectra of (a) (dbtmen)Br$_2$.2H$_2$O **30**, (b) (dbtmen)[MoS$_4$] **31**, (c) (dbtmen)[WS$_4$] **32**
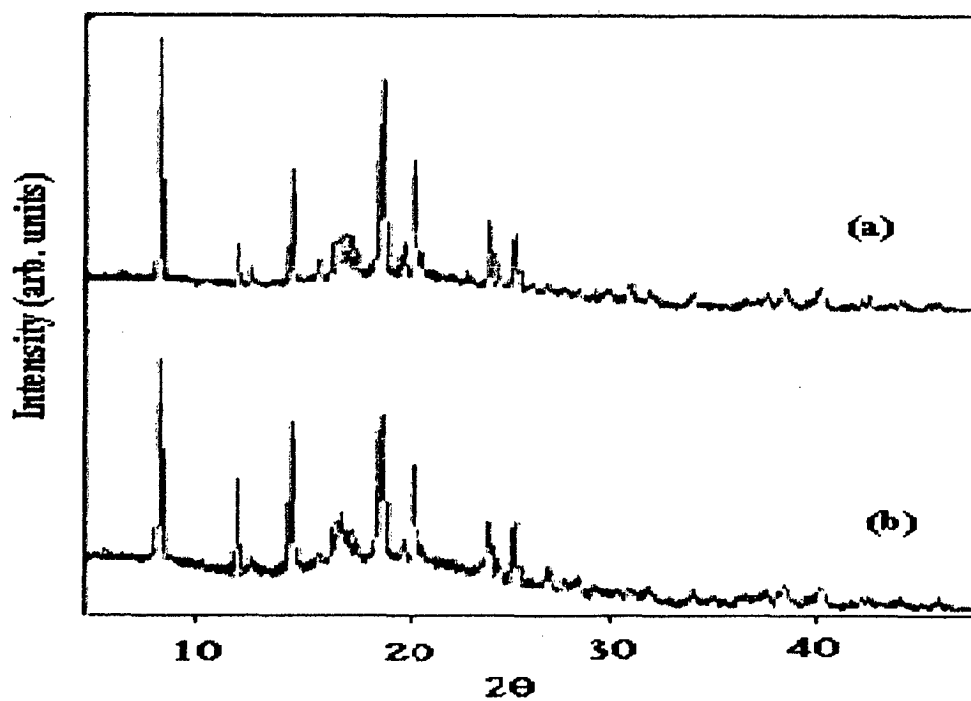
Fig 4.4.22 XRD powder patterns of (a) (dbtmen)[MoS$_4$] **31** (c) (dbtmen)[WS$_4$] **32**
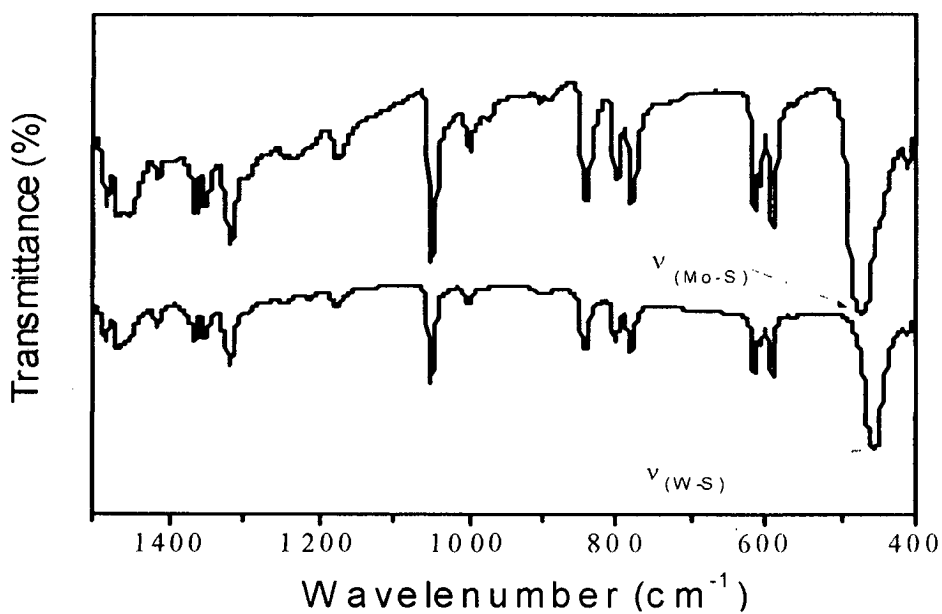
Fig. 4.4.23 IR spectra of (a) (dabcoH)$_2$[MoS$_4$] **25**, (b) (a) (dabcoH)$_2$[WS$_4$] **26**

Fig 4.4.24 XRD powder patterns of (a) (dabcoH)$_2$[MoS$_4$] **25** (b) (dabcoH)$_2$[WS$_4$] **26**

4.4.25 demonstrates this interesting phenomenon of reversible hydration in case of **17**. In Fig 4.3.25a the IR spectrum of the original complex **17** is desplayed which shows a broad signal at 3462 cm^{-1} for O-H vibration of the crystal water. On heating at 140 ^{0}C for about 10-15 min **17** emits its crystal water, which is evidenced from the weight loss that corresponds to a water molecule. The IR spectrum of the anhydrous (trenH$_2$)[MoS$_4$] **19** is shown in Fig 4.3.25b. No O-H bands are observed in the IR spectrum of anhydrous **19** indicating complete emission of water molecule. The phenomenon anhydrous sample was equilibrated over aqueous ammonia mixture in a dessicator. After 2 h the sample was weighed and observed that anhydrous **19** absorb water to give back the original pristine complex (Fig 4.3.25c). The X-ray powder patterns of the pristine complex, dehydrated and rehydrated complexes are presented in Fig 4.4.26. The reversible hydration in (trenH$_2$)[WS$_4$]·H$_2$O **18** can be explained similarly. The IR spectra of pristine complex **18**, anhydrous (trenH$_2$)[WS$_4$] **20** and rehydrated (trenH$_2$)[WS$_4$] are presented in Fig 4.4.27. The X-ray powder patterns of pristine, anhydrous and rehydrated complexes of (trenH$_2$)[WS$_4$]·H$_2$O are displayed in Fig. 4.4.28.

The reversible hydration studies has been also carried out in the case of (dbtmen)Br$_2$·2H$_2$O **30** which is used as starting material for the synthesis of the two highly insoluble tetrathiometallates namely (dbtmen)[MoS$_4$] **31** and (dbtmen)[WS$_4$] **32**. Complex **30** emits its crystal water at round 140 ^{o}C. The mass loss at this temperature corresponds to the emission of water molecule. The resultant anhydrous complex (dbtmen)Br$_2$ when equilibrated over water atmosphere in a dessicator, absorbs its water and results in the formation the hydrated complex. The IR spectra of the pristine **30**, anhydrous (dbtmen)Br$_2$ and rehydrated complex is depicted in (Fig. 4.4.29).
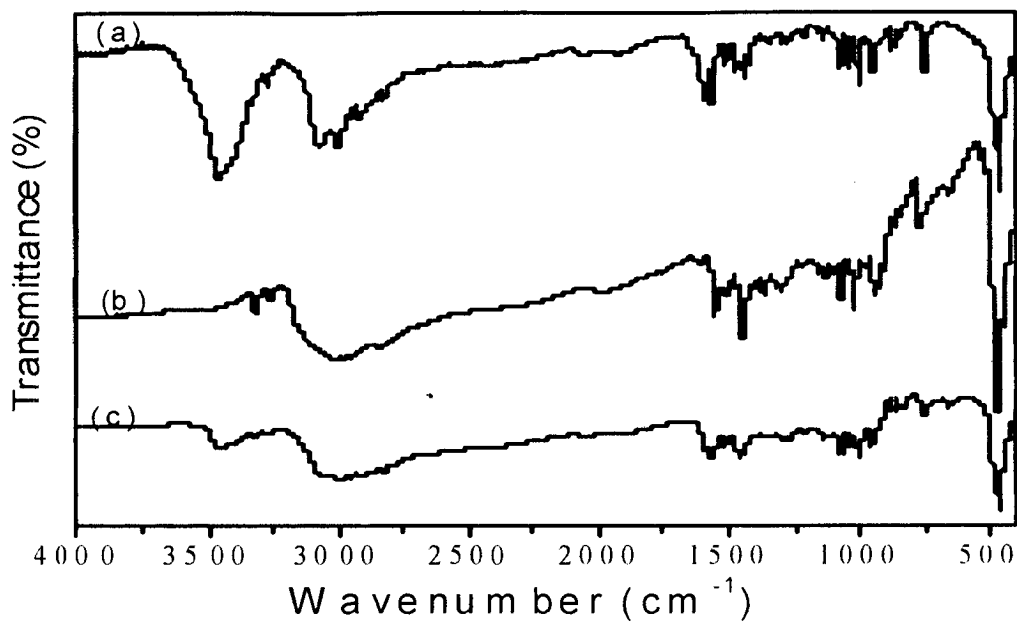
Fig 4.4.25 IR spectra of (a) pristine $\underline{17}$ (b) anhydrous $(trenH_2)[MoS_4]$ (c) rehydrated $(trenH_2)[MoS_4] \cdot H_2O$

2 THETA (degrees)
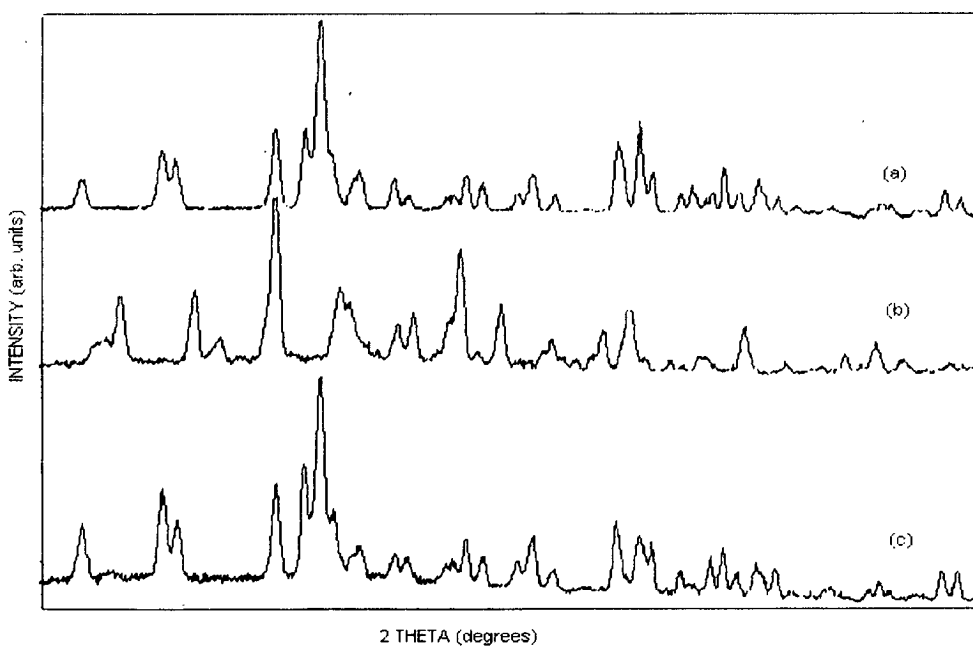
Fig 4.4.26 XRD powder patterns of (a) pristine $\underline{17}$ (b) anhydrous $(trenH_2)[MoS_4]$ (c) rehydrated $(trenH_2)[MoS_4] \cdot H_2O$

179
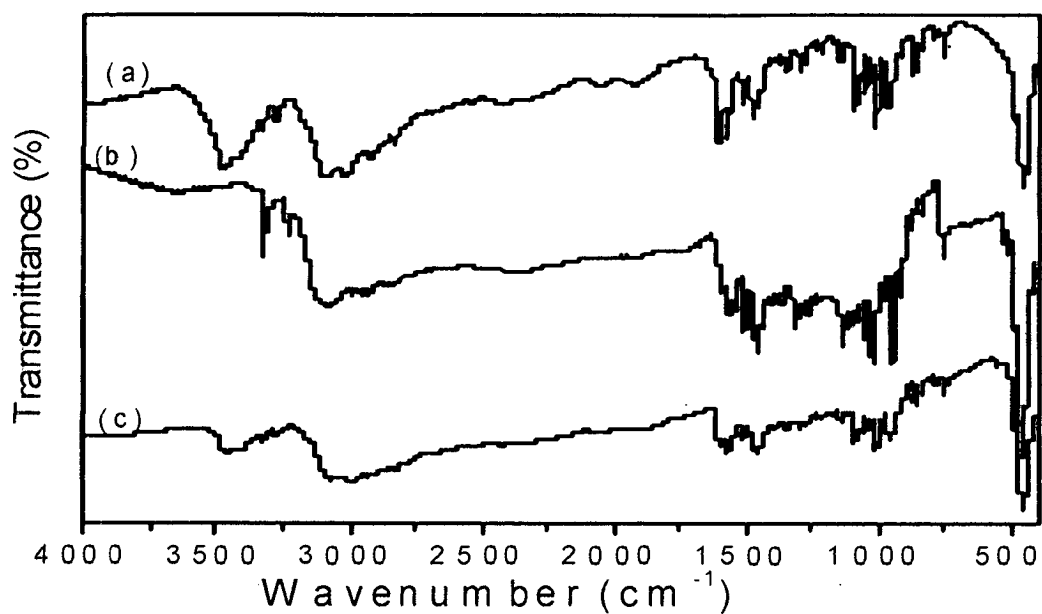
Fig. 4.4.27 IR spectra of (a) pristine **18** (b) anhydrous $(trenH_2)[WS_4]$ (c) rehydrated $(trenH_2)[WS_4] \cdot H_2O$
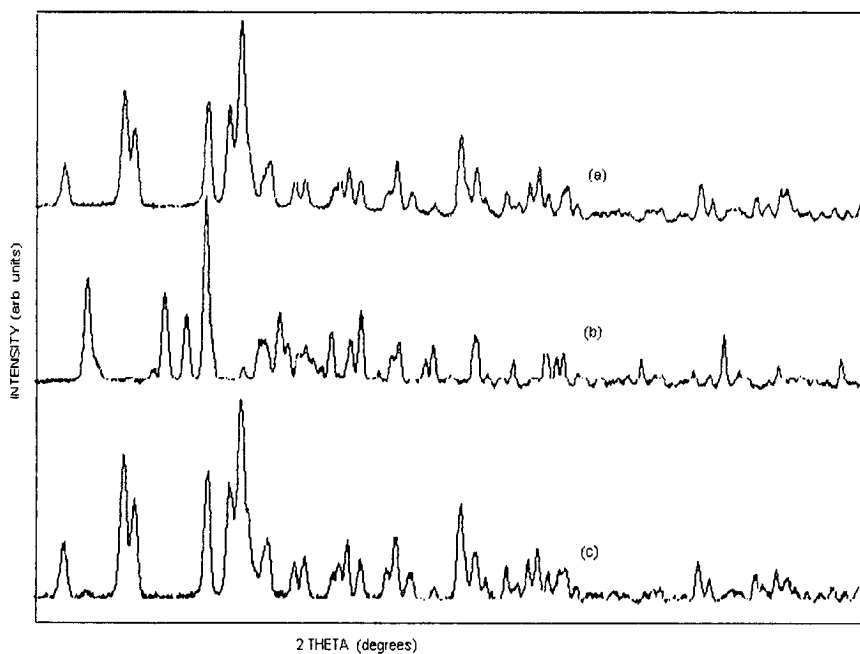
Fig. 4.4.28 XRD powder patterns of (a) pristine **18** (b) anhydrous $(trenH_2)[WS_4]$ (c) rehydrated $(trenH_2)[WS_4] \cdot H_2O$
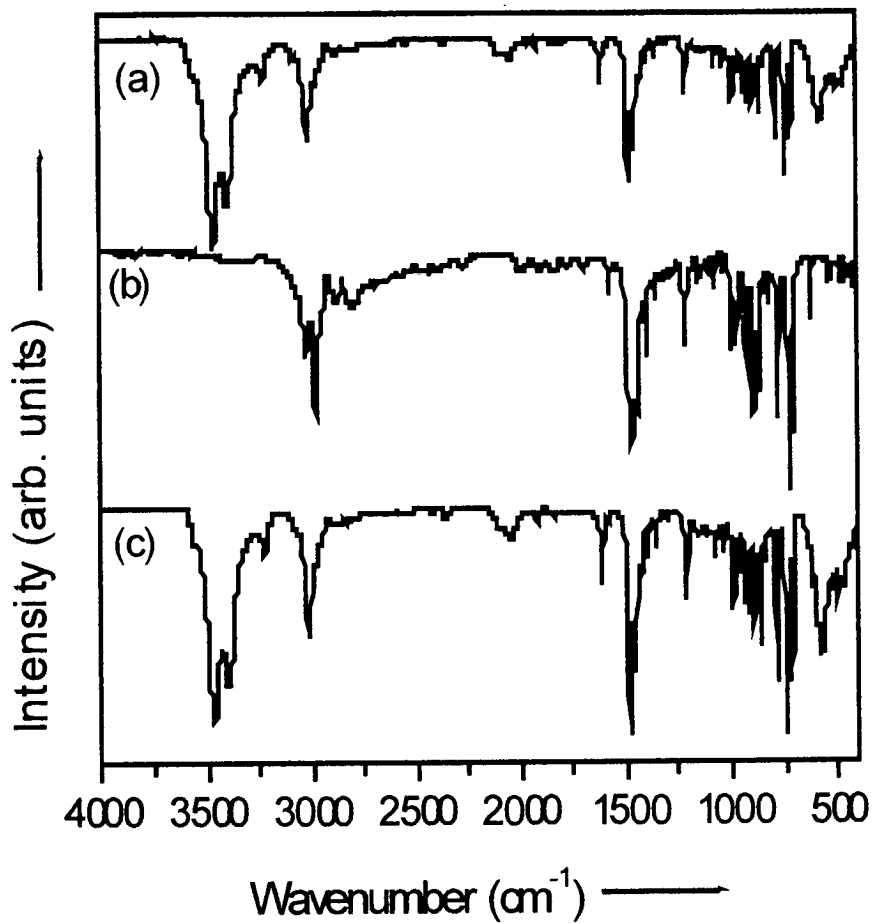
Fig. 4.4.29 IR spectra of (a) pristine **30** (b) anhydrous (dbtmen)Br$_2$ and (c) rehydrated (dbtmen)Br$_2$

4.5 Thermal Investigations

The new organic diammonium tetrathiometalates synthesized in this work have been investigated by TG-DTA technique. In complexes **5** and **6**, TG-DTA coupled with mass spectroscopy have been used to understand the composition of emitting fragments. The thermal decomposition of ammonium tetrathiometalates is well documented in the literature [47,223]. $(NH_4)_2[MoS_4]$ starts decomposing at 155 ^0C while its W analogue at 180 ^0C. In case of $(NH_4)_2[MoS_4]$, an intermediate formed has been reported to be stable till 335 ^0C which then decomposes with elimination of S resulting in the formation of MoS_2. In the case of $(NH_4)_2[WS_4]$, the intermediate WS_3 is stable between 310 and 340 ^0C followed by decomposition into S and WS_2. The formation WS_2 is accompanied by a sharp exothermic event at 339 $^\circ C$ in $(NH_4)_2[WS_4]$. The decomposition reactions for $(NH_4)_2[MS_4]$ are shown below:

$$(NH_4)_2[MS_4] \rightarrow 2\,NH_3 \uparrow + H_2S \uparrow + MS_3 \qquad (4.5.1)$$
$$MS_3 \rightarrow MS_2 + S$$
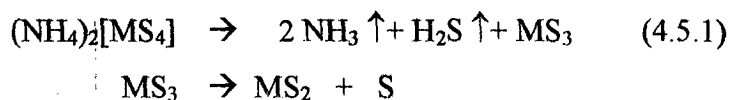
The thermal decomposition of tetraalkylammonium tetrathiometalates to form MS_2 catalysts is documented in the literature [72, 89, 90]. The use of MS_2 and carbon contaminated MS_3 are emerging as good materials in HDS catalysis. In this context, the thermal investigations of organic diammonium tetrathiometalates have been done in the present work and the results are discussed below. TG-DTA data for organic ammonium tetrathiomolybdates and tetrathiotungstates are summarized in Table 4.5.1 and Table 4.5.2.

Table 4.5.1 Thermal decomposition data of tetrathiomolybdates

Compound	DTA results Tpeak (^{0}C)	TG results	
		Mass loss (%)	Composition of residue
(N-MeenH$_2$)[MoS$_4$] **3**	124 endo	37.6 till 600 ^{0}C	MoS$_{2.7}$C$_3$N$_{0.4}$
	153 endo		
(tmenH$_2$)[MoS$_4$] **5**	112 endo	43.0 till 600 ^{0}C	-
(1,3-pnH$_2$)[MoS$_4$] **7**	190 endo	38.2 till 600 ^{0}C	-
(dienH$_2$)[MoS$_4$] **13**	153 endo	37.68 till 500 ^{0}C	MoS$_{2.2}$C$_{2.2}$N$_{0.7}$
	187 endo		
(dipnH$_2$)[MoS$_4$] **15**	136 endo	50.51 till 600 ^{0}C	MoS$_{2.1}$C$_{1.01}$N$_{0.2}$
	183 endo		
(trenH$_2$)[MoS$_4$]· H$_2$O **17**	113 endo	4.6	MoS$_{2.1}$C$_{3.5}$N$_{0.9}$
	162 endo	37.4 till 290 ^{0}C	
	203 endo		
(pipH$_2$)[MoS$_4$] **21**	172 endo	38.3 till 350 ^{0}C	-
	194 endo	39.4 till 800 ^{0}C	
(2-pipH-1-EtNH$_3$)[MoS$_4$]·½H$_2$O **27**	107 endo	2.68	MoS$_{1.7}$C$_{2.3}$N$_{0.7}$
	160 endo	41.75 till 600 ^{0}C	
(dbtmen)[MoS$_4$] **31**	170 endo	62.84 till 600 ^{0}C	MoS$_2$C$_2$
	209 endo		

Table 4.5.2 Thermal decomposition data for tetrathiotungstates.

Compound	DTA results Tpeak (^{0}C)	TG results	
		Mass loss (%)	Composition of residue
(enH$_2$)[WS$_4$] **2**	290 endo	26.6 till 500 ^{0}C	WS$_{2.1}$C$_{1.2}$N$_{0.5}$
(N-MeenH$_2$)[WS$_4$] **4**	232 endo	30.19 till 600 ^{0}C	WS$_{2.2}$C$_{1.4}$N$_{0.4}$
(tmenH$_2$)[WS$_4$] **6**	190 endo	35.9 till 500 ^{0}C	WS$_{2.1}$C$_{1.4}$N$_{0.4}$
	202 endo		
	224 endo		
	395 exo		
(1,3-pnH$_2$)[WS$_4$] **8**	267 endo	29.8 till 500 ^{0}C	WS$_{2.1}$C$_{1.2}$N$_{0.4}$
	333 endo		
(N,N'-dm-1,3-pnH$_2$)[WS$_4$] **10**	223 endo	35.90 till 600 ^{0}C	WS$_{2.1}$C$_{0.9}$N$_{0.2}$
(dienH$_2$)[WS$_4$] **14**	193 endo	26.94 till 600 ^{0}C	WS$_{2.2}$C$_{3.1}$N$_{1.1}$
	247 endo		
	381 endo		
(trenH$_2$)[WS$_4$]· H$_2$O **18**	103 endo	3.43	WS$_{2.1}$C$_3$N$_{0.8}$
	201 endo		
	256 endo	32.8	
(pipH$_2$)[WS$_4$] **22**	289 endo	30.0 till 400 ^{0}C	WS$_{2.1}$C$_{1.2}$N$_{0.3}$
		32.14 till 600 ^{0}C	
(1,4-dmpH$_2$)[WS$_4$] **24**	206 endo	35.9 till 500 ^{0}C	WS$_{2.2}$C$_{1.4}$N$_{0.3}$
	431 endo		
(dbtmen)[WS$_4$] **32**	192 endo	49.88 till 600 ^{0}C	WS$_{1.7}$C$_3$
	232 endo		
	293 endo		

4.5.1 TG-DTA description for (enH₂)[WS₄] 2

The TG-DTA curves of **2** are presented in Fig.4.5.1. The use of an organic ammonium cation like $(enH_2)^{2+}$ enhances the thermal stability of tetrathiotungstate as it starts decomposing at 267 ^{0}C accompanied with a strong endothermic signal at 290 ^{0}C compared to $(NH_4)_2[WS_4]$ which starts decomposing at 180 ^{o}C. Complex **2** is also thermally stable than the reported tetrapropylammonium tetrathiotungstate, which decomposes with two endotherms at 190 and 220 ^{0}C [89]. The single DTA event can be assigned for the simultaneous removal of organic amine en and H₂S. The expected mass loss for the emission of the organic base en and H₂S is 25.17 % and upto to 400 ^{o}C, 25 % mass loss is observed indicating the emission of above fragments. The thermal behavior at this temperature can be represented as shown in the following reaction.

$$(enH_2)[WS_4] \rightarrow en \uparrow + H_2S \uparrow + WS_3 \qquad (4.5.2)$$

On further heating upto 500 ^{0}C, a relatively very little mass loss was observed resulting in the formation of 73.35 % residue. The expected residue for the formation of WS₃ is 74.83 % while a residue of 66.26 % is expected for the formation of WS₂. The black residue was examined by elemental analysis, electron microscopy and X-ray powder diffraction. The residue contains considerable amounts of carbon and N (7.66 %) Based on this data, the residue can be formulated as $WS_2C_{1.8}N_{0.5}$. This result is in good agreement with 1:2 W: S ratio (found 1:1.70) obtained by the ESEM-EDX technique. SEM micrograph of the final residue is displayed in Fig 4.5.2. The decomposed material is porous and the porosity can be attributed to the incomplete removal of carbon. The X-ray powder pattern of the residue showed no intense and sharp peaks but only broad humps indicating the amorphous nature of the residue. The predominant formation of WS₂ residue by decomposition of **2** in a single step at a considerably lower temperature suggests that **2** can be a good precursor for synthesis of WS₂.

Fig. 4.5.1 TG-DTA curves for (enH$_2$)[WS$_4$] **2** (heating rate 4 ^{0}K/min; N$_2$ atmosphere; given are the peak temperatures (T$_p$) in °c and the mass loss in %).

Fig.4.5.2 SEM micrograph of the decomposition product of (enH$_2$)[WS$_4$] **2**

TG and DTA curves for $(N\text{-}Me\text{-}enH_2)[MoS_4]$ **3** are displayed in Fig. 4.5.3. On heating, complex **3** starts decomposing at relatively lower temperature (on set temperature 108 ^{0}C) as compared to complex **2**. The thermal reaction is accompanied by two closely related endothermic peaks in DTA curve at 124 and 153 ^{0}C. These events in the DTA curve can be attributed to the simultaneous emission of N-Me-en and H_2S. The complex is thermally less stable than recently reported $[(prop)_4N]_2[MoS_4]$ [79] which decomposes with endo peak at around 174 ^{0}C. On further heating, TG curve shows mass loss up to 400 ^{0}C and above this temperature the curve remains parallel to the x-axis indicating the formation of a stable sulfide. The complete mass loss up to 600 ^{0}C is 37.6 % and is slightly more than the expected mass loss for emission of N-Me-en and H_2S (35.9%). The observed residue of 62.4% is in between the expected values for MoS_3 (63.99%) and MoS_2 (53.31) formation. The elemental analysis of the residue showed C (8.15%) and N (3.2%) and based on this data the residue has been formulated as $MoS_{2.3}C_{1.3}N_{0.4}$. The formulation of sulfide is in good agreement with EDAX-ESEM results (Mo:S 1:2.1).

The TG-DTA curves for the corresponding W analogue **4** are presented in Fig. 4.5.4. Complex **4** is thermally more stable than **3** as **4** starts decomposing at about 178 ^{0}C unlike **3**, which undergoes this step at relatively lower temperature (on set 108 ^{0}C). Although **3** and **4** have same $(N\text{-}Me\text{-}enH_2)^{2+}$ dication, interestingly **4** decompose in a single event unlike **3** which decomposes in two closely related steps. The TG curve of **4** is parallel to horizontal axis up to 178 ^{0}C and then a considerable drop in mass loss is observed on increasing the temperature. The DTA curve is accompanied by a strong endotherm at 232 ^{0}C which can be shown as below.

$$\underline{3} \quad or \quad \underline{4} \quad \rightarrow \quad MS_3 \quad + \quad N\text{-}Me\text{-}en \quad + \quad H_2S\uparrow \quad (4.5.3)$$

On further heating, TG curve shows mass loss up to 400 ^{0}C and then remains parallel to temperature axis implying sulfide formation. The complete mass loss up to 600 ^{0}C is 30.0 % and is slightly more than the expected mass loss for emission of N-Me-en and H_2S (27.86 %). The final residue amounting to 70 % in TG curve of **4** is in between the expected values for WS_3 (72.13 %) and WS_2 (63.87 %) formation. The
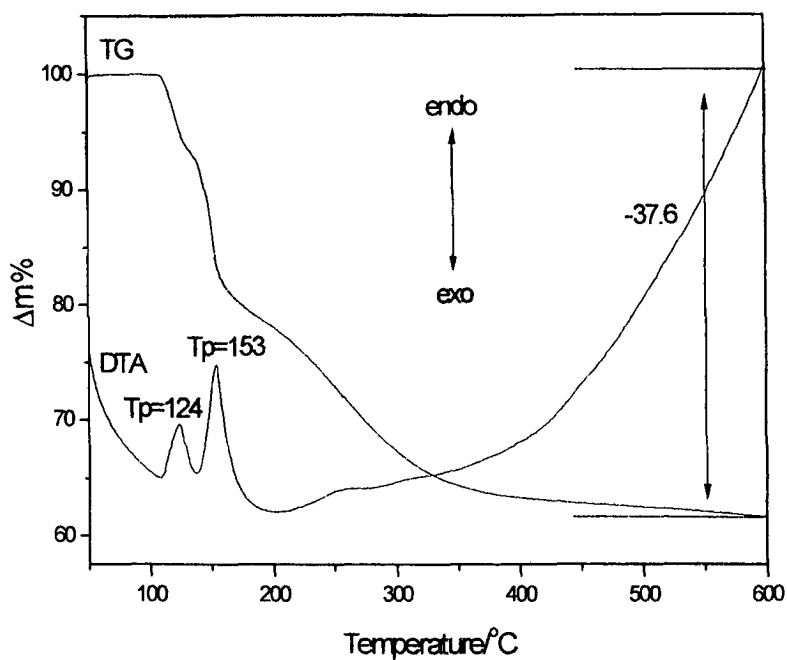
Fig.4.5.3 DTA and TG curves for (N-Me-enH$_2$)[MoS$_4$] **3**
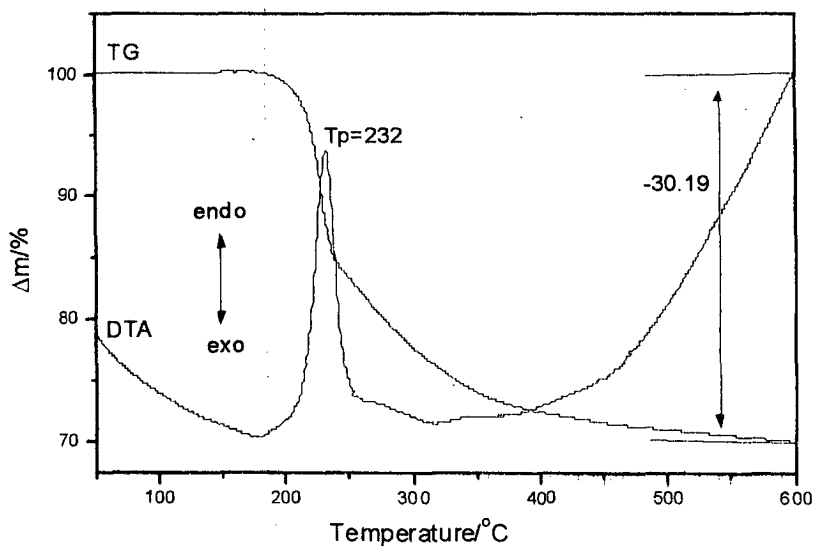
Fig.4.5.4 DTA and TG curves for (N-Me-enH$_2$)[WS$_4$] **4** (heating rate 4 K/min; Ar atmosphere)

187

C, H, N and S analysis showed the presence of C and N (5.18 % & 2.05 %) and this is probably the reason for observed mass loss to occur between the expected WS_3 and WS_2 values. Based on the elemental analysis, the residue has been formulated as $WS_{2.2}C_{1.4}N_{0.4}$ and is in accordance with the ESEM-EDAX data (W: S 1:2.1). The carbon contaminate disulfide is amorphous as evidenced from the X-ray powder pattern.

4.5.3 DTA-TG-DTG-MS description for (tmenH₂)[MoS₄] 5 [79]

On heating, complex **5** starts decomposing at about 112 °C and shows considerable mass loss beyond this temperature in the TG curve. DTA, TG, DTG and MS trend scan curves for **5** are displayed in Fig 4.5.5. The drop in mass loss in the TG curve is accompanied by a strong endothermic peak at 112 °C in DTA curve. The simultaneous emission of tmen and H_2S in the thermal process has been detected by the use of mass spectrometry. Two peaks were observed in the mass spectrum at this temperature with m/z = 58 and m/z = 34 which can be attributed to emission of tmen and H_2S fragments respectively. The total mass loss of 43.0 % is slightly lower than that expected for the emission of only tmen and H_2S (43.9 %).

$$\underline{5} \quad \rightarrow \quad tmen \uparrow + H_2S \uparrow + MoS_3 \qquad (4.5.4)$$

4.5.4 TG-DTA description for (tmenH₂)[WS₄] 6

TG and DTA curves for **6** are displayed in Fig.4.5.6. Complex **6** exhibit four endothermic events in its DTA curve compared to a single step decomposition in **2** and **5**. From the TG curve, it appears that complex **6** is relatively more stable than its isosturctural Mo analogue **5** that starts decomposing only at 112 °C. When compared to decomposition of $(NH_4)_2[WS_4]$, it is worth to note that, complex **6** is less stable then $(NH_4)_2[WS_4]$ that starts decomposing at 180 °C. This thermal behavior of **6** can be attributed to the presence of bulky $(tmenH_2)^{2+}$ cation unlike in $(NH_4)_2[WS_4]$. TG curve of **6** is parallel to the horizontal axis upto 151 °C which then follows endothermic events occurring at 190, 202 and 224 °C in its DTA curve. The observation of three endothermic events indicates that the decomposition is a complex process and in the absence of MS data of the emitted fragments, an exact conclusion on the nature of decomposition cannot be drawn. The expected mass loss for tmen and
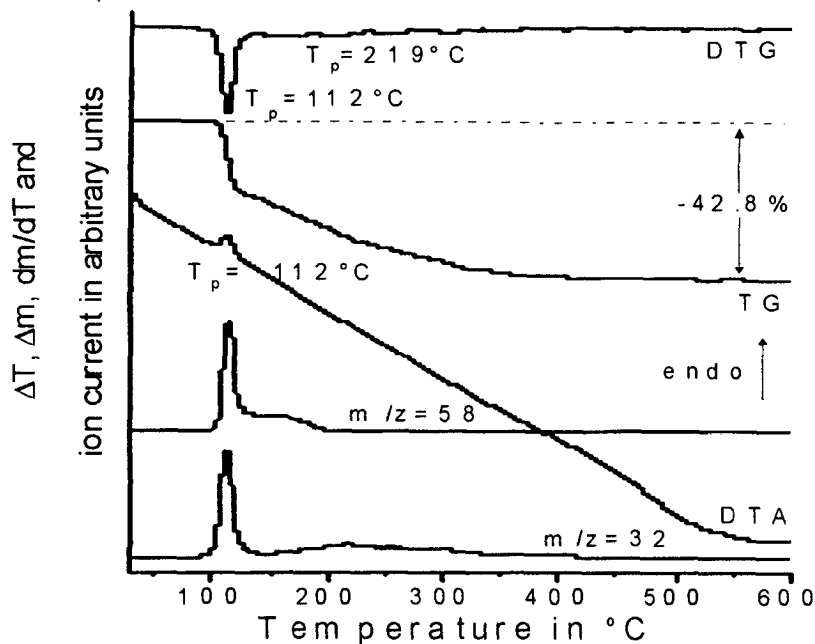
Fig. 4.5.5 DTA, TG, DTG and MS trend scan curves for (tmenH₂)[MoS₄] (heating rate 4 °C/min; m/z = 58 (fragment of N,N,N',N'-tetramethylethyelenediamine); m/z = 34 (H₂S); T$_p$, peak temperatures in °c and the mass loss in %).
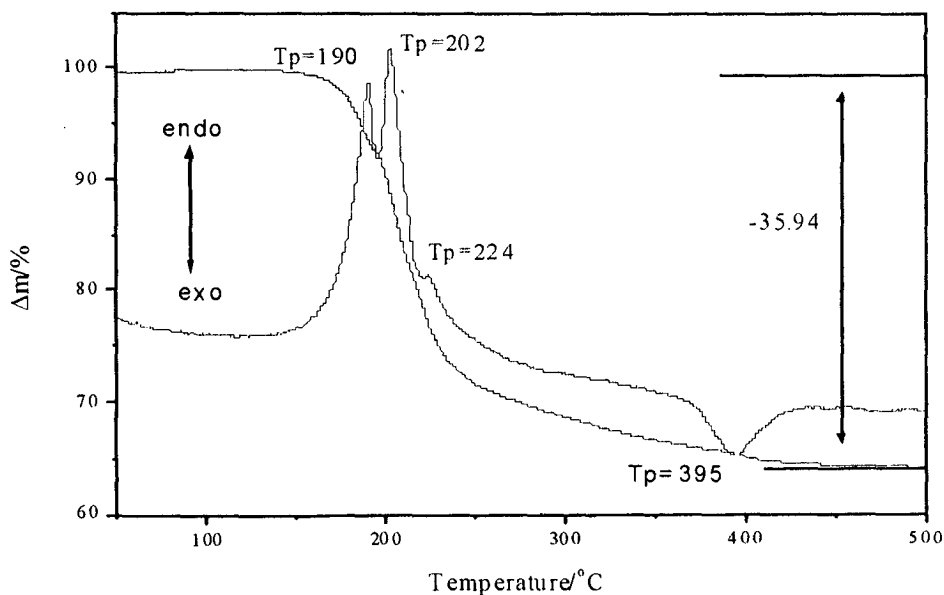
Fig. 4.5.6 TG-DTA curves for (tmenH₂)[WS₄] (heating rate 4 K/min; N₂ atmosphere; given are the peak temperatures (T$_p$) in °c and the mass loss in %).

189

H_2S in (tmenH$_2$)[WS$_4$] is 34.93 %. The mass loss of 35.0 % is observed up to 418 ^{0}C and the total mass loss is about 35.94 % till 500 °C resulting in the formation of 64.06 % of black residue. The expected value for formation of WS$_3$ is 65.07 % while a residue of 57.62 % is expected for the formation of WS$_2$. As the experimental value (64.06 %) is observed between these two, the residue was examined by elemental analysis. The elemental analysis of final residue showed the presence of 7.57 % of C and also N and the residue can be formulated as $WS_{2.2}C_{1.4}N_{0.3}$. ESEM-EDAX experiments gave a W:S ratio very close to 1:2. ESEM picture of decomposed product is presented in Fig. 4.5.7. No intense peaks but only broad humps were observed in the X-ray powder pattern indicating the amorphous nature of the residue.

4.5.5 TG-DTA-MS description for (1,3-pnH$_2$)[MoS$_4$] 7 [79]

Complex (1,3-pnH$_2$)[MoS$_4$] 7 has been investigated by TG-DTA coupled with mass spectrometry with the aim to understand the nature of decomposition processes as well as the intermediate products formed during the heating. DTA, TG, DTG and MS trend scan curves for 7 are depicted in Fig 4.5.8. On heating in thermobalance, 7 exhibits a strong endothermic signal at a peak temperature of about 190 °C. The TG curve is parallel to x-axis till about 190 ^{0}C, suggesting its thermal stability upto this temperature. A strong endothermic signal 190 ^{0}C in DTA curve is accompanied with a mass loss in TG curve. It is obvious form DTG that this event consists of two different steps and the MS curves shows that only 1,3-pn (m/z = 57) and H$_2$S (m/z = 34) are emitted. On further heating the sample mass drops smoothly, which is accompanied with emission of only H$_2$S (m/z = 34). The experimental mass loss up to 600 ^{0}C is 38.2%, which is slightly higher than the expected for the emission of 1,3-pn and H$_2$S (expected 36.0%) However additional measurements using analogue scans gave hints for no emission of elemental sulfur. But the mass change starting from 350 ^{0}C is very smooth and therefore, it is difficult to detect small amounts of S emitted by the sample.

4.5.6 TG-DT description for (1,3-pnH$_2$)[WS$_4$] 8 and (N,N'-dm-1,3-pnH$_2$)[WS$_4$] 10

TG and DTA curves for (1,3-pnH$_2$)[WS$_4$] 8 are presented in Fig.4.5.9. Complex 8 is thermally stable up to around 220 ^{0}C, and then follows decomposition with mass drop in TG curve. Complex 8 is thermally more stable than its corresponding isosturctural Mo analogue 7 that starts decomposing at 190 ^{0}C while
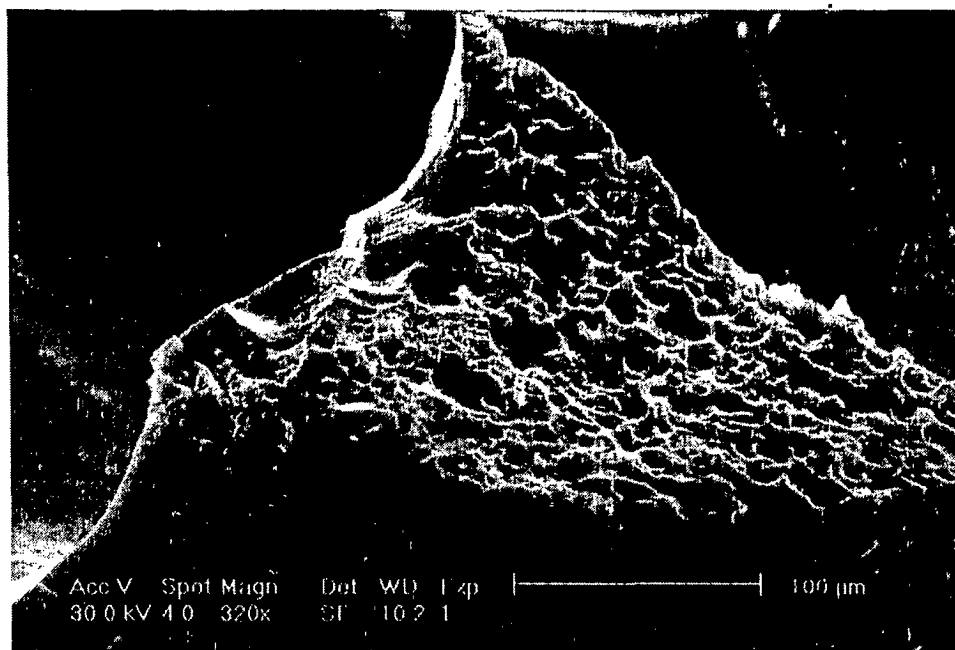
Fig.4.5.7 SEM micrograph of the decomposition product of (tmenH$_2$)[WS$_4$] **6**

$(NH_4)_2[WS_4]$ is thermally less stable compared to **7**. On increasing the temperature, decomposition occurs with a strong endothermic peak at 267 ^{0}C in the DTA curve. The sharp endothermic event in DTA curve can be assigned for the simultaneous removal of 1,3-pn and H_2S. The loss of considerable mass amounting to 28.58 % in two consecutive endothermic steps suggests the loss of 1,3-pn and H_2S. This event can be represented as shown in following equation.

$$\underline{7} \quad or \quad \underline{8} \quad \rightarrow \quad 1,3\text{-pn} \uparrow + \ H_2S \uparrow \ + \ MS_3 \qquad (4.5.5)$$
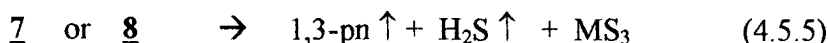
The incomplete removal of 1,3-pn was evident from the elemental analysis of residue which showed considerable amounts of C and N (5.17 and 2.07 %). Based on this data the residue is formulated as $WS_{2.1}C_{1.2}N_{0.4}$ and this is in very good agreement with the ESEM-EDX results (W:S = 1: 1.9). The porous nature of decomposed product is evident from its SEM micrograph, which is displayed in Fig 4.4.10. X-ray powder pattern of the residues exhibits broad humps in indicating the formation of amorphous carbon contaminated disulfide.

TG and DTA curves for **10** are presented in Fig. 4.5.11. Complex **10** is thermally stable up to 170 ^{0}C and on increasing the temperature, starts decomposing with mass drop in TG curve. Complex **10** is thermally less stable than **8** which start decomposing at around 220 ^{0}C. This can be due to the presence of bulky (N,N'-dm-1,3-pnH$_2$)$^{2+}$ cation in **10** where two terminal N atoms are bound to one methyl group each unlike no –CH$_3$ groups bound to N in (1,3-pnH$_2$)$^{2+}$ of **8**. The decomposition process in **10** is accompanied with an endo peak at 220 ^{0}C in DTA curve and can be assigned for the simultaneous emission of organic amine, N,N'-dm-1,3-pn and H_2S. The considerable mass loss of 35.90 % is observed up to 600 ^{0}C in TG curve. The decomposition process can be considered to following manner.

$$\underline{10} \quad \rightarrow \quad N,N'\text{-dm-1,3-pn} \uparrow + \ H_2S \uparrow \ + \ WS_3 \qquad (4.5.6)$$
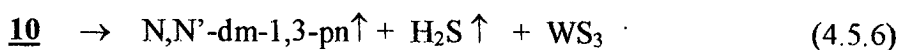
About 4.1 % of C was analyzed in the final decomposed product. Based on the elemental analysis, residue has been formulated as $WS_{2.1}C_{0.9}N_{0.2}$. The SEM micrograph of the final residue indicates the formation of porous material.
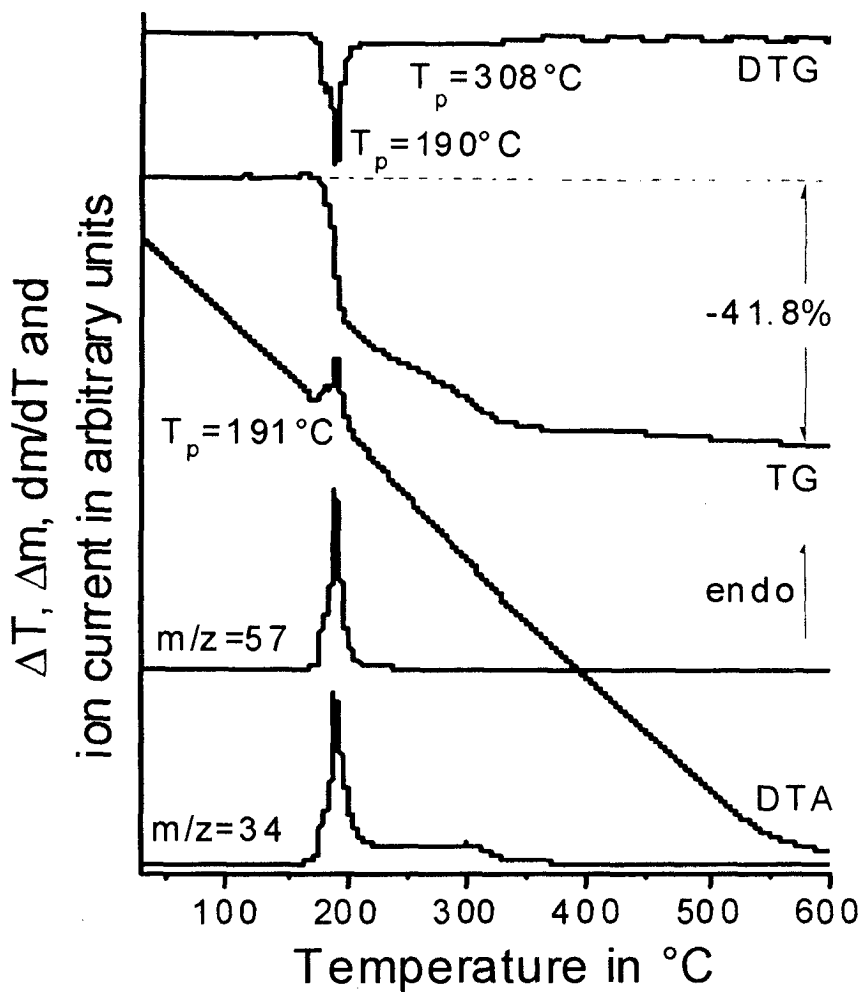
Fig. 4.5.8 DTA, TG, DTG and MS trend scan curves for (1,3-pnH$_2$)[MoS$_4$] (heating rate 4 °C/min; m/z = 57 (fragment of 1,3-propanediamine); m/z = 34 (H$_2$S); T$_p$, peak temperatures in °c and the mass loss in %).

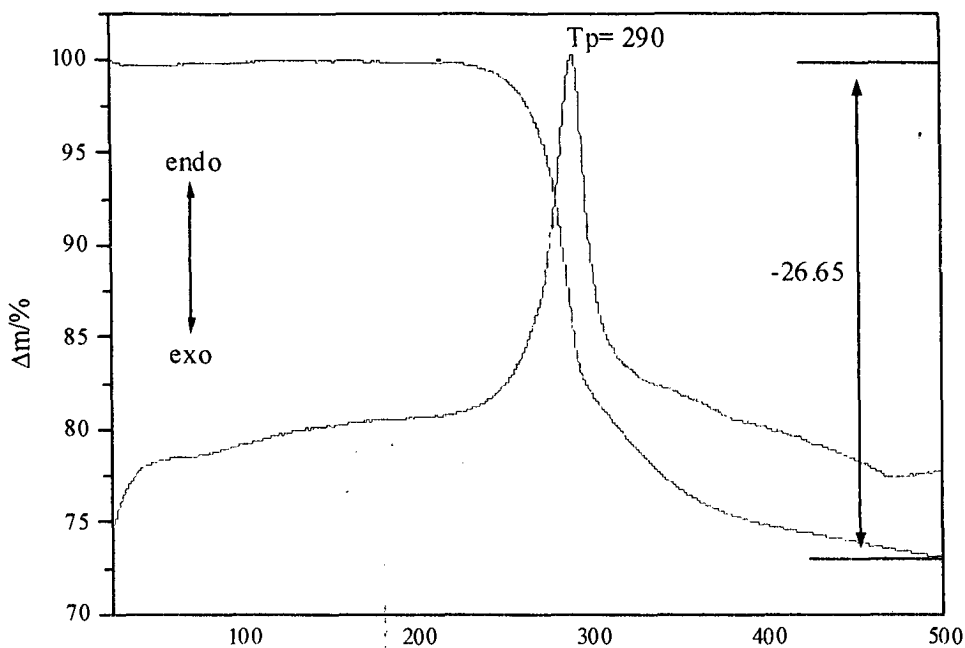Fig. 4.5.9 TG-DTA curves for $(1,3\text{-pnH}_2)[WS_4]$ **8** (heating rate 4 K/min; N_2 atmosphere; given are the peak temperatures (T_p) in °c and the mass loss in %).
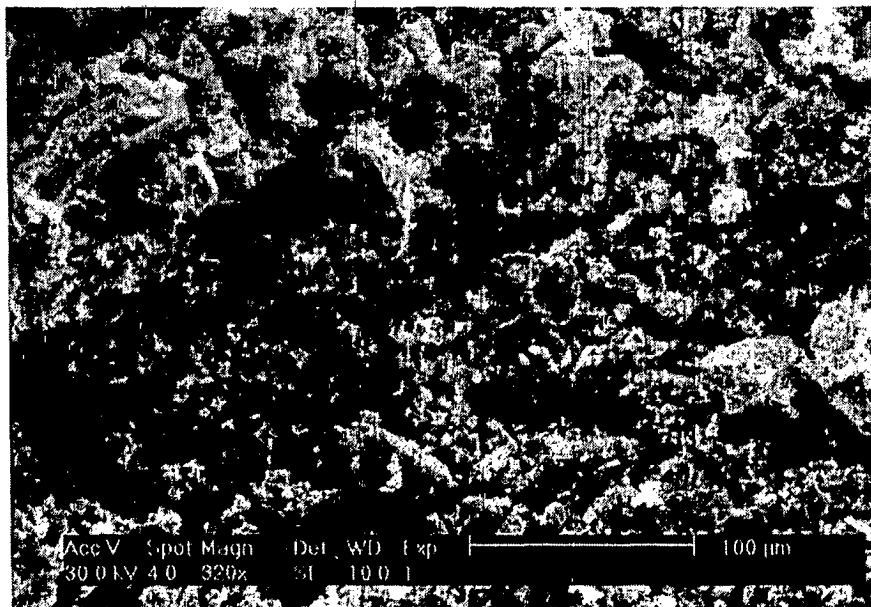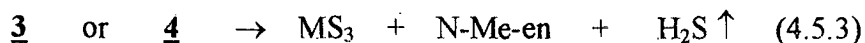

Fig.4.5.10 SEM micrograph of the decomposition product of $(1,3\text{-pnH}_2)[WS_4]$ **8**
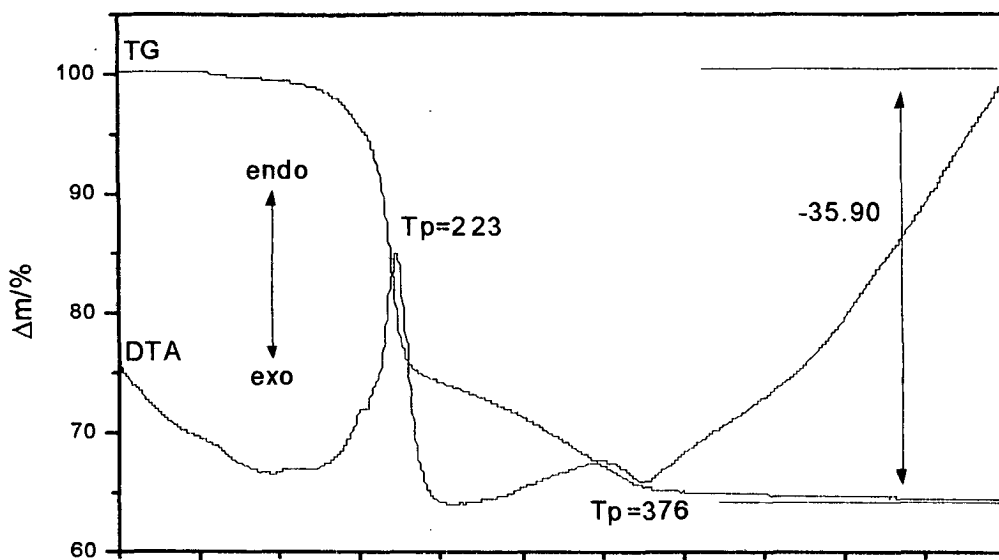
Fig.4.5.11 TG-DTA trace of (N,N'-dm-13-pnH$_2$)[WS$_4$] **10** (heating rate 4 K/min; Ar atmosphere).

4.5.7 TG-DTA description for (dienH$_2$)[MoS$_4$] 13 and (dienH$_2$)[WS$_4$] 14

Complex **13** and **14** were heated in a thermobalance up to 500 ^{0}C in flowing N$_2$ at 4K/min. TG-DTA curves for **13** are presented in Fig 4.5.12. Complex **13** is thermally stable up to 134 ^{0}C and on further heating, starts decomposing with considerable mass loss in TG curve. The mass loss is accompanied by two endothermic events in DTA curves at 153 and 187 ^{0}C that can be attributed to the simultaneous emission of dien and H$_2$S. The total experimental mass loss of 37.68 % up to 500 ^{0}C is quite less than the expected for emission of dien and H$_2$S (41.66 %). C, H, N and S analysis of the final residue showed considerable amount of C (13.03 %) and N (4.7 %), based on which the residue can be formulated MoS$_{2.2}$C$_{2.2}$N$_{0.7}$. This is in good agreement with the results from electron microscopy which showed Mo:S ratio very close to 1:2 (1:21). TG and DTA curves for corresponding W analogue **14** are presented Fig 4.5.13. It can be evidenced from the DTA curve that complex **14** (Tp$_1$ = 193 ^{0}C, Tp$_2$ = 187 ^{0}C) is thermally more stable than its Mo analogue (Tp$_1$ = 153 ^{0}C, Tp$_2$ = 247 ^{0}C). The DTA events can be assigned for the removal of dien and H$_2$S as in **13**. The expected mass loss for the emission of dien and H$_2$S is 32.28% which is quite more that the total mass loss of 26.24 % up to 500 ^{0}C. This indicates the incomplete decomposition of organics. The elemental analysis showed 11.93 % of C and 4.93 % of N and the residue has been formulated as WS$_{2.2}$C$_{3.1}$N$_{1.1}$. The SEM micrograph (Appendix-II) showed that the material is porous and the porosity of the residue can be attributed to the incomplete removal of carbon. The X-ray powder pattern of the residue showed only broad humps indicating formation of amorphous carbon contaminated tungsten sulfide.

4.5.8 TG-DTA description for (dipnH$_2$)[MoS$_4$] 15

TG-DTA trace of the complex (dipnH$_2$)[MoS$_4$] **15** is presented in the Fig 4.5.14. Complex **15** is thermally stable up to 116 ^{0}C and on increasing the temperature considerable mass loss is observed up to 400 ^{0}C which is accompanied by two endothermic events in the DTA curve. The two endothermic DTA curves at 136 and 194 ^{0}C are can be attributed to the removal of dipn and H$_2$S. After 400 ^{0}C, very little mass loss is observed and the TG curve runs parallel to the temperature axis. The total mass loss when heating was stopped at 600 ^{0}C was 50.5 % and is quite high than the expected mass loss for amine and H$_2$S (46.3 %). The X-ray powder pattern of the residue is similar to that observed for decomposed products of other organic ammonium tetrathiomolybdates.
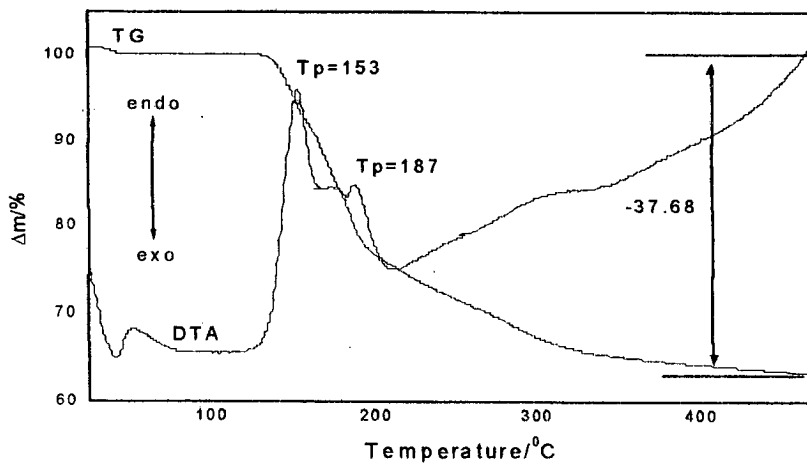
Fig.4.5.12 DTA and TG curves for (dienH₂)[MoS₄] **13** (heating rate 4 K/min; Ar atmosphere).
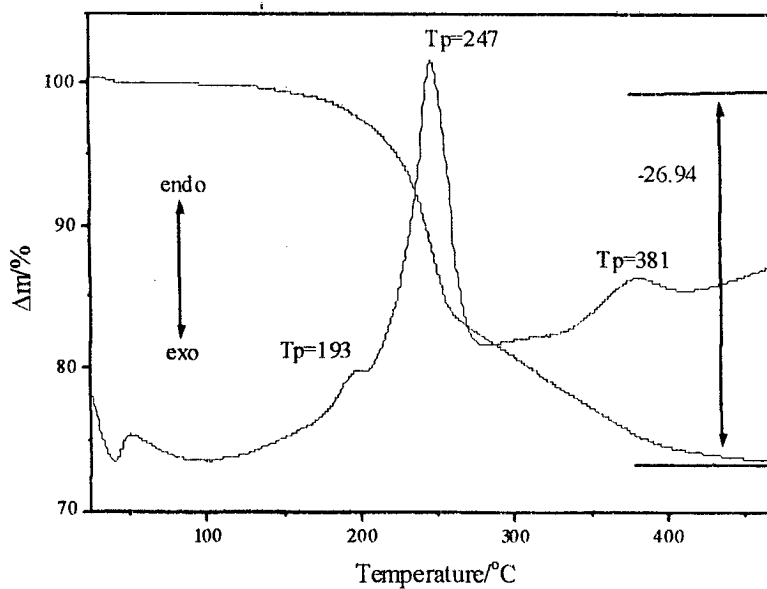
Fig. 4.5.13 DTA,TG curves for (dienH₂)[WS₄] **14** (heating rate 4 K/min; Ar atmosphere)
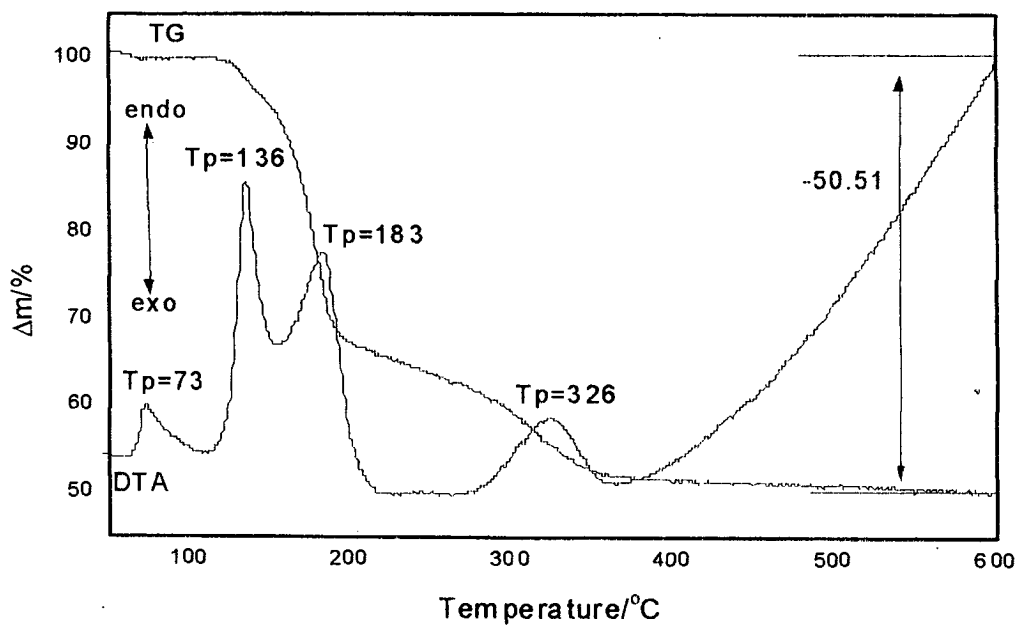
Fig.4.5.14 DTA and TG curves for (dipnH$_2$)[MoS$_4$] **15** (heating rate 4 K/min; Ar atmosphere; given are the peak temperatures (T$_p$) in °C and the mass loss in %).

4.5.9 TG-DTA curves for (trenH₂)[MoS₄]·H₂O $\underline{17}$ *and (trenH₂)[WS₄]·H₂O* $\underline{18}$

TG-DTA curves for $\underline{17}$ are displayed in Fig 4.5.15. When complex $\underline{17}$ was heated, a single mass step of 4.6 % occurred at about 80°C that can be attributed to the elimination of the crystal water (4.6 %). From the DTA and the DTG curve it is obvious that this reaction consists of two endothermic events, which occur at 102 and 113 ^{0}C. The loss of water is complete at about 140 ^{0}C. On further heating the sample mass decreases rapidly and two endothermic events are observed at 162 and 203 ^{0}C. DTG curve shows that the decomposition reaction proceeds in three different steps, which cannot fully be resolved. The experimental mass loss up to about 290 ^{0}C where the DTG curve shows a minimum is about 37.4% which is in good agreement with the loss of tris(2-aminoethyl)amine) (37.4%). Upon a further increase of the temperature the sample mass decreases slowly. C, H, N and S of the residue revealed the presence of large amounts of organic matter and based on this data, the residue can be considered as MoS_{3-x} sulfide.

The TG-DTA trace for $\underline{18}$ is displayed in Fig 4.5.16 exhibits the first mass step of 3.43 % starting at about 70 ^{0}C. The peak temperature for this endothermic event is 103 ^{0}C. This process can be attributed to the emission of crystal water (3.76%). On further heating, two more endothermic events are observed with peak maxima at 201 and 256 ^{0}C resulting in the formation of 63.58% residual mass. It is observed that the profile of the TG-DTA plot of complex (trenH₂)[WS₄]·H₂O is identical to that of the TG-DTA trace of the isostructural Mo analogue namely (trenH₂)[MoS₄] · H₂O discussed earlier. The DTA peak temperatures for the Mo complex were observed 113, 162 and 203 ^{0}C under identical conditions. This indicates that the dehydration of (trenH₂)[WS₄]·H₂O occurs at a slightly lower temperature while the decomposition of the anhydrous tetrathiotungstate thus formed is observed at elevated temperatures as compared to (trenH₂)[MoS₄] · H₂O. This observation is very similar to that observed for other tetrathiotugstates investigated in this work and indicates that $[WS_4]^{2-}$ complexes are thermally more stable than the corresponding $[MoS_4]^{2-}$ analogues. The expected mass loss for the complete removal of tren as well as H₂S in (trenH₂)[WS₄]·H₂O is about 37.7 % while the expected residual mass for the formation of WS₃ is 58.53 %. The residue expected for the formation of WS₂ is 51.83 %. The loss of considerable mass amounting to about 32.78 % in an endothermic step
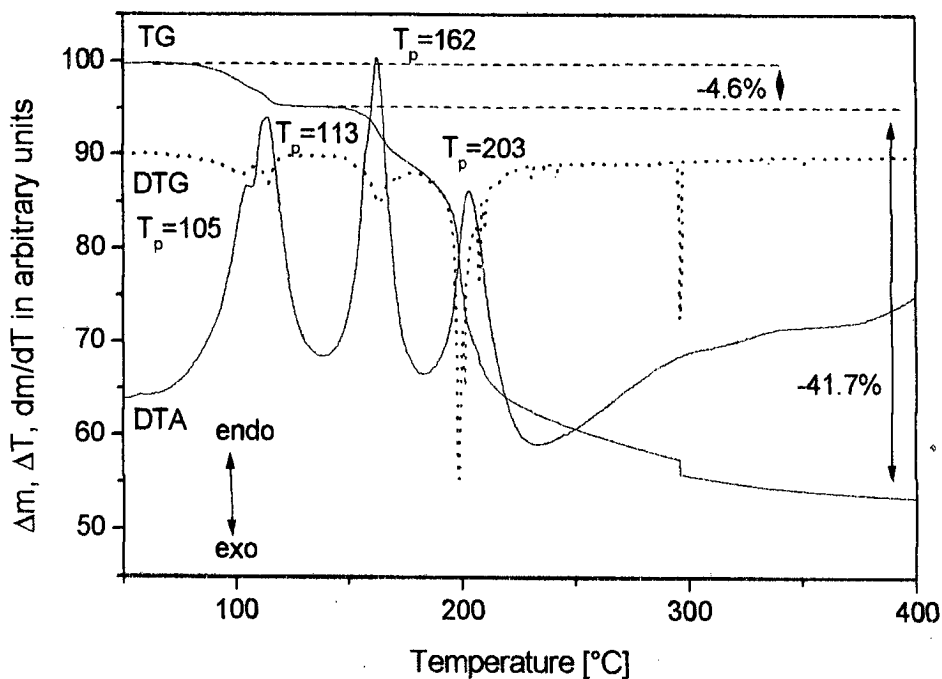
Fig. 4.5.15 DTA, TG and DTG curves for (trenH$_2$)[MoS$_4$].H$_2$O **17** (heating rate 4 K/min; N$_2$ atmosphere; given are the peak temperatures (T$_p$) in °C and the mass loss in %).
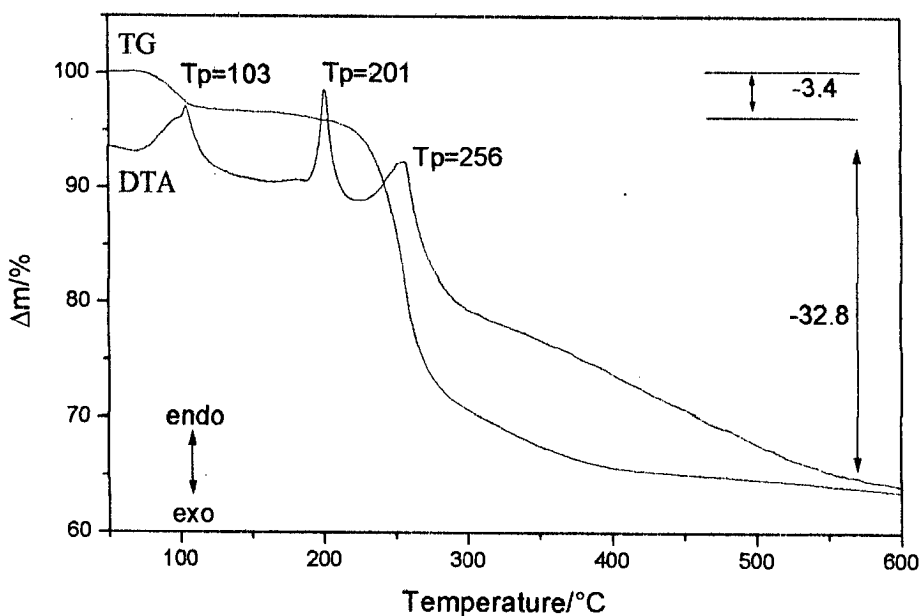
Fig.4.5.16 DTA and TG curves for (trenH$_2$)[WS$_4$] · H$_2$O **18** (heating rate 4 K/min;N$_2$ atmosphere; given are the peak temperatures (T$_p$) in °C and the mass loss in %).

indicates the loss of organics. However the incomplete removal of the organic amine is evident from the elemental analysis of the final product showing the presence of carbon (12.01 %) as well as nitrogen (3.67 %) in the black residue. Based on elemental analysis the residue is formulated as $WS_{2.1}C_3N_{0.8}$ and this formulation is in good agreement with the results (W:S ratio = 1/1.75) from electron microscopy. The amorphous nature of the residue is evident from the X-ray powder pattern.

4.5.10 TG-DTA description for (pipH₂)[MoS₄] 21 and (pipH₂)[WS₄] 22

DTA-TG curves for **21** are presented in Fig 4.5.17. On heating compound $(pipH_2)[MoS_4]$, the decomposition starts at about 170 ^{0}C, which is accompanied by endothermic events in the DTA at 172 and 194 ^{0}C. From the DTG curve it is obvious that this reaction occurs in several steps, which cannot be fully resolved. The complete mass loss up to 330 ^{0}C where the DTG curve shows a minimum is about 38.3 %, which is in good agreement with the emission of hydrogen sulfide and piperazine (38.5 %) resulting in the formation of MoS_3. The simultaneous emission of amine and H_2S has been observed during a thermal decomposition study of **7** discussed earlier. On further heating of the sample, a slow mass decrease was observed and the residual mass of 60.6% at about 800 ^{0}C (not shown in the DTA-TG curve) shows that the intermediately formed MoS_3 is transformed into MoS_2. The elemental analysis of the black residue indicates that a small amount of C and N remained in the product. TG-DTA trace of $(pipH_2)[WS_4]$ is presented in Fig 4.5.18. The use of an organic ammonium cation like $(pipH_2)^{2+}$ in **22** enhances the thermal stability of tetrathiotungstate as it starts decomposing at 208 ^{0}C accompanied with a strong endothermic signal at 289 ^{0}C. This DTA event can be assigned for the simultaneous removal of pip and H_2S. $(pipH_2)[WS_4]$ is also thermally much more stable as compared to the corresponding isostructural Mo analog **21**, which starts decomposing at 140 ^{0}C. The expected mass loss for the emission of the organic base pip and H_2S is 30.04 % and about 30.0 % mass loss is observed till about 400 ^{0}C indicating the emission of the organics. Interestingly no exothermic event is observed at higher temperatures. Above 400 ^{0}C relatively very little mass loss is observed and the total observed mass loss till 600 ^{0}C is 32.14 % resulting in the formation of 67.86 % residue. The expected residue for the formation of WS_3 is 69.96 % while a residue of 61.96 % is expected for the formation of WS_2. As the experimental value (67.86%) is observed between these two, the residue was examined by elemental analysis,
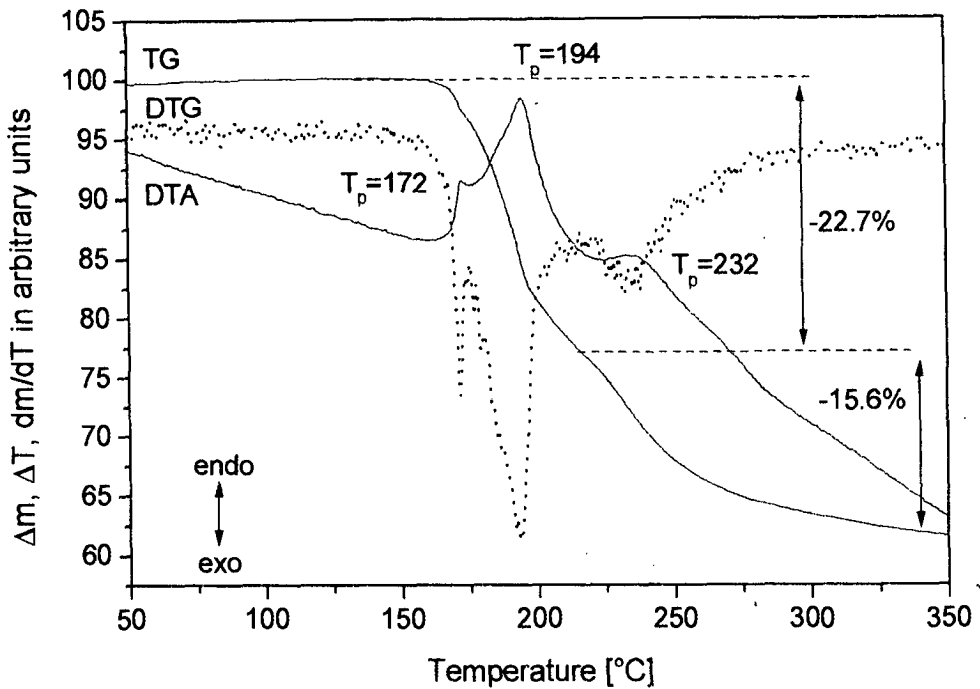
Fig. 4.5.17 DTA, TG and DTG curve for (pipH₂)[MoS₄] **21** (heating rate 4 K/min; N₂ atmosphere; given are the peak temperatures (T_p) in °c and the mass loss in %).
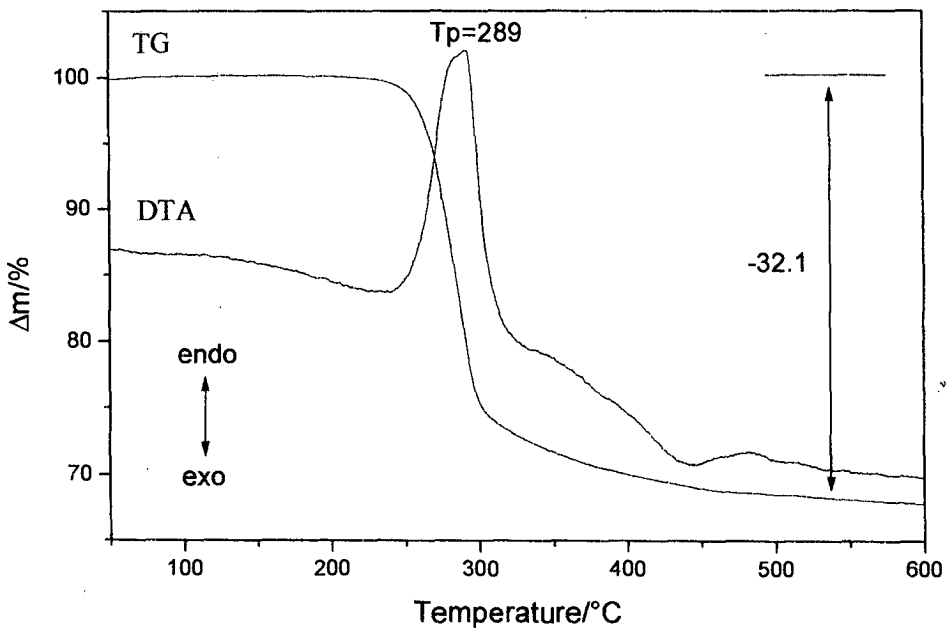
Fig. 4.5.18 DTA and TG curves for (pipH₂)[WS₄] **22** (heating rate 4 K/min; N₂ atmosphere; given are the peak temperatures (T_p) in °C and the mass loss in %).

electron microscopy and powder diffraction. The elemental analysis indicates the presence of 7.41% of C and N based on which the residue can be formulated as $WS_{2.1}C_{1.2}N_{0.3}$. This formulation gains further credence based on the electron microscopy result which gave a W:S ratio very close to 1/2 (1/1.94). The X-ray powder pattern of the residue indicates the amorphous nature of the residue. The formation of a predominantly disulfide residue by the thermal decomposition of **22** in a single step at a considerably lower temperature is not only an interesting aspect of **22** but also indicates that the decomposition process is of complex nature which is also corroborated by the strong and broad signal in the DTA. The decomposition of **21** and **22** can be considered to take place by following manner.

$$\underline{21} \text{ and } \underline{22} \rightarrow \text{pip} + H_2S + MS_3$$
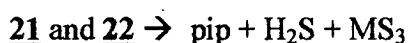
4.5.11 TG-DTA description for (1,4-dmpipH₂)[WS₄] 24

TG and DTA curves of complex **24** are presented in Fig 4.5.19. The TG curve of **24** is parallel to the horizontal axis indicating the thermal stability of **24** till 182 ^{0}C and then decomposition occurs accompanied by strong endothermic event at 206 ^{0}C in its DTA curve. The expected mass loss for the cyclic diamine 1,4-dmp and H_2S is 34.51 %. The experimental mass loss of 34.56 % is observed till 424 ^{0}C indicating the complete removal of organics. The total observed mass loss till 500 ^{0}C is 35.89 % resulting in the formation of 64.11 % of black residue. The expected residue for the formation of WS_3 is 65.39 % and that for WS_2 is 57.89 %. The final thermal product was examined by elemental analysis, electron microscopy and X-ray powder diffractometry. The elemental analysis of the final residue showed considerable amount (7.82 %) of C and N based on which the residue has been formulated as $WS_{2.2}C_{1.4}N_{0.4}$. Interestingly the amount of carbon left in residue of **24** is same as in **6**, which can be related to the number of carbon atoms in organic diamine of two complexes. Both the compounds contain six carbons each. The formulation of residue as $WS_{2.2}C_{1.4}N_{0.4}$ gains further credence based on the electron microscopy result which gave a W:S ratio very close to 1:2 (1:1.8). The X-ray powder pattern of the residue shows no intense peaks, which imply amorphous nature of the residue.
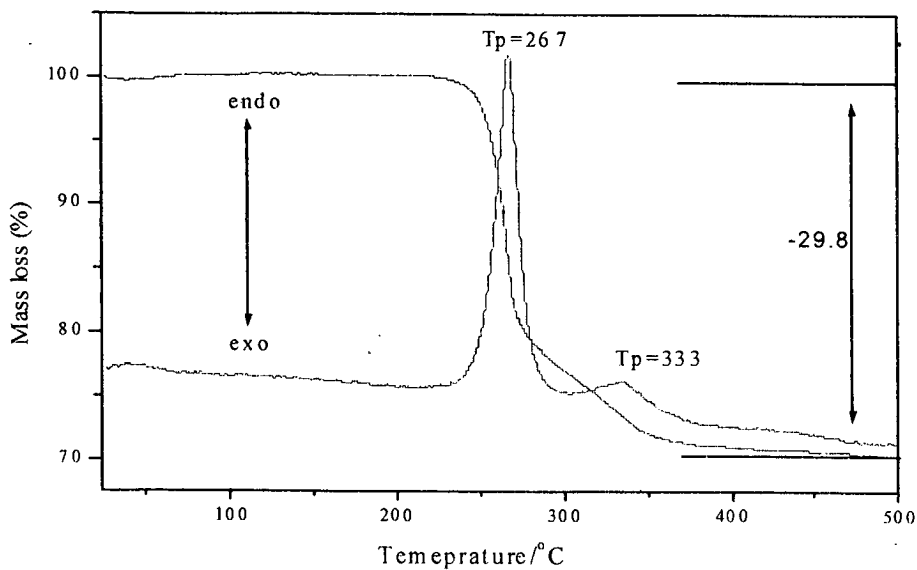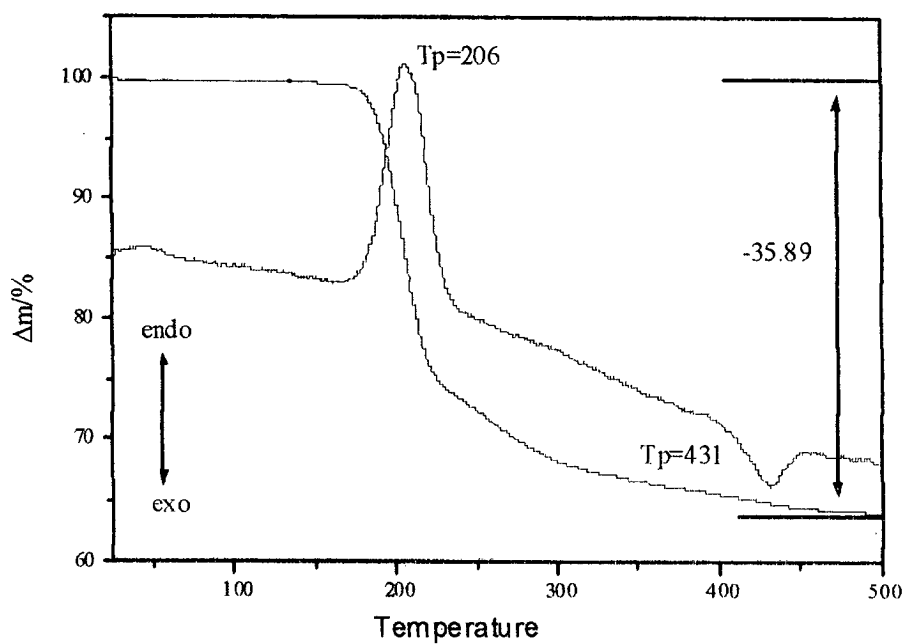
Fig. 4.5.19 TG-DTA curves for (1,4-dmpH$_2$)[WS$_4$] **24** (heating rate 4 K/min; N$_2$ atmosphere; given are the peak temperatures (T$_p$) in °c and the mass loss in %).

4.5.12 TG-DTA description for (2-pipH-1-EtNH₃)[MoS₄] · ½H₂O 27

TG-DTA trace of the hydrated tetrathiomolybdate complex **27** is presented in the Fig 4.5.20. The TG curve of **27** exhibits first mass loss at around $107\ ^0C$ and can be attributed to the emission of half crystal water. The TG curve is accompanied with endothermic signal in DTA curve at this temperature resulting in the mass loss of 2.5 %. The observed mass loss is in good agreement with that of expected mass loss of 2.47 % for removal of half crystal water molecule. On further increasing the temperature, DTA exhibit a sharp endothermic signal at about $160\ ^0C$. For this peak, TG curve shows drop in mass loss and then becomes parallel to horizontal x-axis above $400\ ^0C$. The total experimental mass loss up to $600\ ^0C$ is 44.43 % and is quite less than the expected mass loss for amine and H_2S (47.27 %). The residue showed considerable amounts of carbon and nitrogen indicating incomplete removal of organics. Based on the elemental analysis the residue is formulated as $MoS_{1.7}C_{2.3}N_{0.7}$. However interestingly ESEM-EDAX data gave the semi quantitative of formation MoS_3 as Mo:S ratio was 1:3.3. The X-ray powder pattern of the residue implied the amorphous nature.

4.5.13 TG-DTA description for (dtmen)Br₂·2H₂O 30, (dbtmen)[MoS₄] 31 and (dbtmen)[WS₄] 32

Complexes **30**, **31** and **32** all of which contain same cation (twenty carbons each) has been investigated by TG-DTA studies in argon atmosphere. Thermogravimetry and differential thermal analysis (TG-DTA) curves of **30**, are presented in Fig 4.5.21. Complex **30** start decomposing relatively at low temperature of $105\ ^0C$, which is accompanied by a sharp endothermic peak at $111\ °C$ in its DTA curve. The mass loss in TG curve up to $111\ ^0C$ is 7.4 % and is in good agreement with that expected for mass loss of two crystal waters (7.3 %). The elimination of waters is completed at around $140\ ^0C$ and on further increasing the temperature, anhydrous complex starts decomposing at around $190\ ^0C$, which is followed by strong endothermic event at about $218\ ^0C$ in its DTA. After that decomposition process continues till $600\ ^0C$ and interestingly even at such a higher temperature formation of black carbon residue is observed. The reaction of **30** with $(NH_4)_2[MS_4]$ (M = Mo, W) in aqueous medium results in the formation of the highly insoluble complexes **31** and **32**. TG-DTA curves for **31** are presented in Fig. 4.5.22(a). On heating complex **31**
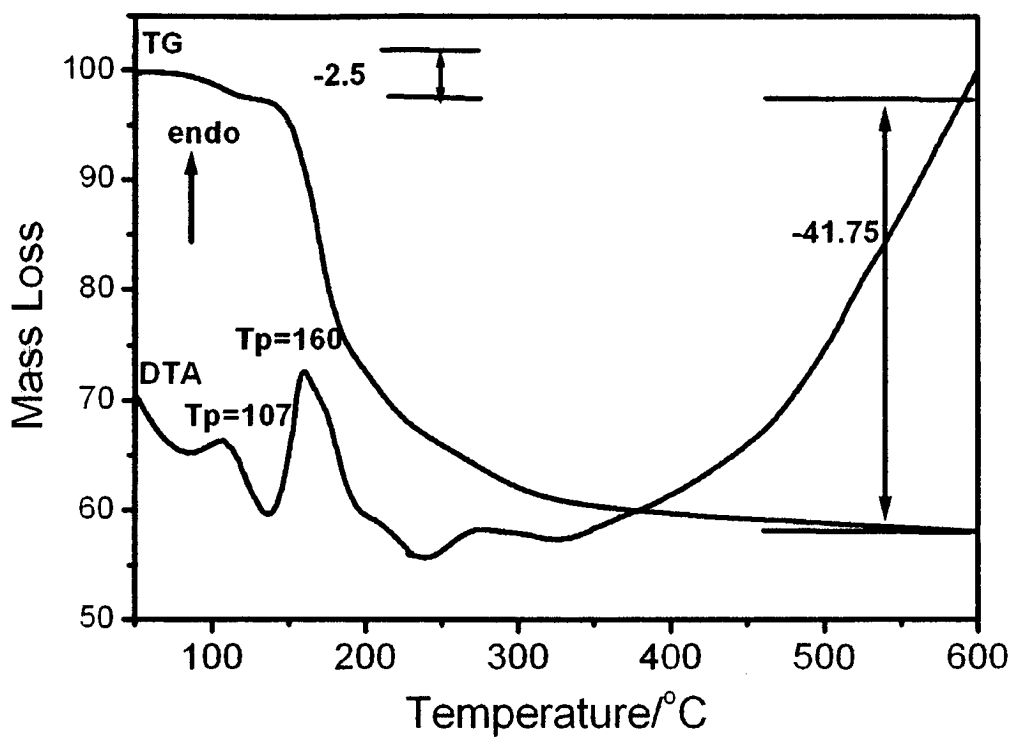
Fig.4.5.20 DTA and TG curves for (a) (2-pipH-1-EtNH$_3$)[MoS$_4$].1/2H$_2$O and (b) (dipnH$_2$)[MoS$_4$] (heating rate 4 K/min; Ar atmosphere; given are the peak temperatures (T$_p$) in °C and the mass loss in %).

start decomposing at about 142 ^{0}C which is evidenced from mass drop in TG curve and is accompanied by two endothermic events at about 170 ^{0}C and 209 ^{0}C. The decomposition process consisting of two endothermic events can be attributed for the simultaneous of decomposition of organic cation and H_2S. The observed endothermic peak temperatures for **31** are comparatively less than for $(NH_4)_2[MoS_4]$ (155 ^{0}C) and **21** (170 ^{0}C) which can be explained on the basis of bulkiness of the cation. On further increasing the temperature, TG curve shows mass loss till up to 400 ^{0}C and then it becomes parallel to temperature axis with very little mass loss up to 600 ^{0}C. The total observed mass loss up to 600 ^{0}C is 62.84 % and is in good agreement with the mass loss expected for emission of organic cation and H_2S (63.24 %). However the elemental analysis of the final residue showed considerable amount of C (13.29 %) indicating incomplete emission of organics. Based the results of elemental analysis, residue has been formulated as MoS_2C_2. Electron microscopy gave a Mo:S ratio which is very close to 1:2 thus indicating the formation of carbon contaminated molybdenum disulfide.

DTA-TG curves of the corresponding W analogue **32** are displayed in Fig. 4.5.22 (b). On heating, complex starts decomposing at about 152 ^{0}C, which is accompanied with mass loss in TG curve. On further increasing temperature, DTA curve exhibits two endothermic events at about 192 and 232 ^{0}C and these events can be attributed to the emissions of organics and hydrogen sulfide. **32** is thermally more stable than its corresponding Mo analogue **31** The thermal decomposition of **32** takes place relatively at lower temperature compared to that observed in other ammonium tetrathiotungstates such as $(NH_4)[WS_4]$ (180 ^{0}C), **21** (208 ^{0}C) and **24** (182 ^{0}C) etc. This interesting thermal behaviour can be attributed to the presence of the bulkier $(dbtmnen)^{2+}$ dication in **32**. TG curve of the complex shows mass loss up to 400 ^{0}C and then after it becomes parallel to the horizontal till 600 ^{0}C. The total observed mass loss up to 600 ^{0}C is 49.88 % resulting in the formation of 50.12 % residue. The expected residue for the formation of WS_3 is 45.86 % while residue of 40.67 % is expected for the formation of WS_2. As the experimental value is quite high compared to above two values, the residue was examined by elemental analysis. The elemental analysis gave the presence of 13.05 % of C which leads to formulate decomposed residue as $WS_{1.75}C_3$. The ESEM picture of final sulfide residue is displayed in Fig.4.5.23, which indicates porous morphology of the material. It indicates that
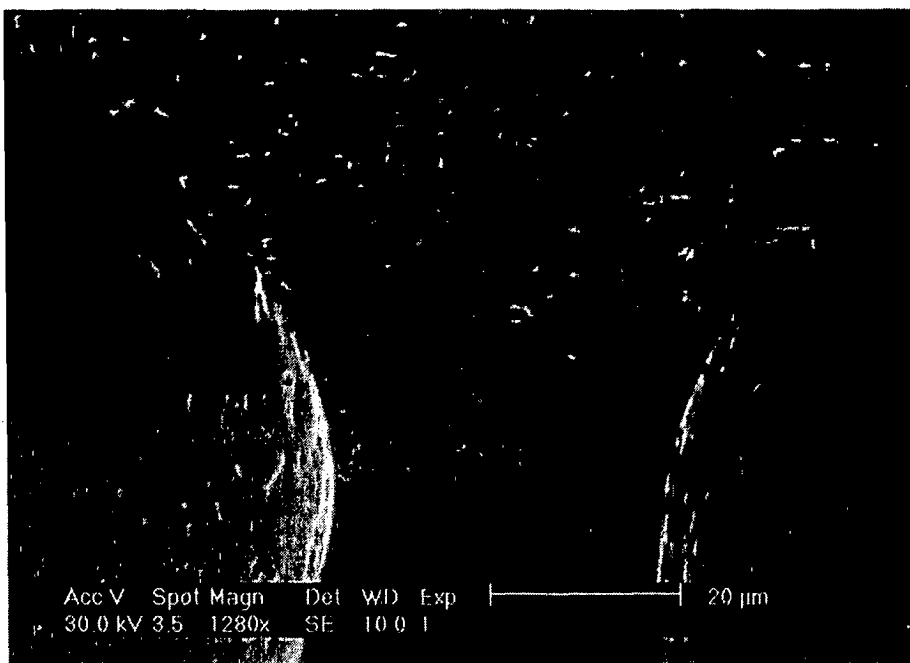
Fig.4.5.23 SEM micrograph of the decomposition product of (dbtmen)[WS₄] **32**

carbon contamination in the final residue has affected the formation of pure WS_2 as particle is more. The X-ray powder pattern of the residue obtained after heating at 600 ^{0}C exhibits only broad bumps like in the case other complexes indicating amorphous nature of the residue.

The organic ammonium tetrathiometalates investigated in this work by the use of TG-DTA analysis, showed considerable amount of carbon in the final decomposed residue. The % C content in final residue of few tetrathiotungstates listed in Table 4.5.3. It can be seen from the table that as the number of carbon atoms in organic amine increases, amount of carbon content in the final residue also increases.

Table 4.5.3 Carbon content of the thermolysed products of tetrathiotungstates

Compound Name	Mol Formula	% C	Final Residue
(enH$_2$)[WS$_4$]	C$_2$H$_{10}$N$_2$WS$_4$	5.23	WS$_{2.1}$C$_{1.2}$N$_{0.5}$
(1,3-pnH$_2$)[WS$_4$]	C$_3$H$_{12}$N$_2$WS$_4$	5.17	WS$_{2.1}$C$_{1.2}$N$_{0.4}$
(N-MeenH$_2$)[WS$_4$]	C$_3$H$_{12}$N2WS$_4$	5.18	WS$_{2.2}$C$_{1.4}$N$_{0.4}$
(pipH$_2$)[WS$_4$]	C$_4$H$_{12}$N$_2$WS$_4$	7.41	WS$_{2.1}$C$_{1.2}$N$_{0.3}$
(trenH$_2$)[WS$_4$.H$_2$O]	C$_6$H$_{22}$N$_4$OWS$_4$	12.01	WS$_{2.1}$C$_3$N$_{0.8}$
(dbtmen)[WS$_4$]	C$_{20}$H$_{30}$N$_2$WS$_4$	13.05	WS$_{1.7}$C$_3$

CHAPTER 5

SUMMARY AND CONCLUSIONS

In recent years, the chemistry of Mo/W-S complexes is an area of intense research investigations owing to the use of the group VI metal sulfides in hydrodesulfurization catalysis (HDS) [202] and the emerging importance of the layered metal disulfides in nanomaterials [203]. The soluble sulfides of the group VI metals Mo and W [98, 99] are a unique class of compounds with a wide range of metal to sulfur stoichiometries, metal oxidation states, coordination geometries and bonding modes of the sulfido ligands. The use of $(NH_4)_2[MS_4]$ (M=Mo, W) as precursors for the soft synthesis of MS_2 nanotubes [28,29], is an important reason for the current interest in the chemistry of tetrathiometalate. Recently it has been reported that the direct pyrolysis of bis(cetyltrimethylammonium) tetrathiotungstate leads to the formation of bulk quantities of uniform WS_2 nanotubules [71]. The use of the corresponding Mo analogue has been reported to yield MoS_2. These reports indicate the emerging importance of organic ammonium salts of $[MS_4]^{2-}$ (M = Mo,W) in material applications.

In the present work the synthesis, spectroscopy, reactivity characteristics, thermal decomposition aspects, as well as structural characterization of several new organic ammonium tetrathiometalates has been achieved. A convenient method has been developed for the high yield synthesis of crystalline tetrathiometalates. The formulation of the synthesized complexes has been arrived at based on elemental analysis, further supported by spectroscopic and X-ray structure determination. In a few cases where X-ray quality crystals could not be prepared, the formulation of the complexes is based on analytical and spectroscopic data. In this context it should be noted that a rapid method for the convenient estimation of $[MS_4]^{2-}$ content of the new tetrathiometalates has been developed based on the high insoluble nature of $[Ni(en)_3][MS_4]$. The synthetic protocol used for the preparation of thiometalates has also been extended to oxochromates and two oxochromates have been characterized. A few of the important conclusions of the present work are given below:

1. A simple base promoted cation exchange method has been developed for the convenient synthesis of crystalline organic ammonium tetrathiometalates.

2. All the complexes exhibit characteristic IR spectra. The IR spectrum of an organic ammonium tetrathiomolybdate is identical to that of the corresponding W analogue excepting that the signals below 500 cm^{-1} are shifted to lower energies in the W compound. The usefulness of IR spectra for the characterization of the tetrathiometalate as well as the organic cation has been discussed in the previous chapter.

3. The structural characterization of the complexes shows that an organic ammonium tetrathiomolybdate is isostructural with its corresponding W analogue.

4. The structures of the synthesized tetrathiometalates can be described as consisting of tetrahedral [MS$_4$]$^{2-}$ (M = Mo, W) ions which are linked to the organic ammonium cations via weak H-bonding interactions in the form of S...H-N bonds.

5. The strength and number of H-bonding interactions affect the M-S bond lengths as evidenced by the observation of long and short M-S bond distances for every complex.

6. With a view to understand the importance of the H-bonding interactions several organic ammonium tetrathiometalates have been characterized. For this purpose a variety of organic amines which differ in terms of this potential H-bonding donors and steric bulk have been employed in this study.

7. The two tetrathiometalates viz (trenH$_2$)[MoS$_4$]·H$_2$O and (trenH$_2$)[WS$_4$]·H$_2$O are the first examples of structurally characterized hydrated organic ammonium tetrathiometalates [83,87]. Both exhibit two types of interactions namely S...H-N and S...H-O. The S...H-O interactions in these complexes appears to be weaker compared to the S...H-N interactions in terms of their ability to elongate M-S bonds.

8. A comparative study of the structural features of several tetrathiometalates which includes known tetrathiometalates, in addition to the new ones described herein has been made to provide a possible explanation for the observed distinct M-S bond distances.

9. Based on the comparative study, it can be inferred that Δ the difference between the longest and the shortest M-S bond can be considered as an important factor to describe the observed distortion.

10. The compounds (pipH$_2$)[MS$_4$] exhibit the maximum Δ value for the tetrathiomolybdate series while the corresponding W analogue exhibits the maximum Δ value for [WS$_4$]$^{2-}$ complexes.

11. When the Δ value is more than 0.030 Å this can be considered as a pronounced distortion of the MS$_4$ tetrahedron as evidenced by the splitting of the asymmetric stretching vibration in the IR spectra.

12. All the tetrathiometalates can be thermally decomposed to the corresponding amorphous sulfides. Tetrathiotungstates are thermally more stable than the corresponding tetrathiomolybdates.

13. Many of the organic ammonium salts of tetrathiometalates can be decomposed in a single endothermic event resulting in the formation of carbon contaminated MS$_2$ unlike the ammonium salts which exhibit an endothermic event followed by an exothermic process to form MS$_2$. The X-ray powder pattern revealed the amorphous nature of the residues.

14. The isostructural complexes viz (dbtmen)[MS$_4$] (M=Mo,W) are the first examples of highly insoluble organic ammonium tetrathiometalates.

15. The reaction of soluble tetrathiometalate with [Ni(en)$_3$]Cl$_2$.2H$_2$O results in the formation of the highly insoluble [Ni(en)$_3$][MS$_4$] (M = Mo, W) complexes in quantitative yield. The formation of the insoluble [Ni(en)$_3$][MS$_4$] has been used as a convenient method for the quantitative estimation of [MS$_4$]$^{2-}$ content.

16 The structurally characterized oxochromates exhibit N-H...O interactions that stabilize the overall structure.

REFERENCES

1. E. I. Stiefel, *Prog. Inorg. Chem.*, **22** (1977) 1.

2. R. Hille, *Chem. Rev.*, **96** (1996) 2757.

3. M. K. Johnson, D. C. Rees, M. W. W. Adams, *Chem, Rev.*, **96** (1996) 2817.

4. B. Burgess, *Chem. Rev.*, **90** (1990) 1377.

5.(a) E. I. Stiefel, W. E. Newton, G. D. Watt, K. L. Hadfield, W. A. Bulen, *Adv. Chem. Ser.*, **162** (1977) 353; (b) R. A. D. Wentworth, *Coord. Chem. Rev.*, **18** (1976) 1.

6. E. I. Stiefel, D. Coucouvanis, N. E. Newton, Eds., *Molybdenum Enzymes, Cofactors and Model Systems*; ACS Symposium, Series 535 (1993).

7. F. A. Cotton, G. Wilkinson, C. A. Murillo, M. Bochman, *Advanced Inorganic Chemistry*, 6th ed., John Wiley, New York, (1999).

8. T. Rauchfuss, *Inorg. Chem.*, **43** (2004) 14 and references cited therein.

09. M. Breysse, E. Furimsky, S. Kasztelan, M. Lacroix, G. Perot, *Catal. Rev.*, **44** (2002) 651.

10. D. D. Whitehurst, T. Isoda, I. Mochida, *Adv. Catal.*, **42** (1988) 345.

11. A. Ennaoui, S. Fiechter, W. Jaegermann, H.J. Tributsch, *J. Electrochem. Soc.*, **133** (1986) 97.

12. F.L. Clauss, *Solid Lubricants and Self-Lubricating Solids*, Academic Press, New York, London, (1974).

13. E. Stoffels, W.W. Stoffels, G. Ceccone, R. Hasnaoui, H. Keune, G. Wahl, F. Rossi, *Appl. Phys.*, **86** (1999) 3442.

14. J. Rouxel, R.A. Bree, *Annu. Rev. Mater. Sci.*, 16 (1986) 137.

15. H. W. Wang, P. W. Skeldon, G. E. Thompson, G. C. Wood, *J. Mater. Sci.*, **32** (1997) 497.

16. H. Topsøe, B.S. Clausen, F.E. Massoth, *Hydrotreating Catalysis*, in: J.R. Anderson, M. Boudart (Eds.), *Catalysis, Science and Technology*, vol. 11, Springer-Verlag, Berlin, (1996).

17. O. Weisser, S. Landa, *Sulfide Catalysts: Their Properties and Applications*, Pergamon Press, New York, (1973).

18. S. P. Cramer, K. S. Liang, A. J. Jacobson, C. H. Chang, R. R. Chianelli, *Inorg. Chem.*, **23** (1984) 1215.

19. A.V. Powell, L. Kosidowski, A. McDowall, *J. Mater. Chem.*, **11** (2001) 1086.

20. G. Alonso, G. Aguirre, I. A. Rivero, S. Fuentes, *Inorg. Chim. Acta.*, **274** (1998) 108.

21. R. Tenne, L. Margulis, M. Genut, G. Hodes, *Nature*, **360** (1992) 444.

22. L. Margulis, G. Salltra, R. Tenne, M. Genut, M. Talianker, *Nature*, **365** (1993) 144 ; Y. Feldman, E. Wasserman, D. J. Srolovita, R. Tenne, *Science*, **267** (1995) 222.

23. P. R. Bonneau, R. F. Jr. Jarvis, R. B. Kaner, *Nature*, **349** (1991) 510.

24. M. R. Close, J. L. Petersen, E. L. Kugler, *Inorg. Chem.*, **38** (1999) 1535.

25. K. Wilkinson, M. D. Merchan, P. T. Vasudevan, *J. Catal.*, **171** (1997) 325.

26. P. Afanasiev, G. F. Xia, G. Berhault, B. Jouguet, M. Lacroix, *Chem.Mater.*, **11** (1999) 3216.

27. I. Bezverkhy, P. Afanasiev, M. Lacroix, *Inorg Chem.* **39** (2000) 5416.

28. M. Nath, A. Govindaraj, C.N.R. Rao, Adv. *Materials*, **13** (2001) 283; C.N.R. Rao, M. Nath, *J. Chem. Soc. Dalton Trans*, (2003) 1.

29. J Chen, S.L. Li, F. Gao, Z.L. Tao, *Chem. Mater.*, **15** (2003) 1012.

30. G. Alonso, G. Berhault, A. Aguilar, V. Collins, C. Ornelas, S. Fuentes, R. R. Chianelli, *J. Catal.*, **208** (2002) 359.

31. G. Alonso, G. Berhault, F. Paraguay, E. Rivera, S. Fuentes, R. R. Chianelli, *Mater. Res. Bull.*, **38** (2003) 1045.

32. Y. Iwata, K. Sato, T. Yoneda, Y. Miki, Y. Sugimoto, A. Nishjima, H. Shiamada, *Catal. Today*, **45** (1998) 353.

33. G. Alonso, M. Del Valle, J. Cruz, V. Petranovskii, A. Licea-Claverie, S. Fuentes, *Catal. Lett.*, **52** (1998) 55.

34. G. Alonso, M. Del Valle, J. Cruz, V. Petranovskii, A. Licea-Claverie, S. Fuentes, *Catal. Today*, **43** (1998) 117.

35. R. R. Chianelli, G. Berhault, *Catal. Today*, **53** (1999) 357.

36. D.J. Sajkowski, S.T. Oyama, *Appl. Catal.*, **134** (1996) 339.

37. F. Pedraza, S. Fuentes, *Catal. Lett.*, **65** (2000) 107.

215

38. D. D. Whitehurst, T. Isoda, I. Mochida, *Adv. Catal.*, **42** (1988) 345.

39. J. Sola, Y Do, J. M. Berg, R. H. Holm, *J. Am. Chem. Soc.*, **105** (1983) 7784; *Inorg. Chem.*, **24** (1985) 1706.

40. Y. Do, E. D. Simhon, R. H. Holm, *Inorg Chem.*, **24** (1985) 2827.

41. M. Latroche, J. A. Ibers, *Inorg. Chem.*, **29** (1990) 1503.

42. J. J. Berzelius, *Poggendorffs Ann. Phys. Chem.*, **7** (1826) 262.

43. J. J. Berzelius, *Poggendorffs Ann. Phys. Lpz.*, **8** (1826) 277.

44. G. Krüss, *Ann. Chem.*, **225** (1884) 1.

45. E. Corlies, J. Leibigs, *Ann. Chem.*, **232** (1886) 244.

46. E. Diemann, A. Müller, *Coord. Chem. Rev.*, **10** (1973) 79.

47. A. Müller, E. Diemann, R. Jostes, H. Bögge, *Angew. Chem.*, **93** (1981) 957; *Angew. Chem. Int. Ed. Engl.*, **20** (1981) 934 and references therein.

48. A. Müller, E. Diemann, *Chem. Commun.* **(1971)** 65 ; A. Müller, E. Ahlborn, H.H. Heinsen, *Z.Anorg. Allg. Chem.*, **386** (1971) 102.

49. A. Müller, E. Diemann, *Z. Naturforsch B; Chem. Sci.*, **23** (1968) 1607.

50. J. W. McDonald, G. D. Friesen, L. D. Rosenhein, W. E. Newton, *Inorg. Chim. Acta.*, **72** (1983) 205.

51. Y. Do, E. D. Simhon, R. H. Holm, *Inorg. Chem.*, **24** (1985) 4635.

52. A. Müller, B. Krebs, E. Dieman, *Angew. Chem. Int. Ed. Engl.*, **6** (1967) 257.

53. K. E. Howard, T. B. Rauchfuss, S. R. Wilson, *Inorg. Chem.*, **27** (1988) 1710.

54. V. Lenher, A. G. Freuhan, *J. Am. Chem. Soc.*, **49** (1927) 3076.

55. R. W. M. Wardle, C. H. Mahler, C. N. Chau, J. Ibers, *Inorg. Chem.*, **27** (1988) 2790.

56. S. C. O'Neal, J. W. Kollis, *Inorg. Chem.*, **28** (1989) 2780.

57. S. C. O'Neal, J. W. Kollis, *J. Am. Chem. Soc.*, **110** (1988) 1971.

58. A. Müller, E. Krickemeyer, H. Bogge, M. Penk, D. Rehdar, *Chimia.*, **40** (1986) 50

59. T. E. Wolff, J. M. Berg, K. O. Hodgson, R. B. Frankel, R. H. Holm, *J. Am. Chem. Soc.*, **101** (1979) 4140.

60 S. H. Lauri, D. E. Dratt, J. H. L. Yong, *Inorg. Chim. Acta.*, **93** (1984) L57-1.

61. M. Emirdag-Eanes, J. A. Ibers, *Z. Krist., -New Cryst. Struct.*, **216** (2001) 484.

62. C. C. Raymond, P. K. Dorhout, S. M. Miller, *Z. Kryst*, **210** (1995) 775.

63. J. Ellermeier, C. Näther, W. Bensch, *Acta Cryst.*, **C55** (1999) 1748.

64. J. Yao, J. A. Ibers, *Acta Cryst.*, **E60** (2004) i10.

65. M. Emirdag-Eanes, J. A. Ibers, *Z. Krist., -New Cryst. Struct.*, **216** (2001) 489.

66. J. Ellermeier, C. Näther, W. Bensch, *Acta Cryst.*, **C55** (1999) 501.

67. J. Ellermeier, *Ph.D. thesis*, Christian-Albrecht Universität-Kiel, (March 2002).

68. J. Ellermeier, W. Bensch, *Z. Naturforsch.*, **56b** (2001) 611.

69. J. Ellermeier, R. Stähler, W. Bensch, *Acta Cryst.*, **C58** (2002) m70.

70. J. Ellermeier, W. Bensch, *Monatsh. Chem.*, **133** (2002) 945.

71. Y. D. Li, X.L. Li, R.R. He, J. Zhu, Z. X. Deng, *J. Am. Chem. Soc.*, **124** (2002) 1411.

72. G. Alonso, M. H. Siadati, G. Berhault, A. Aguilar, S. Fuentes, R. R. Chianelli, *Applied Catalysis*, **263** (2004) 109.

73. I. Bezverkhyy, P. Afanasiev, M. Lacroix, *Mater. Res. Bull.*, **37** (2002) 161.

74. M. A. Ansari, J. Chandrasekaran, S. Sarkar, *Inorg. Chim. Acta.*, **133** (1987) 133.

75. B. R. Srinivasan, B. K. Vernekar, K. Nagarajan, *Indian J. Chem.*, **40A**, (2001) 563.

76. S. Pokhrel, K. S. Nagaraja, B. Varghese, *J. Struc. Chem.*, **44** (2003) 689.

77. S. Pokhrel, K. S. Nagaraja, B. Varghese, *J. Chem. Cryst.*, **33** (2003) 903.

78. (a) M. R. Udupa, G. Aravamudan, Curr. Sci., 42 (1973) 677; (b) P. Dhar, S. Chandrasekaran, *J. Org. Chem.*, **54** (1989) 2998.

79. B. R. Srinivasan, S. N. Dhuri, C. Näther, W. Bensch, *Inorg. Chim Acta*, **358** (2005) 279.

80. A. l. Hadjikyriacou, D. Coucouvanis, *Inorg. Synth.*, **27** (1990) 39.

81. A. R Ramesha, S. Chandrasekaran, *Synth. Commun.*, **22** (1992) 3277.

82. S. Sinha, P. Illakumaran, S. Chandrasekaran, *Tetrahedron*, **55** (1999) 14769.

83. B. R. Srinivasan, S. N. Dhuri, M. Poisot, C. Näther, W. Bensch, Z. *Naturforsch,* **59b** (2004) 1083.

84. B. R. Srinivasan, S. N. Dhuri, C. Näther, W. Bensch, *Acta Cryst.,* **E58** (2002) m622.

85. B. R. Srinivasan, S. N. Dhuri, C. Näther, W. Bensch, *Acta Cryst.,* **C59** (2003) m124.

86. B. R. Srinivasan, S. N. Dhuri, C. Näther, W. Bensch, *Acta Cryst.,* **E59** (2003) m681.

87. B. R. Srinivasan, S. N. Dhuri, M. Poisot, C. Näther, W. Bensch, Z. *Anorg. Allg. Chem.,* **631** (2005) 1087.

88. B. R. Srinivasan, S. N. Dhuri, C. Näther, W. Bensch, *Monats. Chem.,* **137** (2006) 397.

89. G. Alonso, J. Yang , M. H. Siadati, R. R. Chianelli, *Inorg. Chim Acta.,* **325** (2001) 193.

90. G. Alonso, G. Berhault, R. R. Chianelli, *Inorg. Chim. Acta.,* **316** (2001) 105.

91. P. J. Ayamonino, A. C. Ranade, E. Diemann, A. Müller, Z.*Anorg. Allg. Chem.,* **300** (1969) 371.

92. D. V. Partyka, R. H. Holm, *Inorg. Chem.,* **43** (2004) 8609.

93. A. Müller, E. Diemann, *Chem. Ber.,* **102** (1969) 3277.

94. W. S. Sheldrick, M. S. Wachhold, *Angew. Chem. Int. Ed. Engl.,* **36** (1997) 206

95. C. L. Bowes, G. A. Ozin, *Adv. Mater.,* **8** (1996) 13.

96. A. Rabenau, *Angew. Chem.,* **97** (1985) 1017; *Angew. Chem. Int. Ed. Engl.,* **24** (1985) 1026.

97. C. N. Chau, R. W. M. Wardle, J. Ibers, *Inorg. Chem.,* **26** (1987) 2740.

98. D. Coucouvanis, *Adv. Inorg. Chem.,* **45** (1998) 1.

99. T. Shibhahara, *Coord. Chem. Rev.,* **123** (1993) 73.

100. A. Müller, W. Jaegerman, *Inorg. Chem.,* **18** (1979) 2631.

101. E. D. Simhon, N. C. Baenziger, M. G. Kanatzidis, M. Draganjac, D. Coucouvanis, *J. Am. Chem. Soc.,* **103** (1981) 1218.

102. W. -H. Pan, M. A. Harmer, T. R. Halbert, E. I. Stiefel, *J. Am. Chem. Soc.* **106** (1984) 459.

103. M. Draganjac, E. Simhon, L. T. Chan, M. G. Kanatzidis, N. C. Baenziger, D. Coucouvanis, *Inorg. Chem.* **21** (1982) 3321.

104. S. A. Cohen, E. I. Stiefel *Inorg. Chem.* **24** (1985) 4657.

105. W. -H. Pan, M. E. Leonowicz, E. I. Stiefel, *Inorg. Chem.*, **22** (1983) 672.

106. J. M. Manoli, C. Potvin, F. Sécheresse, *Inorg. Chem.*, **26** (1987) 340.

107. F. Sécheresse, J. M. Manoli, C. Potvin, *Inorg. Chem.*, **25** (1986) 3967.

108. S. Bhaduri, J. A. Ibers, *Inorg. Chem.*, **25** (1986) 3.

109. A. Müller, E. Diemann, U. Wienböker, H. Bögge, *Inorg. Chem.*, **28** (1989) 4046.

110. F. Sécheresse, J. Lefebvre, J. C. Daran, Y. Jeannin, *Inorg. Chem.*, **21** (1982) 1311.

111. A. Müller, S. Sarkar, R. G. Bhattacharya, S. Pohl, Dartmann, *Angew. Chem. Int. Ed. Engl.*, **21** (1982) 535.

112. A. Müller, S. Pohl, M. Dartmann, J. P. Cohen, J. M. Bennet, R. M. Kirchner, *Z. Naturforsch.*, **B34** (1979) 434.

113. A. Müller, E. Krickemeyer, *Inorg. Synth.*, **27** (1990) 47.

114. A. Müller, W. O. Nolte, B. Krebs, *Angew. Chem.*, **90** (1978) 286

115. A. Müller, W. O. Nolte, B. Krebs, *Inorg. Chem.*, **19** (1980) 2835.

116. A. Müller, W. Eltzner, N. Mohan, *Angew. Chem. Int. Ed. Engl.*, **18** (1979) 168.

117. D. Coucouvanis, A. Toupadakis, A. Hadjikyriacou, *Inorg. Chem.*, **27** (1988) 3272.

118. R. G. Battacharya, P. K. Chakraborty, P. N. Ghosh, A. K. Mukherji, D. Podder, M. Mukherji, *Inorg. Chem.*, **30** (1991) 3948.

119. P. K. Chakraborty, P. N. Ghosh, R. G. Battacharya, A. K. Mukherji, M. Mukherji, M. Helliwell, *Polyhedron*, **15** (1996) 1443.

120. P. K. Chakraborty, S. Battacharya, C. G. Pierpont, R. G. Battacharya, *Inorg. Chem.*, **31** (1992) 3573.

121. S. L. Crasto, J. D. Martin, G. Christou, *Inorg. Chem.*, **32** (1993) 2978.

122. J. -H. Liao, J. Li, M. G. Kanatidis, *Inorg. Chem.*, **34** (1995) 2658.

123. A. Müller, W. Eltzner, E. Krickemeyer, V. Wittenben, H. Bogge, M. Lemke, *Angew. Chem. Int. Ed. Engl.*, **30** (1991) 1512.

124. A. Müller, W. Eltzner, H. Bogge, S. Sarkar, *Angew. Chem. Int. Ed. Engl.*, **21** (1982) 535.

125. A. Müller, W. Eltzner, H. Bogge, E. Krickemeyer, *Angew. Chem. Int. Ed. Engl.*, **22** (1983) 884.

126. D. Coucouvanis, N. C. Baenziger, E. D. Simhon, P. Stremple, D. Swenson, A. Simopoulos, A. Kostikas, V. Petrouleas, V. Papaefthymiou, *J. Am. Chem. Soc.*, **102** (1980) 1732.

127. A. Müller, Reinsh-Vogell, E. Krickemeyer, H. Bogge, *Angew. Chem. Int. Ed. Engl.*, **21** (1982) 786.

128. S. Sarkar, M. A. Ansari, *J. Am. Soc., Chem. Comun.*, **324** (1986).

129. (a) C. A. McConnachie and E. I. Stiefel, *Inorg. Chem.*, **38** (1999) 964; (b) H. H. Mrrray, L. Wei, S. E. Sherman, M. A. Greany, K. A. Eriksen, T. R. Halbert, E. I. Stiefel, *Inorg. Chem.*, **34** (1995) 841; (c) L. Wei, T. R. Halbert, H. H. III, E. 1 Stiefel, *J. Am. Chem. Soc.*, **112** (1990) 6431; W. –H., Pan, T. R. Halbert, L. L. Hutchings, E. I. Stiefel, *J. Chem. Soc., Chem. Commun.*, (1985) 927; (e) C. L. Coyle, M. A. Harmer, G. N. George, M. Daage, E. I. Stiefel, *Inorg. Chem.*, **29** (1990) 14.

130. Y. Gea, M. A. Greaney, C. L. Coyle, E. I. Stiefel, *J. Chem. Soc., Chem. Commun.*, **160** (1985).

131. T. R. Halbert, L. L. Hutchings, R. Rhodes, E. 1. Stifel, *J. Am. Chem. Soc.*, **108** (1986) 6437.

132. A. Müller, N. Mohan, H. Bogge, *Z. Naturforsch.*, **B33** (1978) 978.

133. I. Paulat-Böschen, B. Krebs, A. Müller, E. Königer-Ahlborn, H. Dornfeld, H. Schulz, *Inorg. Chem.*, **17** (1978) 1440.

134. A. Müller, I. Paulat-Böschen, B. Krebs, H. Dornfeld, *Angew. Chem.*, **88** (1976) 691; *Angew. Chem. Int. Ed. Engl.*, **15** (1976) 633.

135. W. P. Binnie, M. J. Redman, W. J. Mallio, *Inorg. Chem.*, **9** (1970) 1449.

136. A. Müller, S. Sarkar, *Angew. Chem. Int. Ed. Engl.*, **16** (1977) 705.

137. J. -R, Li. Z. –H. Li, D. S. –W. Du, X. –T. Wu, *Polyhedron*, **24** (2005) 481.

138. B. R. Srinivasan, S. Sarkar, *Inorg. Chem.*, **29** (1990) 3898.

139. M. H. Sadr, W. Clegg, H. R. Bijhanzande, *Polyhedron*, **23** (2004) 637.

140. J. Ruiz, V. Rodrígues, G. López, P. A. Chaloner, P. B. Hitchcock, *J. Organometallic Chem.*, **493** (1995) 77.

141. S. Jobic, S. Poirier-Coutansais, M. Evain, R. Brec., *Mater. Res. Bull.*, **36** (2001) 2637.

142. R. Stähler, C. Näther, W. Bensch, *Acta Cryst.*, **C57** (2001) 26; R. Stähler, W. Bensch, *Eur. J. Inorg. Chem.*, **307** (2001) 3.

143. B. Deng, J. A. Ibers, *Acta Cryst.*, **E60** (2004) i147.

144. D. Coucouvanis, *Acc. Chem. Res.*, **14** (1981) 201.

145. B. A. Averill, *Struct. Bonding*, **53** (1983) 59.

146. A. Müller, W. Hellmann, C. Römer, H. Bögge, R. Jostes, M. Römer, U. Schimanski, *Angew. Chem. Int. Ed. Engl.*, **21** (1982) 860.

147. W.G. Zumft, *Eur. J. Biochem.*, **91** (1978) 345.

148. G. J. Brewer, R. D. Dick, D. K. Grover, V. LeClaire, M. Tseng, M. Wicha, K. Pienta, B. D. Redman, T. Jahan, V. K. Sondak, M. Strawderman, G. Lecarpentier, S. D. Merajver, *Clinical Cancer Res.*, **6** (2000) 1.

149. G. N. George, I. J. Pickering, H. H. Harris, J. Galler, D. Klein, J. Lichtmannegger, K. H. Summer, *J. Am. Chem. Soc.*, **125** (2003) 1704.

150. R. B. Rucker, T. Kosonen, M. S. Clegg, A. E. Mitchell., B. R. Rucker, J. Y. Uriu-Hare, C. L. Keen, *Am. J. Clin. Nutr.*, **67** (1998) 996S.

151. S.R. Gooneratne, J.McC. Howell, J.M. Gawthorne, J.S. Kumaratilake, *J. Inorg. Biochem.*, **35** (1989) 23.

152. J.McC. Howell, J.S. Kumaratilake, *J. Comp. Path.*, **103** (1990) 321.

153. A. McQuaid, J. Mason, *J. Inorg. Biochem.*, **41** (1990) 87.

154. G.J. Brewer, R.D. Dick, V. Yuzbasiyan-Gurkin, R. Tankanow, A.B. Young, K.J. Kluin, *Arch. Neurol.*, **48** (1991) 42.

155. K.T. Suzuki, K. Yamamoto, S. Kanno, Y. Aoki, N. Takeichi, *Toxicology*, **83** (1993) 149.

156. Y. Ogra, K.T. Suzuki, *J. Inorg. Biochem.*, **70** (1998) 49.

157. Y. Ogra, Y. Komada, K.T. Suzuki, *J. Inorg. Biochem.*, **75** (1999) 204.

158. Y. Ogra, M. Ohmichi, K.T. Suzuki, *Toxicology*, **106** (1996) 75.

140. J. Ruiz, V. Rodrígues, G. López, P. A. Chaloner, P. B. Hitchcock, *J. Organometallic Chem.*, **493** (1995) 77.

141. S. Jobic, S. Poirier-Coutansais, M. Evain, R. Brec., *Mater. Res. Bull.*, **36** (2001) 2637.

142. R. Stähler, C. Näther, W. Bensch, *Acta Cryst.*, **C57** (2001) 26; R. Stähler, W. Bensch, *Eur. J. Inorg. Chem.*, **307** (2001) 3.

143. B. Deng, J. A. Ibers, *Acta Cryst.*, **E60** (2004) i147.

144. D. Coucouvanis, *Acc. Chem. Res.*, **14** (1981) 201.

145. B. A. Averill, *Struct. Bonding*, **53** (1983) 59.

146. A. Müller, W. Hellmann, C. Römer, H. Bögge, R. Jostes, M. Römer, U. Schimanski, *Angew. Chem. Int. Ed. Engl.*, **21** (1982) 860.

147. W.G. Zumft, *Eur. J. Biochem.*, **91** (1978) 345.

148. G. J. Brewer, R. D. Dick, D. K. Grover, V. LeClaire, M. Tseng, M. Wicha, K. Pienta, B. D. Redman, T. Jahan, V. K. Sondak, M. Strawderman, G. Lecarpentier, S. D. Merajver, *Clinical Cancer Res.*, **6** (2000) 1.

149. G. N. George, I. J. Pickering, H. H. Harris, J. Galler, D. Klein, J. Lichtmannegger, K. H. Summer, *J. Am. Chem. Soc.*, **125** (2003) 1704.

150. R. B. Rucker, T. Kosonen, M. S. Clegg, A. E. Mitchell., B. R. Rucker, J. Y. Uriu-Hare, C. L. Keen, *Am. J. Clin. Nutr.*, **67** (1998) 996S.

151. S.R. Gooneratne, J.McC. Howell, J.M. Gawthorne, J.S. Kumaratilake, *J. Inorg. Biochem.*, **35** (1989) 23.

152. J.McC. Howell, J.S. Kumaratilake, *J. Comp. Path.*, **103** (1990) 321.

153. A. McQuaid, J. Mason, *J. Inorg. Biochem.*, **41** (1990) 87.

154. G.J. Brewer, R.D. Dick, V. Yuzbasiyan-Gurkin, R. Tankanow, A.B. Young, K.J. Kluin, *Arch. Neurol.*, **48** (1991) 42.

155. K.T. Suzuki, K. Yamamoto, S. Kanno, Y. Aoki, N. Takeichi, *Toxicology*, **83** (1993) 149.

156. Y. Ogra, K.T. Suzuki, *J. Inorg. Biochem.*, **70** (1998) 49.

157. Y. Ogra, Y. Komada, K.T. Suzuki, *J. Inorg. Biochem.*, **75** (1999) 204.

158. Y. Ogra, M. Ohmichi, K.T. Suzuki, *Toxicology*, **106** (1996) 75.

159. S. Sarkar, S.B.S. Mishra, *J. Indian Chem. Soc.*, **LXII** (1985) 821.

160. J. LeGall, G. Mazza, N. Dragoni, *Biochim. Biophys. Acta.*, **99** (1965) 385.

161. S.A. Bursakov, O.Yu. Gavel, G.Di Rocco, J. Lampreia, J. Calvete, A.S. Pereira, J.J.G. Moura, I. Moura, *J. Inorg. Biochem.*, **98** (2004) 833.

162. G. N. George, I. J. Pickering, E.Y. Yu, R. C. Prince, S. A. Bursakov, O. Y. Gavel, I. Moura, J. J. G. Moura, *J. Am. Chem. Soc.*, **122** (2000) 8321.

163. J. G. MacDonald, D. N. Harpp, *Tetrahedron Lett.*, **25** (1984) 703.

164. P. Illakumaran, K. R. Prabhu, S. Chandrasekaran, *Synth. Commun.*, **27** (1997) 4031.

165. N. Devan, D. Sureshkumar, I. Beadham, K. R. Prabhu, S. Chandrasekaran, *Indian J. Chem.*, **41B** (2002) 2112.

166. K.R. Prabhu, P.S. Shivanand, S. Chandrasekaran, *Angew. Chem. Int. Ed.Engl.*, **39** (2000) 4316

167 D. Bhar, S. Chandrasekaran, ***Carbohydr. Res.***, **301** (1997) 221.

168. P. Illakumaran, S. Chandrasekaran, *Tetrahedron. Lett.*, **36** (1995) 4881

169. K.R. Prabhu, N. Devan, S. Chandrasekaran, *Synlett*, (2002) 1762 and references therein.

170. R. Cao, K. Tatsumi, Inorg. *Chem.*, **41** (2002) 4102.

171. K. Sasvári, *Acta Crystallogr.*, **16** (1963) 719.

172. H. Schäfer, G. Schäfer, A. Weiss, *Z. Naturforsch.*, **B19** (1964) 76.

173. A. Müller, W. Dieman, M. J. F. Leroy, *Z. Anorg. Allg. Chem.*, **372** (1970) 113.

174. A. Müller, E. J. Baran, R. O. Carter, *Struct. Bonding*, **26** (1976) 81.

175. K. Nakamoto, *Infrared and Raman Spectra of Inorganic and Coordination Compounds*, 4th Edition, John Wiley, New York (1986) 130.

176. D. E. Schwarz, T. B. Rauchfuss, S. R. Wilson, *Inorg. Chem.*, **42** (2003) 2410.

177. B. R. Srinivasan, M. Poisot, C. Näther, W. Bensch, *Acta Cryst.*, **E60** (1983) i136.

178. M. G. Kanatzidis, D. Coucouvanis, *Acta Cryst.*, **C39** (1983) 835.

179. P.J. Lapasset, N. Chezeau, P. Belougne, *Acta Cryst.*, **B32** (1976) 3087.

180. A. Müller, R. Jostes, W. Hellmann, C. Römer, H. Bogge, U. Schimanski, B. Zhuang, L. D. Rossenhein, J. W. McDonald, W. E. Newton, *Z. Anorg. Allg. Chem.*, **533** (1986) 125.

181. B. S. Furniss, A. J. Hannaford, V. Rogers , P. W. G. Smith, A. R. Tatchell, *Vogel's textbook of practical organic chemistry*, 4th Edn (ELBS London) (1978).

182. H. O. House, *Modern Synthetic Reactions*, 2nd Edn, (W A Benjamin Inc., Menlo Park, California), (1972) 257.

183. L. Fieser, M. Fieser, *Reagents for organic synthesis*, (John Wiley, New York), vol.1, (1967) 142.

184. E. J. Corey, J.W. Suggs, *Tetrahedron Lett.*, (1975) 2647.

185. G. Cainilli, G. Cardillo, *Chromium oxidations in organic chemistry* (Springer-Verlag, Berlin), (1984).

186. A. F. Guerrero, H-J. Kim, M. F. Sehlecht, *Tetrahedron Lett.*, **29** (1988) 6707; E. Santaniello, F. Milani, R. Casati, *Synthesis*, (1983) 749.

187. S. Chandrasekhar, M. Takhi, S. Mohapatra, *Synth Commun.*, **26** (1996) 3947.

188. B. Movassagh, M. M. Lakouraj, K. Ghodrati, *Indian J Chem.*, **41B** (2002) 1293.

189. A. J. Norquist, K. R. Heier, P. S. Halasyamani, C. L. Stern, K. R. Poeppelmeier, *Inorg Chem.*, **40** (2001) 2015.

190. N. CH. Panagiotopoulos, I. D. Brown, *Acta Cryst.*, **B28** (1972) 1352.

191. W. Klien, J. Curda, K. Friese, M. Jansen M, *Acta Cryst.*, **C58** (2002) i23.

192. B. M. Casari, V. Langer V, *Acta Cryst.*, **C56** (2000) e36.

193. A. Riou, Y. Gerault, Y. Cudennec, *Acta Cryst.*, **C46** (1990) 1915.

194. N. Seferiadis, HR. Oswald, *Acta Cryst.*, **C43** (1987) 10.

195. H. Montgomery, *Acta Cryst*, **C40** (1984) 14.

196. A. Riou, Y. Gerault, Y. Cudennec, *Acta Cryst.*, **B38** (1982) 1693.

197. K. Ejsmont, M. Wasielewski, J. Zaleski, *Acta Cryst.*, **E58** (2002) m200.

198. P. A. Lorenzo-Luis, P. Martin-Zarza, P. Gili, J. M. Arrieta, G. Germain, L. Dupont, *Acta Cryst.*, **C51** (1995) 1073.

199. H. Chebbi, A. A. Hajem, A. Driss, *Acta Cryst.*, **C56** (2000) e333.

200. H. Chebbi, A. Driss, *Acta Cryst.*, **C57** (2001) 1369.

201. H. Chebbi, A. Driss, *Acta Cryst.*, **E58** (2002) m147.

202. R.R. Chianelli, *Catal. Rev. Sci. Eng.*, **26** (1984) 361.

203. R. Tenne, M. Homyonfer, Y. Feldman, *Chem. Mater.*, **10** (1998) 3225.

204. H. M. State, *Inorganic Synth.*, **6** (1950) 200.

205. B. R. Srinivasan, S. N. Dhuri, A. R. Naik, *Tetrahedron Lett.*, **45** (2004) 2247; B. R. Srinivasan, *J Chem. Sci.*, **116** (2004) 251.

206. V. Polshettiwar, M. Nivsarkar, J. Acharya, M. P. Kaushik, *Tetrahedron Lett.*, **44** (2003) 887.

207. N. N. Greenwood, A. Earnshaw, *Chemistry of The Elements*, 1st ed. ; Pergamon: Oxford, (1984) 1171.

208. X. Xin, N. L. Morris, G. B. Jameson, M. T. Pope, *Inorg. Chem.*, **24** (1985) 3482.

209. J. Chandrasekaran, M. A. Ansari, S. Sarkar, *Inorg. Chem.*, **27** (1998) 3663.

210. G. Svehla, *Vogel's Textbook of Macro and Semimicro Qualitative Inorganic Analysis*, 5th ed.; Orient Longman: New Delhi, (1982) 512.

211. G. M. Sheldrick, *SHELXS-97: Program for the solution of crystal structures*, University of Gottingen, Germany (1994).

212. G. M. Sheldrick, *SHELXL-97: Program for the refinement of crystal structures*, University of Gottingen (1997).

213. A. Bondi, *J. Phys. Chem.*, **68** (1964) 441.

214. T. A. Anan, R. K. Chadha, D. G. Tuck, *Acta Cryst.*, **C57** (1991) 151; M. Kabak, Y. Elerman, C. Ünaleroglu, Y. Mert, T. N. Durlu, *Acta Cryst.*, **C56** (2000) e66.

215. A. Kallel, J. Fail, H. Fuess, A. Daoud, *Acta Cryst.*, **B36** (1980) 2788; P. Toffoli, H. Vénumière, P. Khodadad, N. Rodier, R. Julien, *Acta Cryst.*, **C14** (1985) 1589.

216. A. Chtioui, A. Jouini, *Cryst. Res. Technol.*, 38 (2003) 996.

217. P. A. Koz'min, Z. V. Popova, *Zh. Strukt. Khim. (Russ.)*, **12** (1971) 99.

218. B. R. Srinivasan, C. Näther, W. Bensch, *Acta Cryst.*, **E59** (2003) m639; B. R. Srinivasan, A. R. Naik, C. Näther, W. Bensch, *Acta Cryst.*, **E60** (2004) m1384.

219. J. Tyrselova, L. Kuchta, F. Pavelcik, *Acta Cryst.*, **C52** (1996) 17.

220. D. M. M. Farrell, G. Ferguson, A. L. Lough, C. Glidewell, *Acta Cryst.*, **C57** (2001) 952.

221. B.R.Srinivasan, S. N. Dhuri, C. Näther, W. Bensch, *Indian J. Chem.*, **42A** (2003) 2735.

222. H. Chebbi, A. Driss, *Acta Cryst.* E60 (2004) m904.

223. T. P. Prasad, E. Diemann and A. Müller, *J. Inorg. Nucl. Chem.*, **35** (1973) 1895.

Publications of Sunder N Dhuri

1. "Synthesis and solid state characterization of two insoluble tetrathiometalates", B. R. Srinivasan, **S. N. Dhuri**, C. Näther and W. Bensch, *Transition Met. Chem.*, (2006) (submitted after revision)

2. "Cation-anion interactions in bis(±)*trans*-2-aminocyclohexylammonium tetrathiotungstate, 1,7-diazonia-4-aza-heptane tetrathiotungstate and 1,5-diazonia-9-aza-nonane tetrathiotungstate", B. R. Srinivasan, C. Näther, **S. N. Dhuri** and W. Bensch, *Polyhedron* (2006) (in press).

3. "A novel hydrogen-bonded cyclic dibromide in an organic diammonium salt", B. R. Srinivasan, **S. N. Dhuri**, J. V. Sawant, C. Näther and W Bensch, *J. Chem. Sci.*, **118** (2006) 211-218.

4. "On the Importance of H-bonding Interactions in Organic Ammonium Tetrathiotungstates", B. R. Srinivasan, C. Näther, **S. N. Dhuri** and W. Bensch, *Monatsh. Chem.*, **137** (2005) 397-311.

5. "Synthesis, X-ray Structures, Spectroscopic and Thermal Characterization of Two New Organic Ammonium Tetrathiotungstates", B. R. Srinivasan, **S. N. Dhuri**, M. Poisot, C. Näther and W. Bensch, *Z. Anorg. Allg. Chem.*, **631** (2005) 1087-1094.

6. "Synthesis, spectroscopic, thermal and X-ray structure characterization of 1,3-propanediammonium tetrathiomolybdate and N,N,N',N'-tetramethylethylenediammonium tetrathiomolybdate", B. R. Srinivasan, **S. N. Dhuri**, C. Näther and W. Bensch, *Inorg. Chim. Acta*, **358** (2005) 279-287.

7. "Synthesis, Crystal Structures and Properties of Three New Tetrathiomolybdates with Organic Ammonium Cations", B. R. Srinivasan, **S. N. Dhuri**, M. Poisot, C. Näther and W. Bensch, *Z. Naturforsch*, **59b** (2004) 1083-1092.

8. "The correct formulation of the sulfur transfer reagent benzyltriethylammonium tetracosathioheptamolybdate", B. R. Srinivasan, **S. N. Dhuri** and A. R. Naik, *Tetrahedron Letters*, **45** (2004) 2247-2249.

9. "Synthesis, spectroscopic and X-ray structure characterization of ethylenediammonium chromate and ethylenediammonium dichromate", B. R. Srinivasan, **S. N. Dhuri**, C. Näther and W. Bensch, *Indian J. Chem.*, **42A** (2003) 2735-2741.

10. "1,4-Dimethylpiperazinium tetrathiotungstate", B. R. Srinivasan, **S. N. Dhuri**, C. Näther and W. Bensch, *Acta Cryst.*, **E59** (2003) m681-m683.

11. "1,3-Propanediammonium tetrathiotungstate and N,N,N',N'-tetramethylethylenediammonium tetrathiotungstate", B. R. Srinivasan, **S. N. Dhuri**, C. Näther and W. Bensch, *Acta Cryst*, **C59** (2003) m124-m127.

12. "Ethylenediammonium Tetrathiotungstate (VI)", B. R. Srinivasan, **S. N. Dhuri**, C. Näther and W. Bensch, *Acta Cryst.*, **E58** (2002) m622-m624.

13. "Synthesis, spectroscopic characterization and thermal decomposition studies of magnesium (II) complexes of *ortho* and *para*-aminobenzoic acids" B. R. Srinivasan, S. C. Sawant and **S. N. Dhuri**, *Indian J. Chem.*, **41A** (2002) 290-296.

Papers presented in Symposium and Conferences

14. "Reversible Hydration Characteristics of Group VI Tetrathiometallates Derived from Tris(2-aminoethyl)amine", B. R. Srinivasan, S. N. Dhuri, C. Näther and W. Bensch, Poster presentation in THERMANS 2006 symposium held at Rajasthan University, during 6th-8th Feb 2006.

15. "Thermal and Spectroscopic Investigations of Organic Ammonium Tetrathiotungstates", B. R. Srinivasan, S. N. Dhuri, C. Näther and W. Bensch, poster presentation in THERMANS 2006 symposium held at Rajasthan University, Jaipur, during 6th-8th Feb 2006.

16. "Weak H-bonding Interactions in Organic Ammonium Tetrathiomolybdates and Tetrathiotungstates" B. R. Srinivasan, S. N. Dhuri, C. Näther and W. Bensch presented during 1st-3rd December 2005 in ISCAS Symposium held at Goa University

17. "Reactions of Tetrathiomolybdate with Cu(II) in the Presence of Organic Amines" B. R. Srinivasan, S. N. Dhuri, presented in Third Symposium on Advances of Bio-inorganic Chemistry (SABIC-2004) in conjunction with Second Asian Biological Inorganic Chemsitry Conference (AsBIC-II) organized by TIFR held in Goa during 5-10 Dec 2004.

18. "Organic Diamines as Structure Directing Agents for the synthesis for the Synthesis of Novel $[MoS_4]^{2-}$ (M=Mo, W)", B. R. Srinivasan, S. N. Dhuri, C. Näther and W. Bensch, 6th CRSI National Symposium, IIT Kanpur, Book of Abstacts, Poster-248, page no.270 (2004)

19. "Thermal and Spectroscopic Investigations of Organic Diammonium Salts of Group VI tetrathiometalates" B. R. Srinivasan, S. N. Dhuri, C. Näther and W. Bensch presented in Fourteenth National Symposium in Thermal Analysis (THERMANS 2004) held at MS University Baroda (Jan.2004).

20. "X-ray Characterization of Three New Organic Diammonium Salts of Tetrathiomolybdate: $(1,3-pnH_2)[MoS_4]$ and $(tmenH_2)[MoS_4]$ and $(pipH_2)[MoS_4]$", B. R. Srinivasan, S. N. Dhuri, C. Näther and W. Bensch, presented in Fifth National Symposium in Chemistry held at CLRI Chennai during 7–9 Feb 2003.

21. "X-ray Characterization of Ethylenediammonium Salts of Chromates and Dichromates", B. R. Srinivasan, S. N. Dhuri, C. Näther and W. Bensch, presented in Fifth National Symposium in Chemistry held at CLRI Chennai during 7–9 Feb. 2003.

22. "Thermal Decomposition studies of magnesium (II) complexes of substituted benzoic acids: Substituent effect v/s structural stability" B. R. Srinivasan, S. C. Sawant, and S. N. Dhuri, oral presentation at the Thirteenth National Symposium and Workshop on Thermal analysis (THERMANS 2002) held at BARC Mumbai during 21-25 Jan 2002".

23. "Cation-anion interactions in Oxo and Thiometalates of Group VI metals", B. R. Srinivasan, S. N. Dhuri, presented in the 20th Annual conference of Indian Council of Chemists held in University of Mysore in Dec. 2001.

Table A-I.1 Technical details of data acquisition and selected refinement results for
(enH$_2$)[WS$_4$] **2**, (N-Me-enH$_2$)[WS$_4$] **4** and (N-Me-enH$_2$)[MoS$_4$] **3**

Compound	(enH$_2$)[WS$_4$] **2**	(N-Me-enH$_2$)-[WS$_4$] **4**	(N-Me-enH$_2$)-[MoS$_4$] **3**
Formula	C$_2$H$_{10}$WN$_2$S$_4$	C$_3$H$_{12}$N$_2$S$_4$W	C$_3$H$_{12}$N$_2$S$_4$Mo
Temperature [K]	293	293	293
Wavelength [pm]	71.073	71.073	71.073
Space group	P2$_1$2$_1$2$_1$	P2$_1$2$_1$2$_1$	P2$_1$2$_1$2$_1$
a [Å]	8.6401 (4)	7.8897 (12)	7.8805 (11)
b [Å]	9.3228 (5)	11.831 (2)	11.8098 (16)
c [Å]	11.8281 (7)	11.972 (2)	11.9492 (17)
α, β, γ [°]	90, 90, 90	90, 90, 90	90,90,90
Volume [Å^3]	952.75 (9)	1117.5 (3)	1112.1(3)
Z	4	4	4
μ [mm^{-1}]	12.93	11.028	1.874
F(000)	696	728	600
Molecular weight [g/mol]	374.21	388.24	300.33
Density (calcd.) [g cm^{-3}]	2.609	2.308	1.794
Crystal size (in mm)	0.13 0.1 0.05	0.1 0.09 0.08	0.14 0.12 0.10
h k l range	-11/11;-12/12;-15/15	11/4;-16/1;-16/1	-11/1;-16/1;-16/1
2θ range	3° - 56°	3° - 60°	3° - 60°
Reflections collected	8270	3184	2251
Reflections unique	2308	2646	2141
Data (Fo>4σ(Fo)	2207	2492	1632
R$_{int}$.	0.040	0.0479	0.0367
Min./Max transmission	0.237 / 0.527	0.1858 / 0.2621	0.7214 / 0.8381
Δρ [e/Å^3]	-2.17 / 1.44	-1.238/1.124	-0.731 / 0.625
Parameters	83	92	93
R1 [Fo>4σ(Fo)]^a	0.0230	0.0234	0.0305
WR2 for all unique data	0.0541	0.0601	0.0699
Goodness of fit	1.04	1.032	1.006
CCDC No.		280575	-

^{a}R1 = Σ ||Fo| -|Fc||/Σ|F o|

Table A-I.2 Technical details of data acquisition and selected refinement results for
$(tmenH_2)[MoS_4]$ **5** and $(tmenH_2)[WS_4]$ **6**

Compound	$(tmenH_2)[MoS_4]$ **5**	$(tmenH_2)[WS_4]$ **6**
Formula	$C_6H_{18}MoS_4$	$C_6H_{18}WS_4$
Temperature [K]	293	293
Wavelength [pm]	71.073	71.073
Space group	$P2_1/n$	$P2_1/n$
a [Å]	8.5739 (7)	8.5916 (11)
b [Å]	12.3370 (10)	12.3365 (10)
c [Å]	13.3336 (10)	13.3799 (9)
β [°]	101.082 (6)	101.113 (8)
Volume [$Å^3$]	1384.08 (19)	1391.5 (2)
Z	4	4
μ [mm^{-1}]	1.52	8.87
F(000)	696	824
Molecular weight [g/mol]	342.40	430.31
Density (calcd.) [$g\ cm^{-3}$]	1.643	2.054
Crystal size (in mm)	0.16 0.1 0.07	0.14 0.09 0.07
hkl Range	-0/10;-15/4;-17/16	-1/11;-16/3;-17/17
2θ range	3° - 54°	3° - 56°
Reflections collected	4336	4851
Reflections unique	3019	3363
Data (Fo>4σ(Fo)	2202	2725
$R_{int.}$	0.0219	0.040
Min./Max transmission	–	0.390 / 0.541
$\Delta\rho$ [$e/Å^3$]	-0.34 / 0.37	-2.09 / 0.99
Parameters	118	119
R1 [Fo>4σ(Fo)][a]	0.0242	0.027
WR2 for all unique data	0.0558	0.069
Goodness of fit	0.989	1.07
CCDC No	197080	
[a]$R1 = \Sigma\ |\ |Fo|\ -|Fc|\ |/\Sigma|F\ o|$		

Table A-I.3 Technical details of data acquisition and selected refinement results for $(1,3\text{-pnH}_2)[\text{MoS}_4]$ **7**, $(1,3\text{-pnH}_2)[\text{WS}_4]$ **8** and $(N,N'\text{-dm-}1,3\text{-pnH}_2)[\text{WS}_4]$ **10**

Compound	$(1,3\text{-pnH}_2)[\text{MoS}_4]$ **7**	$(1,3\text{-pnH}_2)[\text{WS}_4]$ **8**	$(N,N'\text{-dm-}1,3\text{-pnH}_2)[\text{WS}_4]$ **10**
Formula	$C_3H_{12}MoN_2S_4$	$C_3H_{12}WN_2S_4$	$C_5H_{16}N_2WS_4$
Temperature [K]	293	293	293
Wavelength [pm]	71.073	71.073	71.073
Space group	$P2_1/c$	$P2_1/c$	$P2_1/n$
a [Å]	10.7690 (8)	10.801 (2)	7.2588 (5)
b [Å]	10.5732 (6)	10.609 (2)	18.5619 (9)
c [Å]	10.7041 (8)	10.774 (2)	9.7335 (7)
α, β, γ [°]	90, 119.569(1), 90	90, 119.60(3), 90	90, 90.283(9), 90
Volume [Å³]	1060.2 (1)	1073.5 (5)	1311.45 (15)
Z	4	4	4
μ [mm^{-1}]	1.97	11.48	9.405
F(000)	600	728	792
Molecular weight [g/mol]	300.33	388.24	416.29
Density (calcd.) [g cm^{-3}]	1.882	2.402	2.108
Crystal size (in mm)	0.15 0.1 0.06	0.11 0.10 0.08	1.0 0.9 0.9
h k l range	-14/14;-13/13;-14/14	-15/13;-2/14;-1/15	-10/10;-26/24;-13/13
2θ range	3° - 56°	3° - 60°	3° - 60°
Reflections collected	10233	4124	17112
Reflections unique	2536	3126	3884
Data (Fo>4σ(Fo))	2366	2663	3231
$R_{int.}$	0.0317	0.042	0.0297
Min./Max transmission	0.6550 / 0.7933	0.291 / 0.401	0.1926/ 0.3926
$\Delta\rho$ [e/Å³]	-0.78 / 0.70	-1.84 / 1.54	-1.843/1.836
Parameters	92	94	110
R1 [Fo>4σ(Fo)][a]	0.0307	0.024	0.0305
WR2 for all unique data	0.0837	0.061	0.0778
Goodness of fit	1.051	1.04	1.047
CCDC No.	197079		280576

[a] $R1 = \Sigma \left| |Fo| - |Fc| \right| / \Sigma |Fo|$

Table A-I.4 Technical details of data acquisition and selected refinement results for $(1,4\text{-bnH}_2)[\text{MoS}_4]$ **11** and $(1,4\text{-bnH}_2)[\text{WS}_4]$ **12**

Compound	$(1,4\text{-bnH}_2)[\text{MoS}_4]$ **11**	$(1,4\text{-bnH}_2)[\text{WS}_4]$ **12**
Formula	$C_4H_{14}N_2MoS_4$	$C_4H_{14}N_2WS_4$
Temperature [K]	293	293
Wavelength [pm]	71.03	71.073
Space group	P-1	P-1
a [Å]	7.1447 (11)	7.1888 (10)
b [Å]	8.2159 (12)	8.1821 (11)
c [Å]	10.5031 (19)	10.634 (2)
α, β, γ [°]	79.558 (10), 81.561 (13), 83.701 (12)	79.647 (12), 81.662 (13), 83.537 (10)
Volume [Å^3]	597.57 (17)	606.4 (2)
Z	2	2
μ [mm^{-1}]	10.17	10.17
F(000)	316	380
Molecular weight [g/mol]	314.35	402.26
Density (calcd.) [g cm^{-3}]	1.747	2.203
Crystal size (in mm)	0.12 0.09 0.07	0.12 0.09 0.07
hkl Range	0/10;-11/11;-14/14	0/10;-11/11;-14/14
2θ range	3° - 60°	3° - 60°
Reflections collected	3726	3795
Reflections unique	3467	3534
Data (Fo>4σ(Fo))	2852	3259
$R_{int.}$	0.0130	0.0130
Min./Max transmission	0.1727 / 0.3800	0.1727 / 0.3800
$\Delta\rho$ [e/Å^3]	-0.65 / 0.71	-0.76 / 0.61
Parameters	103	103
R1 [Fo>4σ(Fo)]^a	0.0265	0.0180
WR2 for all unique data	0.0736	0.0436
Goodness of fit	1.037	1.08
CCDC No	-	280577

^{a}R1 = Σ | |Fo| - |Fc| | /Σ |Fo|

Table A-1.5 Technical details of data acquisition and selected refinement results for $(dienH_2)[MoS_4]$ and $(dienH_2)[WS_4]$

Compound	$(dienH_2)[MoS_4]$ **13**	$(dienH_2)[WS_4]$ **14**
Formula	$C_4H_{15}N_3MoS_4$	$C_4H_{15}N_3WS_4$
Temperature [K]	293	293
Wavelength [pm]	71.073	71.073
Space group	Pmmn	Pmmn
a [Å]	11.5279 (10)	11.559 (1)
b [Å]	7.1941 (4)	7.2424 (6)
c [Å]	7.5474 (5)	7.4956 (5)
Volume [Å^3]	625.9 (2)	627.50 (9)
Z	2	2
μ [mm^{-1}]	1.68	11.48
F(000)	332	396
Molecular weight [g/mol]	329.37	417.28
Density (calcd.) [g cm^{-3}]	1.748	2.402
Crystal size (in mm)	0.12 0.09 0.06	0.11 0.09 0.08
hkl Range	-15/15;-9/9;-9/9	-15/15;-9/8;-9/1
2θ range	3° - 56°	3° - 56°
Reflections collected	5423	3620
Reflections unique	851	859
Data $(Fo>4\sigma(Fo))$	767	812
$R_{int.}$	0.0344	0.0257
Min./Max transmission	-	0.2088 / 0.3116
$\Delta\rho$ [e/Å^3]	-0.49 / 0.57	-0.66 / 0.40
Parameters	42	42
R1 $[Fo>4\sigma(Fo)]^a$	0.0306	0.0131
WR2 for all unique data	0.0885	0.0323
Goodness of fit	1.071	1.128
CCDC No	-	601987
$^aR1 = \Sigma \mid \mid Fo\mid -\mid Fc\mid \mid /\Sigma \mid Fo\mid$		

Table A-I.6 Technical details of data acquisition and selected refinement results for $(dipnH_2)[MoS_4]\underline{14}$ and $(dipnH_2)[WS_4]$ $\underline{15}$

Compound	$(dipnH_2)[MoS_4]$ $\underline{15}$	$(dipnH_2)[WS_4]$ $\underline{16}$
Formula	$C_6H_{19}N_3MoS_4$	$C_6H_{19}N_3WS_4$
Temperature [K]	293	293
Wavelength [pm]	71.073	71.073
Space group	$Pca2_1$	$Pca2_1$
a [Å]	13.7377 (13)	13.8110 (8)
b [Å]	7.4901 (7)	7.5327 (6)
c [Å]	13.4526 (11)	13.4999 (7)
α, β, γ [°]	90, 90, 90	90, 90 90
Volume [Å^3]	1384.2 (2)	1404.45 (16)
Z	4	4
μ [mm^{-1}]	1.522	8.791
F(000)	728	856
Molecular weight [g/mol]	357.42	445.33
Density (calcd.) [g cm^{-3}]	1.715	2.106
Crystal size (in mm)	0.2 0.18 0.16	0.1 0.09 0.08
hkl Range	-19/2;-10/1;-18/6	-19/3;-10/4;-18/3
2θ range	3° - 60°	3° - 60°
Reflections collected	4107	4895
Reflections unique	2959	2582
Data (Fo>4σ(Fo)	2385	2019
R$_{int.}$	0.0404	0.0350
Min./Max transmission	0.7029 / 0.8501	0.1431 / 0.4355
$\Delta\rho$ [e/Å^3]	-0.568 / 0.574	-1.051 / 1.200
Parameters	129	130
R1 [Fo>4σ(Fo)]^a	0.0295	0.0218
WR2 for all unique data	0.0700	0.0531
Goodness of fit	1.028	1.006
CCDC No	-	601988
^{a}R1 = Σ ||Fo| -|Fc||/Σ|F o|		

Table A-I.7 Technical details of data acquisition and selected refinement results for $(trenH_2)[MoS_4] \cdot H_2O$ **17** and $(trenH_2)[WS_4] \cdot H_2O$ **18**

Compound	$(trenH_2)[MoS_4] \cdot H_2O$ **17**	$(trenH_2)[WS_4] \cdot H_2O$ **18**
Formula	$C_6H_{22}N_4OMoS_4$	$C_6H_{22}N_4OWS_4$
Temperature [K]	293	293
Wavelength [pm]	71.073	71.073
Space group	$P2_1/c$	$P2_1/c$
a [Å]	11.470 (2)	11.495 (1)
b [Å]	11.793 (2)	11.810 (1)
c [Å]	12.483 (2)	12.519 (1)
β [°]	111.63 (1)	111.70 (1)
Volume [Å^3]	1569.5 (4)	1579.2 (2)
Z	4	4
μ [mm^{-1}]	1.356	7.83
F(000)	800	928
Molecular weight [g/mol]	390.47	478.37
Density (calcd.) [g cm^{-3}]	1.652	2.012
Crystal size (in mm)	-	0.07 0.08 0.11
hkl Range	-16/1;-16/16;-16/17	-16/1;-16/16;-16/17
2θ range	3° - 60°	3° - 60°
Reflections collected	9614	10399
Reflections unique	4588	4600
Data (Fo>4σ(Fo)	3990	3961
$R_{int.}$	0.0229	0.0193
Min./Max transmission	0.7867 / 0.8513	0.2413 / 0.3650
$\Delta\rho$ [e/Å^3]	-0.80 /0.46	-0.99 / 0.72
Parameters	146	146
R1 [Fo>4σ(Fo)]^a	0.0209	0.0170
WR2 for all unique data	0.0560	0.0401
Goodness of fit	1.042	1.062
CCDC No.	241132	249578

^{a}R1 = Σ | |Fo| -|Fc| |/Σ |F o|

Table A-I.8 Technical details of data acquisition and selected refinement results for $(pipH_2)[MoS_4]$ **21**, $(pipH_2)[WS_4]$ **22** and $(1,4\text{-}dmpH_2)[WS_4]$ **23**

Compound	$(pipH_2)[MoS_4]$ **21**	$(pipH_2)[WS_4]$ **23**	$(1,4\text{-}dmpH_2)[WS_4]$ **24**
Formula	$C_4H_{12}MoN_2S_4$	$C_4H_{12}WN_2S_4$	$C_6H_{16}N_2WS_4$
Temperature [K]	293	293	293
Wavelength [pm]	71.073	71.073	71.073
Space group	$P2_1/c$	$P2_1/c$	Pbca
a [Å]	8.2520 (9)	8.2534 (7)	13.3792 (11)
b [Å]	11.238 (1)	11.271 (1)	12.6369 (7)
c [Å]	11.929 (2)	11.996 (1)	14.9381 (9)
β [°]	95.20 (2)	95.11 (1)	90, 90, 90
Volume [Å^3]	1101.7 (2)	1111.6 (2)	2525.6 (3)
Z	4	4	8
μ [mm^{-1}]	1.90	11.12	9.77
F(000)	624	752	1632
Molecular weight [g/mol]	312.36	400.25	428.30
Density (calcd.) [g cm^{-3}]	1.883	2.392	2.253
Crystal size (in mm)	0.16 0.1 0.07	0.12 0.09 0.06	0.14 0.09 0.06
hkl Range	0/11;-14/4;-16/16	0/11;-15/5;-16/16	-17/17;-15/15;-18/19
2θ range	3° - 60°	3° - 60°	3° - 60°
Reflections collected	5058	4913	23034
Reflections unique	3217	3241	2946
Data (Fo>4σ(Fo)	2258	2632	2398
$R_{int.}$	0.0535	0.0162	0.041
Min./Max transmission	-	0.1631 0.3001	0.360 / 0.555
Δρ [e/Å^3]	-0.69 / 0.670	-0.57 /0.58	-1.39 / 1.66
Parameters	101	101	119
R1 [Fo>4σ(Fo)]^a	0.0290	0.0176	0.025
WR2 for all unique data	0.0730	0.0400	0.067
Goodness of fit	1.017	0.990	1.01
CCDC No	241131	249579	

^{a}R1 = Σ | |Fo| -|Fc| |/Σ|F o|

Table A-I.9 Technical details of data acquisition and selected refinement results for(2-pipH-1-EtNH₃) [MoS₄]· ½H₂O **27**, (trans-1,2-cnH)₂ [WS₄] **28** and (mipaH)₂[WS₄] **29**

Compound	(2-pipH-1-EtNH₃) [MoS₄]· ½H₂O **27**	(trans-1,2-cnH)₂ [WS₄] **28**	(mipaH)₂[WS₄] **29**
Formula	$C_6H_{18}N_3MoS_4O_{0.5}$	$C_{12}H_{30}N_4S_4W$	$C_6H_{20}N_2S_4W$
Temperature [K]	293	293	293
Wavelength [pm]	71.073	71.073	71.073
Space group	C2/c	C2/c	C2/c
A [Å]	24.451 (3)	19.3669(13)	20.4038 (15)
B [Å]	7.1150 (10)	9.4959(5)	14.0813 (9)
C [Å]	17.864 (2)	11.3836(7)	11.2681(8)
α, β, γ [°]	90, 115.0 (10), 90	90, 107.713 (7), 90	90, 110.277(8), 90
Volume [Å³]	2815.9 (6)	1994.3 (2)	3036.8(4)
Z	8	4	8
μ [mm⁻¹]	1.501	6.210	8.127
F(000)	1480	1072	1664
Molecular weight [g/mol]	364.41	542.49	432.33
Density (calcd.) [g cm⁻³]	1.719	1.807	1.891
Crystal size (in mm)	0.12 0.09 0.07	0.13 0.09 0.07	0.12 0.09 0.08
hkl Range	0/34;-1/10;-25/22	-27/27;-13/13;-16/16	-28/28;-19/19;-15/15
2θ range	4° - 60°	3° - 60°	3° - 60°
Reflections collected	4833	11868	16917
Reflections unique	4095	2978	4486
Data (Fo>4σ(Fo)	3008	2675	3365
Rint.	0.0223	0.0369	0.0519
Min./Max transmission	0.7075/ 0.8530	0.3399/0.4861	0.2291/0.4174
Δρ [e/Å³]	-0.445/0.426	-1.336/1.191	-1.664/1.222
Parameters	134	98	125
R1 [Fo>4σ(Fo)]ᵃ	0.0285	0.0305	0.0312
WR2 for all unique data	0.0684	0.0740	0.0820
Goodness of fit	0985	1.102	0.999
CCDC No	-	601986	280578

ᵃR1 = Σ | |Fo| -|Fc| |/Σ|F o|

Table A-I.10 Technical details of data acquisition and selected refinement results for (dbtmen)$Br_2 \cdot 2H_2O$ **30**

Compound	(dbtmen)$Br_2 \cdot 2H_2O$ **30**
Formula	$C_{20}H_{34}Br_2N_2N_2O_2$
Temperature [K]	170 (2)
Wavelength [pm]	71.073
Space group	P-1
a [Å]	8.6672 (6)
b [Å]	11.7046 (8)
c [Å]	11.7731 (8)
α [°]	76.988 (8)
β [°]	88.978 (8)
γ [°]	76.198 (8)
Volume [$Å^3$]	1129.26 (13)
Z	2
μ [mm^{-1}]	3.605
F(000)	508
Molecular weight [g/mol]	494.31
Density (calcd.) [g cm^{-3}]	1.454
Crystal size (in mm)	0.5 0.2 0.2
hkl Range	-11/11; -15/15; -15/15
2θ range	4.5°-56°
Reflections collected	9858
Reflections unique	5133
Data (Fo>4σ(Fo)	4162
$R_{int.}$	0.0319
Min./Max transmission	0.5628/0.6349
$\Delta\rho$ [e/$Å^3$]	-0.721/0.464
Parameters	236
R1 [Fo>4σ(Fo)][a]	0.0297
WR2 for all unique data	0.0760
Goodness of fit	1.007
CCDC No	284867
[a]R1 = Σ | |Fo| -|Fc| |/Σ|F o|	

Table A-I.11 Technical details of data acquisition and selected refinement results for (enH$_2$)[CrO$_4$] **33** and (enH$_2$)[Cr$_2$O$_7$]**34**.

Compound	(enH$_2$)[CrO$_4$] **33**	(enH$_2$)[Cr$_2$O$_7$] **34**
Formula	C$_2$H$_{10}$CrN$_2$O$_4$	C$_2$H$_{10}$Cr$_2$N$_2$O$_7$
Temperature [K]	293	293
Wavelength [pm]	71.073	71.073
Space group	P2$_1$2$_1$2$_1$	C2/c
a [Å]	6.656 (1)	13.464 (2)
b [Å]	8.869 (1)	7.791 (1)
c [Å]	11.831 (2)	8.639 (1)
β [°]	90	108.97 (1)
Volume [Å^3]	698.4 (2)	857.0 (2)
Z	4	4
μ [mm^{-1}]	1.59	2.55
F(000)	368	560
Molecular weight [g/mol]	178.12	278.12
Density (calcd.) [g cm^{-3}]	1.694	2.156
Crystal size (in mm)	0.16 × 0.1 × 0.05	0.16 × 0.1 × 0.07
2θ range	3° - 60°	3° - 60°
Reflections collected	5213	2218
Reflections unique	2041	1245
Data (Fo>4σ(Fo)	1977	1106
R$_{int.}$	0.0542	0.0333
Min./Max. transmission	0.5997 / 0.8406	0.5248 / 0.7555
?ρ [e/Å^3]	-0.59 / 0.32	-0.41 / 0.40
Parameters/Restraints	85 / 0	62 / 0
R1 for all Fo>4σ(Fo)[a]	0.0221	0.0233
WR2 for all unique data	0.0590	0.0690
Goodness of fit	1.104	1.113
CCDC No.	196333	196334

[a]R1 = Σ | |Fo| - |Fc| |/Σ|F o|

Table A-II.12 Atomic coordinates [$\times 10^4$] and equivalent isotropic displacement parameters [$\text{Å}^2 \times 10^3$] for Tetrathiometalates

Atom	x	y	z	U_{eq}
(enH$_2$)[WS$_4$] **2**				
W(1)	2287(1)	9513(1)	3956 (1)	19(1)
S(1)	57(2)	10628 (2)	4060 (1)	29 (1)
S(2)	2486(2)	8455 (2)	2314 (1)	28 (1)
S(3)	2466(2)	7911 (2)	5309 (1)	28 (1)
S(4)	4142(2)	11091 (2)	4129 (1)	28 (1)
N(1)	9322(5)	9442 (7)	6633 (4)	30 (1)
C(1)	8188(7)	10466 (8)	7118 (5)	32 (1)
C(2)	6847(8)	10747 (7)	6344 (6)	35 (2)
N(2)	5706(5)	9580 (7)	6330 (4)	28 (1)
(N-MeenH$_2$)[MoS$_4$] **3**				
Mo(1)	5398 (1)	3632 (1)	2959 (1)	27(1)
S(1)	2737 (1)	3593 (1)	2399 (1)	35(1)
S(2)	5862 (2)	5185 (1)	3870 (1)	39(1)
S(3)	7096 (2)	3592 (1)	1498 (1)	45(1)
S(4)	5875 (2)	2164 (1)	4018 (1)	38(1)
N(1)	6828 (5)	3759 (4)	6269 (4)	36(1)
C(1)	5056 (6)	3778 (5)	6704 (4)	40(1)
C(2)	5071 (5)	3982 (4)	7944 (4)	36(1)
N(2)	3339 (5)	3977 (4)	8406 (3)	33(1)
C(3)	3321 (8)	4088 (6)	9647 (5)	54(2)
(N-Me-enH$_2$)[WS$_4$] **4**				
W1	4610(1)	6374(1)	7041(1)	26(1)
S(1)	7275(2)	6415(1)	7598(1)	34(1)
S(2)	4147(2)	4814(1)	6132(1)	38(1)
S(3)	2907(2)	6417(2)	8499(1)	44(1)
S(4)	4127(2)	7839(1)	5976(1)	37(1)
N(1)	3185(6)	6229(4)	3732(4)	36(1)
C(1)	4935(7)	6211(6)	3296(5)	37(1)
C(2)	4920(7)	6002(5)	2049(5)	38(1)
N(2)	6661(7)	6013(4)	1600(4)	31(1)
C(3)	6677(11)	5908(7)	351(5)	53(2)
(tmenH$_2$)[MoS$_4$] **5**				
Mo(1)	7283(1)	7402 (1)	5232 (1)	25(1)
S(1)	6430(1)	7408 (1)	3577 (1)	35(1)
S(2)	7789(1)	5725 (1)	5751 (1)	39(1)
S(3)	5451(1)	8082 (1)	5976 (1)	39 (1)
S(4)	9430(1)	8368 (1)	5608 (1)	41(1)

C(1)	7882(3)	3878 (2)	3769 (2)	41(1)
C(2)	7975(4)	5197 (2)	2389 (2)	43(1)
N(1)	7114(2)	4848 (2)	3205 (2)	28(1)
C(3)	5364(3)	4708 (2)	2830 (2)	29(1)
C(4)	4998(3)	3802 (2)	2058 (2)	33(1)
N(2)	3293(2)	3466 (2)	1919 (2)	28(1)
C(5)	3019(4)	2445 (3)	1321 (3)	48(1)
C(6)	2174(4)	4327 (3)	1449 (3)	54(1)

(tmenH₂)[WS₄] 6

W(1)	7287(1)	7397 (1)	5238 (1)	26 (1)
S(1)	5456(2)	8079 (1)	5983 (1)	41 (1)
S(2)	9438(2)	8368 (1)	5608 (1)	43 (1)
S(3)	7790(2)	5719 (1)	5756 (1)	42 (1)
S(4)	6429(2)	7401 (1)	3584 (1)	37 (1)
C(1)	7826(7)	5689 (5)	8550 (6)	56 (2)
C(2)	6967(8)	7567 (4)	8691 (6)	50 (2)
N(1)	6704(5)	6547 (3)	8085 (3)	32 (1)
C(3)	4999(6)	6205 (4)	7953 (4)	36 (1)
C(4)	4635(5)	5295 (4)	7181 (4)	30 (1)
N(2)	2894(5)	5155 (3)	6805 (3)	31 (1)
C(5)	2041(7)	4804 (5)	7622 (5)	47 (1)
C(6)	2125(7)	6114 (5)	6241 (4)	43 (1)

(1,3-pnH₂)[MoS₄] 7

Mo(1)	2430 (1)	1451 (1)	4849 (1)	22 (1)
S(1)	1160 (1)	3155 (1)	4550 (1)	29 (1)
S(2)	2351 (1)	239 (1)	6462 (1)	33 (1)
S(3)	1511 (1)	451 (1)	2816 (1)	34 (1)
S(4)	4629 (1)	1988 (1)	5526 (1)	43 (1)
N(1)	5906 (3)	5281 (3)	3032 (3)	37 (1)
C(1)	6352 (3)	4428 (3)	4285 (4)	36 (1)
C(2)	7545 (4)	3563 (3)	4470 (4)	35 (1)
C(3)	8173 (3)	2849 (3)	5865 (3)	35 (1)
N(2)	9365 (3)	2037 (2)	6043 (3)	31 (1)

(1,3-pnH₂)[WS₄] 8

W(1)	2563 (1)	1441 (1)	5143 (1)	26 (1)
S(1)	3841 (1)	3140 (1)	5449 (1)	33 (1)
S(2)	2647 (1)	222 (1)	3542 (1)	37 (1)
S(3)	3473 (1)	443 (1)	7175 (1)	39 (1)
S(4)	357 (1)	1987 (1)	4451 (2)	47 (1)
N(1)	4380 (4)	7960 (3)	6060 (4)	35 (1)
C(1)	3169 (5)	7149 (5)	5871 (5)	39 (1)
C(2)	2558 (5)	6436 (4)	4481 (5)	39 (1)
C(3)	1352 (5)	5576 (4)	4290 (5)	42 (1)

N(2)	916 (4)	4723 (3)	3052 (4)	41 (1)

(N,N'-dm-1,3-pnH₂)[WS₄] 10

W(1)	8399 (1)	1153 (1)	7843 (1)	33 (1)
S(1)	5930(2)	1210 (1)	9140 (1)	46 (1)
S(2)	10827(2)	951(1)	9145(1)	39(1)
S(3)	8766(2)	2180(1)	6754(2)	59(1)
S(4)	8083(3)	289(1)	6349(2)	59(1)
C(1)	3461(10)	1440(4)	5421(7)	62(2)
N(1)	3265(6)	1879(2)	6667(4)	41(1)
C(2)	3821(8)	2632(3)	6522(5)	43(1)
C(3)	3575(10)	3024(3)	7880(5)	55(2)
C(4)	4316(11)	3776(3)	7878(7)	60(2)
N(2)	3206(7)	4297(2)	7031(4)	48(1)
C(5)	1357(10)	4479(4)	7521(7)	61(2)

(1,4-bnH₂)[MoS₄] 11

Mo	7847(1)	4675 (1)	7688 (1)	35(1)
S(1)	10293(1)	3440 (1)	6647 (1)	47(1)
S(2)	8156(1)	7357 (1)	7378 (1)	49(1)
S(3)	7676(1)	3693 (1)	9767 (1)	47(1)
S(4)	5303(1)	4232 (1)	6936 (1)	56(1)
N(1)	7553(3)	7381 (3)	10547 (2)	47(1)
C(1)	7362(4)	9161 (3)	10685 (3)	53(1)
C(2)	5329(4)	9917 (3)	10658 (3)	43(1)
N(2)	7677(4)	2874 (3)	4312 (3)	56(1)
C(3)	7122(5)	1222 (4)	4242 (4)	70(1)
C(4)	5298(4)	828 (3)	5064(3)	50(1)

(1,4-bnH₂)[WS₄] 12

W(1)	7868(1)	4689(1)	7686(1)	30(1)
S(1)	10303(1)	3443(1)	6654(1)	41(1)
S(2)	8173(1)	7385(1)	7390(1)	44(1)
S(3)	7691(1)	3696(1)	9742(1)	43(1)
S(4)	5303(1)	4244(1)	6936(1)	46(1)
N(1)	7562(4)	7381(3)	10547(3)	41(1)
C(1)	7351(5)	9169(4)	10690(4)	50(1)
C(2)	5331(4)	9915(4)	10656(3)	39(1)
N(2)	7715(4)	2849(3)	4344(3)	44(1)
C(3)	7143(6)	1187(5)	4273(5)	64(1)
C(4)	5308(5)	835(4)	5057(4)	46(1)

(dienH₂)[MoS₄] 13

Mo(1)	7500	2500	4561(1)	31(1)
S(1)	5941(1)	2500	2900(2)	53(1)
S(2)	7500	44(2)	6228(2)	60(1)
N(1)	4326(3)	250	6592(5)	55(1)

	x	y	z	U(eq)
C(1)	4586(4)	25008	475(6)	58(1)
C(2)	3552(5)	2500	9589(6)	71(2)
N(2)	2500	1957(9)	8912(9)	42(2)

(dienH$_2$)[WS$_4$] 14

	x	y	z	U(eq)
W(1)	7500	2500	4557(1)	30(1)
S(1)	5948(1)	2500	2884(2)	54(1)
S(2)	7500	57(1)	6236(2)	61(1)
N(1)	4316(3)	2500	6568(4)	54(1)
C(1)	4576(3)	2500	8468(5)	58(1)
C(2)	3550(4)	2500	9595(5)	70(2)
N(2)	2500	1935(8)	8905(7)	39(1)

(dipnH$_2$)[MoS$_4$] 15

	x	y	z	U(eq)
Mo(1)	7530(1)	7192(1)	4613(1)	23(1)
S(1)	8308(1)	7706(2)	5989(1)	44(1)
S(2)	6662(1)	4754(1)	4763(1)	35(1)
S(3)	6591(1)	9465(1)	4285(1)	35(1)
S(4)	8577(1)	6841(2)	3407(1)	47(1)
N(1)	3150(2)	9009(5)	1779(3)	42(1)
C(1)	4206(3)	8789(6)	1808(3)	33(1)
C(2)	4520(3)	7544(6)	2649(3)	29(1)
C(3)	4162(3)	8180(6)	3645(3)	30(1)
N(2)	4526(2)	7022(4)	4465(3)	25(1)
C(4)	4105(3)	7569(5)	5450(3)	28(1)
C(5)	4561(3)	6534(6)	6305(3)	28(1)
C(6)	4039(3)	6872(6)	7272(3)	35(1)
N(3)	3031(2)	6175(5)	7270(3)	37(1)

(dipnH$_2$)[WS$_4$] 16

	x	y	z	U(eq)
W(1)	7468(1)	7192(1)	5283(1)	23(1)
S(1)	8338(1)	4754(2)	5126(1)	35(1)
S(2)	8410(1)	9464(2)	5609(1)	35(1)
S(3)	6692(1)	7705(2)	3899(2)	45(1)
S(4)	6417(1)	6837(2)	6486(2)	47(1)
N(1)	6855(3)	990(7)	8106(5)	44(1)
C(1)	5791(4)	1231(8)	8085(5)	34(1)
C(2)	5480(4)	2455(8)	7258(5)	32(1)
C(3)	5841(5)	1814(9)	6241(5)	33(2)
N(2)	5479(3)	2963(5)	5433(4)	25(1)
C(4)	5890(5)	2424(7)	4439(5)	28(1)
C(5)	5434(4)	3435(8)	3589(4)	26(1)
C(6)	5963(5)	3123(8)	2621(4)	35(2)
N(3)	6964(3)	3831(7)	2625(4)	36(1)

(trenH$_2$)[MoS$_4$].H$_2$O 17

	x	y	z	U(eq)
Mo(1)	1787(1)	3575(1)	2323(1)	26(1)
S(1)	53(1)	3020(1)	2509(1)	41(1)
S(2)	1543(1)	3576(1)	498(1)	35(1)

S(3)	3266(1)	2420(1)	3299(1)	40(1)
S(4)	2250(1)	5303(1)	3001(1)	39(1)
N(1)	6392(1)	3908(1)	3075(1)	29(1)
C(1)	6714(1)	2725(1)	3417(1)	33(1)
C(2)	8024(1)	2645(1)	4327(1)	34(1)
N(2)	8369(1)	1440(1)	4636(1)	34(1)
C(3)	5928(2)	4490(1)	3883(1)	34(1)
C(4)	6272(2)	5731(2)	4004(1)	43(1)
N(3)	7644(2)	5876(1)	4469(1)	46(1)
C(5)	5477(2)	4004(2)	1886(1)	36(1)
C(6)	6023(2)	3710(2)	981(1)	39(1)
N(4)	7069(2)	4412(1)	976(1)	43(1)
O(1)	9395(2)	5453(2)	3441(2)	86(1)

(trenH$_2$)[WS$_4$].H$_2$O **18**

W(1)	1790 (1)	3573 (1)	2326 (1)	26 (1)
S(1)	51 (1)	3022 (1)	2507(1)	41 (1)
S(2)	1546 (1)	3574 (1)	502 (1)	35 (1)
S(3)	3272 (1)	2415 (1)	3301 (1)	41 (1)
S(4)	2255 (1)	5302 (1)	3006 (1)	40 (1)
N(1)	6402 (2)	3910 (2)	3076 (2)	30 (1)
C(1)	6720 (2)	2725 (2)	3419 (2)	33 (1)
C(2)	8027 (2)	2642 (2)	4321 (2)	34 (1)
N(2)	8368 (2)	*1437 (2)	4633 (2)	35 (1)
C(3)	5935 (2)	4492 (2)	3881 (2)	34 (1)
C(4)	6274 (3)	5729 (2)	4001 (2)	43 (1)
N(3)	7648 (2)	5873 (2)	4462 (2)	48 (1)
C(5)	5490 (2)	4003 (2)	1890 (2)	37 (1)
C(6)	6027 (3)	3708 (2)	982 (2)	39 (1)
N(4)	7071 (2)	4404 (2)	974 (2)	44 (1)
O(1)	9402 (3)	5450(2)	3447 (3)	85 (1)

(pipH$_2$)[MoS$_4$] **21**

Mo(1)	7927(1)	2790(1)	5944(1)	22(1)
S(1)	7930(1)	3920(1)	7418(1)	30(1)
S(2)	5739(1)	1646(1)	5854(1)	29(1)
S(3)	10115(1)	1663(1)	6118(1)	29(1)
S(4)	7924(1)	3860(1)	4431(1)	33(1)
N(1)	4594(3)	2698(2)	8239(2)	29(1)
C(1)	3680(3)	1576(3)	8328(2)	29(1)
C(2)	2314(3)	1739(3)	9079(2)	28(1)
N(2)	1242(3)	2737(2)	8668(2)	28(1)
C(3)	2168(4)	3864(3)	8582(3)	34(1)
C(4)	3525(4)	3693(3)	7823(3)	32(1)

(pipH$_2$)[WS$_4$] **22**

W(1)	7906(1)	2207(1)	5940(1)	22 (1)
S(1)	10103 (1)	3328 (1)	6112 (1)	30 (1)
S(2)	5721 (1)	3355 (1)	5853 (1)	30 (1)
S(3)	7901 (1)	1134 (1)	4432 (1)	34 (1)

S(4)	7908 (1)	1077 (1)	7415 (1)	30 (1)
N(1)	4583 (3)	2706 (2)	3242 (2)	28 (1)
C(1)	3508 (4)	3698 (3)	2829 (3)	32 (1)
C(2)	2140 (4)	3867 (3)	3570 (3)	34 (1)
N(2)	1221 (3)	2725 (2)	3659 (2)	28 (1)
C(3)	2297 (3)	1740 (3)	4071 (2)	30 (1)
C(4)	3655 (3)	1577 (3)	3320 (3)	30 (1)

(1,4-dmpH$_2$)[WS$_4$] _24_

W(1)	2484 (1)	3453 (1)	6280 (1)	19 (1)
S(1)	1019 (1)	2894 (1)	6724 (1)	30 (1)
S(2)	2721 (1)	2959 (1)	4875 (1)	32 (1)
S(3)	3678 (1)	2865 (1)	7138 (1)	42 (1)
S(4)	2492 (1)	5192 (1)	6332 (1)	32 (1)
N(1)	4087 (2)	5130 (2)	4485 (2)	26 (1)
C(1)	4875 (2)	4348 (3)	4221 (2)	30 (1)
C(2)	5454 (2)	3958 (3)	5027 (2)	30 (1)
C(3)	3513 (3)	5492 (4)	3687 (2)	46 (1)
N(11)	4933 (2)	5178 (2)	-961 (2)	24 (1)
C(11)	5237 (2)	6048 (3)	-332 (2)	27 (1)
C(12)	5736 (2)	5597 (3)	492 (2)	27 (1)
C(13)	4438 (3)	5618 (3)	-1780 (2)	39 (1)

(2-pip-1-EtNH$_3$)[MoS$_4$] · ½ H$_2$O _27_

Mo(1)	8809(1)	5231(1)	5751(1)	26(1)
S(1)	8048(1)	5320(1)	4520(1)	40(1)
S(2)	8904(1)	2381(1)	6251(1)	37(1)
S(3)	9643(1)	6009(1)	5670(1)	47(1)
S(4)	8631(1)	7204(1)	6548(1)	46(1)
N(1)	6361(1)	5290(3)	6346(1)	30(1)
C(1)	5793(1)	4401(4)	6247(2)	34(1)
C(2)	5295(1)	5835(4)	5989(2)	37(1)
N(2)	5454(1)	7342(3)	6621(1)	37(1)
C(3)	6038(1)	8231(4)	6749(2)	41(1)
C(4)	6526(1)	6748(4)	6977(2)	37(1)
C(5)	6835(1)	3876(4)	6543(2)	41(1)
C(6)	7318(1)	4498(4)	6281(2)	40(1)
N(3)	7050(1)	4956(3)	5392(1)	42(1)
O(1)	5000	4458(4)	7500	45(1)

(±) (trans-1,2-cnH)$_2$[WS$_4$] _28_

W(1)	5000	8223(1)	2500	22(1)
S(1)	4207(1)	9582(1)	1200(1)	36(1)
S(2)	5532(1)	6874(1)	1478(1)	43(1)
N(1)	5537(2)	2144(4)	1448(3)	29(1)
N(2)	5754(2)	3767(5)	3647(4)	41(1)
C(1)	6185(2)	3102(4)	1905(3)	25(1)
C(2)	6819(3)	2538(6)	1512(5)	43(1)

C(3)	7493(3)	3446(7)	2011(5)	48(1)
C(4)	7693(3)	3580(6)	3398(5)	46(1)
C(5)	7065(3)	4186(5)	3769(4)	41(1)
C(6)	6384(2)	3260(4)	3303(4)	31(1)
(mipaH)$_2$[WS$_4$] **29**				
W(1)	2780(1)	6596(1)	7623(1)	34(1)
S(1)	1636(1)	6605(1)	7126(2)	52(1)
S(2)	3274(1)	6453(1)	9667(1)	47(1)
S(3)	3110(1)	7928(1)	7019(1)	52(1)
S(4)	3099(1)	5385(1)	6696(1)	53(1)
N(1)	3497(2)	6148(3)	4207(4)	49(1)
C(1)	4277(3)	6074(4)	4726(6)	60(2)
C(2)	4567(3)	6212(5)	3670(7)	71(2)
C(3)	4559(5)	6756(7)	5759(8)	102(3)
N(2)	1747(2)	3984(3)	5150(5)	54(1)
C(4)	1036(3)	4403(4)	4914(5)	50(1)
C(5)	939(4)	5229(4)	4014(7)	75(2)
C(6)	514(4)	3621(5)	4437(9)	82(2)

U_{eq} is calculated as one third of the trace of the orthogonalised U_{ij} tensor

Table A-II.13 Atomic coordinates [$\times 10^4$] and equivalent isotropic displacement parameters [$\text{Å}^2 \times 10^3$] for (dbtmen)B$_2$·2H$_2$O **30**

Atom	x	y	z	U(eq)
Br(1)	3569(1)	3604(1)	-435(1)	23(1)
Br(2)	1002(1)	6403(1)	5472(1)	28(1)
C(1)	5793(2)	2765(2)	2584(2)	19(1)
N(1)	4217(2)	3358(1)	3069(1)	15(1)
C(2)	3780(2)	4652(2)	2359(2)	16(1)
C(3)	2095(2)	5314(2)	2584(2)	18(1)
N(2)	1681(2)	6632(2)	1942(2)	16(1)
C(4)	2709(3)	7313(2)	2438(2)	18(1)
C(5)	4440(3)	3332(2)	4338(2)	26(1)
C(6)	2957(3)	2713(2)	2923(2)	20(1)
C(7)	1880(3)	6744(2)	651(2)	23(1)
C(8)	-50(3)	7112(2)	2147(2)	23(1)
C(11)	6349(2)	1418(2)	3073(2)	18(1)
C(12)	7343(3)	965(2)	4075(2)	25(1)
C(13)	7874(3)	-286(2)	4497(2)	29(1)
C(14)	7428(3)	-1067(2)	3921(2)	28(1)
C(15)	6453(3)	-624(2)	2920(2)	30(1)
C(16)	5927(3)	619(2)	2491(2)	25(1)
C(21)	2289(2)	8662(2)	1942(2)	16(1)
C(22)	1222(3)	9425(2)	2513(2)	23(1)
C(23)	857(3)	10671(2)	2072(2)	29(1)

Atom					
C(26)	2999(3)	9168(2)	948(2)	24(1)
C(24)	1550(3)	11164(2)	1078(2)	28(1)
C(25)	2633(3)	10412(2)	513(2)	29(1)
O(1)	672(2)	6025(2)	-1647(2)	41(1)
O(2)	3470(2)	3785(2)	6723(2)	37(1)

U_{eq} is calculated as one third of the trace of the orthogonalised U_{ij} tensor

Table A-I.13 Atomic coordinates [$\times 10^4$] and equivalent isotropic displacement parameters [$\mathring{A}^2 \times 10^3$] for (enH$_2$)[CrO$_4$] **33** and (enH$_2$)[Cr$_2O_7$] **34**

Atom	X		Y		Z		U_{eq}	
(enH$_2$)[CrO$_4$]								
Cr(1)	8291	(1)	9877	(1)	6098	(1)	22	(1)
O(1)	6725	(1)	11378	(1)	6077	(1)	27	(1)
O(2)	7836	(2)	8823	(1)	4996	(1)	39	(1)
O(3)	7860	(2)	8897	(1)	7271	(1)	34	(1)
O(4)	10571	(2)	10511	(2)	6074	(1)	42	(1)
N(1)	5505	(2)	6172	(1)	10908	(1)	27	(1)
C(1)	6665	(2)	4748	(1)	10982	(1)	27	(1)
C(2)	8388	(2)	4962	(1)	11806	(1)	28	(1)
N(2)	9610	(2)	3573	(1)	11882	(1)	29	(1)
(enH$_2$)[Cr$_2$O$_7$]								
Cr(1)	3785	(1)	5993	(1)	6577	(1)	19	(1)
O(1)	3602	(1)	7341	(2)	7882	(2)	35	(1)
O(2)	5000		4926	(2)	7500		26	(1)
O(3)	2870	(1)	4541	(2)	6100	(2)	30	(1)
O(4)	3820	(1)	7012	(2)	4978	(2)	39	(1)
N(1)	1467	(1)	4065	(2)	2930	(2)	27	(1)
C(1)	458	(1)	4044	(2)	3285	(2)	22	(1)

U_{eq} is defined as one third of the trace of the orthogonalised U_{ij} tensors